

7-25-2019

Capabilities and Limitations of the Spin Hamiltonian Formalism in Single Molecule Magnets

Philip Ferko

University of Missouri-St. Louis, pjjm84@mail.umsl.edu

Follow this and additional works at: <https://irl.umsl.edu/dissertation>



Part of the [Inorganic Chemistry Commons](#)

Recommended Citation

Ferko, Philip, "Capabilities and Limitations of the Spin Hamiltonian Formalism in Single Molecule Magnets" (2019). *Dissertations*. 845.

<https://irl.umsl.edu/dissertation/845>

This Dissertation is brought to you for free and open access by the UMSL Graduate Works at IRL @ UMSL. It has been accepted for inclusion in Dissertations by an authorized administrator of IRL @ UMSL. For more information, please contact marvinh@umsl.edu.

Capabilities and Limitations of the Spin Hamiltonian Formalism in Single
Molecule Magnets

Philip J. Ferko

M.S. Chemistry, University of Missouri-St. Louis, 2015

B.S. Chemistry, University of Missouri-St. Louis, 2010

A Dissertation Submitted to The Graduate School at the University of Missouri-St.
Louis in partial fulfillment of the requirements for the degree
Doctor of Philosophy in Chemistry

August 2019

Advisory Committee

Wesley Harris, Ph.D.
Chairperson

Benjamin Bythell, Ph.D

Joyce Corey, Ph.D

Stephen Holmes, Ph.D

Acknowledgements

The work reported in this dissertation was supported by numerous people and institutions, including the members of my committee, Drs. W. Harris, B. Bythell, J. Corey, and S. Holmes.

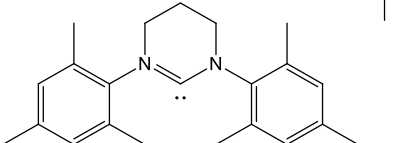
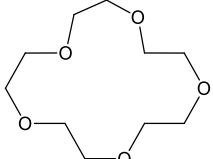
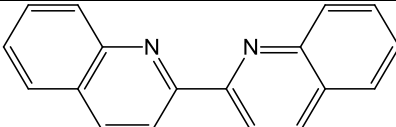
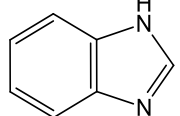
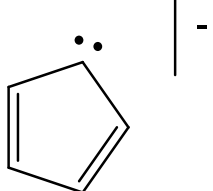
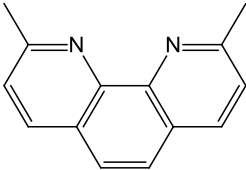
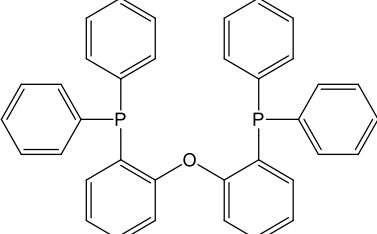
DFT calculations presented in this work were undertaken by Dr. Eric Majzoub at the University of Missouri – Saint Louis, AC magnetic susceptibility measurements were conducted by Dr. Rodolphe Clerac at Centre de Recherches Paul Pascal, and high field EPR measurements were conducted at the National High Magnetic Field Laboratory by Dr. Steve Hill. Near-infrared spectroscopy measurements were completed in the laboratory of Dr. Michael Shaw at Southern Illinois University – Edwardsville.

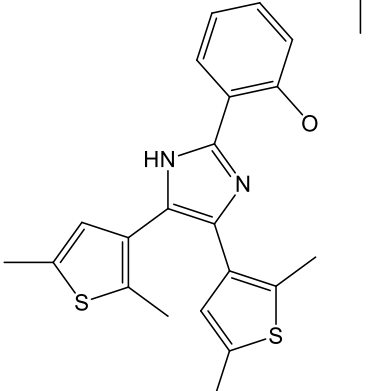
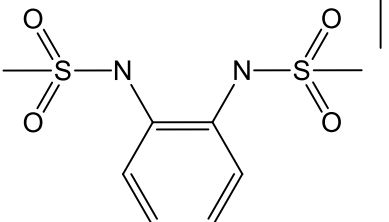
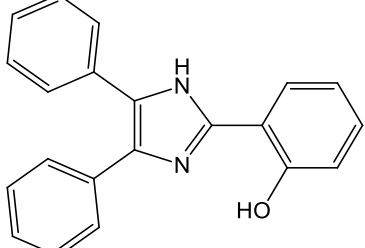
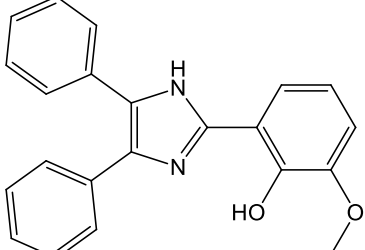
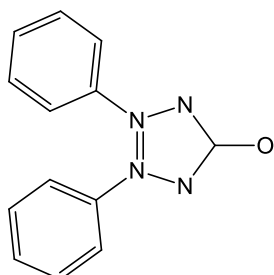
This work was funded in part by NSF grants, CHE 0914935, CHE 0939987, and CHE 1214063.

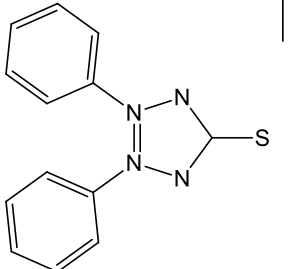
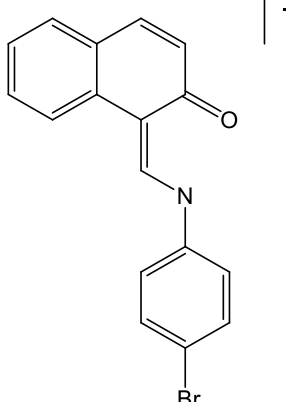
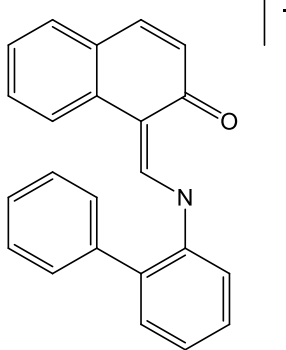
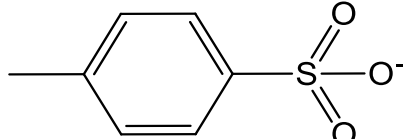
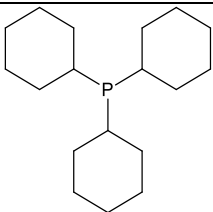
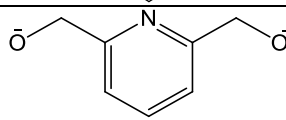
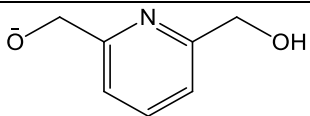
Abstract

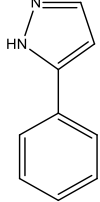
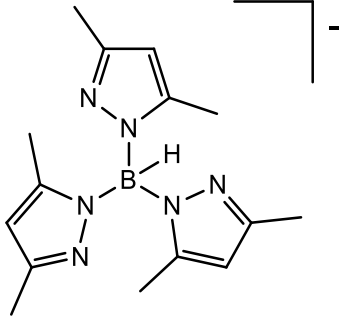
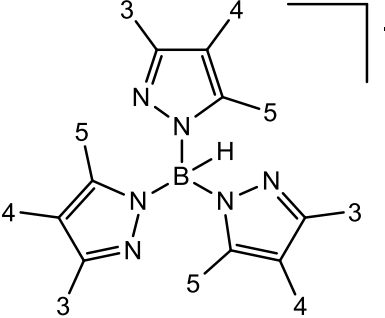
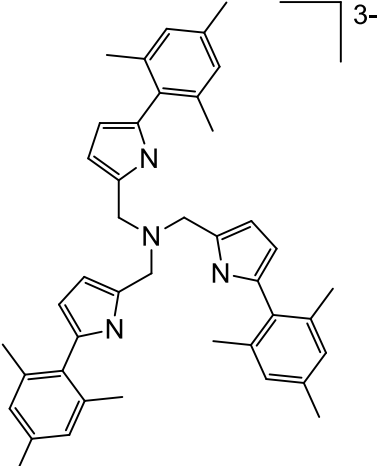
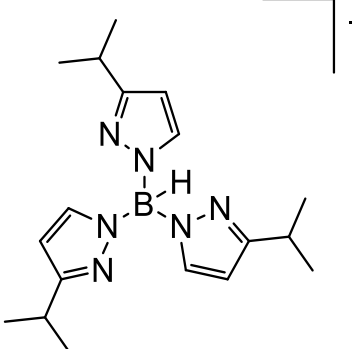
The rational design of molecular magnetic materials is an ongoing effort involving physics, materials science, and chemistry. A common approach to design of complexes and interpretation of magnetic data is the spin Hamiltonian formalism. In this approach, magnetic data is interpreted through constants extracted from the parameterization of data. In design, certain structural motifs are pursued, rationalized by the minimization or maximization of terms in the spin Hamiltonian. In this work, monometallic complexes were prepared to simplify magnetic behavior and allow the examination of specific factors that influence single molecule magnetism like coordination geometry, ligand identity, symmetry, and spin-orbit coupling. A series of hydridotris(3-phenylpyrazolylborato) scorpionate compounds are presented, some of which are inadequately described by the parameterization of magnetic data, and others for which the alteration of terms within the spin Hamiltonian gives the predicted result. These discoveries and ramifications for single molecule magnetism will be discussed. A series of dmf adducts of transition metal para-toluenesulfonates is also presented.

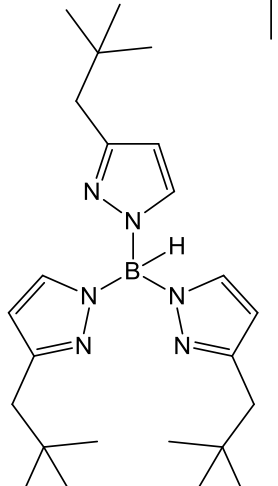
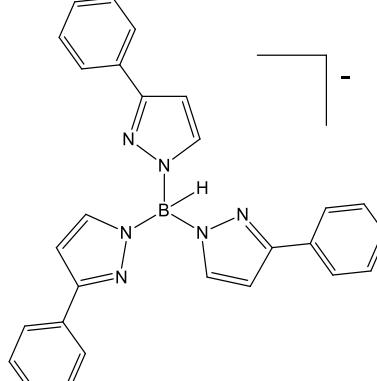
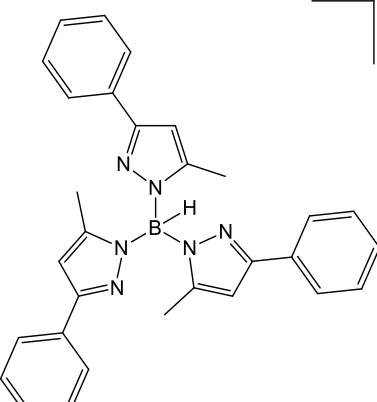
List of Ligands

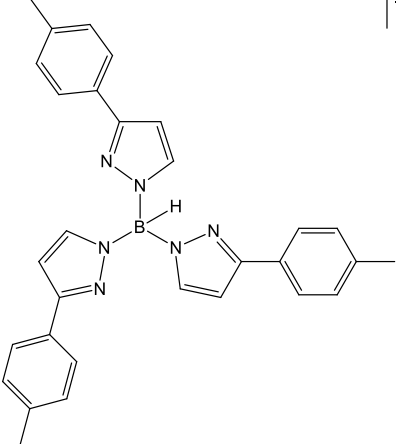
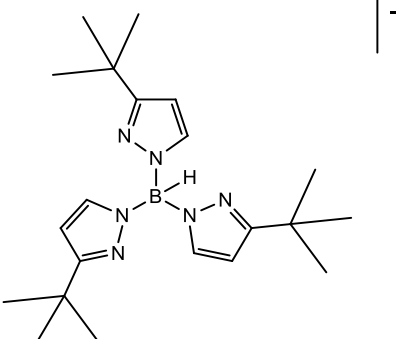
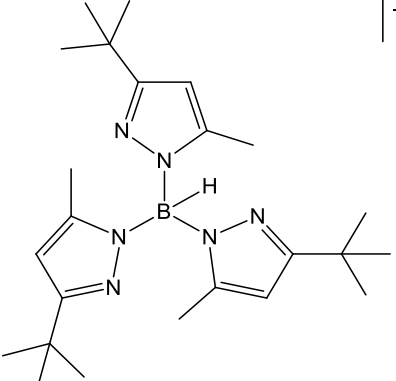
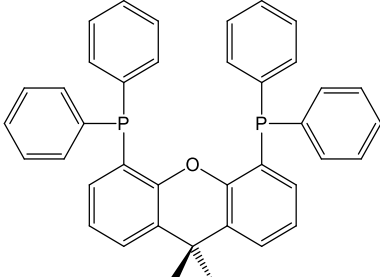
| | |
|-----------------|--|
| 6-Mes |  |
| 15-crown-5 |  |
| Biq |  |
| Bzi |  |
| Cp ⁻ |  |
| Dmph |  |
| DPEphos |  |

| | |
|--------------------------|--|
| <p>Hpbdti</p> |  |
| <p>(L1)²⁻</p> |  |
| <p>L2</p> |  |
| <p>L3</p> |  |
| <p>L4</p> |  |

| | |
|---------------------|--|
| L5 |  |
| (LBr) ⁻ |  |
| (LPh) ⁻ |  |
| (OTs) ⁻ |  |
| PCy ₃ |  |
| (Pdm) ²⁻ |  |
| (pdmH) ⁻ |  |

| | |
|-------------------------------------|--|
| Phpy |  |
| (Tp*) ⁻ |  |
| (Tp') |  |
| (tpa ^{Mes}) ³⁻ |  |
| (Tp ^{i-Pr}) ⁻ |  |

| | |
|---|--|
| <p>(Tp^{Np})⁻</p> |  <p>The structure shows a central boron atom bonded to a hydrogen atom and three nitrogen atoms. Each nitrogen atom is part of a 5-membered ring containing two other nitrogen atoms. The top ring is substituted with a tert-butylmethylcarbamoyl group. The two bottom rings are substituted with tert-butylmethyl groups. A negative charge is indicated by a minus sign in the top right corner.</p> |
| <p>(Tp^{Ph})⁻</p> |  <p>The structure shows a central boron atom bonded to a hydrogen atom and three nitrogen atoms. Each nitrogen atom is part of a 5-membered ring containing two other nitrogen atoms. Each of the three rings is substituted with a phenyl group. A negative charge is indicated by a minus sign in the top right corner.</p> |
| <p>(Tp^{Ph,Me})⁻</p> |  <p>The structure shows a central boron atom bonded to a hydrogen atom and three nitrogen atoms. Each nitrogen atom is part of a 5-membered ring containing two other nitrogen atoms. The top ring is substituted with a phenyl group and a methyl group. The two bottom rings are substituted with a phenyl group and a methyl group. A negative charge is indicated by a minus sign in the top right corner.</p> |

| | |
|---|--|
| <p>(Tp^{p-tol})⁻</p> |  |
| <p>(Tp^{t-Bu})⁻</p> |  |
| <p>(Tp^{t-Bu,Me})⁻</p> |  |
| <p>Xantphos</p> |  |

List of Abbreviations, Units, Symbols

| | |
|---|---|
| AO | Atomic Orbital |
| \vec{B} | magnetic flux density |
| $c_0 = 299\,792\,458\text{ m s}^{-1}$ | speed of light in a vacuum ¹ |
| C_n | rotation by $2\pi/n$ |
| $\epsilon_0 = 8.854\,187\,817 \times 10^{-12}\text{ C}^2\text{ m}^{-1}\text{ J}^{-1}$ | permittivity of vacuum ¹ |
| $e^- = -1.602\,176\,487(4) \times 10^{-19}\text{ C}$ | charge of electron ¹ |
| $g_e = -2.002\,319\,304\,362\,2(15)$ | Landé g factor for free electron ¹ |
| $h = 6.626\,068\,96(3) \times 10^{-34}\text{ J s}$ | Planck constant ¹ |
| \vec{H} | magnetic field strength |
| \hat{H} | Hamiltonian operator |
| i | inversion |
| <i>IUPAC</i> | International Union of Pure and Applied Chemistry |
| $k_B = 1.380\,658(12) \times 10^{-23}\text{ J K}^{-1}$ | Boltzmann constant ¹ |
| $ L\rangle$ | summation of orbital angular momentum |
| $ l\rangle$ | azimuthal quantum vector |
| $\mu_0 = 4\pi \times 10^{-7}\text{ N A}^{-2}$ | permeability of vacuum ¹ |
| $\mu_B = 9.274\,009\,15(2) \times 10^{-24}\text{ J T}^{-1}$ | Bohr magneton ¹ |
| \vec{M} | magnetization |
| $ M_s\rangle$ | summation of spin angular momentum |
| $ m_l\rangle$ | magnetic quantum vector |
| $ m_s\rangle$ | spin magnetic moment quantum vector |
| $m_e = 9.109\,382\,15(5) \times 10^{-31}\text{ kg}$ | mass of electron ¹ |
| n | principal quantum number |
| r | radius |
| <i>SMM</i> | single molecule magnet |
| T | temperature (K) |
| T_C | Curie temperature |
| T_N | Néel temperature |
| θ | Weiss constant |
| χ | magnetic susceptibility |

| | |
|----------|-------------------------------|
| χ_M | molar magnetic susceptibility |
| Z | atomic number |

Table of Contents

| | |
|--|-----|
| Chapter 1. Overview of Magnetism and Instrumental Methods..... | 14 |
| 1.1. Objectives..... | 14 |
| 1.2. Introduction..... | 14 |
| 1.3. Classical Magnetism..... | 17 |
| 1.4. Quantum Mechanical Origins of Magnetism | 23 |
| 1.5. Molecular Orbital Model of Exchange | 31 |
| 1.6. Single Molecule Magnetism | 35 |
| 1.7. Instrumental Methods | 56 |
| 1.7.1. UV-vis Spectroscopy | 56 |
| 1.7.2. Bulk Magnetic Susceptibility | 58 |
| 1.7.3. Alternating Current Magnetic Susceptibility..... | 59 |
| 1.7.4. References | 60 |
| Chapter 2. Synthesis and Characterization of 4-Coordinate Scorpionates for Single Molecule Magnetism..... | 83 |
| 2.1. Overview of 4-Coordinate Scorpionates..... | 83 |
| 2.2. Introduction to the Present Work | 88 |
| 2.3. Results and Discussion | 91 |
| 2.3.1. Synthesis..... | 91 |
| 2.3.2. Infrared Spectroscopy..... | 95 |
| 2.3.3. UV/vis/NIR Spectroscopy..... | 102 |
| 2.3.4. High Field Electron Paramagnetic Resonance Spectroscopy | 115 |
| 2.3.5. X-ray Structural Studies | 118 |
| 2.3.6. Magnetic Characterization | 133 |
| 2.4. Conclusions..... | 151 |
| 2.5. Experimental | 153 |

| | |
|--|-----|
| 2.6. References | 159 |
| Chapter 3. Chapter 3. Para-toluenesulfonates of Divalent First Row Transition Metals | 176 |
| 3.1. Introduction..... | 176 |
| 3.2. Results and Discussion | 181 |
| 3.2.1. Syntheses and Solubilities | 181 |
| 3.2.2. Infrared Spectroscopy..... | 182 |
| 3.2.3. UV-vis Spectroscopy | 185 |
| 3.2.4. Single Crystal X-Ray Diffraction Studies | 187 |
| 3.2.5. Bulk Magnetic Measurements..... | 200 |
| 3.3. Conclusions..... | 200 |
| 3.4. Experimental | 201 |
| 3.5. References | 206 |
| Chapter 4. Partially Completed Work..... | 216 |
| 4.1. Introduction..... | 216 |
| 4.2. Results and Discussion | 217 |
| 4.3. Conclusions..... | 230 |
| 4.4. Experimental | 231 |
| Chapter 5. Conclusions | 236 |
| 5.1. The Limitations of the Spin Hamiltonian Formalism in Single Molecule Magnetism | 236 |
| Appendix A. Supplemental Data for Chapter 2..... | 242 |
| Appendix B. Supplemental Data for Chapter 3..... | 287 |
| Appendix C. Supplemental Data for Chapter 4..... | 317 |

Chapter 1. Overview of Magnetism and Instrumental Methods

1.1. Objectives

The research undertaken in this dissertation was done with the objective of preparing and examining monometallic transition metal single molecule magnets. By preparing monometallic paramagnetic transition metal clusters, several benefits can be realized. These materials can readily be characterized by traditional chemistry methods, variables of magnetic behavior like spin-spin coupling and transverse magnetic anisotropy can be minimized or eliminated, and single molecule magnetism can be studied in simple systems that can later be incorporated into more complicated systems.²⁻³

1.2. Introduction

Before outlining the general principles of molecular magnetism, it is appropriate to justify the effort by briefly considering the uses of magnetic materials.

Magnetism, for all its unanswered questions, has been known to man since prehistoric times and plays a central role in modern technology, the often-scapegoated foundation of civilization itself.⁴⁻⁷ As we will see, magnetism also provided an impetus for the development of quantum mechanics, since it could not be described by classical approaches.⁸⁻¹¹ Current applications of magnetic materials include information storage, medicine, interconversion of mechanical and electrical energy in alternators, generators, relays, speakers, power

distribution, and communication equipment; ^{5, 12-14} as recently as 2000, the world market for magnetic materials exceeded that of semiconductors.⁴

Moreover, the economic benefits of miniaturization have driven much recent technological advancement in electronic devices, and this incentive is still present for magnetic materials.¹⁵⁻¹⁷ Currently, however, the superparamagnetic limit poses a barrier to further reductions in size of magnetic devices, particularly magnetic data storage.^{4, 14} This superparamagnetic limit is a minimum domain size ($r = 10 - 100$ nm at room temperature) at which a material still exhibits the superparamagnetism necessary for magnetic data storage. Below this size, the magnetization is overcome by thermal effects, and the recorded data is lost. Advances in engineering like perpendicular recording have led to moderately increased storage density, but a novel method for storage appears to be a longer-lasting answer to the superparamagnetic limit.¹⁸⁻²⁰

Single molecule magnets (SMMs) show promise as new magnetic materials to improve current devices or deliver new devices without classical counterparts through their novel properties.^{4, 12-13, 21-28} Information storage,^{13, 21} (nuclear) magnetic resonance imaging (MRI) contrast agents,¹² molecular spintronics,²⁶ quantum computing,^{23-24, 27-28} and magnetic refrigeration²² are some proposed applications. Since the remnant magnetization in SMMs arises from a different process than in superparamagnetism, the superparamagnetic limit does not apply and storage densities can approach a single molecule in size, an improvement of 3-4 orders of magnitude over commercial technologies.⁴ The origins of this remnant magnetization will be examined in greater detail in

section 1.4. For MRI contrast agents, spin relaxation in SMMs can be used to contrast MRI images to improve signal to noise ratios, relaxation rates, and reduce the use of more toxic elements like Gd.¹² Lastly, SMMs may be suitable materials for molecular spintronics, devices that use charge and spin to carry information in circuits.^{26, 29-31} As a single molecule can operate in this capacity, it may prove to be a large step in miniaturization and the combining of multiple functionalities into a single device.²⁶ It has been observed that some applications have yet to be envisioned as there are no classical analogies to SMMs so that entirely new devices and functionalities may be possible.²⁶

Already advances have been made not only in the development of materials but in their incorporation into devices.^{24, 28, 30-33} The readout of magnetic memory for a single Fe₄ SMM was reported in 2009, demonstrating that the SMM behavior was retained even when tethered to Au surfaces.²⁴ In 2012, Wernsdorfer et al. reported the electronic readout of a single nuclear spin in a Tb^{III} SMM.²⁸ Discrete states exhibited lifetimes on the order of tens of seconds, and the Kondo effect was observed. The Kondo effect is an anomalous scattering of conduction band electrons caused by magnetic impurities, in this case a single Tb^{III} complex. Molecular layers of an SMM have shown exchange bias, an important step towards spin valves.³⁰ Furthermore, this particular material is operative near room temperature, an important advance.

This optimistic picture of advances is tempered by current challenges to the creation of new SMMs and their incorporation in devices.^{4, 34-36} The design of SMMs is chemically challenging, and the predictive principles are not analogous

to other areas of chemistry.^{4, 34, 37-38} While quantum mechanical effects cause some of the useful properties of SMMs, quantum tunneling of the magnetization (QTM) undermines remnant magnetization in these materials.³⁷⁻³⁸ As the energy separations between states can be low, most SMMs are only 'operative' (exhibit zero field magnetization) at very low temperatures.³⁹⁻⁴⁰ Nevertheless, SMMs provide a route to improvement of current magnetic technology, new devices, and compounds to study the physics in the transition between single paramagnetic centers and extended structures.²²

As many have observed, there is a tendency for physicists and chemists to continue using cgs units in describing magnetic properties. In this work the SI system is used to follow the guidelines of the International Union for Pure and Applied Chemistry (IUPAC).¹

1.3. Classical Magnetism

The classical mechanics interpretation of magnetism models a bulk material interacting with a magnetic field and is described by continuous functions.^{8, 41-43} This model was developed to describe the experimental observations of macroscopic quantities of materials interacting with magnetic fields, so a consideration of phenomena at the molecular level is not intrinsically part of the treatment.⁴¹ However, the idea that a macroscopic paramagnetic insulator consists of magnetic moments associated with spatial points was often accepted in the classical treatment, and leads to the idea of a paramagnetic center. A paramagnetic center is simply an atom or collection of atoms with

significant unpaired spin density.⁴³ While this definition is not placed in chronological order, it is an assumption that underpins all modern treatments and much of the classical approach. All materials, when placed in an inhomogeneous magnetic field, experience a net attraction or repulsion to the stronger portion of the field.⁴² The repulsion is called diamagnetism and is exhibited by all materials, in the sense that the net interaction of a material will include a diamagnetic contribution. This arises when the applied field causes the paired electrons to move in their orbitals to create an opposing field, so that the magnetic field lines are directed away from the sample via Lenz's law. Since all stable compounds contain paired electrons, all materials exhibit this diamagnetism. If one or more unpaired electrons in a material align with the applied field, it concentrates magnetic flux lines through the material and results in paramagnetism.

Figure 1.1 provides a visualization of the interaction of diamagnetic and paramagnetic materials with a magnetic field.⁴² The sample material is represented by the circle in the center, with the squares standing for the north and south poles of magnets providing the field with which the sample interacts. Given that the paramagnetic spins give magnetic moments that are typically one to two orders of magnitude greater than diamagnetic contributions, both must be accounted for in real systems, and the paramagnetic contribution almost always overcomes the diamagnetic contribution.

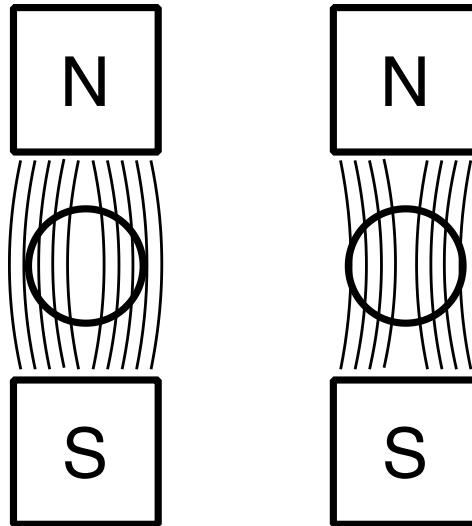


Figure 1.1. Left: Magnetic flux lines directed outside a diamagnetic material. Right: Magnetic flux lines concentrated in a paramagnetic material. Adapted from reference 42.

The magnetization \vec{M} is the magnetic moment per unit of volume, expressed in amperes per meter, $A\ m^{-1}$. \vec{H} is the magnetic field, also measured in $A\ m^{-1}$. \vec{B} is the induction or magnetic flux density acting on matter, measured in Tesla (T) or Gauss (G) ($1T = 10^4\ G$). The three are related by

$$\vec{B} = \mu_0(\vec{H} + \vec{M}) \quad \text{Equation 1.1}$$

At the weak field limit ($|\vec{H}| \ll k_B T$) the magnetization of a paramagnetic material is related to field strength by

$$\vec{M} = \chi \vec{H} \quad \text{Equation 1.2}$$

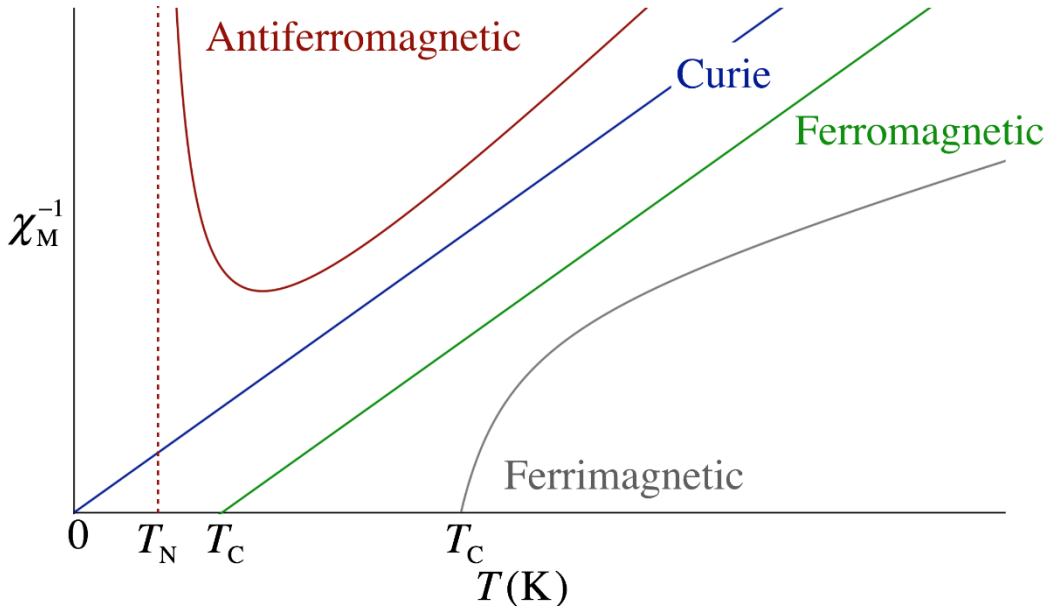


Figure 1.2. Reciprocal molar susceptibilities versus temperature for antiferromagnetic, paramagnetic (Curie), ferromagnetic, and ferrimagnetic materials. Adapted from 44.

where χ is magnetic susceptibility, a dimensionless constant for each material at a given temperature. At higher field strengths, the magnetization levels off to a constant and the material is said to be magnetically saturated.⁴⁴ Physically, the spins of the material are largely aligned with \vec{H} and since the number of spins is finite, the magnetization cannot increase to infinity. The constant χ can also be expressed on a per mole basis, χ_M . This magnetic susceptibility can be expressed as the sum of paramagnetic and diamagnetic contributions by the equation

$$\chi = \chi_{\text{diamagnetic}} + \chi_{\text{paramagnetic}} \tag{Equation 1.3}$$

which also holds for magnetic susceptibility on a per mole or per volume basis.⁴²

The temperature dependence of χ_M is described in the Curie-Weiss law,

$$\chi_M^{-1} = \frac{T - \theta}{C} \tag{Equation 1.4}$$

relating χ_M to θ and C , the Weiss and Curie constants respectively.^{42, 44} This relationship is empirical, and when plotted, curves of χ_M^{-1} versus T will yield the values for θ and C .^{7, 44} The deviations from linearity and the x-intercept provide additional information.

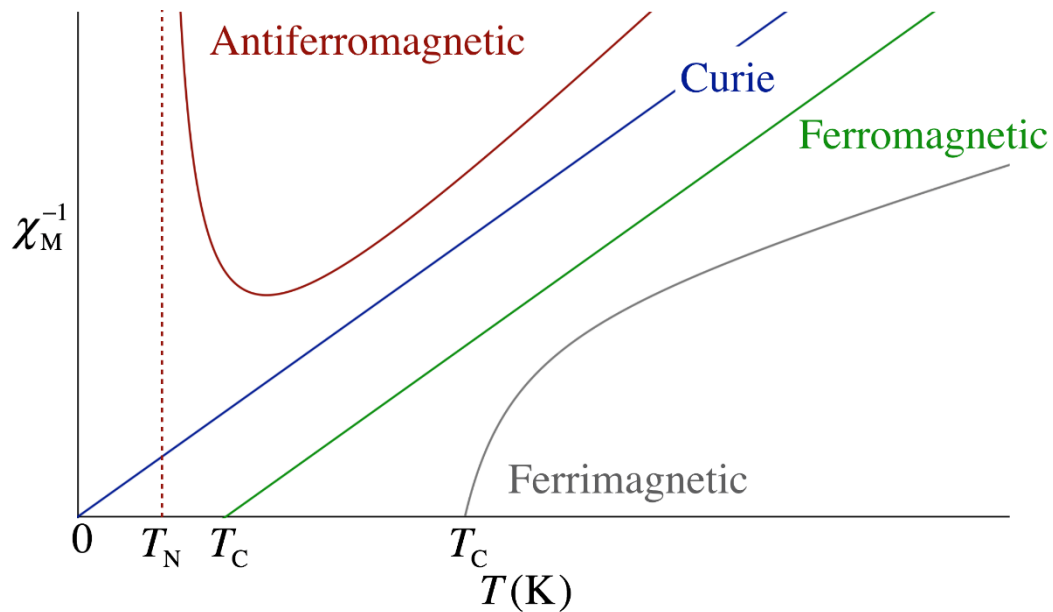


Figure 1.2 shows four hypothetical plots of typical results from this procedure. In the simplest case, a line passes through the origin of the graph and the material exhibits simple paramagnetism. If a line intercepts the x-axis at a value above zero, the material is ferromagnetic. In two instances the plots are curved, and the materials are then ferrimagnetic or antiferromagnetic. At higher temperatures, these two types exhibit roughly linear plots, but deviate at lower temperatures. For antiferromagnetic materials, the plot asymptotically approaches a value called the Néel temperature, T_N . For ferrimagnetic materials the plot exhibits a negative deviation and intercepts the x-axis at the critical temperature, T_C . More compactly,

$$\theta > 0 \Rightarrow \text{ferromagnetism} \quad \text{Equation 1.5}$$

$$\theta < 0 \Rightarrow \text{antiferromagnetism or ferrimagnetism.} \quad \text{Equation 1.6}$$

Combined, these plots show that at high temperatures all paramagnetic materials show a linear trace, but deviations from this behavior occur at low temperature, with the details differentiating the four classes of materials. For a ferromagnetic material, an interaction between paramagnetic centers leads to the maximum unpaired spin being the ground state. For an antiferromagnetic material, interaction between paramagnetic centers makes the spin-paired state the ground state where all electrons are paired. Ferrimagnetic materials also have a spin-paired state that is the ground state, but the pairing is incomplete, and a residual magnetic moment is present. The paramagnetic behavior at higher temperatures for all four types of materials led researchers to consider the origins of the effect as a competition between magnetic ordering of the materials and thermal disorder.

For a paramagnetic material where $|\vec{H}| \ll k_B T$, the paramagnetic component of the magnetic susceptibility (see Equation 1.3) is described by the Langevin equation,

$$\chi_{\text{paramagnetic}} = \mu_0 N_A \left(\frac{\mu^2}{3k_B T} \right) \quad \text{Equation 1.7}$$

where μ_0 is the permeability constant, μ is the magnetic moment of the atom, N_A is Avogadro's number, and k_B is Boltzmann's constant.⁴⁴ The diamagnetic contribution is described by the term

$$\chi_{\text{diamagnetic}} = -\frac{N_A e^2}{6m_e c^2} \sum_n \langle r_n \rangle^2 \quad \text{Equation 1.8}$$

where $\langle r_n \rangle$ is the radius of an atom, m_e is the mass of the electron, and the contribution is summed for all electrons on an atom.⁷ Equation 1.7 treats the magnetic moments of atoms as dipoles present in a lattice able to assume any orientation and undergo a disordering that is temperature-dependent, in line with the previous observation regarding the interplay of magnetic ordering and temperature. At high temperature, the denominator of Equation 1.7 becomes larger than the numerator and $\chi \rightarrow 0$. As the temperature approaches 0, $\chi \rightarrow \infty$, but in real systems χ approaches a constant value. In earlier work a constant, α , was included in the numerator and described "high frequency terms" which accounted for a temperature-independent contribution to the magnetic susceptibility.⁴³

While Equation 1.7 describes the linear range and the deviations can be attributed to interactions between the magnetic moments of the atoms, later work showed the Langevin treatment of magnetic susceptibility to be inadequate and in fact inconsistent.⁸⁻¹¹ Niels Bohr and Henrika van Leeuwen independently published work showing that "in a constant magnetic field and in thermal equilibrium the magnetization of an electron gas in the classical Drude-Lorentz model is identically zero."^{8-9, 11} In a classical statistical mechanics treatment, the application of an external field to the paramagnetic material would induce an opposing field on its surface. This opposing field would shield the remainder of the material from the external field, leading to no net magnetization. Bohr's report of this result has been referred to as "the most deflationary publication of all time in physics."⁷

1.4. Quantum Mechanical Origins of Magnetism

The failure of classical mechanics to describe magnetism in a self-consistent manner pushed workers towards a more complete description of the phenomenon.⁸ A step towards this was published by Van Vleck,⁴³ who described the magnetization of materials in a complementary method to that of Langevin.^{7,}
⁴³⁻⁴⁶ In the Van Vleck equation,

$$\chi_M = \frac{N_A \sum \left[\frac{(E_n^1)^2}{k_B T} - 2 \sum E_n^2 \right] \exp\left(-\frac{E_n^0}{k_B T}\right)}{\sum_n \exp\left(-\frac{E_n^0}{k_B T}\right)} \quad \text{Equation 1.9}$$

the resultant microstates (E_n^m) of a magnetic system are described instead of individual spins where N_A = Avogadro's number, k_B = Boltzmann constant, and T = temperature.⁴⁵ E_n^0 is the energy of a given level n in zero field, and E_n^1 and E_n^2 are the first and second Zeeman coefficients giving the energies dependent upon an applied field. These are populated by the familiar partition function, and a summation over all states is taken. This equation holds true for paramagnetic systems with no cooperativity between spins (magnetically dilute) and $|\vec{H}| \ll k_B T$.^{42, 44} The importance of the Van Vleck equation for magnetic susceptibility is that it was the first to provide a justification for the Curie law that incorporates Boltzmann statistics and quantum mechanics.⁸ In practice, the ground state or states are often sufficient to model the magnetic susceptibility of a material and if this fails, inclusion of excited states that are thermally accessible often remedies the problem. Next, the origin of the magnetic moments that lead to the observed microstates will be examined.

The magnetic moment of inorganic materials is derived mostly from contributions of electron spin and orbital angular momentum present on the metal ions.⁴¹ If the magnetic moment is solely attributable to electron spin, the Bose-Stoner formula for the magnetic moment in weak fields ($|\vec{H}| \ll k_B T$) holds,¹

$$\mu_{SO} = 2\sqrt{S(S+1)} \quad \text{Equation 1.10}$$

where

$$S = \sum_i |m_{s,i}| \quad \text{Equation 1.11}$$

and

$$\mu = \chi \vec{H} \quad \text{Equation 1.12}$$

for unpaired electrons on a paramagnetic center.⁴⁷⁻⁴⁹ Equation 1.11 describes the relationship between the spin of a paramagnetic center and the individual electron spins. The magnetic moment associated with a paramagnetic center is a vector, an important point when considering the mathematical treatment of magnetic systems. When orbital angular momentum and other effects begin to contribute to the magnetic properties of a material, a more thorough description becomes necessary. Prior to outlining the spin Hamiltonian approach to paramagnetism, it is appropriate to state the problem or conditions that are being met. This approach seeks to accurately describe bulk magnetic, atomic magnetic, and spectroscopic properties of paramagnetic insulators. It must also use discrete math or wave mechanical descriptions to reflect the quantum

¹ This formula is in accord with present sources, earlier papers often gave the formula as $\sqrt{4S(S+1)}$.

mechanical origins of magnetism. To do this, observables--i.e., values that can be directly measured via experiment--must be related to the quantum numbers describing the system and potentially additional constants that also describe the system. In this formalism, the system is the smallest unit that exhibits the complete magnetic properties of the material. Two sources of error can stem from a misunderstanding of this definition, the first being that in which a spin system is too small and interactions between parts are neglected. In the other, the spin system is defined as larger than it is. The latter often occurs in systems that are chemically linked but where the paramagnetic centers behave independently. As will be shown, the first error leads to poor modelling of the behavior, and the second to over-parameterization that accurately models the system but leaves parameters that are physically meaningless.

The electrons in a paramagnetic insulator can often be accurately described by the four quantum numbers $n, l, m_l,$ and m_s . If a paramagnetic material is an insulator, the electrons are localized or associated with a particular atom or atoms. Electron spin angular momentum has no classical analogy since the electron itself cannot spin, having no spatial dimension.⁴¹ The name spin results from the fact that in macroscopic systems, moving current gives rise to a magnetic field, and it was assumed a similar process created the magnetic moment of elementary particles. The spin of an electron $|m_s\rangle$ is described by the spin quantum number which has the allowed values of $\pm \frac{1}{2}$.^{41, 50} The magnetic moment $|\mu\rangle$ of an electron is related to $|m_s\rangle$ by

$$|\mu\rangle = -\frac{e^-}{m_e} |s\rangle \quad \text{Equation 1.13}$$

where

$$||s\rangle| = \frac{h}{4\pi} \quad \text{Equation 1.14}$$

From this the cancellation of the magnetic moment of two electrons in one orbital is apparent if they obey the Pauli exclusion principle. Since the two allowed values are fixed and of equal and opposite magnitude, the magnetic moments of the electrons cancel, and no magnetic moment is observed.

Orbital angular momentum $|m_l\rangle$ takes on the allowed values of $0 = s, 1 = p, 2 = d, \dots$ which result in the familiar shapes of the s, p, d, f, \dots orbital series. The impact of orbital angular momentum on the magnetic moment of an electron depends on its interaction with the electron spin through spin-orbit coupling (SOC).^{7, 41, 50-51} For lighter atoms SOC is a weak effect that can be treated as a perturbation via the Russell-Saunders coupling scheme.⁵² For the first and second row transition metals, SOC can be observed in susceptibility measurements as a small deviation from the spin-only value of μ_{eff} . One of the simplest ways SOC is quantified for transition metals is the Landé g value which is included in the Bose-Stoner equation

$$\mu_{\text{eff}} = g\sqrt{S(S+1)} \text{ (BM)} \quad \text{Equation 1.15}$$

and this Landé g is allowed to vary to match experimental data.⁴¹⁻⁴² This is a restatement of Equation 1.10 where the fixed value 2 becomes g and is allowed to vary. For a material with no SOC, $g = 2.0023$.^{41-42, 50} The deviation from 2.00 is a result of relativistic considerations first described by Dirac in 1928 but still represents only the spin contribution to the magnetic moment of an electron.⁵³ For heavier atoms, the coupling of spin and orbital angular momentum can no

longer be treated as a weak perturbation of the electron spin moment and the $j - j$ coupling scheme is used. Since it is not pertinent to the present work, it will not be examined in detail; it will merely be said that the spin and orbital angular momentum vectors are added to each other and the resulting vector, \vec{j} is used to complete calculation of the eigenstates in the spin Hamiltonian.

The Zeeman effect is the splitting of degenerate magnetic levels in a weak magnetic field.⁵⁴ For an energy level with a given spin, S , the degeneracy is $2S + 1$. These degenerate states, upon application of an external magnetic field \vec{H} , undergo Zeeman splitting to give $2S + 1$ states of energy determined by

$$\hat{H} = E_0 + \mu_B S g \vec{B} \quad \text{Equation 1.16}$$

where E_0 is the energy of the degenerate states in the absence of a magnetic field, and the difference in energy between adjacent states ($\Delta S = \pm 1$) is $\mu_B g \vec{B}$. In cases where SOC is present and the field is sufficiently strong, the spin and orbital momentum is decoupled, and the Paschen-Back effect that leads to further splitting is observed.⁵⁴⁻⁵⁸ It is mentioned for the sake of completeness but will not be considered here as the phenomenon is not observed in this work.

In some cases, a splitting of otherwise degenerate states can occur with no external magnetic field, and this is aptly named zero-field splitting (ZFS). The quantification of ZFS is complicated by often being an anisotropic phenomenon. The orientation of the material in a magnetic field for the measurement of electronic states in an EPR or electronic absorption experiment can influence the results. The Hamiltonian for ZFS is

$$\hat{H} = DS_z^2 + E(S_x^2 - S_y^2) \quad \text{Equation 1.17}$$

where S_x , S_y , and S_z are the projection of spin S in the Cartesian coordinate system, D is the axial component of the ZFS tensor, and E is the transverse component of the ZFS tensor. The ZFS tensor is real, symmetric, and describes the separation of $|\pm S\rangle$ eigenstates in the absence of a magnetic field and is related to the anisotropic projection of the spin in real space.⁴¹ In the case of cubic symmetry (O_h) $D = E = 0$ and for axial symmetry $E = 0$.³⁵ The symmetry refers to the environment of the unpaired electrons under consideration. For O_h complexes ZFS is not present or if seen, very weak. Axial complexes, those possessing a C_n axis, can show ZFS, that is, for Equation 1.17, $D \neq 0$ and $E = 0$. Small changes in the ligand field or symmetry can have an influence on the magnetic properties such that the typically minor distinction between pseudo- C_n and C_n becomes of great importance, as will be discussed in section 1.4. When $D < 0$, the anisotropy is called Ising anisotropy or easy axis anisotropy, and the ground state or states are ones that maximize the magnitude of the spin $|\pm S\rangle$.³⁴ Conversely, when $D > 0$, easy plane anisotropy is present and the ground state is $|S = 0, 1/2\rangle$.

Up to this point we have considered systems with unpaired electrons on one atom or set of atoms to form one paramagnetic center, but it is possible (and common) to have multiple paramagnetic centers that interact with each other to create a single spin system. The interaction between paramagnetic centers is termed "coupling" and described in the spin Hamiltonian formalism via the interaction term

$$\hat{H}_{\text{interaction}} = \sum_{i,j} -J_{ij}S_iS_j + S_iD_{ij}S_j + d_{ij}S_i \times S_j \quad \text{Equation 1.18}$$

which quantifies the isotropic, anisotropic, and antisymmetric exchange between paramagnetic centers, respectively.⁵⁹⁻⁶⁰ J_{ij} is the singlet-triplet energy gap, D_{ij} is the magnetic anisotropy tensor, and d_{ij} is the Dzialoshinski-Moriya vector. This third term is less familiar to most chemists but arises from SOC and results in the spin canting observed in some systems.⁶¹⁻⁶² Often the interaction between paramagnetic centers is modeled by considering only isotropic coupling,

$$\hat{H}_{\text{interaction}} = \sum_{i,j} -S_iJ_{ij}S_j \quad \text{Equation 1.19}$$

If we have a system with Ising-type anisotropy and nonzero spin ground states, it leads to the creation of a spin reversal energy barrier and a double well potential energy curve with $|\pm S\rangle$ maximized for each well, which differs from the other only by sign. Reversal of the magnetization must overcome an energy barrier of

$$U_{\text{eff}} \sim |D|S^2 \quad \text{Equation 1.20}$$

for integer systems and

$$U_{\text{eff}} \sim |D|S^2 - 1/4 \quad \text{Equation 1.21}$$

for half integer systems. The significance of Equation 1.20 and Equation 1.21 will be discussed further in section 1.4. Combining Equation 1.16, Equation 1.17, and Equation 1.19, we arrive at

$$\hat{H}_{\text{spin}} = [DS_z^2 + E(S_x^2 - S_y^2)] + \sum_{i,j} -S_iJ_{ij}S_j + \mu_B Sg\vec{B} \quad \text{Equation 1.22}$$

which is sufficient for understanding the basic properties of many SMMs.

Neglected from this Hamiltonian are terms for hyperfine coupling and the nuclear

Zeeman effect. These can have effects on the observed properties of SMMs and will be discussed further in section 1.4.

Figure 1.3 depicts the eigenstates for an $|M_s\rangle = 10$ SMM with the corresponding barrier to magnetization reversal in zero field. Allowed states within the wells are indicated by horizontal lines in a similar fashion to vibrational energy levels. When a magnetic field is applied, the Zeeman effect increases the splitting on one side and reduces the effect of ZFS on the other, so that the stabilized state can be populated at the expense of the other. When the field is switched off, the population imbalance is maintained and can only be overcome by a thermal redistribution (neglecting quantum tunneling effects, section 1.4).

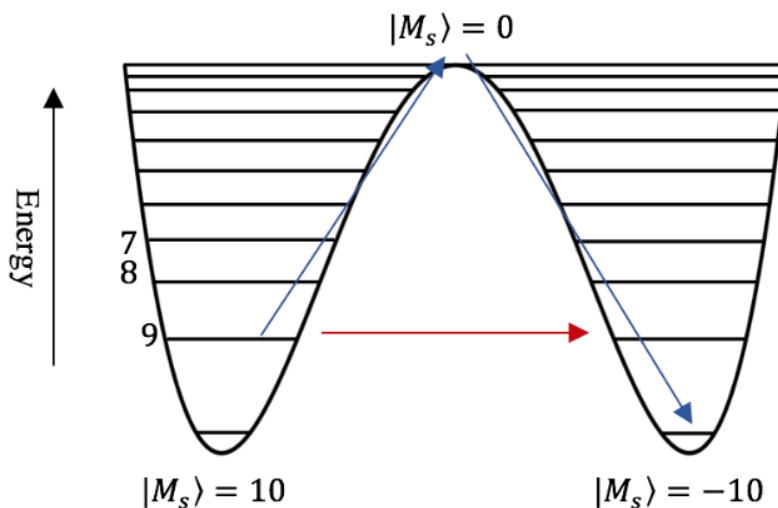


Figure 1.3. Eigenstates and relaxation processes for $[Mn_{12}O_{12}(O_2CMe)_{16}(H_2O)_4]$, an $S = 10$ SMM. The blue arrows indicate thermal processes and the red arrow QTM which can occur below U_{eff} . Reproduced from 4.

1.5. Molecular Orbital Model of Exchange

While the spin Hamiltonian approach is a useful route to interpretations of spectroscopic and magnetic data, it is insufficient to describe the mechanism by

which coupling, ZFS, and SOC occur. Using the concepts of molecular orbital (MO) theory, a description of magnetic exchange in molecules has been developed.⁵⁰ MO theory has several assumptions or features worth listing before a further discussion of the description of magnetic exchange. Metal complexes are ionic in the sense that charged species are combined to prepare them, but significant covalency is present in the resultant complexes.⁵⁰ MO theory assumes a covalent interaction between atoms. Bonding between metal and ligand is predominantly an interaction between the s orbital and ligand orbitals, with a smaller interaction between the metal p orbitals and the ligands due to a large energy mismatch. The d orbitals participate in bonding the least, although they have a significant role in magnetic properties.

According to MO theory, the stabilization of an electron in a molecule or ion is dependent on the overlap integral

$$\hat{S}_{\mu\nu} = \langle \chi_{\mu} | \chi_{\nu} \rangle \quad \text{Equation 1.23}$$

and exchange integral

$$\hat{H}_{\mu\nu} = \langle \chi_{\mu} | \hat{H}_{\text{eff}} | \chi_{\nu} \rangle \quad \text{Equation 1.24}$$

for two atomic orbitals χ_{μ} and χ_{ν} . \hat{H}_{eff} is the one electron Hamiltonian, which gives the energy values for the electron.⁶³ It is important to note that $\hat{S}_{\mu\nu}$ increases as orbital overlap increases and that $\hat{S}_{\mu\nu} = 0$ does not imply that $\hat{H}_{\mu\nu} = 0$. When $\hat{S}_{\mu\nu} \neq 0$, a molecular orbital made from a combination of atomic orbitals χ_{μ} and χ_{ν} is created, and this resultant orbital is then populated via the Pauli exclusion principle. If two electrons are present in this orbital, they must have

spins of $+\frac{1}{2}$ and $-\frac{1}{2}$ respectively. This stabilizes the singlet state as the spin momenta cancel out. For the exchange integral $\hat{H}_{\mu\nu}$, two electrons occupying atomic orbitals χ_{μ} and χ_{ν} can exchange with each other if they both have the same spin quantum number i.e. the spins are aligned. This stabilizes the triplet state. In most cases $\hat{S}_{\mu\nu}$ is significantly larger than $\hat{H}_{\mu\nu}$ so that the singlet state is stabilized, leading to the large singlet-triplet energy gaps observed in many compounds. However, the weaker bonding of transition metal complexes and the smaller overlaps between d and other orbitals leads to the smaller $\hat{H}_{\mu\nu}$ term taking on a larger role in determining the singlet and triplet energies, and in some cases favoring the triplet ground state. The interactions that lead to coupling are quantified by the value J which is the energy difference between the ground and excited states for two coupled spins. It can be decomposed as

$$J = J_F + J_{AF} \quad \text{Equation 1.25}$$

where $J_F > 0$ and $J_{AF} < 0$. In general, the $\hat{H}_{\mu\nu}$ term favors ferromagnetic coupling and the $\hat{S}_{\mu\nu}$ term favors antiferromagnetic coupling.

For the purposes of coupling between magnetic orbitals in first row transition metal complexes, two processes are observed, direct exchange and superexchange. Direct exchange coupling does not occur through mediating atoms between paramagnetic centers; rather, the magnetic orbitals themselves interact.^{41, 64} This depends on the symmetry of the interacting orbitals. The overlap integral typically decreases as it moves through the series of symmetric interactions σ , π , δ , to strict orthogonality (Figure 1.4). The overlap integrals decrease across the series, leading to a smaller antiferromagnetic contribution

while the ferromagnetic contribution from exchange decreases less rapidly, so that even when the overlap integral is zero a ferromagnetic interaction between the magnetic orbitals can exist. This is reflected in a trend from strong antiferromagnetic to weak ferromagnetic coupling (Figure 1.4). A well-known example of direct exchange occurs in bimetallic paddlewheel complexes where the formation of metal-metal bonds results in fewer unpaired electrons than in the individual metal ions.⁶⁵⁻⁶⁷

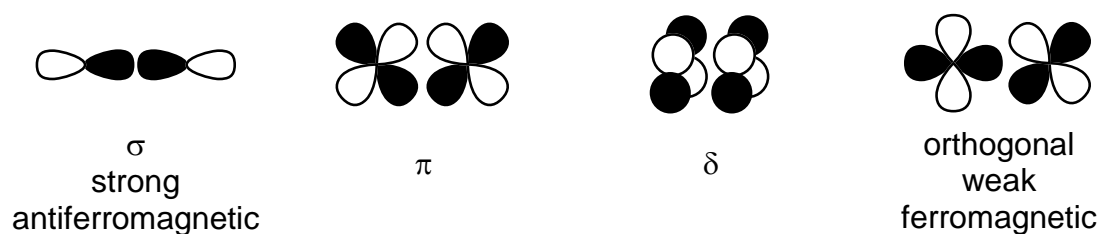


Figure 1.4. The role of orbital overlap symmetry in the direct exchange mechanism. From left to right the bonding interaction decreases to zero. Reproduced from 41.

Superexchange occurs when paramagnetic centers interact through nominally diamagnetic bridging atoms or ligands.^{41, 60} The most common cases of this are in systems with one or two bridging atoms between paramagnetic centers. Bridges with higher atom counts typically couple too weakly to be observed, and the paramagnetic centers instead behave as magnetically dilute, isolated atoms where no spin-spin interactions occur. For the purposes of the present work the discussion will focus on diatomic bridging ligands, especially cyanides. In superexchange through cyanides, σ and π interactions must be taken into consideration. Figure 1.5 A. depicts a right-handed coordinate system for a bimetallic species with a cyanide bridge. Lone pairs on the C and N termini act as σ donors to the metal centers A and B. Figure 1.5 B shows how an unshared electron on atom B can delocalize onto the ligand into an orbital with π symmetry and an unshared electron can delocalize onto the cyanide into an

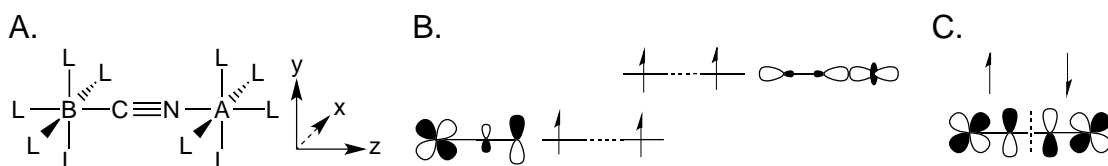


Figure 1.5. A. Coordinate system for two six coordinate metal ions bridged by a cyanide with C_{4v} symmetry. B. Superexchange in orthogonal orbitals across cyanide bridge leading to ferromagnetic coupling. C. Superexchange between orbitals with stronger overlap leading to antiferromagnetic coupling. Reproduced from 41.

orbital with σ symmetry. Since the two orbitals on the ligand are orthogonal $\hat{S}_{\mu\nu} = 0$ but the proximity of the two orbitals leads to $\hat{H}_{\mu\nu} \neq 0$ so that the two resulting MOs constructed from atomic orbitals (AOs) on the metal and ligand are populated via Hund's rules, i.e. with aligned spin. Figure 1.5 C shows the case where unpaired electrons interact via a common π^* orbital on the ligand leading

to spin pairing as two electrons in the same orbital cannot have the same spin. In many systems of interest these two schemes, direct exchange and superexchange, can be used to harness the power of MO theory to describe and even predict magnetic coupling in polymetallic systems.

1.6. Single Molecule Magnetism

From a physical standpoint, a SMM can be viewed as a molecular material that has unpaired electron spin that has preferred spatial orientations and exhibits magnetic hysteresis in an AC magnetic field.^{38, 68-70} The application of a magnetic field can orient the spins in one of the two preferred directions, and upon removal of the field this spin alignment can become disordered (relaxed). Relaxation from this metastable state can be accomplished by three routes: spin-lattice interactions, spin-spin-interactions, and quantum tunneling of the magnetization.³⁸ In recent work, spin-spin interactions are sometimes considered negligible in SMMs, explained by the distances between paramagnetic centers.⁷¹ Older literature discusses the possible effects of spin-spin interactions as non-negligible, and some workers chose magnetically dilute systems to avoid this problem.^{7, 72-74} The few recent papers examining this in SMM experiments have sometimes found significant interactions between spin centers perturbing relaxation dynamics.^{34, 75-77} The largest effect can be seen in zero field as well as bias fields that render two states degenerate, allowing the spin-spin transitions. In principle, interactions with nearest neighbors ultimately couple all the spin centers together, but in practice the couplings past the nearest neighbors drop in

strength and probability rendering all but the nearest neighbors irrelevant. Selection of a bias field that suppresses spin-spin interactions is also an effective strategy to examine the relaxation dynamics of an isolated spin center. For this work we will consider spin-lattice interactions and quantum tunneling of the magnetization as the dominant relaxation pathways. There are three spin-lattice interactions that we will consider: direct relaxation, the Raman process, and the Orbach process (Figure 1.6). The energies absorbed or emitted by a paramagnetic center to move between $|S\rangle$ states are small so the quanta for these transitions are absorbed or provided by the lattice as vibrational energy (phonons).

Quantum tunneling of the magnetization (QTM) occurs between degenerate $|S\rangle$ states whether they are degenerate in zero field or made degenerate by an applied magnetic field.³⁸ Since the $|S\rangle$ states are degenerate, total energy is conserved without the absorption or emission of a phonon so the process itself is unaffected by temperature. However, if multiple degenerate states exist, the tunneling probability between each can differ. The population of the states is dependent on temperature, and so the tunneling rate can be indirectly affected by temperature. Quantum tunneling of the magnetization

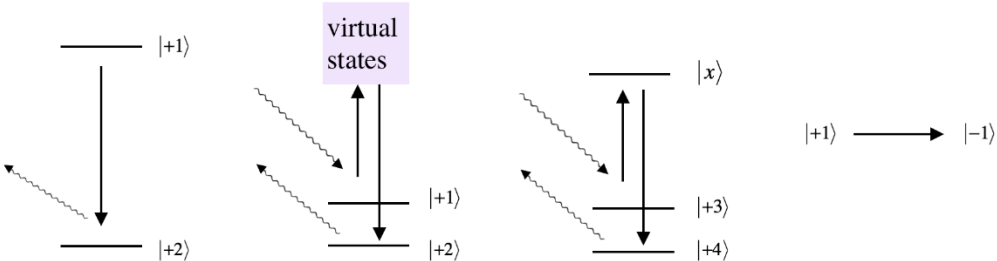


Figure 1.6. Schematic representation of A.) direct relaxation, B.) Raman process, C.) Orbach process, and D.) quantum tunneling of the magnetization.

(QTM) can occur at temperatures below those necessary to thermally overcome U_{eff} .^{38, 78} Macroscopic systems with two stable configurations assume one or the other, whereas in QTM the wave-like nature of the magnetic moment means that in the case of degenerate $| + S \rangle$ and $| - S \rangle$ states, the eigenfunction can take on non-zero values on both sides of the barrier. Consequently, in these cases there is a probability of finding either value upon measurement. This QTM allows for spin flipping below the thermal barrier, undermining the remnant magnetization even below U_{eff} , and is often a relevant process for the magnetic dynamics of SMMs. In SMMs, the rate of QTM is influenced not only by temperature but also by the eigenstates between which the tunneling occurs, which can be thermally populated below the barrier. Specifically, the probability of QTM increases in excited states compared to the ground state. Application of an external magnetic field breaks the degeneracy of the double wells, but QTM is still possible in the instance where two energy levels are the same in energy even if $| |S_i \rangle |$ values are not the same.³⁸

Direct relaxation is dropping from an excited state to a lower energy state with the emission of a phonon.^{72, 74} A paramagnetic center in an excited state will drop and the photon will be removed into the lattice, ultimately lost as thermal energy to the surroundings in the same way dark processes will conserve energy in the absorption of a photon. The direct process is linearly proportional to temperature.

Raman and Orbach processes are both two-phonon in nature.^{72, 74, 79-83} In each process, an excited state absorbs a phonon before emitting a phonon of

higher energy to relax to a lower state. These phonons consist of quantized energy transferring between the microstate of the magnetic center and the crystal lattice. The difference between the two is the lifetime of the second excited state. Raman processes are instantaneous, while the second excited state of the Orbach process has a measurable lifetime.⁷⁴

The overall relaxation rate as a function of temperature, as proposed by Scott and Jeffries and including terms for direct relaxation, tunneling, Raman, and Orbach mechanisms respectively is:

$$\tau^{-1} = AH^2T + \frac{B_1}{1 + B_2H^2} + CT^n + \tau_0^{-1} \exp\left(\frac{-U_{\text{eff}}}{k_B T}\right) \quad \text{Equation 1.26}$$

where A , B_1 , B_2 , and C are parametric terms fitted from data, τ_0^{-1} is the pre-exponential term from Orbach relaxation, H is field strength, k_B is the Boltzmann constant, and T is the temperature.^{70, 72} For a Kramers ion, $n = 9$ and for a non-Kramers ion $n = 7$ although the validity of this has been questioned. Some workers opt to fit the data with n as a variable and often find lower values to provide a better fit.^{70, 84-86} Often the numerous terms are found by fitting data which risks over-parameterization, yet they do describe valid, observable processes which undermine the remnant magnetization of SMMs.^{38, 70, 74}

According to early approaches to modeling spin-lattice interactions, a paramagnetic crystalline material can be modeled as a collection of paramagnetic centers. These paramagnetic centers in a crystal are canonical ensembles in thermal equilibrium with a heat bath such that Boltzmann statistics can model the thermodynamics of the system.⁸⁷ In other words, each paramagnetic center has ground and excited states. In order to conserve

energy, any transition from an excited state to the ground state must be accompanied by an increase of thermal energy. The initial assumption was that this energy is transferred to vibrations of the lattice (the phonon system) and this phonon system is strongly coupled to the bath so that the temperature of the lattice and the bath are identical. This assumption is not necessarily valid, however, and leads to the discrepancy between the above-described Waller model and its derivatives and observation.^{74, 87-89} Given the extremely low temperatures at which these magnetic measurements are made, certain peculiarities cause the Waller model to be insufficient to explain the relaxation times of SMMs at lower temperatures. Figure 1.7 depicts the plot of phonon mode density of states as a function of phonon mode energy. At low energies (and by extension, at low temperatures) the density of phonon states obeys a cubic relationship to energy up to the Debye temperature (dashed line).⁹⁰ Above this phonon energy value, the density of states breaks from ideal behavior. For some SMMs the relaxation rate deviates from prediction to a slower value.

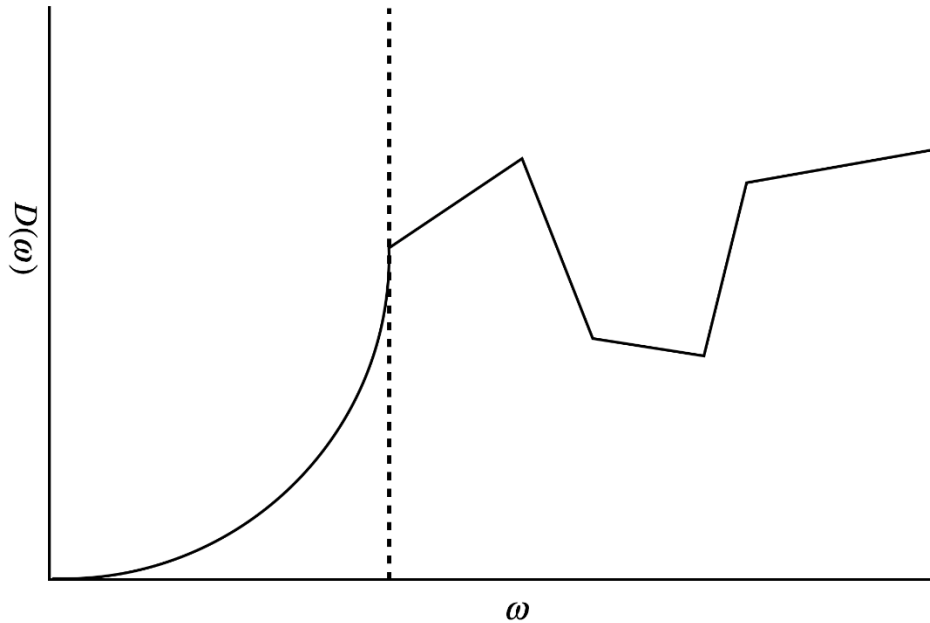


Figure 1.7. A qualitative plot of phonon mode density of states as a function of phonon mode energy for a non-conducting solid. Adapted from reference 90.

This is the observation that led to improved models at extremely low temperature, which account for Raman and Orbach relaxation, and specifically the deviations observed to a lower value. An individual paramagnetic center or spin interacts with the lattice through the spin-lattice interactions. The lattice then interacts with the thermal bath. The initial assumption was that the thermal bath is always of the same temperature as the lattice, that any excess energy in the lattice is immediately absorbed into the bath. This assumption is incorrect and leads to the eventual failure of Waller's model.

The energy differences between ground and excited spin states for a paramagnetic center are small, especially in comparison to most phonon modes in a lattice. According to Debye theory, the phonon modes are not distributed evenly in energy.⁹⁰ At lower temperatures the density of phonon states obeys a power law such that the number of low energy phonons in a lattice are small. The

number of spin centers can be greater than this number of low energy phonon modes so that relaxation of the spin centers can saturate the available low energy phonon modes if the probability of lattice-bath energy transfer is less than the probability of spin-lattice interaction.^{72, 74, 81} If true, this populates a few excited phonon states in the lattice and creates a deviation from the Boltzmann distribution. Further relaxation of spin centers is dependent on the transfer of energy from these phonon modes to the thermal bath. This slows the relaxation rate and is referred to as the phonon bottleneck.

For the Orbach process, a transfer of energy from the lattice to the spin center moves the spin center to a higher energy state from which it can relax to the ground state.⁷⁴ This is advantageous for faster relaxation. By including the small energy difference between the two states into a larger emitted phonon, the resultant lattice vibration will fall in a region of the phonon spectrum that is more dense.⁹¹ The increased density of states increases the heat capacity and sometimes avoids the bottleneck. Since the Orbach process accesses a specific phonon mode, a bottleneck can still be observed when this mode becomes saturated, again, if the probability of lattice-bath interaction is lower than spin-lattice interaction. As the temperature of the sample increases, more excited states become accessible so that the bottleneck is avoided by distributing energy into multiple phonon modes.

The Raman process is a more general case of the Orbach process where wide bands of phonon modes instead of specific phonons are accessed. This requires a greater lattice temperature to reach sufficiently dense states, but once

it has occurred the heat capacity of these bands is far greater than that of all the paramagnetic centers and no bottleneck is typically observed. It is important to note the strong temperature dependence of the Raman and Orbach processes. These two spin-lattice interactions are effectively gated by thermal energy in the lattice as a threshold temperature must be met to provide the phonons necessary for accessing the excited states necessary for emission and relaxation to the ground state.

Having discussed interactions between the spin and lattice, we now turn to the interaction of the lattice with the thermal bath. In the classic thermodynamics treatment, the efficient transfer of heat between a system and its surroundings is assumed, which in the case of magnetic systems at very low temperatures is not always the case. This point was raised in earlier work where it was observed that the frequency of phonon transfer to the heat bath can be lower than that of the spin-lattice interactions.^{72, 74, 91} The resistance to the transfer of energy from a lattice to a thermal bath (thermal transfer resistance) depends on the surface of the interfacing materials as well as the speed of sound in the materials.⁹²⁻⁹⁴ A large mismatch in the speed of sound leads to internal reflections of phonons in much the same way a large difference in refractive indices leads to internal reflection of light.⁹² This suggests that material preparation and the interface through which low temperatures are maintained may have a strong influence on the magnetic relaxation dynamics.⁹⁴

In consideration of the relaxation pathways described above, the ideal SMM would have an isolated ground state well-separated from excited states

and no transverse anisotropy ($E = 0$). The isolated ground state prevents Orbach and Raman relaxation and $E = 0$ suppresses QTM.⁷⁰

The above-mentioned ZFS term describes a further splitting of the microstates for a paramagnetic system and is dependent upon coupling of spin and orbital angular momentum, leading to a deviation of the magnetic moment from the spin-only value.⁹⁵⁻⁹⁷ The two relevant contributions to this splitting are referred to as first- and second-order, first-order being in-state mixing and second-order out-of-state.⁹⁸ First-order contributions arise from spin-orbit coupling that occurs in the ground state. In order for this to occur, two orbitals with angular momentum $m_l \neq 0$ and related by a rotation axis must be degenerate and partially occupied so as to generate an E or T state (**Error! Not a valid bookmark self-reference..A, B**).³⁵ The electronic configuration in **Error! Not a valid bookmark self-reference..A** is a T state, which would have first-order contributions to spin-orbit coupling. Typically, Jahn-Teller distortions will undermine first order SOC in SMMs.⁹⁹ One exception is a group of structurally-related linear monometallic Fe complexes reported by Long et al. where the linear two coordinate geometry precludes any Jahn-Teller distortions.^{23, 70, 100-101}

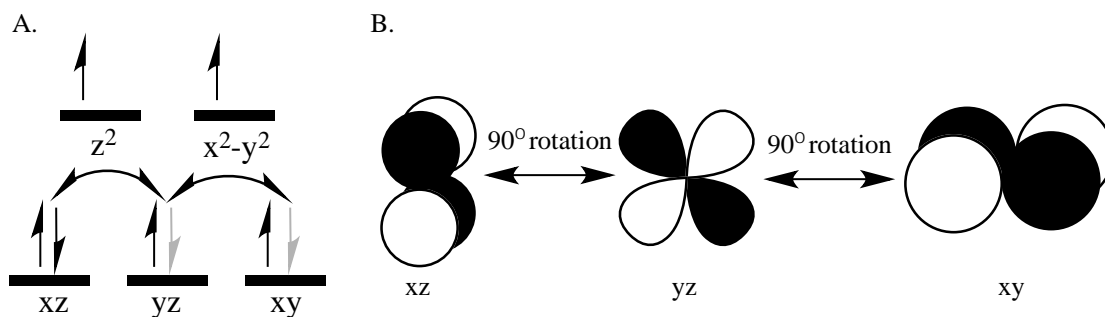


Figure 1.8. A. High spin d^6 configuration in octahedral symmetry giving rise to a 5T state. B. The xz , yz , and xy orbitals related by rotation.

Second-order spin-orbit coupling arises when a low-lying excited state of the appropriate symmetry mixes with the ground state.¹⁰² Spin-orbit coupling will then become active, and is typically manifested in a deviation of the Landé g from 2.00023. Previous work has demonstrated the impact of second-order spin-orbit coupling on ZFS, namely that it can increase SOC sufficiently to deviate g from the spin-only value.¹⁰³ Spin-orbit coupling also undermines spin selection rules by rendering the quantum numbers of ground and excited states less well-defined.⁵⁰ This allows spin-forbidden transitions to states which can also contribute angular momentum.³⁵ Regardless of whether SOC is first or second order, the result is a radially asymmetric magnetic susceptibility of the complex, e.g. magnetic anisotropy.¹⁰⁴

Given the numerous factors that influence single molecule magnetism, it is not surprising that there are multiple approaches to preparing these materials that are being actively pursued.^{2, 25, 35, 85, 105-118} Among the more extreme of these approaches, there are efforts to maximize S or D , while others attempt to optimize both in small nuclearity clusters. Perhaps the best-known examples of approaches to maximizing S are the Mn_{12} polymetallic complexes.^{2, 114-115} Other high-spin approaches are the development of single-chain magnets and large combinations of $3d$ and $4f$ metals in polynuclear clusters.^{109, 116-118} In these clusters and chains, the large S value is intended to contribute to U_{eff} via Equation 1.20 and Equation 1.21.

In single-chain magnets, an additional term to the energy barrier to magnetization reversal is included.^{109, 116-117, 119} The spontaneous spin-flip of one link in the chain creates two domain walls in the chain, one on either side of the flipped link.¹⁰⁹ Depending on the strength of the coupling between adjacent metal centers, this effect can be quite strong. For mixtures of $3d$ and $4f$ ions, the $4f$ ions are intended to contribute the majority of the magnetic anisotropy through their substantial SOC.⁵⁰ Between $4f$ ions, spin-spin coupling is typically weak so $3d$ ions are included as linkers between these $4f$ ions, which couples them more effectively, allowing greater communication of spin alignment between the $4f$ metal centers.¹¹⁸

The alignment of magnetic anisotropy vectors in $[(Tp^R)M^n(CN)_3]^{n-4}$ complexes is important in controlling uniaxial magnetic anisotropy and consequently, blocking temperature in polynuclear clusters.¹⁰⁴ The conjectured anisotropy tensor is aligned with the principal rotation axis in these complexes so that preparation of multi-metallic clusters with close alignment of these axes affords an enhancement of the magnetization reversal barrier. A 2011 report by Holmes et al. demonstrated this principle in the case of two SMMs where differences in the spin ground states and nuclearity gave similar blocking temperatures, attributed to the larger magnitude of the D term (-1.1 vs. -0.5 cm⁻¹).¹⁰⁴ This is in accord with a growing body of theoretical work and experimental evidence that emphasizes the role of D in determining the blocking temperature, undermining the viewpoint that solely increasing S is paramount.^{35-36, 120}

Motivated by the above-mentioned relationships of S and D to U_{eff} , (Equation 1.20 and Equation 1.21) workers have endeavored to maximize the magnitude of S . As an example, Murugesu et al. reported the synthesis and characterization of $[\text{Mn}_{25}\text{O}_{18}(\text{OH}_2)(\text{N}_3)_{12}(\text{pdm})_6(\text{pdmH})_6](\text{Cl})_2 \cdot 12\text{MeCN}$.¹⁰⁸ It was anticipated to have a substantial thermal barrier to magnetization reversal. Subsequent analysis found $D = -0.022 \text{ cm}^{-1}$ and a thermal barrier of 8.3 cm^{-1} . This illustrates the trend that in large clusters, ZFS tends to be small or stabilize $m_s = 0$ states, that coupling between multiple metal centers is sensitive to small changes in bond angles, that super-exchange in better-known bridging ligands tends to be weak, and that excited states are frequently only a few wavenumbers higher in energy than the ground state.^{35-36, 40, 121} Additionally, QTM can also be operative, leading to complexes with no out-of-phase magnetic susceptibility in the absence of a magnetic bias field.³⁸ These effects in various permutations often cause the temperatures at which SMM behavior is observed to be below liquid nitrogen temperature, since thermal energy readily overcomes the low U_{eff} and QTM is rampant. Furthermore, temperature control is of no avail in preventing quantum tunneling processes. Instead, the local field must break the degeneracy of spin states or the transverse magnetic field must be zero, as the admixing of states allows tunneling. Because of these challenges, effort could be put towards controlling the sign and magnitude of D .³⁵⁻³⁶ In the ZFS tensor magnitude and direction both play a role. Often in large spin systems misalignment of ZFS tensors for the building blocks cancels most of the effect, leading to a small U_{eff} .¹⁰⁴

For transition metals, this approach entails the use of rigid ligands or those with high steric demand to prepare complexes of reduced coordination numbers, as well as axial symmetry.^{70, 100, 122} This aims to render the ground state well separated from excited states, minimize intermolecular interactions, and (for transition metals) to increase orbital contributions to the magnetic moment.¹²³ This also increases the ZFS for these complexes by allowing for first or second order SOC and relaxing selection rules that allow more states to contribute angular momentum to the magnetic anisotropy^{35, 124} The first report of a monometallic transition metal SMM was $K[(\text{tpa}^{\text{Mes}})\text{Fe}]$ (tpa^{Mes} = tris((5-mesitylpyrrol-2-yl)methyl)amine) in 2010 by Long, featuring a tetradentate N coordination environment.¹²² The ZFS for this complex is almost 40 cm^{-1} .¹²² Since then others have been reported, including a series of two coordinate linear Fe(II) complexes.^{3, 70, 125-126} In these complexes, the low coordination number and symmetry of the ligand field lead to orbital degeneracies and significant SOC arising from the $^5\Delta$ ground state and relaxed selection rules for electronic transitions.⁷⁰

Since the first published example of a $3d$ monometallic transition metal SMM in 2010,¹²² work has focused on increasing the number of known compounds in this category and understanding their design and properties. The coordination number, geometry, and metal identity have all been varied in an effort to increase D and U_{eff} .^{3, 70, 76, 84, 101, 122, 125-135} Theoretical studies and other experiments have sought to elucidate structure/activity relationships.^{3, 23, 35, 120, 132,}

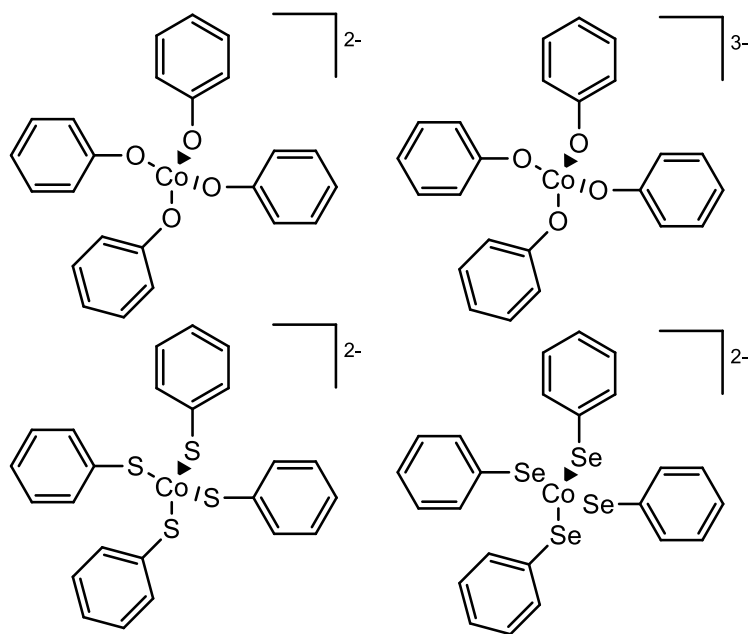


Figure 1.9. Structures of $(\text{Ph}_4\text{P})_2[\text{Co}(\text{OPh})_4] \cdot (\text{CH}_3\text{CN})$ (top left), $\text{K}(\text{Ph}_4\text{P})[\text{Co}(\text{OPh})_4]$ (top right), $(\text{Ph}_4\text{P})_2[\text{Co}(\text{SPh})_4]$ (bottom left), and $(\text{Ph}_4\text{P})_2[\text{Co}(\text{SePh})_4]$ (bottom right).

Cobalt complexes have also proven to be viable candidates for SMM behavior (**Error! Reference source not found.**). Most reported Co single molecule magnets have tetrahedral or distorted tetrahedral coordination geometries.^{76, 84, 125, 128, 130, 132, 140-141} These fall into pseudo C_3 or D_2 space groups.^{76, 84, 128, 132, 140-141} Examples of other geometries and higher coordination numbers are known, but the present discussion will be limited to the four-coordinate case as this is most relevant.^{140, 142} One series of related complexes consists of homoleptic distorted tetrahedral Co^{II} compounds $((\text{Ph}_4\text{P})_2[\text{Co}(\text{OPh})_4] \cdot (\text{CH}_3\text{CN})$, $\text{K}(\text{Ph}_4\text{P})[\text{Co}(\text{OPh})_4]$, $(\text{Ph}_4\text{P})_2[\text{Co}(\text{SPh})_4]$, $(\text{Ph}_4\text{P})_2[\text{Co}(\text{SePh})_4]$) (Figure 1.9).¹²⁵ These complexes have a local D_{2d} or pseudo D_{2d} symmetry at the metal center. All have easy axis magnetic anisotropy, which creates barriers to magnetization reversal. Three of the compounds show zero

field remnant magnetization. The alteration of the coordinating atom through the series O, S, Se has an impact, increasing the magnitude of the ZFS. In contrast, the observed blocking temperatures do not show the same consistent trend, highlighting the limitations of D in determining SMM dynamics.

$K(\text{Ph}_4\text{P})[\text{Co}(\text{OPh})_4]$ shows a strong curvature in the Arrhenius plot, suggesting that intermolecular interactions are operative in magnetic relaxation throughout the temperature range investigated.¹²⁵ Regardless, the impact of heavier atoms and increased covalency on ZFS is demonstrated in this series of compounds.

Carl et al. report a compound, $\text{Co}\{(\text{NtBu})_3\text{SMe}\}_2$, which exhibits a similar $[\text{N}_4]$ environment imposed by two bidentate ligands.¹⁴³ Thermally assisted relaxation of the magnetization is observed at about 10 K, but below this temperature QTM becomes the dominant relaxation pathway. Experiments were conducted to show hysteresis exhibiting the characteristic sigmoidal lineshape. Inclusion of a Raman term was necessary to fit the magnetic data and suggests that mixing of the $|\pm 3/2\rangle$ and $|\pm 1/2\rangle$ states is occurring. $(\text{HNEt}_3)_2[\text{Co}(\text{L}1)_2]$ also exhibits slow relaxation in zero field.⁸⁴ However, the ligand field appears to suppress Raman relaxation to a greater extent, giving a higher blocking temperature.

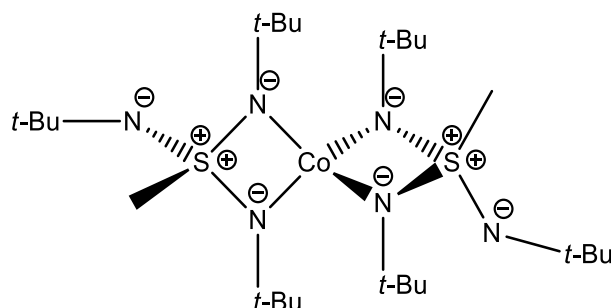


Figure 1.10. Structure of $\text{Co}\{(\text{NtBu})_3\text{SMe}\}_2$. The charge assignments are adapted from 143.

[Co(LBr)₂], [Co(LPh)₂], [Co^{II}(L2)₂], [Co(L3)₂], and [Co(hpbdti)₂] all contain a Co^{II} ion coordinated in a [N₂O₂] environment with the ligands creating distortions away from the angles expected for purely tetrahedral bonds.¹⁴⁴ For [Co(LBr)₂] and [Co(LPh)₂], Arrhenius plots are linear down to 4 and 3 K respectively,¹⁴⁴ below which QTM is the dominant relaxation pathway. [Co^{II}(L2)₂] and [Co(L3)₂] have linear Arrhenius plots down to ca. 6.5 K,¹⁴⁵ with QTM being the dominant process below this range. Magnetic characterization of [Co(hpbdti)₂] reveals the existence of two relaxation modes in the range 2.5-5.2 K, which is confirmed by Argand plots.¹⁴⁶ Argand plots are discussed in Section 1.5 AC Magnetic Susceptibility. At higher temperatures, a single relaxation pathway is observed. The multiple relaxation pathways at lower temperatures were ascribed to the non-collinearity of magnetic anisotropy vectors at low temperature. The formation of dimers in the crystal structure through hydrogen bonds and π - π interactions is proposed to occur. These types of close contacts are often considered responsible for dipole-mediated QTM, but the three different relaxation modes can be fitted as Orbach processes.^{144, 146}

The next structural type to consider are 4-coordinate complexes with two N, P, or As atoms and two halogen or pseudo-halogens coordinated in a cis fashion.^{25, 76, 128, 141, 144, 147} While the bond angles are reminiscent of distorted tetrahedral complexes, they are in fact closer to C₂ because of the different ligands present. None of these complexes ([Co(dmph)CoBr₂], [Co(biq)Cl₂],

[Co(biq)Br₂], [Co(biq)I₂], [Co(bzi)₂(NSC)₂], [Co(PPh₃)₂Cl₂], [Co(DPEphos)Cl₂], [Co(Xantphos)Cl₂], [Co(PPh₃)₂Br₂], [Co(PPh₃)₂I₂], or [Co(AsPh₃)₂I₂]) exhibit zero field remnant magnetization.^{25, 76, 128, 141, 144, 147} In some cases, incorporation of heavier coordinating atoms increases the ZFS ([Co(PPh₃)₂Br₂], [Co(PPh₃)₂I₂], or [Co(AsPh₃)₂I₂]), but this is not always the case (see [Co(biq)Cl₂], [Co(biq)Br₂], and [Co(biq)I₂]).^{128, 141} [(dmph)CoBr₂], [Co(biq)Cl₂], [Co(biq)Br₂], and [Co(biq)I₂] exhibit easy axis magnetic anisotropy.^{25, 76} Application of a DC bias field allows for the observation of SMM behavior, yet there is not a clear relationship between ZFS and U_{eff} . For [Co(biq)I₂], fitting of the magnetic data arrives at $E = 4.1 \text{ cm}^{-1}$ which may be allowing for QTM that leads to faster relaxation.²⁵ [(L3)CoCl](CF₃SO₃) is the sole member of the C₃ structural family for Co^{II}, with easy axis magnetic anisotropy and a putative phonon bottleneck that allows for observation of out-of-phase magnetic susceptibility.¹³⁰ The three compounds reported by Eichöfer, [Li(15-crown-5)] [Co{N(SiMe₃)₂}₃], [Co{N(SiMe₃)₂}₂(thf)], and [Co{N(SiMe₃)₂}₂(PCy₃)], are a few degrees from trigonal planar and possess easy axis magnetic anisotropy.¹⁴⁸ Calculations indicate that excited state mixing must introduce most of the SOC as the ground states are all $L = 0$. The last series, [Co(L4)(Cl)₂(MeCN)], [Co(L4)(Br)₂(MeCN)], [Co(L5)(Cl)₂(MeCN)], and [Co(L5)(Br)₂(MeCN)], are four-coordinate complexes with low symmetry from the inclusion of three different ligands. Switching from O to S atoms on the tetrazolium ligand appears to change the sign of D , moving from positive values for [Co(L4)(Cl)₂(MeCN)] and [Co(L4)(Br)₂(MeCN)] to negative values for [Co(L5)(Cl)₂(MeCN)] and [Co(L5)(Br)₂(MeCN)].¹⁴⁹

With a greater number of examples some conclusions can be drawn that the limited number of Fe examples does not provide. There are several examples ((HNEt₃)₂[Co(L1)₂], [Co(LBr)₂], [Co(LPh)₂], [Co^{II}(L2)₂], [Co(hpbdti)₂], [Co(L4)(Cl)₂(MeCN)], and [Co(L4)(Br)₂(MeCN)]) with $D > 0$ that exhibit remnant magnetization, the origin of which is unclear but has been ascribed to the phonon bottleneck.^{25, 76, 130} The use of heavier atoms in the ligands appears to often increase the magnitude of D as well as change the magnetic anisotropy of the spin systems to easy axis versus easy plane. Lastly, it is worth noting that the estimated U_{eff} values found from D are not necessarily accurate, demonstrated particularly well by [Co(AsPh₃)₂]₂ and [(L3)CoCl](CF₃SO₃), indicating the role of multiple relaxation pathways.

Table 1.1. Magnetic and structural data for low coordinate monometallic Co single molecule magnets. Reproduced from 144.

| Compound | D (cm ⁻¹) | U_{eff} (cm ⁻¹) | τ_0 (s) | ref |
|--|-------------------------|---|------------------------|-----|
| (Ph ₄ P) ₂ [Co(OPh) ₄](CH ₃ CN) | -11.1 | 21 | 7.0x10 ⁻¹⁰ | 125 |
| K(Ph ₄ P)[Co(OPh) ₄] | -23.8 | - | - | 125 |
| (Ph ₄ P) ₂ [Co(SPh) ₄] | -62 | 19 | 1.0x10 ⁻⁶ | 125 |
| (Ph ₄ P) ₂ [Co(SePh) ₄] | -83 | 34 | 3x10 ⁻⁶ | 125 |
| Co{(NtBu) ₃ SMe} ₂ | -58 | 75 | 2.64x10 ⁻⁸ | 143 |
| (HNEt ₃) ₂ [Co(L1) ₂] ^a | -115 | 118 | 3.89x10 ⁻⁸ | 84 |
| [Co(LBr) ₂] ^b | -36.7 | 36 | 5.6x10 ⁻¹⁰ | 144 |
| [Co(LPh) ₂] ^c | -39.8 | 43 | 8.4x10 ⁻¹⁰ | 144 |
| [Co ^{II} (L2) ₂] ^d | ±31 | 62 | 1.0x10 ⁻¹⁰ | 145 |
| [Co(L3) ₂] ^e | ±22 | 44 | 2.6x10 ⁻⁹ | 145 |
| [Co(hpbdti) ₂] ^f | not reported | 39.4 | 1.3x10 ⁻⁸ | 146 |
| [(dmph)CoBr ₂] ^g | +10.6 | 22.9 | 3.7x10 ⁻¹⁰ | 76 |
| [Co(biq)Cl ₂] ^h | +10.5 | 29.6 | 1.9x10 ⁻¹⁰ | 25 |
| [Co(biq)Br ₂] ^h | +12.5 | 27.5 | 1.2x10 ⁻¹⁰ | 25 |
| [Co(biq)I ₂] ^h | +10.3 | 39.6 | 3.2x10 ⁻¹³ | 25 |
| [Co(bzi) ₂ (NSC) ₂] ⁱ | -10.1 | 14.7 | 1.86x10 ⁻⁸ | 150 |
| [Co(PPh ₃) ₂ Cl ₂] | -14 | 25.8 | 1.2x10 ⁻⁹ | 147 |
| [Co(DPEphos)Cl ₂] ^j | -14.4 | 24.3 | 2.1x10 ⁻¹⁰ | 147 |
| [Co(Xantphos)Cl ₂] ^k | -15.4 | 20.8 | 6.0x10 ⁻⁹ | 147 |
| [Co(PPh ₃) ₂ Br ₂] | -12.5 | 25.9 | 9.44x10 ⁻¹¹ | 128 |
| [Co(PPh ₃) ₂ I ₂] | -36.9 | 21.3 | 4.65x10 ⁻¹⁰ | 141 |

| | | | | |
|--|--------|------|-----------------------|-----|
| [Co(AsPh ₃) ₂ l ₂] | -74.7 | 22.7 | 1.5x10 ⁻⁸ | 141 |
| [(L3)CoCl](CF ₃ SO ₃) ^m | +12.7 | 24 | 1.9x10 ⁻¹⁰ | 130 |
| [Li(15-crown-5)] [Co{N(SiMe ₃) ₂ } ₃] | -57 | 16.1 | 3.5x10 ⁻⁷ | 148 |
| [Co{N(SiMe ₃) ₂ } ₂ (thf)] | -72 | 18.1 | 9.3x10 ⁻⁸ | 148 |
| [Co{N(SiMe ₃) ₂ } ₂ (PCy ₃)] | -82 | 19.1 | 3.0x10 ⁻⁷ | 148 |
| [Co(L4)(Cl) ₂ (MeCN)] ⁿ | +15.61 | 10.3 | 7.68x10 ⁻⁷ | 149 |
| [Co(L4)(Br) ₂ (MeCN)] ⁿ | +11.16 | 8.2 | 8.39x10 ⁻⁷ | 149 |
| [Co(L5)(Cl) ₂ (MeCN)] ^p | -11.30 | 20.2 | 1.49x10 ⁻⁹ | 149 |
| [Co(L5)(Br) ₂ (MeCN)] ^p | -10.32 | 13.8 | 8.12x10 ⁻⁸ | 149 |

In the case of Ni, at least two compounds relevant to SMMs have been reported.^{135, 151} K{Ni(N[CH₂C(O)NC(CH₃)₃]₃)} was found to have $D = -200 \text{ cm}^{-1}$ but shows no out-of-phase susceptibility even under a DC bias magnetic field.¹³⁵ The origins of the lack of a barrier to magnetization reversal were not investigated further. [Ni(6-Mes)₂]Br (6-Mes= 1,3-bis(2,4,6-trimethylphenyl)-3,4,5,6-tetrahydropyrimidin-2-ylidene) is another Ni complex showing SMM behavior.¹⁵¹ The synthetic strategy of using bulky ligands to enforce a nearly linear geometry was applied in this work, similar to the method described for Fe complexes (*vide supra*). AC magnetic susceptibility studies found that under an applied DC magnetic bias field, frequency dependent behavior was observed. Fitting of the curves found $U_{\text{eff}} = 12 \text{ cm}^{-1}$ and $\tau_0 = 4.6 \times 10^{-6} \text{ s}$. Interestingly, a structurally related complex with a formal Ni^{II} center was found to exhibit no SMM

behavior, which was ascribed to the creation of a nondegenerate ground state versus the degenerate ground state of $[\text{Ni}(\text{6-Mes})_2]\text{Br}$.

As shown above, monometallic transition metal complexes have demonstrated potential as materials to exhibit single molecule magnetism. In preparing monometallic complexes the effects of magnetic coupling can be minimized to allow the examination of magnetic anisotropy in the individual magnetic centers. Combined with structural information, structure/activity relationships may be determined allowing for the engineering of magnetic materials with desirable properties.

Whether a given complex has in-state or out-of-state SOC, it is desirable that it have axial symmetry to minimize the transverse anisotropy term which allows for QTM.^{35-36, 70, 100} For the following work, altering the divalent first row transition metal changes the number of electrons in the d subshell. If a ligand field has some degenerate orbitals, the population of that subshell arrangement will determine if in-state or out-of-state SOC is allowed. The examination of magnetic data should then support or refute the hypothesis that in-state SOC will have a greater effect on the ZFS than out-of-state contributions. The ligand field can also contribute to SOC through the bonding interactions themselves. Bonds with greater covalency and to heavier atoms can increase the contributions to SOC and further increase the ZFS. Related complexes can be prepared with systematic alteration of one ligand and then studied for the impact on SMM properties. Lastly, the coupling of well-characterized monometallic complexes can provide an entry into polymetallic clusters. Bimetallics are particularly

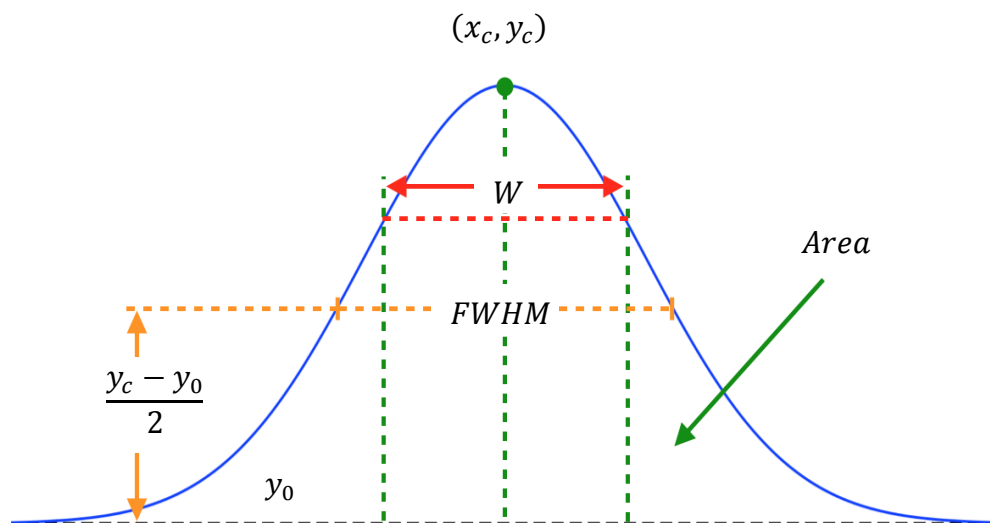
desirable as there is only one coupling interaction between the two metal centers. The comparison between well-characterized monometallic complexes and their coupling products will allow for greater understanding of the changes in the magnetic properties.

1.7. Instrumental Methods

1.7.1. UV-vis Spectroscopy

The absorption bands in electronic spectra in liquids are typically inhomogeneously broadened meaning that they can be accurately modeled as Gaussian line shapes, a treatment that has a firm basis in theory.¹⁵²⁻¹⁵⁴ The experimental value of this fact is the ability to extract λ_{max} values by curve fitting, especially in the case of overlapping bands. In doing so more accurate values can be determined with this accuracy being propagated through crystal field splitting calculations. There are some qualifying assumptions made in this theoretical treatment; that the solvent is nonpolar, the solutions are dilute, and the volume of the analyte molecule or ion is larger than that of the solvent molecules.¹⁵²⁻¹⁵⁴ If the volume of the analyte molecule is larger than that of the solvent, interactions between solvent are averaged out and solvent effects are minimized, provided that the solvent is nonpolar. The use of nonpolar solvents had the additional benefit of not coordinating to the metal center, which would lead to erroneous electronic spectra as the species in solution would not be the same as the solid state. Since the magnetic phenomena are examined in the solid state, care must be taken to ensure that the coordination environment in

electronic spectra measurements is the same as the solid-state environment. In



accordance with previous literature work, the extinction coefficients are reported from the original spectrum, not the fitted value.¹⁵⁵

The equation for a Gaussian peak is of the form

$$y = y_0 + \frac{A}{w\sqrt{\pi/2}} e^{-2\frac{(x-x_c)^2}{w^2}} \quad \text{Equation 1.27}$$

where y_0 is the baseline, A is the area, W is the peak width, and x_c is the local maximum of the peak.^{154, 156} Figure 1.11 depicts a peak with the relevant parameters labelled. The values w and $FWHM$ are similar in that they quantify the peak width.^{154, 157} The former is a measure derived from the statistical approach, while the latter is more commonly used to quantify peak width in spectroscopy. Peak positions were visually estimated and then iteratively fitted until convergence was reached. The condition for convergence was defined as $\chi^2 < 1 \cdot 10^{-9}$. In instances where the number of peaks was not visually apparent a count was determined by multiple factors. The number of peaks was not

allowed to exceed those justifiable by the Tanabe-Sugano secular equations or comparison to related compounds.¹⁵⁸ Comparison to related compounds was necessary because of the reduction of symmetry that could split peaks further and SOC effects that also led to splitting.⁵⁰ The minimum number of peaks necessary for a fit with $R^2 > 0.999$ was used as long as it did not exceed the number from the previous condition.

1.7.2. Bulk Magnetic Susceptibility

Despite some limitations, bulk magnetic susceptibility can provide important magnetic information more rapidly than intensive cryogenic methods. Through it, the S value and Landé g factor can be measured at room temperature.^{45, 48} The Bose-Stoner formula for transition metals, Equation 1.10, relates the number of unpaired electrons to the magnetic moment of the spin center.^{42, 44-45, 48-49} This characterizes a material as low or high spin and can indicate SOC contributions to the magnetic moment.⁴⁹ The limitation present is that at room temperature and weak external magnetic field values, magnetic systems can readily occupy excited states such that S and g are in fact averages for a thermal population of the ground state as well as low-lying excited states. For this reason, the magnetometry measurements conducted with more sensitive instruments at low temperature remain essential experiments.⁴⁴

The magnetic susceptibility balance measures the response of a material placed in an inhomogeneous magnetic field as a weight change as the solid is either attracted or repulsed by the magnetic field.⁴² A torsion balance is the

component that measures this change of weight as for a paramagnetic material the change is small. From the apparent mass difference the magnetic susceptibility of the sample can be calculated by Equation 1.15.⁴⁸

1.7.3. Alternating Current Magnetic Susceptibility

Another use of magnetic techniques involves the oscillation of the magnetic field at a frequency (ν) and measuring the magnetic moment.⁴⁴ This experiment can be conducted in a few different ways and the data also processed differently to provide insight into the dynamics of the SMM behavior.^{38, 121, 149} If a magnetic material is placed in an oscillating (AC) magnetic field, the response can be decomposed into in-phase (χ') and out-of-phase (χ'') components related to the susceptibility as

$$\chi = \chi' + i\chi'' \quad \text{Equation 1.28}$$

where

$$\chi' = \chi \cos \varphi \quad \text{Equation 1.29}$$

and

$$\chi'' = \chi \sin \varphi \quad \text{Equation 1.30}$$

If the magnetization of the material follows the oscillation of the field completely $\chi'' = 0$, but χ'' takes on significant nonzero values when the relaxation rate is roughly equal to ω , $\omega = 2\pi\nu$. (If a material does not follow the oscillating field at all, the phase relationship is not constant with respect to time, so the model breaks down). A peak is observed in $\chi''(T)$ when the relaxation rate is equal to ω . Figure 1.12 left plots typical results from this experiment. The x-axis is often plotted logarithmically to better show the lineshape, and the individual plots can

hold temperature or DC magnetic bias field strength constant. The relaxation rate can be found this way, and then the intrinsic barrier to magnetization reversal can be found using the Arrhenius equation¹²¹,

$$\tau = \tau_0 \exp\left(\frac{U_{\text{eff}}}{k_{\text{B}}T}\right) \quad \text{Equation 1.31}$$

This assumes that the Arrhenius plot is linear; deviations indicate more than one relaxation pathway is active. A typical Arrhenius plot is shown in Figure 1.12 right. The fitted line and extracted parameters are shown in red.

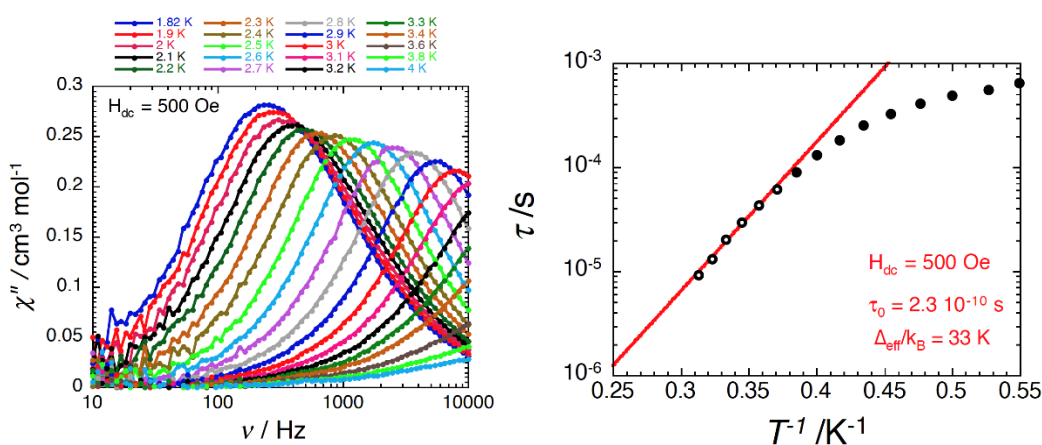


Figure 1.12. Left: Plots of χ'' versus frequency for $(\text{Tp}^{\text{Ph}})\text{CoCl}$ in a bias field of 500 Oe at selected temperatures in the range of 1.8 to 4 K. Right: Arrhenius plot of the characteristic frequencies (ω) for the out-of-phase magnetic susceptibility of $(\text{Tp}^{\text{Ph}})\text{CoCl}$.

1.7.4. References

1. Cohen, E.R.; Cvitas, T.; Frey, J.G.; Holmström, B.; Kuchitsu, K.; Marquardt, R.; Mills, I.; Pavese, F.; Quack, M.; Stohner, J.; Strauss, H.L.; Takami, M.; Thor, A.J., *Quantities, Units, and Symbols in Physical Chemistry, Iupac Green Book*. third ed.; IUPAC and RSC Publishing: Cambridge, 2008.
2. Bagai, R.; Christou, G., The Drosophila of Single-Molecule Magnetism: $[\text{Mn}_{12}\text{O}_{12}(\text{O}_2\text{Cr})_{16}(\text{H}_2\text{O})_4]$. *Chemical Society Reviews* **2009**, 38 (4), 1011-26.

3. Harman, W.H.; Harris, T.D.; Freedman, D.E.; Fong, H.; Chang, A.; Rinehart, J.D.; Ozarowski, A.; Sougrati, M.T.; Grandjean, F.; Long, G.J.; Long, J.R.; Chang, C.J., Slow Magnetic Relaxation in a Family of Trigonal Pyramidal Iron(II) Pyrrolide Complexes. *Journal of the American Chemical Society* **2010**, *132* (51), 18115-18126.
4. Christou, G.; Gatteschi, D.; Hendrickson, D.N.; Sessoli, R., Single-Molecule Magnets. *MRS Bulletin* **2000**, *25* (11), 66-71.
5. Lewis, L.H.; Jiménez-Villacorta, F., Perspectives on Permanent Magnetic Materials for Energy Conversion and Power Generation. *Metallurgical and Materials Transactions A* **2013**, *44* (1), 2-20.
6. Sánchez, J.R.; Vila, L.; Desfonds, G.; Gambarelli, S.; Attané, J.; De Teresa, J.; Magén, C.; Fert, A., Spin-to-Charge Conversion Using Rashba Coupling at the Interface between Non-Magnetic Materials. *Nature Communications* **2013**, *4*, 2944.
7. Van Vleck, J., Quantum Mechanics-the Key to Understanding Magnetism. *Reviews of Modern Physics* **1978**, *50* (2), 181.
8. Savoie, B., A Rigorous Proof of the Bohr–Van Leeuwen Theorem in the Semiclassical Limit. *Reviews in Mathematical Physics* **2015**, *27* (08), 1550019.
9. Van Leeuwen, H.J., *Vraagstukken Uit De Electronentheorie Van Het Magnetisme*. Eduard Ijdo: 1919.
10. Leeuwen, H.J.v., Problèmes De La Théorie Électronique Du Magnétisme. *J. Phys. Radium* **1921**, *2*, 361-377.

11. Bohr, N., *Studier over Metallernes Elektrontheori*. Thaning et Appel in Komm.: 1911.
12. Cucinotta, G.; Perfetti, M.; Luzon, J.; Etienne, M.; Car, P.E.; Caneschi, A.; Calvez, G.; Bernot, K.; Sessoli, R., Magnetic Anisotropy in a Dysprosium/Dota Single-Molecule Magnet: Beyond Simple Magneto-Structural Correlations. *Angewandte Chemie International Edition* **2012**, 51 (7), 1606-1610.
13. Ghosh, S.; Datta, S.; Friend, L.; Cardona-Serra, S.; Gaita-Ariño, A.; Coronado, E.; Hill, S., Multi-Frequency Epr Studies of a Mononuclear Holmium Single-Molecule Magnet Based on the Polyoxometalate [Ho^{III}(W₅O₁₈)₂]⁹⁻. *Dalton Transactions* **2012**, 41 (44), 13697-13704.
14. Wood, R., The Feasibility of Magnetic Recording at 1 Terabit Per Square Inch. *IEEE Trans. Magn.* **2000**, 36, 36-42.
15. Díaz-Michelena, M., Small Magnetic Sensors for Space Applications. *Sensors* **2009**, 9 (4), 2271-2288.
16. Meier, F.; Zhou, L.; Wiebe, J.; Wiesendanger, R., Revealing Magnetic Interactions from Single-Atom Magnetization Curves. *Science* **2008**, 320 (5872), 82-86.
17. Arnold, D.P., Review of Microscale Magnetic Power Generation. *IEEE Transactions on Magnetics* **2007**, 43 (11), 3940-3951.
18. Skumryev, V.; Stoyanov, S.; Zhang, Y.; Hadjipanayis, G., Beating the Superparamagnetic Limit with Exchange Bias. *Nature* **2003**, 423 (6942), 850.
19. Thompson, D.A.; Best, J.S., The Future of Magnetic Data Storage Technology. *IBM Journal of Research and Development* **2000**, 44 (3), 311-322.

20. Shiroishi, Y.; Fukuda, K.; Tagawa, I.; Iwasaki, H.; Takenoiri, S.; Tanaka, H.; Mutoh, H.; Yoshikawa, N., Future Options for Hdd Storage. *IEEE Transactions on Magnetics* **2009**, *45* (10), 3816-3822.
21. Rinehart, J.D.; Long, J.R., Exploiting Single-Ion Anisotropy in the Design of F-Element Single-Molecule Magnets. *Chemical Science* **2011**, *2* (11), 2078.
22. Mossin, S.; Tran, B.L.; Adhikari, D.; Pink, M.; Heinemann, F.W.; Sutter, J.r.; Szilagyi, R.K.; Meyer, K.; Mindiola, D.J., A Mononuclear Fe (Iii) Single Molecule Magnet with a $3/2 \leftrightarrow 5/2$ Spin Crossover. *Journal of the American Chemical Society* **2012**, *134* (33), 13651-13661.
23. Atanasov, M.; Zadrozny, J.M.; Long, J.R.; Neese, F., A Theoretical Analysis of Chemical Bonding, Vibronic Coupling, and Magnetic Anisotropy in Linear Iron (Ii) Complexes with Single-Molecule Magnet Behavior. *Chemical Science* **2013**, *4* (1), 139-156.
24. Mannini, M.; Pineider, F.; Sainctavit, P.; Danieli, C.; Otero, E.; Sciancalepore, C.; Talarico, A.M.; Arrio, M.-A.; Cornia, A.; Gatteschi, D., Magnetic Memory of a Single-Molecule Quantum Magnet Wired to a Gold Surface. *Nature materials* **2009**, *8* (3), 194-197.
25. Smolko, L.; Černák, J.; Dušek, M.; Miklovič, J.; Titiš, J.; Boča, R., Three Tetracoordinate Co(Ii) Complexes [Co(Biq)X₂](X = Cl, Br, I) with Easy-Plane Magnetic Anisotropy as Field-Induced Single-Molecule Magnets. *Dalton Transactions* **2015**, *44* (40), 17565-17571.
26. Winpenny, R.E., Molecular Spintronics: Stretch for a Moment. *Nature nanotechnology* **2013**, *8* (3), 159-160.

27. Ardavan, A.; Rival, O.; Morton, J.J.; Blundell, S.J.; Tyryshkin, A.M.; Timco, G.A.; Winnpenny, R.E., Will Spin-Relaxation Times in Molecular Magnets Permit Quantum Information Processing? *arXiv preprint quant-ph/0609143* **2006**.
28. Vincent, R.; Klyatskaya, S.; Ruben, M.; Wernsdorfer, W.; Balestro, F., Electronic Read-out of a Single Nuclear Spin Using a Molecular Spin Transistor. *Nature* **2012**, *488* (7411), 357-60.
29. Yamada, T.; Schmaus, S.; Bagrets, A.; Yamagishi, Y.; Evers, F.; Wulfhekel, W. In *Single Molecular Spintronics: Giant Magnetoresistance through a Single Molecule*, 2013 NSFC-JSPS seminar on magnetic surface and films with novel characterization techniques, 2013; p 4.
30. Heutz, S., Molecular Spintronics: A Warm Exchange. *Nature materials* **2015**, *14* (10), 967-968.
31. Bogani, L.; Wernsdorfer, W., Molecular Spintronics Using Single-Molecule Magnets. *Nature materials* **2008**, *7* (3), 179-186.
32. Thiele, S.; Balestro, F.; Ballou, R.; Klyatskaya, S.; Ruben, M.; Wernsdorfer, W., Electrically Driven Nuclear Spin Resonance in Single-Molecule Magnets. *Science* **2014**, *344* (6188), 1135-1138.
33. Schwöbel, J.; Fu, Y.; Brede, J.; Dilullo, A.; Hoffmann, G.; Klyatskaya, S.; Ruben, M.; Wiesendanger, R., Real-Space Observation of Spin-Split Molecular Orbitals of Adsorbed Single-Molecule Magnets. *Nature communications* **2012**, *3*, 953.

34. Gómez-Coca, S.; Aravena, D.; Morales, R.; Ruiz, E., Large Magnetic Anisotropy in Mononuclear Metal Complexes. *Coordination Chemistry Reviews* **2015**, *289*, 379–392.
35. Neese, F.; Pantazis, D.A., What Is Not Required to Make a Single Molecule Magnet. *Faraday Discussions* **2011**, *148*, 229-238.
36. Ruiz, E.; Cirera, J.; Cano, J.; Alvarez, S.; Loose, C.; Kortus, J., Can Large Magnetic Anisotropy and High Spin Really Coexist? *Chemical Communications* **2008**, (1), 52-54.
37. Ishikawa, N.; Sugita, M.; Wernsdorfer, W., Quantum Tunneling of Magnetization in Lanthanide Single-Molecule Magnets: Bis(Phthalocyaninato)Terbium and Bis(Phthalocyaninato)Dysprosium Anions. *Angewandte Chemie, International Edition in English* **2005**, *44* (19), 2931-5.
38. Gatteschi, D.; Sessoli, R., Quantum Tunneling of Magnetization and Related Phenomena in Molecular Materials. *Angewandte Chemie International Edition* **2003**, *42* (3), 268-297.
39. Rinehart, J.D.; Fang, M.; Evans, W.J.; Long, J.R., Strong Exchange and Magnetic Blocking in N_2^{3-} -Radical-Bridged Lanthanide Complexes. *Nat Chem* **2011**, *3* (7), 538-42.
40. Ungur, L.; Le Roy, J.J.; Korobkov, I.; Murugesu, M.; Chibotaru, L.F., Fine-Tuning the Local Symmetry to Attain Record Blocking Temperature and Magnetic Remanence in a Single-Ion Magnet. *Angewandte Chemie International Edition* **2014**, *53* (17), 4413-4417.

41. Launay, J.-P.; Verdaguer, M., Basic Concepts. In *Electrons in Molecules: From Basic Principles to Molecular Electronics*, Oxford University Press: Oxford, 2014; pp 1-77.
42. Drago, R.S., Appendix A. In *Physical Methods in Inorganic Chemistry*, Reinhold: New York, 1965.
43. Van Vleck, J., On Dielectric Constants and Magnetic Susceptibilities in the New Quantum Mechanics Part I. A General Proof of the Langevin-Debye Formula. *Physical Review* **1927**, 29 (5), 727.
44. Launay, J.-P.; Verdaguer, M., The Localized Electron: Magnetic Properties. In *Electrons in Molecules: From Basic Principles to Molecular Electronics*, Oxford University Press: Oxford, 2014; pp 78-202.
45. Griffith, J.S., Magnetic Effects in Atomic Structure. In *The Theory of Transition-Metal Ions*, University Press: Cambridge, 1961.
46. Griffith, J.S., Optical Spectra and Thermodynamic Properties. In *The Theory of Transition-Metal Ions*, University Press: Cambridge, 1961.
47. Bose, D.M., Die Rolle Des Kreiselektrons Bei Paramagnetischen Erscheinungen. *Zeitschrift für Physik* **1927**, 43 (11), 864-882.
48. Bhatnagar, S.S.; Prakash, B.; Hamid, A., 270. Magnetism and Molecular Constitution of Some Chromium Compounds. *Journal of the Chemical Society (Resumed)* **1938**, (0), 1428-1434.
49. Van Vleck, J., Valence Strength and the Magnetism of Complex Salts. *The Journal of Chemical Physics* **1935**, 3 (12), 807-813.

50. Figgis, B.N.; Hitchman, M.A., Introduction. In *Ligand Field Theory and Its Applications*, Second Edition ed.; Wiley Interscience: New York, 1999; pp 1-26.
51. Drago, R.S., Electronic Absorption Spectroscopy. In *Physical Methods in Inorganic Chemistry*, Reinhold: New York, 1965.
52. Figgis, B.N.; Hitchman, M.A., Chapter 1. Introduction. In *Ligand Field Theory and Its Applications*, Wiley-VCH: New York, 2000.
53. Dirac, P.A. In *The Quantum Theory of the Electron*, Proceedings of the Royal Society of London A: Mathematical, Physical and Engineering Sciences, The Royal Society: 1928; pp 610-624.
54. Kapitza, P.; Strelkov, P.; Laurman, E., The Zeeman and Paschen-Back Effects in Strong Magnetic Fields. *Proceedings of the Royal Society of London. Series A, Mathematical and Physical Sciences* **1938**, 1-15.
55. Gawlik, W., Hyperfine Interaction Versus Strong Laser Field-Optical Back-Goudsmit (Paschen-Back) Effect. *American Journal of Physics* **1991**, 59 (8), 706-710.
56. Goudsmit, S.; Bacher, R., The Paschen-Back Effect of Hyperfine Structure. *Physical Review* **1929**, 34 (11), 1499.
57. Shapiro, A.; Fluri, D.; Berdyugina, S.V.; Stenflo, J., Molecular Hanle Effect in the Paschen-Back Regime. *Astronomy & Astrophysics* **2007**, 461 (1), 339-349.
58. Zentile, M.A.; Andrews, R.; Weller, L.; Knappe, S.; Adams, C.S.; Hughes, I.G., The Hyperfine Paschen-Back Faraday Effect. *Journal of Physics B: Atomic, Molecular and Optical Physics* **2014**, 47 (7), 075005.

59. Moriya, T., Anisotropic Superexchange Interaction and Weak Ferromagnetism. *Physical Review* **1960**, 120 (1), 91.
60. Curély, J., Magnetic Orbitals and Mechanisms of Exchange II. Superexchange. *Monatshefte für Chemie - Chemical Monthly* **2005**, 136 (6), 1013-1036.
61. Dai, D.; Xiang, H.; Whangbo, M.-H., Effects of Spin-Orbit Coupling on Magnetic Properties of Discrete and Extended Magnetic Systems. *Journal of Computational Chemistry* **2008**, 29 (13), 2187-2209.
62. Cao, S.; Zhang, X.; Paudel, T.R.; Sinha, K.; Wang, X.; Jiang, X.; Wang, W.; Brutsche, S.; Wang, J.; Ryan, P.J.; Kim, J.-W.; Cheng, X.; Tsymbal, E.Y.; Dowben, P.A.; Xu, X., On the Structural Origin of the Single-Ion Magnetic Anisotropy in LuFeO₃. *Journal of Physics-Condensed Matter* **2016**, 28 (15), 56001-56001.
63. Albright, T.A.; Burdett, J.K.; Whangbo, M.H., Atomic and Molecular Orbitals. In *Orbital Interactions in Chemistry*, John Wiley and Sons: New York, 1985; pp 1-11.
64. Curély, J., Magnetic Orbitals and Mechanisms of Exchange I. Direct Exchange. *Monatshefte für Chemie - Chemical Monthly* **2005**, 136 (6), 987-1011.
65. Cotton, F.A.; Daniels, L.M.; Murillo, C.A.; Pascual, I.; Zhou, H.-C., Remarkable Effects of Axial Π^* Coordination on the Cr–Cr Quadruple Bond in Dichromium Paddlewheel Complexes. *Journal of the American Chemical Society* **1999**, 121 (29), 6856-6861.

66. Hansen, J.r.; Li, B.; Dikarev, E.; Autschbach, J.; Davies, H.M.L., Combined Experimental and Computational Studies of Heterobimetallic Bi–Rh Paddlewheel Carboxylates as Catalysts for Metal Carbenoid Transformations. *The Journal of Organic Chemistry* **2009**, *74* (17), 6564-6571.
67. Patra, S.K.; Sadhukhan, N.; Bera, J.K., Effects of Axial Coordination on the Ru– Ru Single Bond in Diruthenium Paddlewheel Complexes. *Inorganic Chemistry* **2006**, *45* (10), 4007-4015.
68. Pedersen, K.S.; Dreiser, J.; Weihe, H.; Sibille, R.; Johannesen, H.V.; Sørensen, M.A.; Nielsen, B.E.; Sigrist, M.; Mutka, H.; Rols, S.; Bendix, J.; Piligkos, S., Design of Single-Molecule Magnets: Insufficiency of the Anisotropy Barrier as the Sole Criterion. *Inorganic Chemistry* **2015**, *54*, 7600–7606.
69. Poulten, R.C.; Page, M.J.; Algarra, A.s.G.; Le Roy, J.J.; López, I.; Carter, E.; Llobet, A.; Macgregor, S.A.; Mahon, M.F.; Murphy, D.M., Synthesis, Electronic Structure, and Magnetism of [Ni (6-Mes) ₂]⁺: A Two-Coordinate Nickel (I) Complex Stabilized by Bulky N-Heterocyclic Carbenes. *Journal of the American Chemical Society* **2013**, *135* (37), 13640-13643.
70. Zadrozny, J.M.; Atanasov, M.; Bryan, A.M.; Lin, C.-Y.; Rekken, B.D.; Power, P.P.; Neese, F.; Long, J.R., Slow Magnetization Dynamics in a Series of Two-Coordinate Iron(II) Complexes. *Chemical Science* **2013**, *4* (1), 125-138.
71. Reiff, W.M.; LaPointe, A.M.; Witten, E.H., Virtual Free Ion Magnetism and the Absence of Jahn-Teller Distortion in a Linear Two-Coordinate Complex of High-Spin Iron (II). *Journal of the American Chemical Society* **2004**, *126* (33), 10206-10207.

72. Scott, P.L.; Jeffries, C.D., Spin-Lattice Relaxation in Some Rare-Earth Salts at Helium Temperatures; Observation of the Phonon Bottleneck. *Physical Review* **1962**, *127* (1), 32-51.
73. Bloembergen, N.; Shapiro, S.; Pershan, P.; Artman, J., Cross-Relaxation in Spin Systems. *Physical Review* **1959**, *114* (2), 445.
74. Orbach, R., Spin-Lattice Relaxation in Rare-Earth Salts. *Proceedings of the Royal Society of London Series A* **1961**, *264* (1319), 458-484.
75. Wernsdorfer, W.; Bhaduri, S.; Tiron, R.; Hendrickson, D.N.; Christou, G., Spin-Spin Cross Relaxation in Single-Molecule Magnets. *Physical Review Letters* **2002**, *89* (19).
76. Huang, W.; Liu, T.; Wu, D.; Cheng, J.; Ouyang, Z.; Duan, C., Field-Induced Slow Relaxation of Magnetization in a Tetrahedral Co(II) Complex with Easy Plane Anisotropy. *Dalton Transactions* **2013**, *42* (43), 15326-15331.
77. Ruamps, R.; Batchelor, L.J.; Guillot, R.; Zakhia, G.; Barra, A.-L.; Wernsdorfer, W.; Guihéry, N.; Mallah, T., Ising-Type Magnetic Anisotropy and Single Molecule Magnet Behaviour in Mononuclear Trigonal Bipyramidal Co (II) Complexes. *Chemical Science* **2014**, *5* (9), 3418-3424.
78. Wernsdorfer, W.; Sessoli, R.; Caneschi, A.; Gatteschi, D.; Cornia, A., Nonadiabatic Landau-Zener Tunneling in Fe₈ Molecular Nanomagnets. *EPL (Europhysics Letters)* **2000**, *50* (4), 552.
79. Finn, C.B.P.; Orbach, R.; Wolf, W.P., Spin-Lattice Relaxation in Cerium Magnesium Nitrate at Liquid Helium Temperature: A New Process. *Proceedings of the Physical Society* **1961**, *77* (2), 261.

80. Orbach, R.; Blume, M., Spin-Lattice Relaxation in Multilevel Spin Systems. *Physical Review Letters* **1962**, 8 (12), 478-480.
81. Orbach, R., Spin-Lattice Relaxation in Rare-Earth Salts: Field Dependence of the Two-Phonon Process. *Proceedings of the Royal Society of London Series A* **1961**, 264 (1319), 485-495.
82. Alexander, S.; Entin-Wohlman, O.; Orbach, R., Relaxation and Nonradiative Decay in Disordered Systems. Iii. Statistical Character of Raman (Two-Quanta) Spin-Lattice Relaxation. *Physical Review B* **1987**, 35 (3), 1166-1173.
83. Orbach, R., On the Theory of Spin-Lattice Relaxation in Paramagnetic Salts. *Proceedings of the Physical Society* **1961**, 77 (4), 821.
84. Rechkemmer, Y.; Breitgoff, F.D.; van der Meer, M.; Atanasov, M.; Haki, M.; Orlita, M.; Neugebauer, P.; Neese, F.; Sarkar, B.; van Slageren, J., A Four-Coordinate Cobalt(II) Single-Ion Magnet with Coercivity and a Very High Energy Barrier. *Nature communications* **2016**, 7, 10467.
85. Novikov, V.V.; Pavlov, A.A.; Nelyubina, Y.V.; Boulon, M.-E.; Varzatskii, O.A.; Voloshin, Y.Z.; Winpenny, R.E., A Trigonal Prismatic Mononuclear Cobalt (II) Complex Showing Single-Molecule Magnet Behavior. *Journal of the American Chemical Society* **2015**, 137 (31), 9792-9795.
86. Herchel, R.; Váhovská, L.; Potočňák, I.; Trávníček, Z.k., Slow Magnetic Relaxation in Octahedral Cobalt(II) Field-Induced Single-Ion Magnet with Positive Axial and Large Rhombic Anisotropy. *Inorganic Chemistry* **2014**, 53 (12), 5896-5898.

87. Waller, I., Über Die Magnetisierung Von Paramagnetischen Kristallen in Wechselfeldern. *Zeitschrift für Physik* **1932**, 79 (5-6), 370-388.
88. Gorter, C., Paramagnetic Relaxation in a Transversal Magnetic Field. *Physica* **1936**, 3 (9), 1006-1008.
89. Gorter, C.J., Paramagnetic Relaxation. *Physica* **1936**, 3 (6), 503-514.
90. Kittel, C., *Introduction to Solid State Physics* Sixth Edition ed.; John Wiley and Sons: New York, 1986.
91. Van Vleck, J.H., Paramagnetic Relaxation and the Equilibrium of Lattice Oscillators. *Physical Review* **1941**, 59 (9), 724-729.
92. Barrat, J.-L.; Chiaruttini, F., Kapitza Resistance at the Liquid—Solid Interface. *Molecular Physics* **2003**, 101 (11), 1605-1610.
93. Pollack, G.L., Kapitza Resistance. *Reviews of Modern Physics* **1969**, 41 (1), 48.
94. Nan, C.-W.; Birringer, R., Determining the Kapitza Resistance and the Thermal Conductivity of Polycrystals: A Simple Model. *Physical Review B* **1998**, 57 (14), 8264.
95. Niemeyer, M.; Hirsch, K.; Zamudio-Bayer, V.; Langenberg, A.; Vogel, M.; Kossick, M.; Ebrecht, C.; Egashira, K.; Terasaki, A.; Möller, T.; v. Issendorff, B.; Lau, J.T., Spin Coupling and Orbital Angular Momentum Quenching in Free Iron Clusters. *Physical Review Letters* **2012**, 108 (5), 057201.
96. Lin, P.H.; Smythe, N.C.; Gorelsky, S.I.; Maguire, S.; Henson, N.J.; Korobkov, I.; Scott, B.L.; Gordon, J.C.; Baker, R.T.; Murugesu, M., Importance of out-of-State Spin-Orbit Coupling for Slow Magnetic Relaxation in Mononuclear

Fe(II) Complexes. *Journal of the American Chemical Society* **2011**, 133 (40), 15806-9.

97. Perić, M.; García-Fuente, A.; Zlatar, M.; Daul, C.; Stepanović, S.; García-Fernández, P.; Gruden-Pavlović, M., Magnetic Anisotropy in “Scorpionate” First-Row Transition-Metal Complexes: A Theoretical Investigation. *Chemistry – A European Journal* **2015**, 21 (9), 3716-3726.

98. Ganyushin, D.; Neese, F., First-Principles Calculations of Zero-Field Splitting Parameters. *Journal of Chemical Physics* **2006**, 125 (2), 24103.

99. Kahn, O., Dinuclear Complexes with Predictable Magnetic Properties. *Angewandte Chemie International Edition in English* **1985**, 24 (10), 834-850.

100. Zadrozny, J.M.; Xiao, D.J.; Atanasov, M.; Long, G.J.; Grandjean, F.; Neese, F.; Long, J.R., Magnetic Blocking in a Linear Iron(I) Complex. *Nat Chem* **2013**, 5 (7), 577-81.

101. Zadrozny, J.M.; Xiao, D.J.; Long, J.R.; Atanasov, M.; Neese, F.; Grandjean, F.; Long, G.J., Mossbauer Spectroscopy as a Probe of Magnetization Dynamics in the Linear Iron(I) and Iron(II) Complexes $[\text{Fe}(\text{C}(\text{SiMe}_3)_2)]^{1-/0}$. *Inorganic Chemistry* **2013**, 52 (22), 13123-31.

102. Jahn, H.A.; Teller, E., Stability of Polyatomic Molecules in Degenerate Electronic States I-Orbital Degeneracy. *Proc. R. Soc. London A* **1937**, 161, 220-235.

103. Lin, P.-H.; Smythe, N.C.; Gorelsky, S.I.; Maguire, S.; Henson, N.J.; Korobkov, I.; Scott, B.L.; Gordon, J.C.; Baker, R.T.; Murugesu, M., Importance of out-of-State Spin–Orbit Coupling for Slow Magnetic Relaxation in Mononuclear

Feii Complexes. *Journal of the American Chemical Society* **2011**, 133 (40), 15806-15809.

104. Zhang, Y.Z.; Mallik, U.P.; Clerac, R.; Rath, N.P.; Holmes, S.M., Irreversible Solvent-Driven Conversion in Cyanometalate $\{\text{Fe}_2\text{Ni}\}_N$ ($N=2, 3$) Single-Molecule Magnets. *Chemical Communications* **2011**, 47 (25), 7194-6.

105. Zhu, Y.-Y.; Cui, C.; Zhang, Y.-Q.; Jia, J.-H.; Guo, X.; Gao, C.; Qian, K.; Jiang, S.-D.; Wang, B.-W.; Wang, Z.-M., Zero-Field Slow Magnetic Relaxation from Single Co(II) Ion: A Transition Metal Single-Molecule Magnet with High Anisotropy Barrier. *Chemical Science* **2013**, 4 (4), 1802-1806.

106. Farrell, A.R.; Coome, J.A.; Probert, M.R.; Goeta, A.E.; Howard, J.A.; Lemée-Cailleau, M.-H.; Parsons, S.; Murrie, M., Ultra-Low Temperature Structure Determination of a Mn 12 Single-Molecule Magnet and the Interplay between Lattice Solvent and Structural Disorder. *CrystEngComm* **2013**, 15 (17), 3423-3429.

107. Wang, S.; Zuo, J.L.; Zhou, H.C.; Choi, H.J.; Ke, Y.; Long, J.R.; You, X.Z., $[(\text{Tp})_8(\text{H}_2\text{O})_6\text{Cu}(\text{II})_6\text{Fe}(\text{III})_8(\text{CN})_{24}]^{4+}$: A Cyanide-Bridged Face-Centered-Cubic Cluster with Single-Molecule-Magnet Behavior. *Angewandte Chemie, International Edition in English* **2004**, 43 (44), 5940-3.

108. Murugesu, M.; Habrych, M.; Wernsdorfer, W.; Abboud, K.A.; Christou, G., Single-Molecule Magnets: A Mn_{25} Complex with a Record $S=51/2$ Spin for a Molecular Species. *Journal of the American Chemical Society* **2004**, 126 (15), 4766-4767.

109. Ferbinteanu, M.; Miyasaka, H.; Wernsdorfer, W.; Nakata, K.; Sugiura, K.-i.; Yamashita, M.; Coulon, C.; Clérac, R., Single-Chain Magnet (Net₄)[Mn₂(5-MeOsalen)₂Fe(CN)₆] Made of Mn^{III}-Fe^{III}-Mn^{III} Trinuclear Single-Molecule Magnet with an S = 9/2 Spin Ground State. *Journal of the American Chemical Society* **2005**, *127* (9), 3090-3099.
110. Coutinho, J.T.; Antunes, M.A.; Pereira, L.C.; Bolvin, H.; Marcalo, J.; Mazzanti, M.; Almeida, M., Single-Ion Magnet Behaviour in [U(Tp^{me2})₂]. *Dalton Transactions* **2012**, *41* (44), 13568-71.
111. Habib, F.; Brunet, G.; Vieru, V.; Korobkov, I.; Chibotaru, L.F.; Murugesu, M., Significant Enhancement of Energy Barriers in Dinuclear Dysprosium Single-Molecule Magnets through Electron-Withdrawing Effects. *Journal of the American Chemical Society* **2013**, *135* (36), 13242-13245.
112. Blagg, R.J.; Tuna, F.; McInnes, E.J.; Winpenny, R.E., Pentametallic Lanthanide-Alkoxide Square-Based Pyramids: High Energy Barrier for Thermal Relaxation in a Holmium Single Molecule Magnet. *Chem Commun (Camb)* **2011**, *47* (38), 10587-9.
113. Ishikawa, N.; Sugita, M.; Wernsdorfer, W., Quantum Tunneling of Magnetization in Lanthanide Single-Molecule Magnets: Bis (Phthalocyaninato) Terbium and Bis (Phthalocyaninato) Dysprosium Anions. *Angewandte Chemie International Edition* **2005**, *44* (19), 2931-2935.
114. Tasiopoulos, A.J.; Vinslava, A.; Wernsdorfer, W.; Abboud, K.A.; Christou, G., Giant Single-Molecule Magnets: A {Mn₈₄} Torus and Its Supramolecular Nanotubes. *Angewandte Chemie* **2004**, *116* (16), 2169-2173.

115. Mougel, V.; Chatelain, L.; Pécaut, J.; Caciuffo, R.; Colineau, E.; Griveau, J.-C.; Mazzanti, M., Uranium and Manganese Assembled in a Wheel-Shaped Nanoscale Single-Molecule Magnet with High Spin-Reversal Barrier. *Nature Chemistry* **2012**, *4* (12), 1011-1017.
116. Miyasaka, H.; Madanbashi, T.; Sugimoto, K.; Nakazawa, Y.; Wernsdorfer, W.; Sugiura, K.i.; Yamashita, M.; Coulon, C.; Clérac, R., Single-Chain Magnet Behavior in an Alternated One-Dimensional Assembly of a Mn^{III} Schiff-Base Complex and a TCNQ Radical. *Chemistry—A European Journal* **2006**, *12* (27), 7028-7040.
117. Clérac, R.; Miyasaka, H.; Yamashita, M.; Coulon, C., Evidence for Single-Chain Magnet Behavior in a Mn^{III}-N^{III} Chain Designed with High Spin Magnetic Units: A Route to High Temperature Metastable Magnets. *Journal of the American Chemical Society* **2002**, *124* (43), 12837-12844.
118. Peng, J.-B.; Zhang, Q.-C.; Kong, X.-J.; Zheng, Y.-Z.; Ren, Y.-P.; Long, L.-S.; Huang, R.-B.; Zheng, L.-S.; Zheng, Z., High-Nuclearity 3d–4f Clusters as Enhanced Magnetic Coolers and Molecular Magnets. *Journal of the American Chemical Society* **2012**, *134* (7), 3314-3317.
119. Feng, X.; Liu, J.; Harris, T.D.; Hill, S.; Long, J.R., Slow Magnetic Relaxation Induced by a Large Transverse Zero-Field Splitting in a Mn^{II}Re^{IV}(CN)₂ Single-Chain Magnet. *Journal of the American Chemical Society* **2012**, *134* (17), 7521-7529.
120. Waldmann, O., A Criterion for the Anisotropy Barrier in Single-Molecule Magnets. *Inorganic Chemistry* **2007**, *46* (24), 10035-10037.

121. Jurca, T.; Farghal, A.; Lin, P.-H.; Korobkov, I.; Murugesu, M.; Richeson, D.S., Single-Molecule Magnet Behavior with a Single Metal Center Enhanced through Peripheral Ligand Modifications. *Journal of the American Chemical Society* **2011**, *133* (40), 15814-15817.
122. Freedman, D.E.; Harman, W.H.; Harris, T.D.; Long, G.J.; Chang, C.J.; Long, J.R., Slow Magnetic Relaxation in a High-Spin Iron(II) Complex. *Journal of the American Chemical Society* **2010**, *132* (4), 1224-1225.
123. Park, K.; Holmes, S.M., Exchange Coupling and Contribution of Induced Orbital Angular Momentum of Low-Spin Fe³⁺ Ions to Magnetic Anisotropy in Cyanide-Bridged Fe₂m₂ Molecular Magnets: Spin-Polarized Density-Functional Calculations. *Physical Review B* **2006**, *74* (22), 224440.
124. Boča, R., Zero-Field Splitting in Metal Complexes. *Coordination Chemistry Reviews* **2004**, *248* (9-10), 757-815.
125. Zadrozny, J.M.; Telsler, J.; Long, J.R., Slow Magnetic Relaxation in the Tetrahedral Cobalt(II) Complexes [Co (Eph)₄]²⁻ (E=O, S, Se). *Polyhedron* **2013**, *64*, 209-217.
126. Fataftah, M.S.; Zadrozny, J.M.; Rogers, D.M.; Freedman, D.E., A Mononuclear Transition Metal Single-Molecule Magnet in a Nuclear Spin-Free Ligand Environment. *Inorganic Chemistry* **2014**, *53* (19), 10716-10721.
127. Rajnák, C.; Titiš, J.n.; Fuhr, O.; Ruben, M.; Boča, R., Single-Molecule Magnetism in a Pentacoordinate Cobalt (II) Complex Supported by an Antenna Ligand. *Inorganic Chemistry* **2014**, *53* (16), 8200-8202.

128. Boča, R.; Miklovič, J.; Titiš, J.N., Simple Mononuclear Cobalt(II) Complex: A Single-Molecule Magnet Showing Two Slow Relaxation Processes. *Inorganic Chemistry* **2014**, *53* (5), 2367-2369.
129. Titis, J.; Boca, R.; Miklovic, J.; Valigura, D., Mononuclear Ni (II) Complex: A Field Induced Single-Molecule Magnet Showing Two Slow Relaxation Processes. *Dalton Transactions* **2015**, 12484.
130. Zadrozny, J.M.; Liu, J.; Piro, N.A.; Chang, C.J.; Hill, S.; Long, J.R., Slow Magnetic Relaxation in a Pseudotetrahedral Cobalt(II) Complex with Easy-Plane Anisotropy. *Chemical Communications* **2012**, *48* (33), 3927-9.
131. Zadrozny, J.M.; Long, J.R., Slow Magnetic Relaxation at Zero Field in the Tetrahedral Complex $[\text{Co}(\text{SPh})_4]^{2-}$. *Journal of the American Chemical Society* **2011**, *133* (51), 20732-4.
132. Titiš, J.; Miklovič, J.; Boča, R., Magnetostructural Study of Tetracoordinate Cobalt(II) Complexes. *Inorganic Chemistry Communications* **2013**, *35*, 72-75.
133. Zhang, Y.-Z.; Gómez-Coca, S.; Brown, A.J.; Saber, M.R.; Zhang, X.; Dunbar, K.R., Trigonal Antiprismatic Co (II) Single Molecule Magnets with Large Uniaxial Anisotropies: Importance of Raman and Tunneling Mechanisms. *Chemical Science* **2016**, *7* (10), 6519-6527.
134. Ding, M.; Cutsail, G.; Aravena, D.; Amoza, M.; Rouzieres, M.; Dechambenoit, P.; Lozovyy, Y.; Pink, M.; Ruiz, E.; Clerac, R., A Low Spin Manganese (IV) Nitride Single Molecule Magnet. *Chemical Science* **2016**.

135. Gómez-Coca, S.; Cremades, E.; Aliaga-Alcalde, N.; Ruiz, E., Huge Magnetic Anisotropy in a Trigonal-Pyramidal Nickel(II) Complex. *Inorganic Chemistry* **2013**, *53* (2), 676-678.
136. Graham, M.J.; Zadrozny, J.M.; Shiddiq, M.; Anderson, J.S.; Fataftah, M.S.; Hill, S.; Freedman, D.E., Influence of Electronic Spin and Spin–Orbit Coupling on Decoherence in Mononuclear Transition Metal Complexes. *Journal of the American Chemical Society* **2014**, *136* (21), 7623-7626.
137. Titis, J.; Boca, R., Magnetostructural D Correlation in Nickel(II) Complexes: Reinvestigation of the Zero-Field Splitting. *Inorganic Chemistry* **2010**, *49* (9), 3971-3.
138. Gomez-Coca, S.; Cremades, E.; Aliaga-Alcalde, N.r.; Ruiz, E., Mononuclear Single-Molecule Magnets: Tailoring the Magnetic Anisotropy of First-Row Transition-Metal Complexes. *Journal of the American Chemical Society* **2013**, *135* (18), 7010-7018.
139. Gómez-Coca, S.; Urtizbera, A.; Cremades, E.; Alonso, P.J.; Camón, A.; Ruiz, E.; Luis, F., Origin of Slow Magnetic Relaxation in Kramers Ions with Non-Uniaxial Anisotropy. *Nature communications* **2014**, *5*, 4300.
140. Vallejo, J.; Castro, I.; Ruiz-García, R.; Cano, J.; Julve, M.; Lloret, F.; De Munno, G.; Wernsdorfer, W.; Pardo, E., Field-Induced Slow Magnetic Relaxation in a Six-Coordinate Mononuclear Cobalt(II) Complex with a Positive Anisotropy. *Journal of the American Chemical Society* **2012**, *134* (38), 15704-15707.

141. Saber, M.R.; Dunbar, K.R., Ligands Effects on the Magnetic Anisotropy of Tetrahedral Cobalt Complexes. *Chemical Communications* **2014**, 50 (82), 12266-12269.
142. Chen, L.; Wang, J.; Wei, J.-M.; Wernsdorfer, W.; Chen, X.-T.; Zhang, Y.-Q.; Song, Y.; Xue, Z.-L., Slow Magnetic Relaxation in a Mononuclear Eight-Coordinate Cobalt(II) Complex. *Journal of the American Chemical Society* **2014**, 136 (35), 12213-12216.
143. Carl, E.; Demeshko, S.; Meyer, F.; Stalke, D., Triimidosulfonates as Acute Bite-Angle Chelates: Slow Relaxation of the Magnetization in Zero Field and Hysteresis Loop of a Co^{II} Complex. *Chemistry–A European Journal* **2015**, 21 (28), 10109-10115.
144. Ziegenbalg, S.; Hornig, D.; Görls, H.; Plass, W., Cobalt(II)-Based Single-Ion Magnets with Distorted Pseudotetrahedral [N₂O₂] Coordination: Experimental and Theoretical Investigations. *Inorganic Chemistry* **2016**, 55, 4047-4058.
145. Buchholz, A.; Eseola, A.O.; Plass, W., Slow Magnetic Relaxation in Mononuclear Tetrahedral Cobalt(II) Complexes with 2-(1H-imidazol-2-yl) Phenol Based Ligands. *Comptes Rendus Chimie* **2012**, 15 (10), 929-936.
146. Cao, D.-K.; Feng, J.-Q.; Ren, M.; Gu, Y.-W.; Song, Y.; Ward, M.D., A Mononuclear Cobalt(II)–Dithienylethene Complex Showing Slow Magnetic Relaxation and Photochromic Behavior. *Chemical Communications* **2013**, 49 (78), 8863-8865.
147. Yang, F.; Zhou, Q.; Zhang, Y.; Zeng, G.; Li, G.; Shi, Z.; Wang, B.; Feng, S., Inspiration from Old Molecules: Field-Induced Slow Magnetic Relaxation in

Three Air-Stable Tetrahedral Cobalt(II) Compounds. *Chemical Communications* **2013**, 49 (46), 5289-5291.

148. Eichhöfer, A.; Lan, Y.; Mereacre, V.; Bodenstein, T.; Weigend, F., Slow Magnetic Relaxation in Trigonal-Planar Mononuclear Fe(II) and Co(II) Bis(trimethylsilyl) Amido Complexes: A Comparative Study. *Inorganic Chemistry* **2014**, 53 (4), 1962-1974.

149. Vaidya, S.; Upadhyay, A.; Singh, S.K.; Gupta, T.; Tewary, S.; Langley, S.K.; Walsh, J.P.; Murray, K.S.; Rajaraman, G.; Shanmugam, M., A Synthetic Strategy for Switching the Single Ion Anisotropy in Tetrahedral Co(II) Complexes. *Chemical Communications* **2015**, 51 (18), 3739-3742.

150. Nemeč, I.; Herchel, R.; Trávníček, Z., Suppressing of Slow Magnetic Relaxation in Tetracoordinate Co (II) Field-Induced Single-Molecule Magnet in Hybrid Material with Ferromagnetic Barium Ferrite. *Scientific reports* **2015**, 5, 10761.

151. Poulten, R.C.; Page, M.J.; Algarra, A.s.G.; Le Roy, J.J.; López, I.; Carter, E.; Llobet, A.; Macgregor, S.A.; Mahon, M.F.; Murphy, D.M., Synthesis, Electronic Structure, and Magnetism of $[\text{Ni}(\text{6-Mes})_2]^+$: A Two-Coordinate Nickel(I) Complex Stabilized by Bulky N-Heterocyclic Carbenes. *Journal of the American Chemical Society* **2013**, 135 (37), 13640-13643.

152. Blume, M., Stochastic Theory of Line Shape: Generalization of the Kubo-Anderson Model. *Physical Review* **1968**, 174 (2), 351-358.

153. Kador, L., Stochastic Theory of Inhomogeneous Spectroscopic Line Shapes Reinvestigated. *The Journal of Chemical Physics* **1991**, 95 (8), 5574-5581.
154. Saven, J.G.; Skinner, J.L., A Molecular Theory of the Line Shape: Inhomogeneous and Homogeneous Electronic Spectra of Dilute Chromophores in Nonpolar Fluids. *The Journal of Chemical Physics* **1993**, 99 (6), 4391.
155. Desrochers, P.J.; Telser, J.; Zvyagin, S.A.; Ozarowski, A.; Krzystek, J.; Vivic, D.A., Electronic Structure of Four-Coordinate C_{3v} Nickel(II) Scorpionate Complexes: Investigation by High-Frequency and -Field Electron Paramagnetic Resonance and Electronic Absorption Spectroscopies. *Inorganic Chemistry* **2006**, 45, 8930-8941.
156. Langhals, H., A Re-Examination of the Line Shape of the Electronic Spectra of Complex Molecules in Solution: Log-Normal Function Versus Gaussian. *Spectrochimica Acta Part A: Molecular and Biomolecular Spectroscopy* **2000**, 56 (11), 2207-2210.
157. Deming, W.E.; Birge, R.T., On the Statistical Theory of Errors. *Reviews of Modern Physics* **1934**, 6 (3), 119-161.
158. Tanabe, Y.; Sugano, S., On the Absorption Spectra of Complex Ions. I. *Journal of the Physical Society of Japan* **1954**, 9 (5), 753-766.

Chapter 2. Synthesis and Characterization of 4-Coordinate Scorpionates for Single Molecule Magnetism

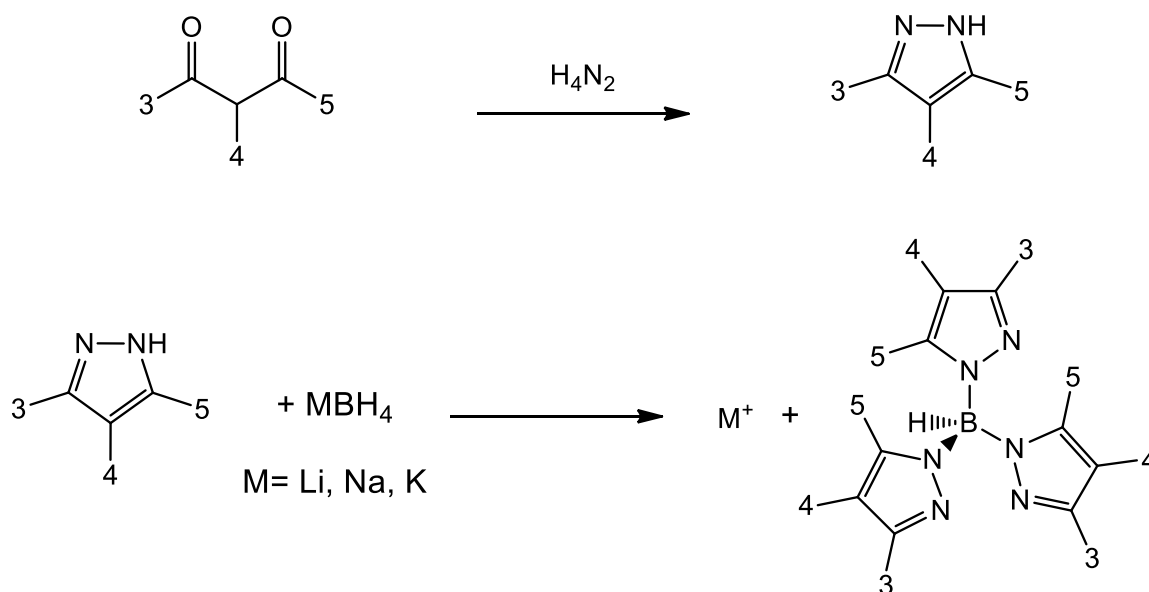
2.1. Overview of 4-Coordinate Scorpionates

Since their first description in 1967, scorpionates have been an intensely studied class of ligands.¹⁵⁹⁻¹⁶¹ While initial reports focused on first row transition metal complexes¹⁶²⁻¹⁶⁴, second and third row, lanthanide, and main group complexes are known and have been studied for a variety of applications.¹⁵⁹ The results of these efforts are over a thousand papers and multiple monographs.¹⁶⁰ The applications investigated include model complexes of enzyme active sites, catalysts, luminescent materials, contrast agents, spin-crossover systems, radio-tracers, and the present matter, SMMs.^{104, 110, 165-174} The axial symmetry of C_{3v} or C_3 monometallic scorpionates may give rise to ZFS, which is associated with SMM behavior.¹⁷⁵

The substitution of the pyrazole rings in the 3, 4, and 5 positions allows for steric effects on the coordination geometry of the metal.^{160-161, 176} The substitution also affects the electronic properties of the ligand.¹⁷² Combined, these properties make scorpionates a useful ligand for the preparation of complexes of interest to the SMM community.^{104, 155, 173, 175, 177} The coordination geometry can be manipulated towards axial symmetry causing the transverse anisotropy term, E , to approach zero. If E is zero, no mixing of the degenerate ground states can occur, and quantum tunneling of the magnetization is suppressed.³⁸ The reduction of the coordination number also allows for SOC, which is largely

nonexistent in coordinatively saturated complexes, particularly 6-coordinate O_h complexes. By altering the electron donating ability of the ligand, the electron density on the metal can be altered and influence the interaction with other ligands that may be present besides the scorpionate.

Tris-pyrazol-1-yl and tetrakis-pyrazol-1-yl borates ("scorpionates") are prepared by Scheme 2.1 wherein pyrazoles of a given structure can be prepared by the reaction of a substituted 1,3-dione with hydrazine.¹⁶¹ These pyrazoles can then be heated with MBH_4 salts ($M = Li, Na, K$) to prepare the scorpionate ligands as alkali salts.^{161, 163-164, 178} Three factors controlling the degree of substitution on the boron atom are the steric bulk of the pyrazole, the stoichiometry of the reaction, and the maximum temperature of the reaction mixture.^{161, 163}



Scheme 2.1 The synthesis of pyrazolyborates or "scorpionates".

The addition of pyrazole to a hydridoborate passes through a five-membered ring transition state that is sensitive to the steric bulk of the pyrazole

ring (Figure 2.1, middle).¹⁶¹⁻¹⁶² Bulky pyrazoles such as 3-phenylpyrazole can only add to form the tris-pyrazolylborate as the boron atom becomes increasingly sterically hindered with each substitution to a point where the fourth substitution is prevented.¹⁶¹ However, tris- and tetrakis- scorpionates are known for the unsubstituted pyrazole derivative.¹⁶³ Stoichiometry and temperature are also used to control whether three or four pyrazoles are added since the addition of pyrazole rings to the boron atom proceeds in a stepwise fashion.¹⁶⁰ Typically, asymmetric pyrazoles add to give the less sterically-demanding product.^{161, 174}

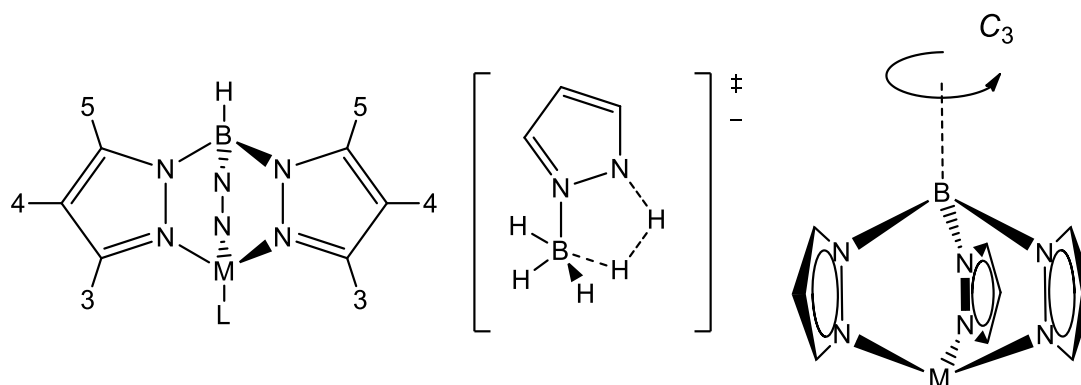


Figure 2.1 Left: Numbering scheme for the potentially substituted positions on the scorpionate ligand. L indicates the position of the axial ligand. Middle: The five-membered ring transition state of the reaction between pyrazoles and the borohydride anion. Right: The C_3 symmetry of the coordinated scorpionate ligand.

Synthesis of metal complexes with scorpionates proceeds by a variety of reaction types.^{155, 160-161, 174, 179-180} Simple salt metathesis reactions were the first reported routes, typically involving the addition of a group IA salt of the scorpionate to a metal halide with the precipitation of MX (M = Na, K; X = group VIIA). The use of Tl or Sn salts of scorpionates was later reported.¹⁸¹⁻¹⁸² The strong lattice energy of TlX (X = group VIIA) salts favors the products to a greater degree, generally improving the yield. Later work focused on introduction of other

ligands in the remaining axial position.¹⁵⁹ The use of thiocyanate and cyanate salts of the metal to prepare the initial complex or their incorporation into a mixture of scorpionate and metal halide led to the isolation of many "pseudo-halide" complexes.^{159, 161}

Subsequent ligand substitution can occur by a variety of methods.^{167, 183-186} Simple substitution of labile solvent ligands has been observed.¹⁸³ Treatment with reducing agents like Mg or KC_8 increases electron density on the metal centers and allows for coordination to normally inert molecules like N_2 .¹⁸⁴ Halide ligands can be substituted with alkyl and aryl fragments by reaction with Grignard reagents. The precipitation of MgX_2 salts drives these reactions forward.¹⁸⁵ More covalent ligands can be substituted through salt metathesis as well, not limiting the route to more electrostatic products.¹⁸⁵ Scorpionate complexes with an alkyl ligand in the axial position are reactive towards compounds with activated H atoms such that -SH, -SMe, -OEt, -OiPr, and -NHPH complexes have been prepared.¹⁵⁹

The relevance of the numerous reaction pathways is that the combination of axial symmetry and synthetic versatility makes this ligand system attractive for future work. Systematic alteration of the axial ligand can provide structurally related complexes wherein the axial ligand alters the magnetic properties and may provide for bridging between metal centers to examine magnetic properties in bimetallics.¹⁸⁷⁻¹⁸⁸

Sterically demanding hydrido-(trispyrazolyl)borates (Tp^R)⁻ are often referred to as "tetrahedral enforcers" to recognize their propensity to form 4-

coordinate, non-square planar complexes of first row transition metals.^{179, 182, 184, 189-190} Tetrahedral is somewhat misleading as the bond angles are closer to the 90° of an octahedral complex than the 109.47° of a true tetrahedral environment.^{161, 174} The $(\text{Tp}^{\text{R}})^-$ family of ligands is isolobal to the Cp^- ligand and often coordinates in the same fashion, occupying three positions on one face of a metal ion.¹⁵⁹ This often results in a C_3 symmetry about the metal center (Figure 2.2, right).

In contrast to $(\text{Cp})^-$, the electronic and steric effects can be more readily tuned, and this has led to some of the interest in $(\text{Tp}^{\text{R}})^-$ ligands in coordination and organometallic chemistry.^{161, 172} For catalytic and biomimetic chemistry much of the interest is engendered by the reduction of symmetry and coordination numbers that often accompany novel or increased reactivity of transition metal complexes.^{167, 171-172, 184, 191-194} Synthetically this can be challenging as $(\text{Tp}^{\text{R}})\text{MX}$ complexes are generally unstable and will undergo ligand exchange reactions to form $(\text{Tp}^{\text{R}})_2\text{M}$ complexes.¹⁶¹ These may or may not have all three pyrazole rings from the second scorpionate coordinated to the metal, dependent upon steric considerations.^{159, 191, 195}

The electronic structure and tunability of scorpionate complexes is being harnessed in the present work and has been investigated by other researchers.^{34, 97, 155, 172, 175, 186, 196-197} Of interest is the relationship between T_d and C_{3v} -symmetric mononuclear complexes. Interpretation of spectroscopic data for Ni has been accomplished by treating the C_{3v} case as a distorted T_d symmetry (Figure 2.3).^{155, 175} In this model the z^2 orbital is the most sensitive to

changes in donor strength, which can be seen in Figure 2.3 as the orbital increases in energy from left to right. From T_d to C_{3v} with a weak axial ligand, the electronic density oriented directly at the orbital increases, thus increasing the energy of the orbital. As the donor strength of the axial ligand increases, it further destabilizes the z^2 orbital.

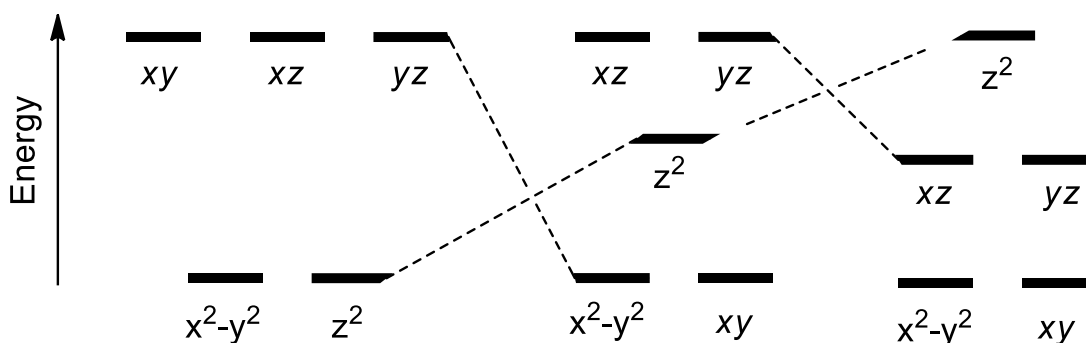


Figure 2.3. Relative orbital energies for T_d (Left) and C_{3v} -symmetric (Middle, Right) ligand fields. Adapted from 155.

2.2. Introduction to the Present Work

The preparation of $(\text{Tp}^{\text{Ph}})\text{MnCl}$ offers a material useful for comparison to other monometallic complexes and a possible reagent to prepare other complexes. Given the relatively weak ligand field of an $[\text{N}-3 \text{Cl}-1]$ environment, the complex is expected to have an $S = 5/2$ ground state with no orbital angular momentum contributions. No in-state SOC is possible in the 6A_1 ground state, as there is no electronic degeneracy and excited states violate spin selection rules or are very high in energy. From this it is expected that $(\text{Tp}^{\text{Ph}})\text{MnCl}$ will have a room temperature magnetic susceptibility close to the spin-only value and exhibit no out-of-phase to the AC magnetic susceptibility with or without a bias field.

Preparation and characterization of the complex as described in this work confirms these predictions.

Investigation of $(\text{Tp}^{\text{Ph}})\text{CoX}$ complexes is motivated by predicted magnetic properties and literature reports of SMM behavior in Co^{II} complexes.^{84, 86, 125, 128, 130, 140-142, 144, 146-147, 198} The syntheses of $(\text{Tp}^{\text{Ph}})\text{CoCl}$ and $(\text{Tp}^{\text{Ph}})\text{CoBr}$ were previously reported, albeit with limited infrared, UV-vis, and magnetic data.¹⁹¹ However, the axial symmetry, degenerate ground state, and large magnetic moment make the complexes attractive for investigation of magnetic properties. In C_{3v} symmetry, Co^{II} complexes are predicted to have a degenerate ground state, creating in-state SOC (Figure 2.4).¹⁵⁵ This can increase the magnetic anisotropy of the molecule, and the axial symmetry of the C_{3v} space group can render the transverse anisotropy $E = 0$. This suppresses quantum tunneling of the magnetization.³⁸

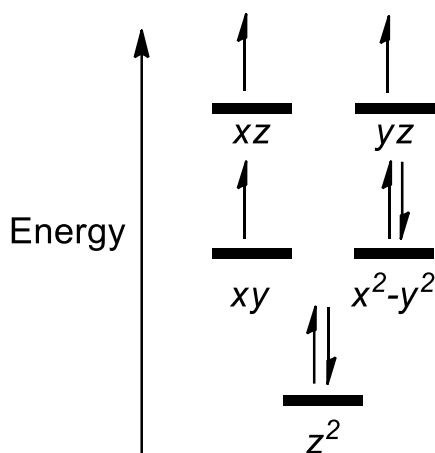


Figure 2.4. Relative ordering of orbitals for $(\text{Tp}^{\text{Ph}})\text{CoX}$ ($X = \text{Cl}, \text{Br}, \text{I}$). The z^2 orbital is most sensitive to the identity of the axial ligand. Here the orbital energies are plotted with a weak field ligand (halide) in the axial position.

Some of these possibilities have been realized in other Co^{II} complexes.

Monometallic SMMs with Co^{II} ions have been reported in the literature, including

one that shows zero field remnant magnetization.^{76, 84, 125, 128, 130, 132, 140-141} A series reported by Zdrozny et al.¹²⁵ contains $(\text{Ph}_4\text{P})_2[\text{Co}(\text{OPh})_4] \cdot (\text{CH}_3\text{CN})$, $(\text{Ph}_4\text{P})_2[\text{Co}(\text{SPh})_4]$, and $(\text{Ph}_4\text{P})_2[\text{Co}(\text{SePh})_4]$, three structurally related compounds with the largest change between them being the alteration of the coordinating atom of the ligands through the series, O, S, and Se (Figure 2.5).

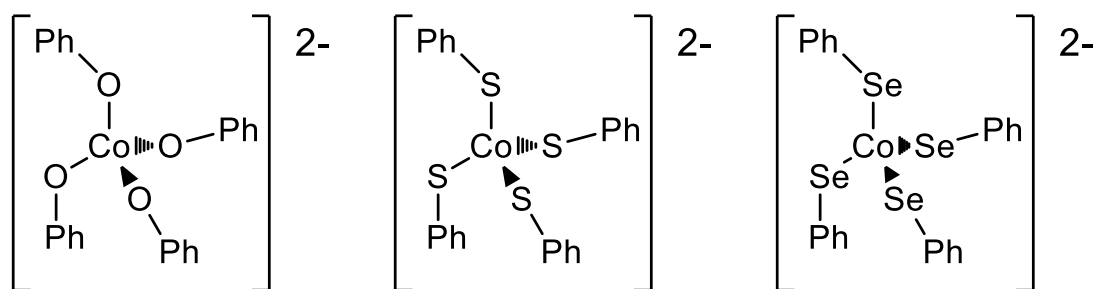


Figure 2.5. Structures of the anion of $(\text{Ph}_4\text{P})_2[\text{Co}(\text{OPh})_4] \cdot (\text{CH}_3\text{CN})$, $(\text{Ph}_4\text{P})_2[\text{Co}(\text{SPh})_4]$, and $(\text{Ph}_4\text{P})_2[\text{Co}(\text{SePh})_4]$ as reported by Zdrozny et al.¹²⁵

As Z increases for the coordinating atom, the ZFS value found by magnetic susceptibility measurements also increases. For $(\text{Ph}_4\text{P})_2[\text{Co}(\text{OPh})_4] \cdot (\text{CH}_3\text{CN})$ $D = -11.1 \text{ cm}^{-1}$, $(\text{Ph}_4\text{P})_2[\text{Co}(\text{SPh})_4]$ $D = -62 \text{ cm}^{-1}$, and $(\text{Ph}_4\text{P})_2[\text{Co}(\text{SePh})_4]$ $D = -83 \text{ cm}^{-1}$. While all three are approximately D_{2d} in symmetry, $(\text{Ph}_4\text{P})_2[\text{Co}(\text{OPh})_4] \cdot (\text{CH}_3\text{CN})$ shows tetragonal compression in contrast to $(\text{Ph}_4\text{P})_2[\text{Co}(\text{SPh})_4]$, and $(\text{Ph}_4\text{P})_2[\text{Co}(\text{SePh})_4]$, which both show tetragonal elongation. The authors argue that SOC, tetragonal distortion, and covalent interactions through larger orbitals in a weaker ligand field all contribute to increase the magnetic anisotropy. In examining $(\text{Tp}^{\text{Ph}})\text{CoX}$ ($X = \text{Cl}, \text{Br}, \text{I}$), it is reasonable to expect a similar trend to arise. This has been observed in a series of related Ni^{II} complexes, $(\text{Tp}^*)\text{NiX}$ ($X = \text{Cl}, \text{Br}, \text{I}$).¹⁵⁵ HFEPR measurements enabled detailed spin Hamiltonian analysis, which found strong contributions to

the ZFS parameter from the halides.¹⁵⁵ This resulted in experimentally determined D values of $+3.93(2) \text{ cm}^{-1}$, $-11.43(3) \text{ cm}^{-1}$, and $-23.01(4) \text{ cm}^{-1}$ for $(\text{Tp}^*)\text{NiCl}$, $(\text{Tp}^*)\text{NiBr}$, and $(\text{Tp}^*)\text{NiI}$. This supports the idea that substitution of Cl atoms with heavier halides can increase the SOC and in turn the magnetic anisotropy.¹⁷⁵ The increased magnetic anisotropy could result in greater magnetic hysteresis arising from a large D value, minimal E , and higher blocking temperatures, QTM notwithstanding.

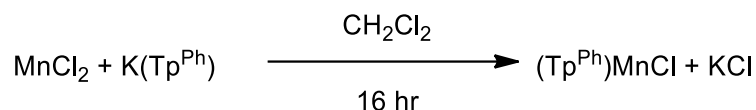
Previously, Ni^{II} complexes with axial symmetry have been reported to exhibit SMM behavior.¹⁵¹ This arises from out-of-state or excited state SOC as they assume a non-degenerate ground state.¹⁵⁵ Since excited states may be low in energy, it is possible that significant mixing could occur. Additionally, preparation of Ni^{II} scorpionate complexes will yield reagents for the preparation of heterobimetallics and Ni^{I} and Ni^{III} complexes that may show in-state SOC.

As a diamagnetic control for comparison purposes, the synthesis of $(\text{Tp}^{\text{Ph}})\text{ZnCl}$ was completed and the product characterized. This compound also provides a reagent for magnetic dilution experiments.^{131, 199}

2.3. Results and Discussion

2.3.1. Synthesis

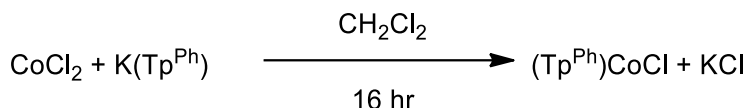
The first compound in the series moving across the first row is $(\text{Tp}^{\text{Ph}})\text{MnCl}$. This was prepared by a salt metathesis reaction between MnCl_2 and $\text{K}(\text{Tp}^{\text{Ph}})$ (Scheme 2.2).



Scheme 2.2. Salt metathesis reaction to prepare (Tp^{Ph})MnCl.

K(Tp^{Ph}) is soluble in dichloromethane while the MnCl₂ is insoluble.¹⁶¹ However, after stirring for an extended period of time the ligand chelates MnCl₂ and the product is soluble. The insolubility of KCl in dichloromethane precludes the reverse reaction, driving it to completion. After 16 hr of stirring the supernatant takes on a straw or tan color and can be filtered. This salt metathesis route in low polarity, poorly coordinating solvents proves to be effective for the preparation of other complexes in the series.

The synthesis of (Tp^{Ph})CoCl is shown in Scheme 2.3.

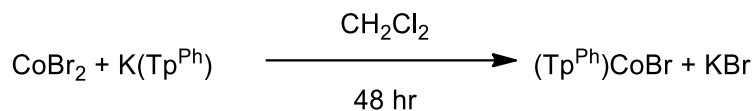


Scheme 2.3. The synthesis of (Tp^{Ph})CoCl by salt metathesis.

Again, salt metathesis and the production of insoluble KCl drives the reaction forward. Purification was accomplished by drying the reaction mixture in vacuo at 60 °C and extracting with tetrahydrofuran. This was more effective than re-dissolving in dichloromethane, which did not extract the product as effectively, and prolonged stirring would pulverize the KCl making it more difficult to remove via filtration. After filtering, layering with hexanes and standing at -20 °C gave a crystalline product.

The synthesis of (Tp^{Ph})CoBr (Scheme 2.4) proved more complicated than

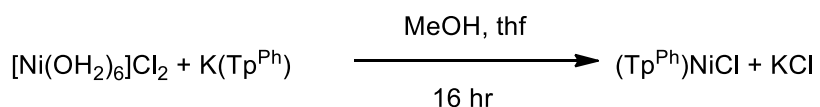
that of other compounds.



Scheme 2.4. Synthesis of α - and β -(Tp^{Ph})CoBr

The stirring time was increased as the reaction progressed more slowly than the preparation of the chloride complex. The evacuation, extraction, and filtration were carried out similarly to (Tp^{Ph})CoCl except that dichloromethane was used to re-dissolve the crude reaction mixture. It appears that the bromide complex is more soluble in dichloromethane than the chloride complex. Layering with pentanes and standing at -20 °C gives not one but two crystalline products, the α - and β -polymorphs. No lattice solvent is incorporated in either, the only difference is in the crystal packing arrangement and bond distances and angles. These can be separated by the Pasteur method (visual inspection and manual separation with the aid of a microscope). Alternately, the crystals can be rinsed with cold acetone, in which the β -polymorph dissolves more rapidly and can be washed away.

The preparation of (Tp^{Ph})NiCl proceeded by (Scheme 2.5).



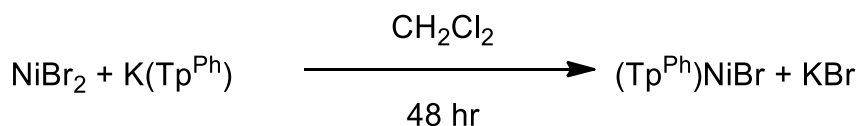
Scheme 2.5. Synthesis of (Tp^{Ph})NiCl.

The crude reaction mixture included two products, the desired (Tp^{Ph})NiCl and (Tp^{Ph})Ni(phpy)Cl (phpy = 5-phenylpyrazole) resulting in a mustard color.

Fractional recrystallization in dichloromethane and diethyl ether separated the

two complexes as $(\text{Tp}^{\text{Ph}})\text{NiCl}$ was less soluble in nonpolar solvents. The isolation of pyrazole adducts of other Ni scorpionate complexes has been reported.^{182, 185} Attempts to prepare $(\text{Tp}^{\text{Ph}})\text{NiCl}$ from anhydrous NiCl_2 resulted in low yields due to the insolubility of NiCl_2 in nonpolar solvents and the increased acidity of partially dehydrated hydrates of Ni^{II} . This leads to hydrolysis of the scorpionate.¹⁸⁵

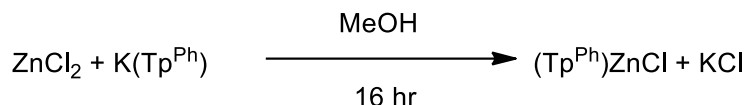
In contrast to $(\text{Tp}^{\text{Ph}})\text{NiCl}$, the bromide could be prepared from anhydrous NiBr_2 (Scheme 2.6). Stirring for two days was sufficient for the reaction to proceed, suggesting that anhydrous NiBr_2 is more soluble in dichloromethane, perhaps due to the larger polarizability of Br^- versus Cl^- . Purification was accomplished by decanting to remove KBr , drying to isolate a crude solid, and recrystallization from dichloromethane and pentanes.



Scheme 2.6. Preparation of $(\text{Tp}^{\text{Ph}})\text{NiBr}$ by salt metathesis in dichloromethane.

The preparation of $(\text{Tp}^{\text{Ph}})\text{ZnCl}$ was performed again by salt metathesis (Scheme 2.7).

Owing to the d^{10} configuration, no colors were observed. A white precipitate of KCl formed from the clear solution, which was then decanted and evaporated. The white crude product was then recrystallized from dichloromethane with pentanes as a counter solvent to yield a clear crystalline product.



Scheme 2.7. Synthesis of (Tp^{Ph})ZnCl by salt metathesis.

The yields for these reactions ranged from 43-65%, which is in line with yields reported for similar compounds and syntheses.^{161, 184} The yields may be determined by the solubility of the metal salts as similar reactions with tetrafluoroborate salts of transition metals typically have higher yields.¹⁹⁶ Higher yields are also possible with TI salts of scorpionate ligands, but these were avoided due to toxicity.¹⁸² Trace amounts of water can cause hydrolysis of the (Tp^{Ph})⁻ ligand, which may have impacted the yields, especially in the case of (Tp^{Ph})NiCl, where a six-fold stoichiometry of water was introduced into the reaction mixture by use of the hydrated salt of Ni.¹⁸²

2.3.2. Infrared Spectroscopy

The B-H bond in hydridotrispyrazolylborato complexes provides a spectroscopic handle that correlates with the electron donation from ligand to metal ion.²⁰⁰ Potassium hydridotris(3-phenylpyrazolyl)borate shows a single absorption band at 2415 cm⁻¹ which shifts to higher energies upon binding with first row transition metals.¹⁶¹ The B-H stretches for the compounds described above are listed in Table 2.1.

Table 2.1. B-H bond stretching energies.

| Compound | ν (B-H) (cm ⁻¹) |
|-------------------------------|---------------------------------|
| K(Tp ^{Ph}) | 2415 |
| (Tp ^{Ph})MnCl | 2474 |
| (Tp ^{Ph})CoCl | 2495 |
| (Tp ^{Ph})CoBr | 2479 |
| (Tp ^{Ph})CoI | 2478 |
| (Tp ^{Ph})NiCl | 2478 |
| (Tp ^{Ph})NiBr | 2504 |
| (Tp ^{Ph})NiI | 2503 |
| (Tp ^{Ph})Ni(phpy)Cl | 2503 |
| (Tp ^{Ph})ZnCl | 2512 |

The negative charge of the ligand, when uncompensated by covalent binding of a metal ion, results in more antibonding character for the B-H bond, weakening it and resulting in a lower vibrational energy.

Overall, the compounds follow a trend of increasing B-H stretching energies moving from left to right across the first-row transition metals. This is attributable to the increase of Z_{eff} moving from left to right, caused by incomplete shielding of the nuclear charge by d electrons. The increased charge draws more electron density away from the (Tp^{Ph})⁻ ligand, increasing the B-H stretch energy. It is important to note that the pattern is not strict, overlap exists between the

ranges of Co and Ni complexes. This indicates that multiple effects are in play, and they are similar in magnitude.

For Co complexes, the ν (B-H) values decrease as the halides increase in mass. This is consistent with stronger bonding between metal and halide, lessening the inductive effect by the metal on the (Tp^{Ph})⁻ ligand. In contrast to the changing of the metal ion present, descending the halide series greatly increases Z . This is relevant as SOC is proportional to Z , so changing from Cl ($Z = 17$) to Br ($Z = 35$) to I ($Z = 53$) has the potential to greatly increase SOC affecting the magnetic properties, if the magnetic orbitals of the resulting complex include substantial halide character.¹⁷⁵

For Co, many complexes with weaker ligands are known, including halides and pseudo-halides, which are included in Table 2.2 and used for comparison. Comparison of the cobalt complexes in Table 2.1 to these compounds shows that they fall on the lower end of ν (B-H) energies. This suggests a weaker interaction between ligand and metal than seen in most analogous compounds. If the interaction is weaker, two processes could have a greater impact on the magnetic properties. First, the interaction between halide and metal can be stronger, leading to greater SOC in the heavier halides. The second is a weaker crystal field, which will also reduce the quenching of SOC. Based on this, it is expected that the magnetic anisotropy will follow the order (Tp^{Ph})CoCl < (Tp^{Ph})CoBr < (Tp^{Ph})CoI.

In the case of Ni, descending group VIIA does not systematically alter the ν (BH) frequency. The chloride ν (BH) = 2478 cm⁻¹, bromide ν (BH) = 2504 cm⁻¹,

and iodide $\nu(\text{BH}) = 2503 \text{ cm}^{-1}$. Comparison of $\nu(\text{BH})$ values for $(\text{Tp}^{\text{Ph}})\text{NiCl}$, $(\text{Tp}^{\text{Ph}})\text{NiBr}$, and $(\text{Tp}^{\text{Ph}})\text{NiI}$ to related complexes shows that the values are redshifted versus the analogous $(\text{Tp}^{\text{Ph,Me}})$ complexes $(\text{Tp}^{\text{Ph,Me}})\text{NiCl}$ (2544 cm^{-1}), $(\text{Tp}^{\text{Ph,Me}})\text{NiBr}$ 2547 cm^{-1} , $(\text{Tp}^{\text{Ph,Me}})\text{NiI}$ (2544 cm^{-1}).¹⁸² This is an average difference of 50 cm^{-1} , surprisingly large given the structural similarity of $(\text{Tp}^{\text{Ph}})^-$ and $(\text{Tp}^{\text{Ph,Me}})^-$. Measurements and calculations on similar compounds suggest that increasing covalency is present in the Ni-X bond moving from $(\text{Tp}^{\text{Ph}})\text{NiCl}$ to $(\text{Tp}^{\text{Ph}})\text{NiI}$.^{155, 175} As the covalency increases, presumably from improved orbital overlap, the effective charge of the metal ion is decreased, leaving more electron density on the scorpionate ligand. Based on the $\nu(\text{BH})$ and Z values, we propose that magnetic anisotropy, if observed, will be $(\text{Tp}^{\text{Ph}})\text{NiCl} < (\text{Tp}^{\text{Ph}})\text{NiBr} < (\text{Tp}^{\text{Ph}})\text{NiI}$ since Z is proportional to SOC and the increasing energy of $\nu(\text{B-H})$ indicates a stronger interaction between the halide and metal, introducing more halide character to the magnetic orbitals.

Table 2.2. Literature $\nu(\text{BH})$ values for selected complexes.

| compound | $\nu(\text{BH})$ (cm^{-1}) | sample preparation | reference |
|---|---------------------------------------|--------------------|-----------|
| $(\text{Tp}^{\text{t}})\text{MnCl}$ | 2506 | KBr pellet | 201 |
| $(\text{Tp}^{\text{t-Bu}})\text{MnCl}$ | 2519 | Nujol mull | 202 |
| $(\text{Tp}^{\text{Ph,Me}})\text{MnCH}_2\text{Si}(\text{Me})_3$ | 2543 | Nujol mull | 185 |
| $(\text{Tp}^{\text{Ph,Me}})\text{MnCH}_2\text{Ph}$ | 2543 | Nujol mull | 185 |
| $(\text{Tp}^{\text{Np}})\text{Co}(\text{NNN})$ | 2490 | Nujol mull | 203 |

| | | | |
|-------------------------------|------|---------------|-----|
| (Tp ^{Np})Co(NCO) | 2495 | Nujol mull | 203 |
| (Tp ^{i-Pr})Co(NCS) | 2495 | Nujol mull | 204 |
| (Tp ^{Np})CoCl | 2495 | Nujol mull | 203 |
| (Tp ^{Ph})CoBr | 2502 | None reported | 191 |
| (Tp ^{Ph})CoCl | 2503 | None reported | 191 |
| (Tp ^{t-Bu})Co(NNN) | 2505 | Nujol mull | 161 |
| (Tp ^{Ph})Co(NCS) | 2510 | Nujol mull | 161 |
| (Tp ^{Ph})Co(NCO) | 2510 | Nujol mull | 161 |
| (Tp ^{t-Bu})Co(NCO) | 2515 | Nujol mull | 161 |
| (Tp')CoCl | 2520 | KBr pellet | 201 |
| (Tp ^{i-Pr})Co(NCO) | 2524 | Nujol mull | 204 |
| (Tp ^{t-Bu})CoCl | 2540 | Nujol mull | 161 |
| (Tp ^{t-Bu})CoF | 2545 | Nujol mull | 202 |
| (Tp ^{Ph,Me})Co(NNN) | 2549 | Nujol mull | 185 |
| (Tp')Co(NCS) | 2550 | KBr pellet | 201 |
| (Tp ^{Np})CoI | None | None reported | 205 |
| | | reported | |

| | | | |
|--|------|------------|-----|
| (Tp ^{Ph,Me})NiCH ₂ Ph | 2472 | Nujol mull | 185 |
| (Tp ^{i-Pr})Ni(NCS) | 2480 | Nujol mull | 204 |
| (Tp ^{Np})Ni(NNN) | 2490 | KBr pellet | 174 |
| (Tp ^{Np})NiCl | 2495 | Nujol mull | 203 |
| (Tp ^{Np})Ni(NCO) | 2495 | Nujol mull | 203 |
| (Tp ^{Np})Ni(NCS) | 2495 | Nujol mull | 203 |

| | | | |
|---|----------|---------------|-----|
| (Tp ^{Np})Ni(NNN) | 2495 | Nujol mull | 203 |
| (Tp ^{Np})Ni(NCO) | 2495 | Nujol mull | 174 |
| (Tp ^{t-Bu})Ni(NCO) | 2495 | KBr pellet | 174 |
| (Tp') | 2495 | KBr pellet | 174 |
| (Tp ^{ρ-tol})Ni(NCS) | 2504 | KBr pellet | 174 |
| (Tp ^{i-Pr})Ni(NCO) | 2505 | Nujol mull | 204 |
| (Tp ^{Np})Ni(NCS) | 2510 | Nujol mull | 174 |
| (Tp ^{t-Bu})Ni(NCS) | 2510 | KBr pellet | 174 |
| (Tp ^{t-Bu})Ni(NCO) | 2515 | Nujol mull | 161 |
| (Tp ^{t-Bu})Ni(NNN) | 2515 | Nujol mull | 161 |
| (Tp ^{t-Bu})Ni(NCS) | 2527 | Nujol mull | 161 |
| (Tp ^{Ph,Me})NiCH ₂ Si(Me) ₃ | 2527 | Nujol mull | 185 |
| (Tp ^{Ph,Me})Ni(NNN) | 2543 | Nujol mull | 185 |
| (Tp ^{Ph,Me})NiCl | 2544 | KBr pellet | 182 |
| (Tp ^{Ph,Me})NiI | 2544 | KBr pellet | 182 |
| (Tp ^{t-Bu,Me})Ni(NNN) | 2545 | KBr pellet | 174 |
| (Tp ^{t-Bu,Me})Ni(NCO) | 2545 | KBr pellet | 174 |
| (Tp ^{Ph,Me})NiBr | 2547 | KBr pellet | 182 |
| (Tp') | None | None reported | 204 |
| (Tp')Ni(NCS) | reported | | |
| <hr/> | | | |
| (Tp ^{Np})Zn(NNN) | 2495 | Nujol mull | 203 |
| (Tp ^{Np})ZnCl | 2495 | Nujol mull | 203 |
| (Tp ^{Np})Zn(NCO) | 2495 | Nujol mull | 203 |

| | | | |
|------------------------------|------|------------|-----|
| (Tp ^{t-Bu})Zn(NNN) | 2502 | Nujol mull | 161 |
| (Tp ^{Ph})Zn(NNN) | 2505 | Nujol mull | 161 |
| (Tp ^{Ph})Zn(NCS) | 2508 | Nujol mull | 161 |
| (Tp ^{t-Bu})Zn(NCO) | 2510 | Nujol mull | 161 |
| (Tp ^{Ph})Zn(NCO) | 2510 | Nujol mull | 161 |
| (Tp')Zn(Cl) | 2510 | Nujol mull | 204 |
| (Tp ^{i-Pr})Zn(NNN) | 2510 | Nujol mull | 178 |
| (Tp ^{i-Pr})Zn(NCS) | 2512 | Nujol mull | 204 |
| (Tp ^{Np})Zn(NCS) | 2515 | Nujol mull | 203 |
| (Tp ^{i-Pr})Zn(NCO) | 2520 | Nujol mull | 204 |
| (Tp ^{t-Bu})Zn(NCS) | 2529 | Nujol mull | 161 |
| (Tp')Zn(NNN) | 2550 | Nujol mull | 204 |
| (Tp')Zn(NCS) | 2550 | Nujol mull | 204 |
| (Tp')Zn(NCO) | 2550 | Nujol mull | 204 |

Electrochemical study of (Tp^{Ph})NiX (X = Cl, Br, I) by Dougherty et. al indicates a dissimilar electronic environment from (Tp^{t-Bu})NiX (X = Cl, Br, I) complexes.¹⁷⁹

This precludes a closer comparison or reasoning by analogy to describe the chemical properties of (Tp^{Ph})⁻ complexes. The electron-withdrawing effect of phenyl rings vs. *t*-Bu substituents decreases the donor strength of the scorpionate ligand. This is shown in reduction potentials for (Tp^{t-Bu})⁻ vs. (Tp^{Ph})⁻ scorpionates where the reduction of the (Tp^{Ph})⁻ complexes occurs under less reducing conditions vs. the (Tp^{t-Bu})⁻. With alteration of the halide little change is seen in the reduction potentials, which they hypothesize is related to distortion of

the coordination environments, which tempers the orbital overlap trends.¹⁷⁹ This fits with the ν (B-H) frequencies to a degree. For $(\text{Tp}^{\text{Ph}})\text{NiBr}$ and $(\text{Tp}^{\text{Ph}})\text{NiI}$, the stretching frequencies are almost identical. Since the reduction potentials of the Cl and Br are within 0.04 V of each other, and the stretching frequencies for $(\text{Tp}^{\text{Ph}})\text{NiBr}$ and $(\text{Tp}^{\text{Ph}})\text{NiI}$ are also close, it suggests that the $(\text{Tp}^{\text{Ph}})^-$ ligand and halides are similar in donor strength such that as one increases donation the other decreases, resulting in a very similar electronic environment for the Ni^{II} ion. This will be further demonstrated in the UV-vis measurements (*vide infra*). While it appears that axial ligand identity can alter the ν (B-H) frequency, the determining factor remains the identity of the transition metal.

2.3.3. UV/vis/NIR Spectroscopy

To determine the electronic ground state and in some cases estimate the strength of the ligand field, electronic spectra were collected for $(\text{Tp}^{\text{Ph}})\text{MnCl}$, $(\text{Tp}^{\text{Ph}})\text{CoCl}$, α - $(\text{Tp}^{\text{Ph}})\text{CoBr}$, and β - $(\text{Tp}^{\text{Ph}})\text{CoBr}$.⁵⁰ If the complexes were of T_d or O_h symmetry, interpretation would be as straightforward as consulting Tanabe Sugano diagrams.^{158, 206-207} While the complexes are not, the electronic spectra can sometimes be interpreted by treating the deviation from higher symmetry as a perturbation of the parent symmetry group, and this approach is applied to the Co compounds in this work.^{155, 172, 195} A given band present in T_d or O_h symmetry can be split into two or more bands in a manner that can be predicted to a certain degree based on symmetry arguments with mixing being the predominant factor in deviations. This approach has literature precedence especially for the Co and

Ni compounds.^{191, 208-209} Calculations and band assignments have been determined by comparison to the tetrahedral Tanabe-Sugano secular equations for the appropriate electron count for many related complexes.¹⁵⁸ There is no indication in the electronic spectra, magnetic data, or X-ray structures of ligand non-innocence, which would alter the electron count at the metal center necessitating the use of Tanabe-Sugano secular equations for a different d electron count than those for the reagent metal ion.^{50, 210-211}

For (Tp^{Ph})MnCl, The UV-vis spectrum in dichloromethane shows no absorptions, which is consistent with the 6A_1 ground state. Given that there are no excited states above 6A_1 easily accessed at room temperature, all transitions are spin-forbidden with the effect that there can be minimal excited state contributions to SOC. This does not preclude excited state contributions to the ZFS, however, as the selection rule is that any transition where $\Delta S = 0, \pm 1$ contributes to the ZFS.³⁵ The large energy differences between ground and excited states that meet the $\Delta S = 0, \pm 1$ selection rule likely minimize this effect, which would lead to an isotropic, spin only magnetic moment. These two inferences are supported by magnetic data (*vide infra*, Section 2.3.3). Since the ground state is isotropic and well-separated from any excited states that could contribute to SOC or ZFS, the magnetic moment is expected to be spin-only and isotropic overall.

For the (Tp^{Ph})CoX complexes (Tp^{Ph})CoCl and (Tp^{Ph})CoBr, the collected spectral data is similar to spectroscopy data and calculations available in literature sources.^{97, 125, 172, 174, 189, 191, 205, 208-209, 212-214} As mentioned previously,

C_3 and D_2 symmetric chromophores are treated as variations of T_d spectra, that is to say, the spectra are analyzed as a distortion of the T_d T-S diagram for tetrahedral d^7 ions. Naturally, a splitting of bands arises, yet the Co^{II} spectra of 4-coordinate complexes with C_3 or D_2 symmetry still show similarities to the T_d spectrum.^{84, 172, 191, 196, 212} For a free d^7 ion, two terms of relevance are present: the 4F ground state and the 4P excited state.^{50, 158} In a tetrahedral crystal field the 4F ground state splits into a 4A_2 ground state and 4T_1 and 4T_2 excited states. The 4P term changes to 4T_1 .⁸⁴

It has been proposed that excited state J-T effects leads to splitting of the $^4T_1(P)$ band even in T_d environments, which fits with the fine structure observed for these types of complexes.²⁰⁸ In C_{3v} , d^7 configurations still have a degenerate ground state whereas in D_2 they do not, yet D_2 complexes still show fine structure.⁸⁴ To explain the wider phenomenon, SOC and vibronic coupling have both been invoked.¹⁷² In C_{3v} symmetry mixing between the xz , yz , and xy , x^2-y^2 orbital pairs is allowed, which could also be the origin of the splitting.⁹⁷ Theoretical investigations support the conclusion that accurate interpretation of Co^{II} spectral data requires full configuration interaction calculations.²¹⁵

The Co^{II} complexes exhibit similar spectra. They both have several convolved peaks around 625 nm, a broad absorption above 900 nm, and another around 1650 nm in the near infrared (Figure 2.7, Figure 2.8). The extinction coefficients are in the range ($\epsilon = 50\text{-}800 \text{ M}^{-1}\text{cm}^{-1}$) expected for $d-d$ transitions in a tetrahedral ligand field where transitions are spin-forbidden but Laporte-allowed (Table 2.3).⁵⁰

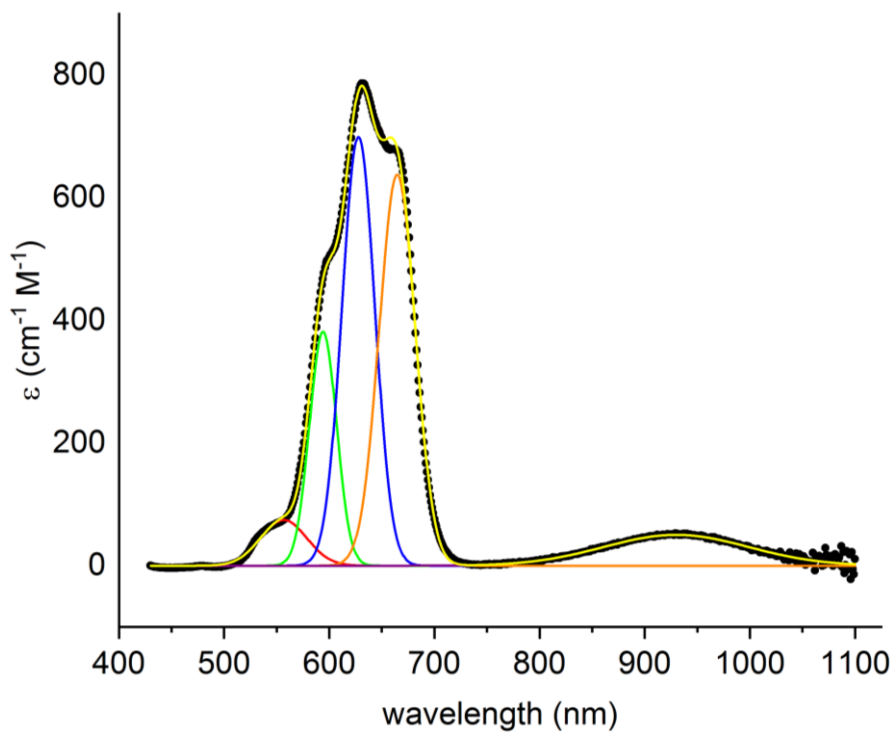


Figure 2.7. Deconvolution of UV-visible absorption spectrum of $(Tp^{Ph})CoCl$. • = experimental spectrum, •,•,•,•,• = fitted peaks, • = fitted curve.

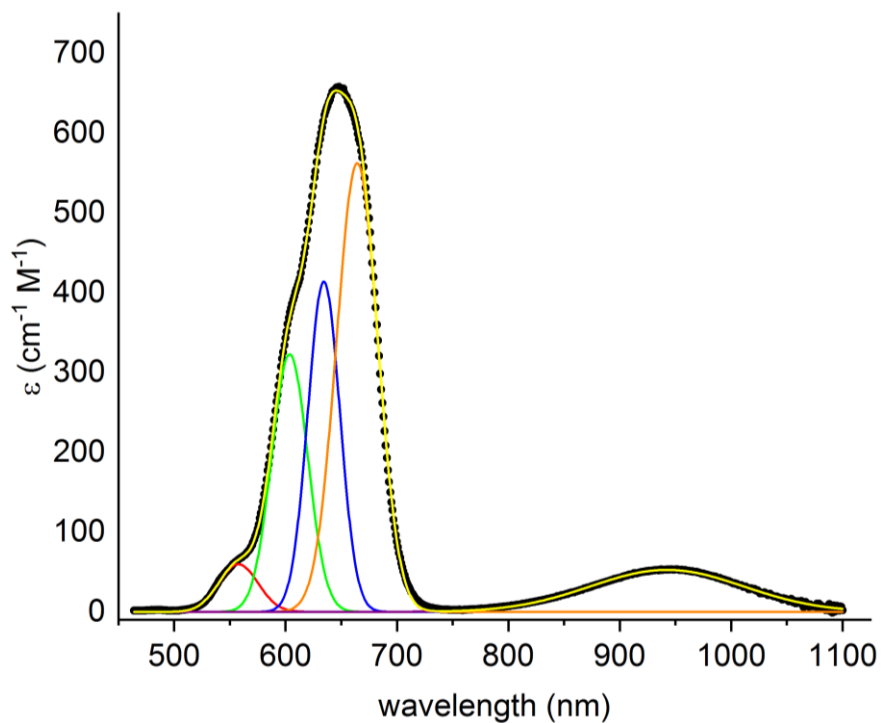


Figure 2.8. Deconvolution of UV-visible absorption spectrum of $(Tp^{Ph})CoBr$. • = experimental spectrum, •,•,•,•,• = fitted peaks, • = fitted curve.

Table 2.3. Electronic spectra of (Tp^{Ph})CoCl and (Tp^{Ph})CoBr.

| Compound | Solvent | ${}^4T_1(P) \leftarrow {}^4A_2$ | ${}^4T_1(F) \leftarrow {}^4A_2$ | ${}^4T_2(F) \leftarrow {}^4A_2$ |
|-------------------------|---------------------------------|---------------------------------|---------------------------------|---------------------------------|
| (Tp ^{Ph})CoCl | CH ₂ Cl ₂ | 544 (60) sh | | |
| | | 586 (400) sh | | |
| | | 632 (800) | | |
| | | 663 (700) sh | | |
| | CCl ₄ | | 933 (50) | 1653 (70) |
| (Tp ^{Ph})CoBr | CH ₂ Cl ₂ | 561 (70) sh | | |
| | | 598 (300) sh | | |
| | | 643 (600) | | |
| | | 673 (500) sh | | |
| | CCl ₄ | | 942 (50) | 1691 (80) |

The electronic spectrum for (Tp^{Ph})CoCl is plotted in Figure 2.7. The peaks at 544, 586, 632, and 663 nm are all assigned to the ${}^4T_1(P) \leftarrow {}^4A_2$ transition.^{172, 216-217} The splitting of a single band into multiple absorptions has been noted in many 4-coordinate Co^{II} systems.^{172, 191, 208}

Peaks in the (Tp^{Ph})CoBr spectrum (Figure 2.8) are red-shifted in comparison to (Tp^{Ph})CoCl, and the peaks around 625 nm are less distinct than in (Tp^{Ph})CoCl. Nevertheless, attempts to fit the spectrum with fewer peaks resulted in poorer fits, and the spectra are otherwise quite similar. The results of the peak fitting are presented in Table 2.3 and further parameters for all fittings are presented in Table A.1.

The spectra of $(\text{Tp}^{\text{Ph}})\text{CoCl}$ and $(\text{Tp}^{\text{Ph}})\text{CoBr}$ can be discussed together as they are similar. Several challenges to the traditional electronic spectra interpretation methods have been observed.²¹⁸ The absence of an inversion center allows the mixing of p and d orbitals, which is reflected in the increased extinction coefficients for formally $d-d$ transitions in comparison to octahedral complexes, which possess an inversion center. SOC is allowed, which splits bands, as well as bands present due to low symmetry components of the ligand field. It has also been noted that excited states for the $^4A_2 \text{Co}^{\text{II}}$ ion could be perturbed due to second order J-T distortions. Even in the case of tetrahedral Co^{II} complexes with halide ligands the electronic spectra differ from that predicted by the Tanabe-Sugano diagram, which indicates some mixing of electronic states.^{172, 208, 217} The listed effects make Co^{II} ions magnetically interesting, but also complicates the interpretation of electronic spectra. Herein we will attempt an interpretation of the data using the approach of Telser et al.¹⁷², which builds on the work of Jesson and Larrabee.^{172, 217-218} In this approach, the multiplet near 625 nm is analogous to the $^4T_1(\text{P}) \leftarrow ^4A_2$ transition, which splits into 4A_2 and 4E bands in C_{3v} . At lower energies, the $^4T_2(\text{F}) \leftarrow ^4A_2$ and $^4T_1(\text{F}) \leftarrow ^4A_2$ absorptions are observed. It is interesting to note that the multiplet observed around 600 nm is also observed in tetrahedral Co^{II} complexes where the Tanabe-Sugano secular equations predict a single absorption band.^{172, 208, 217} This has been ascribed to vibronic coupling, which can occur in higher symmetry systems, leaving open to debate the origin of this multiplet, whether from vibronic coupling or the reduction in symmetry. From these band assignments Racah

parameters can be calculated to estimate the effect of the ligand field on SOC. The coupling of spin and orbital angular momentum is maximized in the free ion, and the Racah parameter B can be used to calculate the nephelauxetic parameter. As the nephelauxetic parameter approaches the free ion value, so too will the SOC. For $(\text{Tp}^{\text{Ph}})\text{CoCl}$ and $(\text{Tp}^{\text{Ph}})\text{CoBr}$ the calculations were made using the ${}^4T_2(\text{F}) \leftarrow {}^4A_2$ and ${}^4T_1(\text{F}) \leftarrow {}^4A_2$ bands as these are not split by SOC or vibronic coupling. Table 1.4 shows the results. The β values in Table 1.4 indicate that SOC gives $(\text{Tp}^{\text{Ph}})\text{CoCl}$ and $(\text{Tp}^{\text{Ph}})\text{CoBr}$ over 85% of the free ion value. The nephelauxetic ratios are higher than the values for $(\text{CoCl}_4)^{2-}$ and $(\text{CoBr}_4)^{2-}$ which are 0.72 and 0.70, respectively.⁵⁰ These results seem implausibly high and as such bring the underlying assumptions into question.

Table 2.4. Transitions and calculated crystal field values for Co^{II} complexes.

| | Transitions as assigned in T_d | | Calculated values | | |
|--------------------------------------|--|--|-------------------------|---------|--------------------------------|
| | (cm ⁻¹) | | B (cm ⁻¹) | β | Δ_T (cm ⁻¹) |
| | ${}^4T_1(\text{F}) \leftarrow {}^4A_2$ | ${}^4T_2(\text{F}) \leftarrow {}^4A_2$ | | | |
| $(\text{Tp}^{\text{Ph}})\text{CoCl}$ | 10616 | 5928 | 861 | 0.87 | 2635 |
| $(\text{Tp}^{\text{Ph}})\text{CoBr}$ | 10616 | 5910 | 866 | 0.88 | 2627 |

To better examine the electronic structure, calculations were performed by Dr. Eric Majzoub. The structure was taken from X-ray data and used without optimization. Calculations were completed with GAMESS-US with multiple basis

sets including unrestricted Hartree-Fock and High Spin Open Shell Self-Consistent Field Theory methods.²¹⁹⁻²²¹ Basis sets used were TZV, N31, PW91, and B3LLYP.²²²⁻²²⁴ All calculations that converged arrived at the same ordering of the *d* subshell as depicted below. The results are shown in Figure 2.9. This ordering places an 4E state lowest in energy which is consistent with the large, presumably in-state SOC seen in the magnetic data (vide supra). The calculations show significant SOC coupling that spreads electron density over multiple atoms, especially Co and Cl. This renders the quantum numbers less descriptive as the microstates are not orthogonal and significant mixing is present. Since the 4A_2 state is no longer lowest in energy, the values calculated in Table 2.4 can no longer be considered valid. It is not clear from the data, nor can it be determined, how general this change of the ground state from 4A_2 to 4E is for pseudo-tetrahedral Co^{II} complexes. With a 4E ground state, the z^2 orbital of Co must be lowest in energy, which supports the idea that the interaction between the halide and (Tp^{Ph})Co⁺ fragment is largely electrostatic. This is at odds with Telser et al. having observed that the extinction coefficient values are sensitive to the identity of the axial ligand and that this indicates significant ligand character in the *d* orbitals.¹⁷² They argue that one result is that the axial ligand affects the SOC in a significant manner, which is true in the compounds they have studied. However, referring to ions like NCS⁻, NNN⁻, and NCO⁻ as pseudo-halides due to their position on the spectrochemical series may linguistically blur an important distinction: these pseudo-halides tend to be π acceptors whereas

halides are most often π donors. This difference may explain the weak covalent interaction of the halides versus the pseudo-halides.

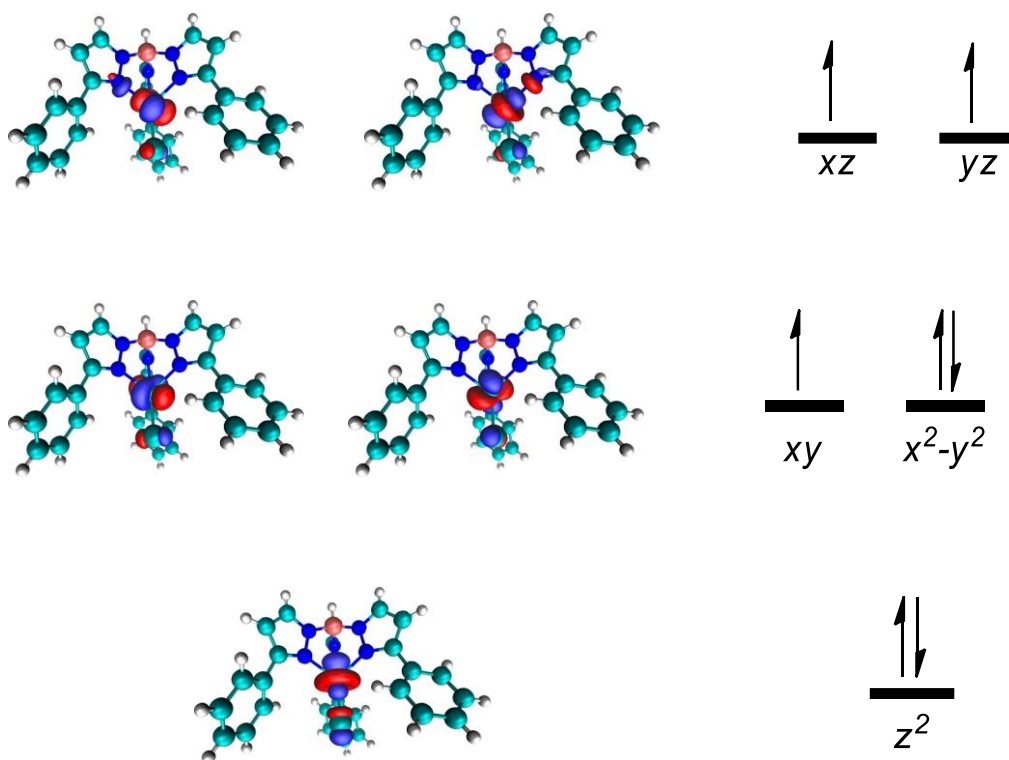


Figure 2.9. Left: Frontier orbitals of $(Tp^{Ph})CoCl$ as determined from preliminary DFT calculations. Right: Corresponding orbitals and the ground state electronic configuration.

Changing the ground state from 4A_2 , which has no expected in-state orbital contribution to the magnetic moment, to 4E with allowed in-state SOC has the potential to alter the ZFS by increasing the magnitude of D . The drop from cubic to axial symmetry also decreases the transverse anisotropy term, E , potentially to zero (not to be confused with the term symbol). The potential increase of SOC is supported by the Racah parameter B and the nephelauxetic ratio, β .

For the Ni^{II} series, the electronic spectra are similar to each other and literature reports of related Ni scorpionates.^{155, 174} Two convolved peaks are

present around 500 nm, with two peaks at 800 and 900 nm (Figure 2.10, Figure 2.11). The peaks at 500 nm and 800 nm are narrow, while the peak at 900 nm is broad.

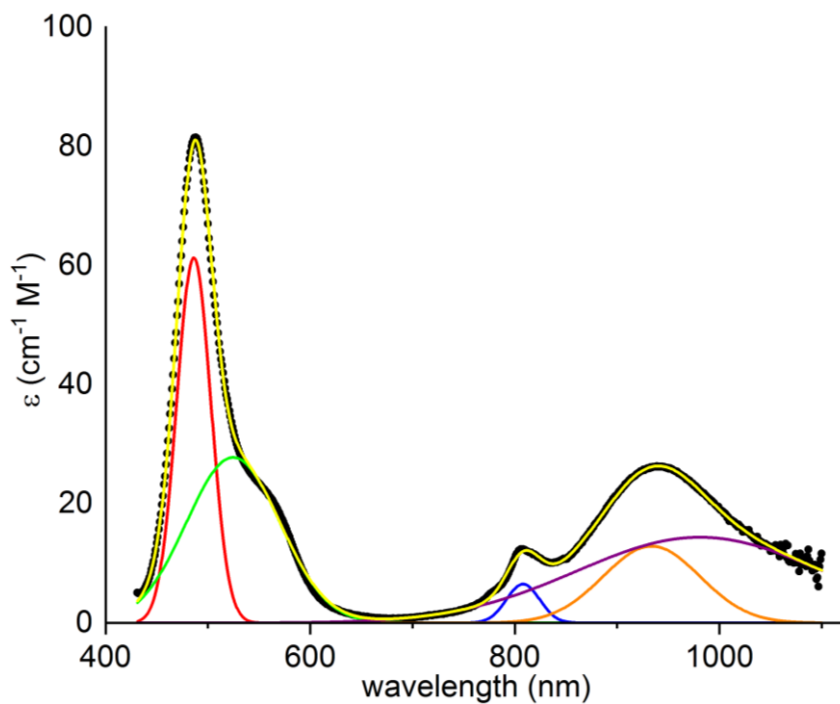


Figure 2.10. Deconvolution of UV-visible absorption spectrum of $(Tp^{Ph})NiCl$. • = experimental spectrum, •,•,•,•,• = fitted peaks, • = fitted curve.

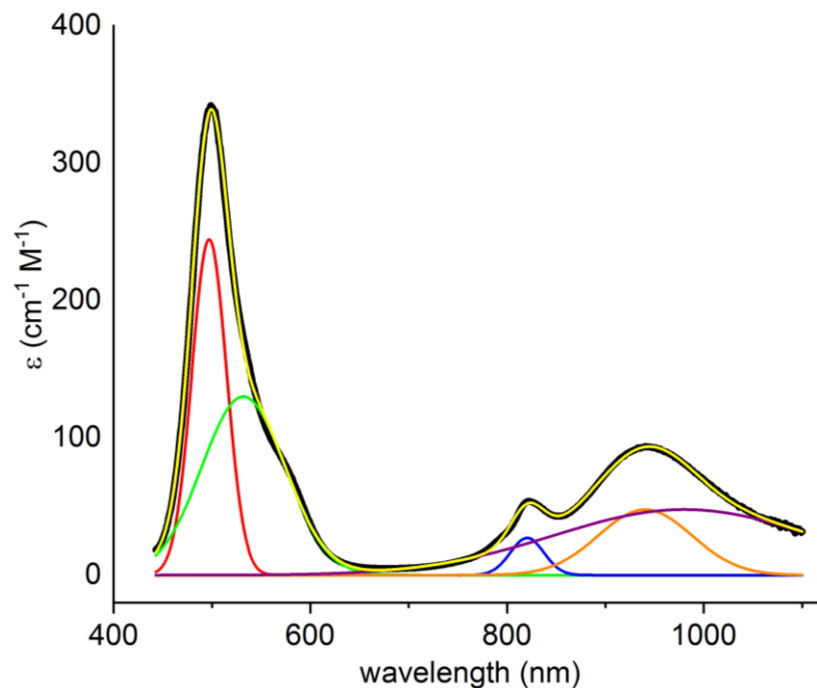


Figure 2.11. Deconvolution of UV-visible absorption spectrum of $(Tp^{Ph})NiBr$. \bullet = experimental spectrum, $\bullet, \bullet, \bullet, \bullet, \bullet$ = fitted peaks, \bullet = fitted curve.

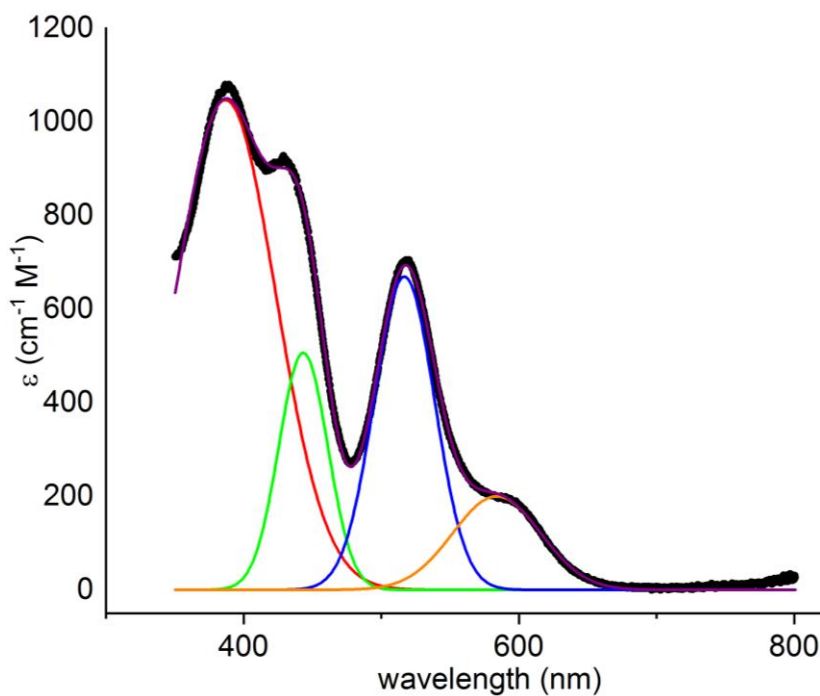


Figure 2.12. Deconvolution of UV-visible absorption spectrum of $(Tp^{Ph})NiI$. \bullet = experimental spectrum, $\bullet, \bullet, \bullet, \bullet$ = fitted peaks, \bullet = fitted curve.

The presence of these numerous peaks has been ascribed to trigonal splitting that is present in C_{3v} symmetry. With this reduction in symmetry ($T_d \rightarrow C_{3v}$), the 3T_1 (F), 3T_2 (F), and 3T_1 (P) states all split into two energy levels each (Figure 2.13). This makes calculation of the Racah parameters by traditional methods impossible.

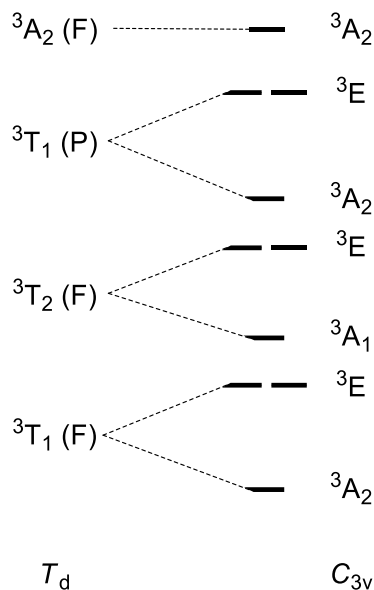


Figure 2.13. Microstate splitting on reduction of symmetry from T_d to C_{3v} for Ni^{II} . Reproduced from 155.

Figure 2.10, Figure 2.11, and Figure 2.12 depict the spectra with the deconvolution results overlaid. Analogous halide complexes with the ligand hydridotris(3,5-dimethylpyrazolyl)borate (Tp^*) have been studied.^{155, 175} These complexes, $(Tp^*)NiX$ ($X = Cl, Br, I$) are interesting and relevant for several reasons. While the steric bulk of a methyl group is less than a phenyl, these form C_3 symmetric four-coordinate complexes similar to the present matter, presumably due to electronic effects.¹⁵⁵ These compounds were also characterized by electronic spectroscopy including NIR measurements. Due to the structural similarities, they are an apt comparison and bands in the electronic

spectra can be assigned by analogy to complexes reported by Desrochers et.

al.¹⁵⁵ For purposes of comparison the electronic spectra data for these

compounds are presented in Table 2.5.

Table 2.5. Electronic spectra of selected nickel complexes in CH₂Cl₂. Wavelengths are reported in nm and extinction coefficients in parentheses (M⁻¹ cm⁻¹).

| compd | ³ A ₂ (³ A ₂ ,F)← | ³ E(³ T ₁ ,P)← | ³ A ₂ (³ T ₁ ,P)← | ³ E(³ T ₁ ,F)← |
|-------------------------|--|---|--|---|
| | ³ A ₂ (³ T ₁ ,F) | ³ A ₂ (³ T ₁ ,F) | ³ A ₂ (³ T ₁ ,F) | ³ A ₂ (³ T ₁ ,F) |
| (Tp [*])NiCl | 481 (500) | 560 (70) | 794 (150) | 883 (170) |
| (Tp [*])NiBr | 498 (450) | 574 (65) | 810 (140) | 894 (138) |
| (Tp [*])NiI | 521 (700) | 575 (120) | 826 (150) | 907 (123) |
| (Tp ^{Ph})NiCl | 486 (80) | 524 (30) | 805 (10) | 950 (30) |
| (Tp ^{Ph})NiBr | 497 (300) | 532 (200) | 817 (50) | 951 (90) |
| (Tp ^{Ph})NiI | 443 (70) | 517 (50) | 584 (30) | ‡ |

‡ The NIR spectrum of this compound has not been collected.

Qualitatively, (Tp^{Ph})NiX exhibits similar spectra to other (Tp^R)NiX complexes. The absorption bands for both (Tp^{*})⁻ and (Tp^{Ph})⁻ complexes show a red shift going down the halide series, consistent with a weaker crystal field. This follows the spectrochemical series for halides. Compared to the (Tp^{*})NiX series, (Tp^{Ph})NiX complexes exhibit similar absorption spectra with small shifts the bands. The exception is the ³E(³T₁,P)←³A₂(³T₁,F) transition which shifts to higher energy in the (Tp^{Ph})⁻ series. The absorptions for the (Tp^{Ph})⁻ series are less intense overall than the (Tp^{*})⁻ series although the absorptions increase in the

order $\text{Cl} < \text{Br} < \text{I}$. The low intensity suggests the transitions are predominantly $d-d$ in character.¹⁵⁵

The electronic spectra are in accordance with a ${}^3\text{A}_2({}^3\text{T}_1, \text{F})$ ground state as found in other systems and theoretical experiments.⁹⁷ This result is of particular importance as it is in agreement with magnetic measurements and supports the hypothesis of an out-of-state origin of magnetic anisotropy for $(\text{Tp}^{\text{Ph}})\text{NiCl}$ since the spectra are similar to other complexes with a ${}^3\text{A}_2({}^3\text{T}_1, \text{F})$ ground state. The spectrum for $(\text{Tp}^{\text{Ph}})\text{NiI}$ (Figure 2.12) stands apart from $(\text{Tp}^{\text{Ph}})\text{NiCl}$ (Figure 2.10) and $(\text{Tp}^{\text{Ph}})\text{NiBr}$ (Figure 2.11) in the difference in relative intensities of the absorptions. The stronger absorptions for $(\text{Tp}^{\text{Ph}})\text{NiI}$ indicate a greater mixing between Ni and I orbitals. This could be the product of a better match in orbital energies or greater overlap. A charge transfer band is observed for $(\text{Tp}^{\text{Ph}})\text{NiI}$ at 387 nm ($\epsilon = 1200 \text{ M}^{-1}\text{cm}^{-1}$) but not in the spectral ranges measured for $(\text{Tp}^{\text{Ph}})\text{NiCl}$ or $(\text{Tp}^{\text{Ph}})\text{NiBr}$. It is plausible that magnetic characterization for $(\text{Tp}^{\text{Ph}})\text{NiI}$ will find a greater magnetic anisotropy and perhaps increased blocking temperature in comparison to $(\text{Tp}^{\text{Ph}})\text{NiCl}$ and $(\text{Tp}^{\text{Ph}})\text{NiBr}$ because of the increased orbital interaction between I and Ni.

2.3.4. High Field Electron Paramagnetic Resonance Spectroscopy

High Field EPR (HF-EPR) data were collected at the National High Magnetic Field Laboratory in Tallahassee, FL by Steven Hill using a transmission probe that propagates microwaves through cylindrical light-pipes. HF microwave radiation was generated by a phase-locked Virginia Diodes solid-state source

operating at 13 ± 1 GHz and followed by a chain of multipliers and amplifiers. High strength magnetic fields were produced by a 17 T superconducting magnet.²²⁵ Single-crystal HFEPR experiments were performed in a Quantum Design PPMS system with a 7 T superconducting magnet. A millimeter-wave Vector Network Analyzer served as a microwave source and detector.²²⁶⁻²²⁷

Due to the large ZFS and $S > 1/2$ for these complexes, high field measurements were necessary to observe the electron paramagnetic spectra. HFEPR measurements were made on $(\text{Tp}^{\text{Ph}})\text{NiCl}$ to better understand the electronic structure and its role in the observed magnetic behavior. Given the $S = 1$ ground state and the C_3 symmetry of the molecule in the solid state, the following spin Hamiltonian was used to fit the data:

$$\mathcal{H}_{spin} = \mu_B \vec{B} \cdot g \cdot \hat{S} + D \hat{S}_z^2 \quad \text{Equation 2.1}$$

Field strength and frequency domains were scanned from 1-14 T and 100-400 GHz and the experimental resonances fitted to the spin Hamiltonian. The following parameters are extracted from this experiment: $D = 1.5 \text{ cm}^{-1}$, $g_x = g_y = 2.28$, $g_z = 2.29$. The positive value of the zero field splitting results in the $|M_S\rangle = 0$ state being the ground state. For this reason, hysteresis is only observed in an applied bias field. A related series of $(\text{Tp}^*)\text{NiX}$ ($X = \text{Cl}, \text{Br}, \text{I}$) complexes have been studied via HFEPR, UV-vis absorbance spectroscopy, DFT, and *ab initio* calculations.^{155, 175} For $(\text{Tp}^*)\text{NiCl}$ D was found to be $+3.93 \text{ cm}^{-1}$. A nonzero E value of $+0.348 \text{ cm}^{-1}$ was found, and g_x , g_y , g_z were extracted as 2.28, 2.27, and 2.25 respectively. The spin Hamiltonian used to extract these parameters was not identical to Equation 2.1; an additional $E(S_x^2 - S_y^2)$ term was included.

Including the transverse anisotropy term accounts for the lowered symmetry of $(\text{Tp}^*)\text{NiCl}$; the chloride ligand deviates from axial symmetry by tilting off the principal rotation axis. This reduced symmetry also leads to the different values of g_x and g_y . The sign and magnitude of D is sensitive to the identity of the axial ligand, substituting Cl for Br and I led to negative values of D with increasing magnitude in the $(\text{Tp}^*)\text{NiX}$ series. Computational studies suggest the metal center has a variety of transitions that influence the SOC, but these terms are overwhelmed by the SOC contributions of the heavier halides.¹⁷⁵ This is in accord with studies of other systems. Figure 2.14 shows the experimental spectra for $(\text{Tp}^{\text{Ph}})\text{NiCl}$ as a function of magnetic field strength at a range of frequencies. The large signal at low field on all four spectra is the half-field transition, the result of a $\Delta m_s = 2$ transition.

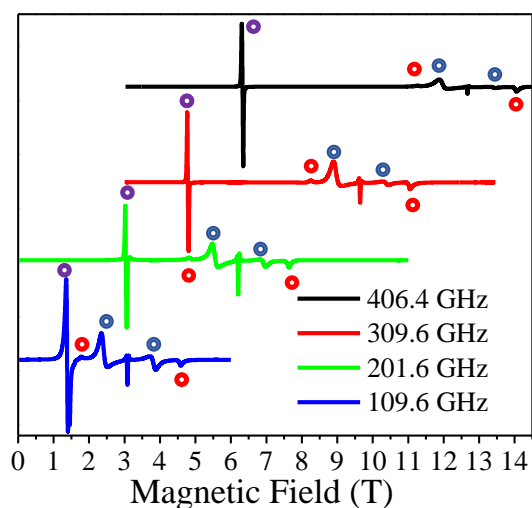


Figure 2.14. HFEPR spectra for $(\text{TpPh})\text{NiCl}$. $B||z$ (\bullet), $B||xy$ (\bullet), and half field transmissions (\bullet) are marked.

Figure 2.15 is a plot of calculated energy levels as lines with experimental data overlaid as black circles. Five of the features are close to parallel with a

sixth having double the slope. The slope reflects the increasing separation of states under an applied field described by the Zeeman term of the spin Hamiltonian. Two lines in red correspond to B||z resonances, two blue lines correspond to B||xy components. An additional transition in Figure 2.15 is plotted with a pink line and indicates a double quantum transition, assigned as it appears at fields close to $g = 2.3$ over the range of the measurements.²²⁸ It can be seen in Figure 2.15 as the feature between the B||xy resonances. The purple line is a half field transition, the slope of roughly twice that of the B||xy components.

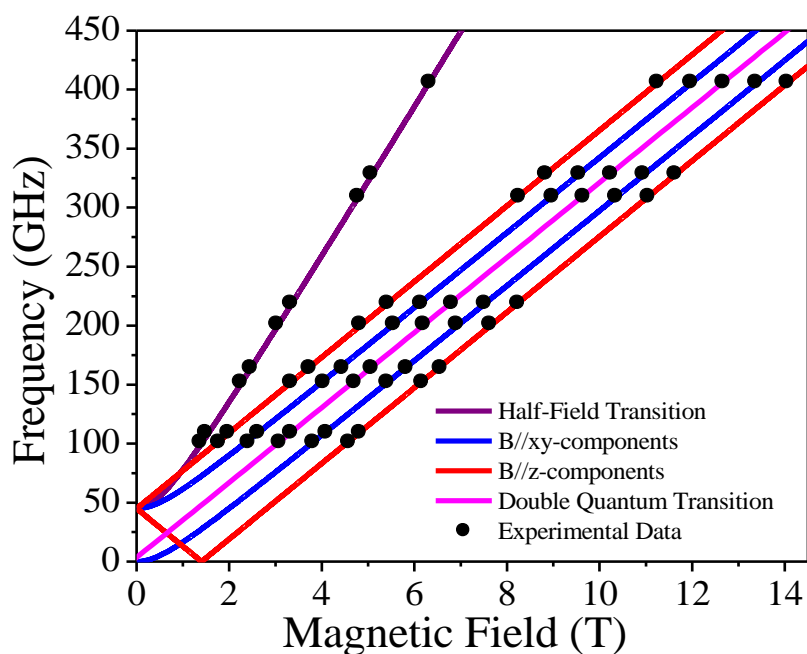


Figure 2.15. HFEPR experimental data points plotted on top of the calculated energy levels for $(Tp^{Ph})NiCl$.

2.3.5. X-ray Structural Studies

X-ray diffraction measurements provide important information about the coordination environment of the metal ions as well as the structure of the crystal

lattice. These are relevant to the modeling of magnetic data and a component of deducing the electronic structure of the metal ions. In particular, static Jahn-Teller effects can be observed or an upper limit to their extent placed.^{97, 205} In contrast, spectroscopic measurements are often made in solution which isolates complexes from each other and at room temperature has a tendency to average out various distortions.²²⁹ Substituents which freely rotate in solution are often locked into position in the solid state, and small changes in the periphery of magnetic complexes can have profound effects on the magnetic properties of these materials. Since the design of monometallic SMMs is built on the creation of orbital degeneracy, Jahn-Teller distortions are possible and can undermine the strictly axial symmetry that gives rise to a barrier to magnetization reversal.²⁰⁵ In the case of four coordinate scorpionates, it has been suggested that a distortion from C_3 symmetry arises as a result of Jahn-Teller distortion.⁹⁷ By shifting the axial ligand off the principal rotation axis the degeneracy of the d_{xz}/d_{yz} and $d_{x^2-y^2}/d_{xy}$ orbital pairs can be broken. To better describe the distortion of 4-coordinate species from ideal T_d symmetry, a geometry index has been devised (τ_4) wherein the two largest angles are defined as α and β as in Equation 2.2 and Figure 2.16.^{97, 205, 230} (It is important to note that the largest angles are often between *trans* ligands). Using Equation 2.2 an index can be calculated with a value of 1 for T_d and 0 for square planar.²³⁰

$$\tau_4 = \frac{(360^\circ - (\alpha^\circ + \beta^\circ))}{141^\circ} \quad \text{Equation 2.2}$$

In the case of these 4-coordinate scorpionates, in a rigorous C_3 symmetric molecule, a single vector passes through the H-B...M-X bonds to form a principal

rotation axis about which the rest of the molecule can be defined. In some instances, a distortion occurs at the M-X bond where the X ligand is no longer collinear with the B...M vector. This breaks the symmetry of the coordination environment of the metal ion with the X-M-N bond angles taking two different values. In addition to the index giving a numerical description of the distortion, the values of α and β also describe if the C_3 symmetry is broken. If $\alpha = \beta$, the rotation axis is maintained but if unequal the rotation axis is broken and an investigation into the origin of the distortion can be made.

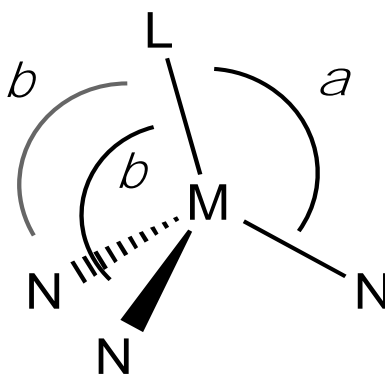


Figure 2.16. The definition of the α and β angles to quantify distortions from tetrahedral symmetry. Adapted from 97.

Table 2.6 lists the angles for each complex and the calculated τ_4 index. As can be seen, the indices show a substantial distortion from T_d symmetry, but often the complexes maintain C_3 symmetry. This is important as it is the axial symmetry that eliminates E (transverse magnetic anisotropy) and suppresses tunneling of the magnetic moment. The τ_4 index can be less than one while the complex still maintains a principal rotation axis.

Table 2.6. Selected geometric data derived from X-ray crystal structures for $(Tp^{Ph})MnCl$, $(Tp^{Ph})CoCl$, α - $(Tp^{Ph})CoBr$, β - $(Tp^{Ph})CoBr$, $(Tp^{Ph})NiCl$, $(Tp^{Ph})NiBr$, $(Tp^{Ph})NiI$, and $(Tp^{Ph})ZnCl$.

| Metal | Axial Ligand | α (°) | β (°) | τ_4 | M-X (Å) | N-M (Å) |
|------------------|--------------|--------------|-------------|----------|------------|------------|
| Mn ^{II} | Cl | 123.77(6) | 125.08(6) | 0.77 | 2.2774(8) | 2.133 (2) |
| | | | 126.07(7) | | | 2.147 (2) |
| | | | | | | 2.156 (3) |
| Co ^{II} | Cl | 122.07(5) | 122.07(5) | 0.85 | 2.1771(11) | 2.0296(19) |
| | α -Br | 121.98(6) | 121.98(6) | 0.85 | 2.3229(5) | 2.0361(9) |
| | β -Br | 120.68(5) | 122.85(5) | 0.85 | 2.3539(3) | 2.0413(16) |
| | | | 122.23(5) | | | 2.0457(18) |
| | | | | | 2.0373(17) | |
| Ni ^{II} | Cl | 123.59(5) | 123.59(5) | 0.79 | 2.1615(5) | 2.0064(8) |
| | Br | 123.47(5) | 123.47(5) | 0.81 | 2.2927(3) | 2.0046(7) |
| | I | 123.46(7) | 123.46(7) | 0.81 | 2.4463(8) | 2.0041(15) |
| Zn ^{II} | Cl | 123.02(3) | 123.02(3) | 0.81 | 2.1565(9) | 2.0350(12) |

(Tp^{Ph})MnCl. The single crystal XRD experiment indicates a monometallic complex of C_1 symmetry that crystallizes in the monoclinic crystal system and the $P2_1/n$ space group. Figure 2.17 depicts the asymmetric unit and atom labeling scheme for $(Tp^{Ph})MnCl$. Four equivalent molecules occupy the unit cell. The

experimental details are given in Table A.2.

Table A.3,

Table A.4, and

Table A.5 tabulate the atom coordinates, bond angles, and bond lengths.

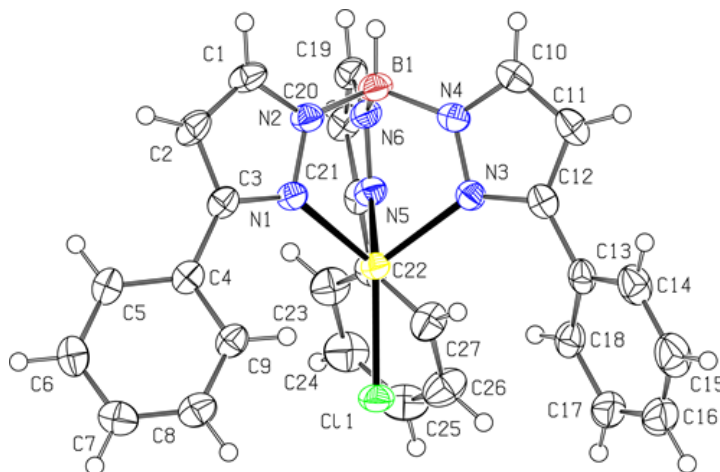


Figure 2.17. Numbering scheme and ORTEP for (Tp^{Ph})MnCl. Ellipsoids plotted at 50% probability.

The Cl ligand is distorted from axial symmetry by tilting away from the principal rotation axis of the molecule, exhibiting three different N-Mn-Cl bond angles. The Mn-N bond lengths are similar, ranging from 2.133(2) to 2.156(3) Å. The Mn-Cl bond is 2.2774(8) Å in length. From this, the τ_4 index can be calculated and is found to be 0.78, showing a significant tilt of the axial ligand. The phenyl rings are not related by symmetry and two of the three are nearly coplanar. This allows for the two phenyl rings to approach pyrazole rings on neighboring molecules at distances of 4.169(6) and 3.568(5) Å. The third ring, containing C22-C27, is not oriented planar or perpendicular to nor does it as closely approach any other aromatic portion of adjacent molecules. This

precludes any strong stabilizing π interactions and suggests that the two coplanar phenyl rings have a greater effect on the crystal packing.

There are two possible causes for the tilt of the axial ligand, either crystal packing is stabilized by the distortion or the Jahn-Teller effect causes a static distortion. The latter is less likely as the 6A ground state should have no first order Jahn Teller effect. However, excited state mixing is possible and has been indirectly observed via ZFS in Mn^{II} complexes in 4-coordinate geometry. Since the ZFS in such cases is no greater than 1 cm^{-1} in magnitude for other Mn^{II} complexes, it seems more likely that the crystal packing causes this tilt and the reduction of the τ_4 index.²³¹

(Tp^{Ph})CoCl. This compound crystallizes in the $P\bar{3}$ space group and the complexes possess C_3 symmetry with the principal rotation axis passing through the collinear H, B, Co, and Cl atoms (Figure 2.18). The unit cell contains two molecules related by an inversion center. As such, the principal rotation axes of the molecules are parallel. The experimental details are given in Table A.6.

Table A.7,

Table A.8, and

Table A.9 tabulate the atom coordinates, bond angles, and bond lengths.

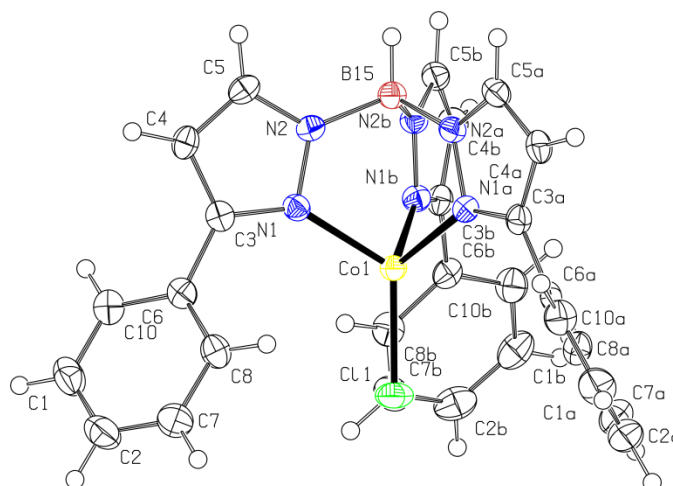


Figure 2.18. Numbering scheme and ORTEP for $(\text{Tp}^{\text{Ph}})\text{CoCl}$. Ellipsoids plotted at 50% probability.

There are none of the typical phenyl ring spatial arrangements associated with π interactions present in the lattice. It appears that the complex crystallizes to minimize void space by placing antiparallel stacks adjacent to each other. The τ_4 index for $(\text{Tp}^{\text{Ph}})\text{CoCl}$ is 0.82, indicating that it is closer to tetrahedral than $(\text{Tp}^{\text{Ph}})\text{MnCl}$. $(\text{Tp}^{\text{Ph}})\text{CoCl}$ shows no distortion despite an E ground state with the N-Co-Cl $\angle = 122.07(5)^\circ$. The deviation in the τ_4 index arises from the difference in bond lengths between Co-N and Co-Cl, but the local coordination environment remains rigorously C_3 within the experimental error of the single crystal XRD experiment. Investigation of similar compounds in the literature indicate that this axial symmetry is not always present.¹⁷² In the case of $(\text{Tp}^{\text{t-Bu,Me}})\text{CoCl}$ the N-Co-Cl $\angle = 121.51(5)^\circ$. For $(\text{Tp}^{\text{t-Bu,Tn}})\text{CoCl}$, the N-Co-Cl angles are unique, with the values $122.51(7)^\circ$, $119.81(7)^\circ$, and $122.11(7)^\circ$. This suggests the compound may show SMM behavior as the E term of the spin Hamiltonian should be zero. Of course, magnetic measurements are the absolute test for SMM behavior.

α -(Tp^{Ph})CoBr, β -(Tp^{Ph})CoBr. This compound has been isolated in two crystal systems, a trigonal and a tetragonal polymorph with space groups of $P\bar{3}$ and $P4_2/n$. The polymorphs are labelled as α -(Tp^{Ph})CoBr and β -(Tp^{Ph})CoBr. Both are solvent-free and α -(Tp^{Ph})CoBr has a Z of 2 whereas β -(Tp^{Ph})CoBr has a Z of 8. The numbering schemes for α -(Tp^{Ph})CoBr and β -(Tp^{Ph})CoBr are presented in Figure 2.19 and Figure 2.20.

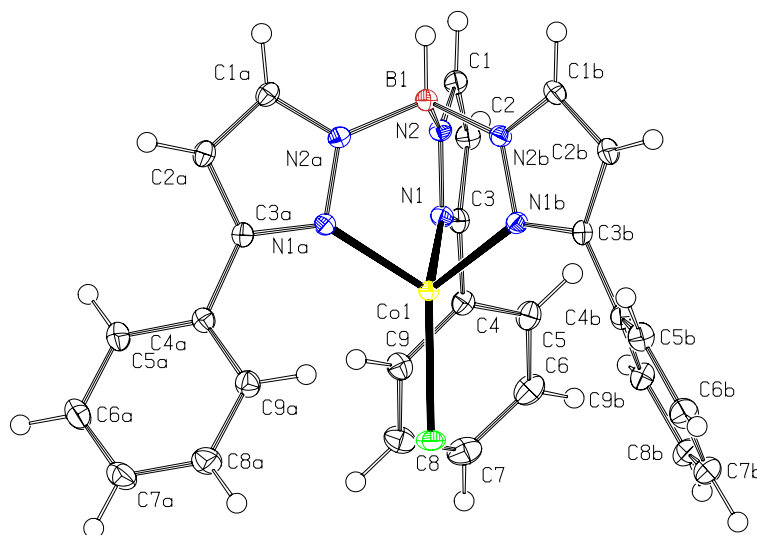


Figure 2.19. Numbering scheme and ORTEP for α -(Tp^{Ph})CoBr. Ellipsoids plotted at 50% probability.

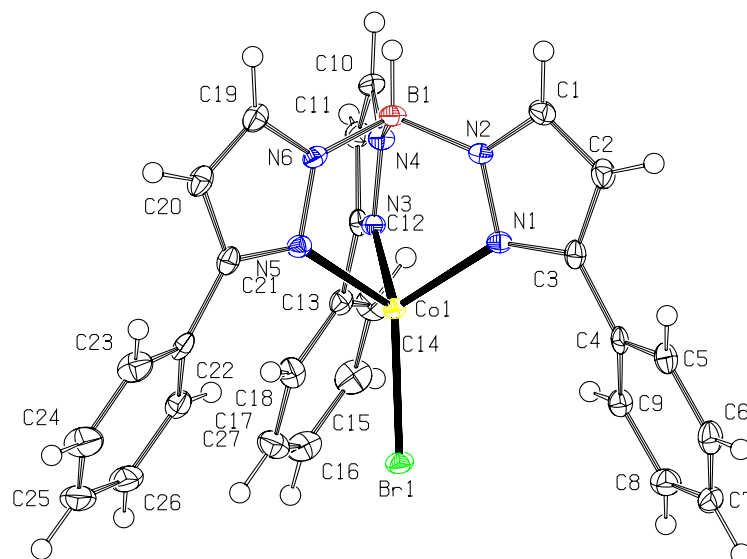


Figure 2.20. Numbering scheme and ORTEP for β -(Tp^{Ph})CoBr. Ellipsoids plotted at 50% probability.

The isolation of two polymorphs of (Tp^{Ph})CoBr provides a chance to examine the role of small changes in coordination geometry and crystal packing in the magnetic properties of the compound in the solid state. Two prominent changes occur between the two polymorphs, a small distortion of the axial ligand position and a large change in the orientation of individual molecules with respect to each other. Figure 2.21 depicts the crystal packing of α -(Tp^{Ph})CoBr with red arrows denoting the principal rotation axes of the individual molecules. These rotation axes are in the plane of the figure, as is the principal rotation axis of the unit cell. Figure 2.22 depicts the β -(Tp^{Ph})CoBr polymorph with the principal rotation axis of the unit cell perpendicular to the plane of the figure. The vectors in α -(Tp^{Ph})CoBr are parallel whereas they are canted in β -(Tp^{Ph})CoBr. To our knowledge there are few reports of polymorphism in monometallic SMMs, and being able to isolate two solvent-free polymorphs gives an opportunity to examine the role of the crystal lattice in SMM phenomena.²³² In other

magnetically anisotropic systems, a spatial orientation of the anisotropy has been shown, and the alignment of the anisotropy for multiple spin centers has a marked effect on the magnetic properties.^{104, 123} Experimental details, atom coordinates, bond angles, and lengths for both polymorphs are recorded in Table A.10 - Table A.17.

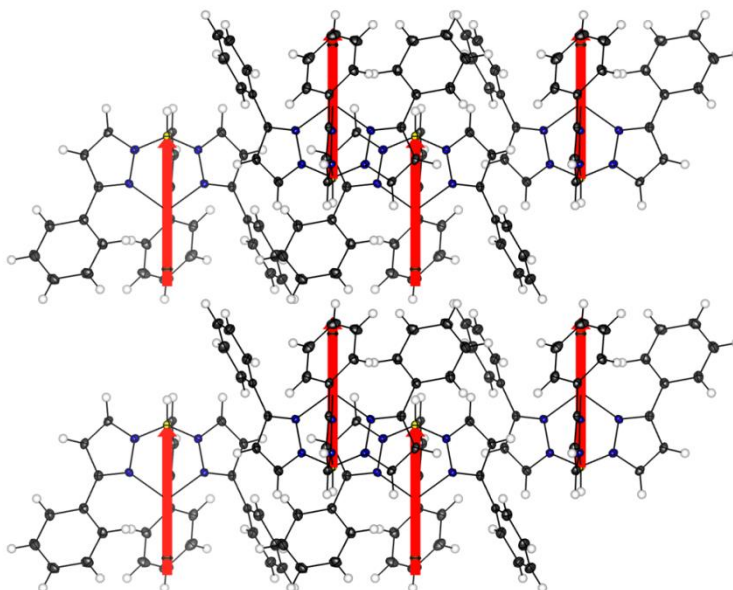


Figure 2.21. Unit cell of α -(Tp^{Ph})CoBr with the Co...Br axis denoted by the red vectors.

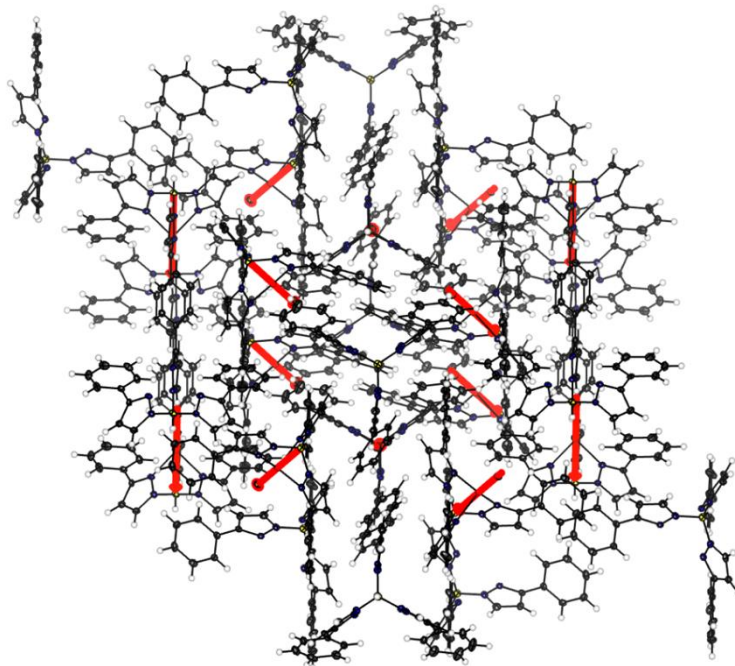


Figure 2.22. Unit cell of β -(Tp^{Ph})CoBr with the Co...Br axis denoted by the red vectors.

(Tp^{Ph})NiCl. This compound crystallizes in the trigonal crystal system in the $P\bar{3}$ space group. The monometallic complexes have C_3 symmetry and the unit cell contains two molecules. Figure 2.23 depicts the numbering scheme and ORTEP. The experimental details, atom coordinates, bond angles, and bond lengths are contained in Table A.18 - Table A.21.

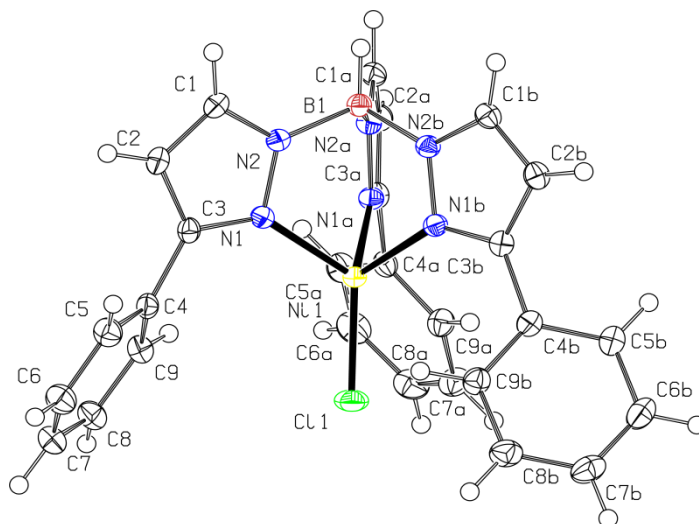


Figure 2.23. ORTEP and numbering scheme for (Tp^{Ph})NiCl plotted at 50% probability.

Overall, the individual complex shows relatively high symmetry. For B1 \cdots Ni1 \cdots Cl1, $\angle = 180^\circ$, and N1,3,5-Ni1-Cl1 $\angle = 92.34(3)^\circ$. Each phenylpyrazole is related by rotation to the other two, as indicated by the numbering scheme. Since these are not completely planar the symmetry of the molecule is lowered to C_3 from C_{3v} . Despite the high symmetry, the τ_4 index is 0.80, attributable solely to angle distortion from perfect tetrahedral from the difference in bond length between the Ni-N bond (2.0064(8) Å) and the Ni-Cl bond (2.1615 (5) Å). In other words, there is no distortion from axial symmetry even though $\tau_4 \neq 1$. From this it can be inferred that neither crystal packing nor potential Jahn-Teller distortion is sufficient to break the symmetry of the complex. While it may appear reasonable to assign a nondegenerate ground state from the X-ray data, it is insufficient as crystal packing could be at odds with a distortion. At best, it may be said that the crystal structure is more consistent with an A ground state. In the crystal lattice the principal rotation axes of the complexes are parallel or antiparallel to each other. This favors the magnetic anisotropy being aligned in the crystalline material.

(Tp^{Ph})Ni(phpy)Cl. The addition of a 5-phenylpyrazole as a ligand to (Tp^{Ph})NiCl causes several large changes in the crystal structure. Moving from four-

coordinate to five-coordinate, the geometry around the metal changes from distorted tetrahedral to a distorted square pyramidal with one N of the scorpionate occupying the axial position and the remaining coordinating atoms in basal positions (Figure 2.24). The potential for high symmetry in the scorpionate is eliminated such that the complex possesses C_1 symmetry. N1, N3, and N5 are the bonding atoms of the scorpionate ligand with bond lengths of 2.0767(11), 2.0407(11), and 2.0693(10) Å. The N7-Ni1 bond is 2.0705(11) Å in length and the Ni1-Cl1 bond is 2.3201 (4) Å long. The increased length of the Ni-Cl bond in comparison to $(\text{Tp}^{\text{Ph}})\text{NiCl}$ is likely caused by the increased electron density on Ni from the additional ligand in $(\text{Tp}^{\text{Ph}})\text{Ni}(\text{phpy})\text{Cl}$. The similar lengths of the three Ni-N bonds trans to other Ni-N bonds suggests roughly equal donor strength while the shorter axial Ni-N bond forming the peak of the square pyramidal geometry likely results from the absence of a ligand in the *trans* position.

$(\text{Tp}^{\text{Ph}})\text{Ni}(\text{phpy})\text{Cl}$ crystallizes in the triclinic crystal system in the $P\bar{1}$ space group with a Z of 2. The experimental details, atom coordinates, bond angles, and bond lengths are contained in Table A.22, - Table A.25. The low symmetry of the coordination environment breaks any degeneracy that would lead to a Jahn-Teller distortion. The τ_4 index is also inapplicable making that form of structural comparison to the other reported compounds impossible.

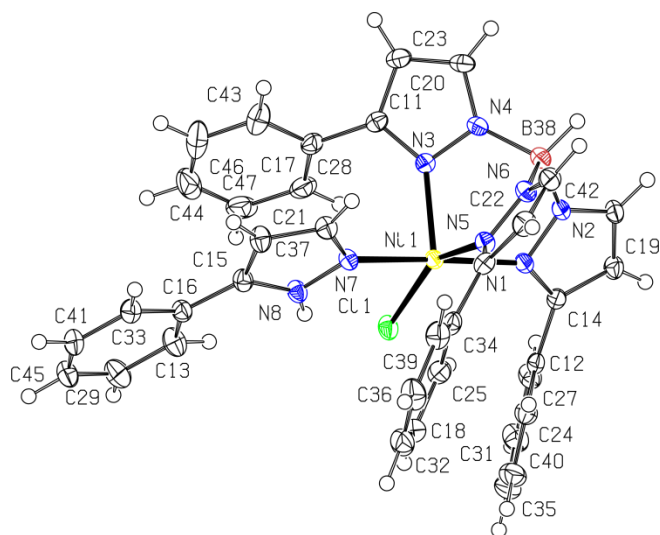


Figure 2.24. ORTEP and numbering scheme of $(Tp^{Ph})Ni(phpy)Cl$ plotted at the 50% probability level.

$(Tp^{Ph})NiBr$. This compound follows the trend of highly symmetrical complexes in space groups with small Z values. It is trigonal and belongs to the $P\bar{3}$ space group with a Z of 2. Each of the molecules in the unit cell exhibits axial symmetry with the principal rotation axis passing through B1, Ni1, and Br1. Figure 2.25 depicts the ORTEP and numbering scheme for the complex. Each phenylpyrazole is related by rotation around the B1 \cdots Ni1 \cdots Br1 axis giving the complex strict axial symmetry. The experimental details, atom coordinates, bond angles, and bond lengths are presented in Table A.26 - Table A.29. The τ_4 index is calculated as 0.81 with the deviation arising solely from the difference in bond length between N-Ni and Ni-Br that in turn influences the angles. In other words, there is no tilting of the Ni-Br bond in $(Tp^{Ph})NiBr$. If the complex has a degenerate ground state, it does not manifest in a Jahn-Teller distortion. The bond length for all three N-Ni1 bonds is 2.0046(7) Å. This is shorter than the length of 2.0064(8)

Å in $(\text{Tp}^{\text{Ph}})\text{NiCl}$. The length of the Ni1-Br1 bond is 2.2927(3) Å, a little over 0.1 Å difference from the Ni-Cl bond in $(\text{Tp}^{\text{Ph}})\text{NiCl}$.

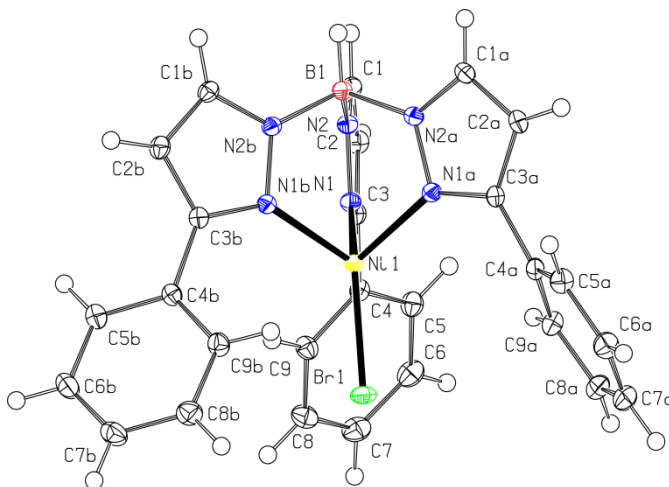


Figure 2.25. ORTEP of $(\text{Tp}^{\text{Ph}})\text{NiBr}$ plotted at 50% probability with the numbering scheme depicted.

$(\text{Tp}^{\text{Ph}})\text{NiI}$. This compound crystallizes as monometallic complexes in the $P\bar{3}$ space group, a member of the trigonal crystal system. The complex itself has C_3 symmetry with the principal rotation axis containing the B, Ni, and I atoms (Figure 2.26). Each of the three phenylpyrazole rings is related to the other two by rotation, but since they are not completely planar there are no mirror planes in the structure. This rotation of the phenyl ring accommodates the iodine atom in the axial position. The N1-Ni1 and Ni1-I1 bonds are 2.0041 (15) and 2.4463 (8) Å in length. For N1-Ni1-I1 $\angle = 123.42$ (4). The τ_4 index is calculated as 0.80, the same as $(\text{Tp}^{\text{Ph}})\text{NiBr}$. In the same way as $(\text{Tp}^{\text{Ph}})\text{NiCl}$ and $(\text{Tp}^{\text{Ph}})\text{NiBr}$, the geometry does not indicate any Jahn-Teller distortion to stabilize a degenerate ground state. Table A.30 - Table A.33 provide experimental details, atom coordinates,

bond angles, and bond lengths.

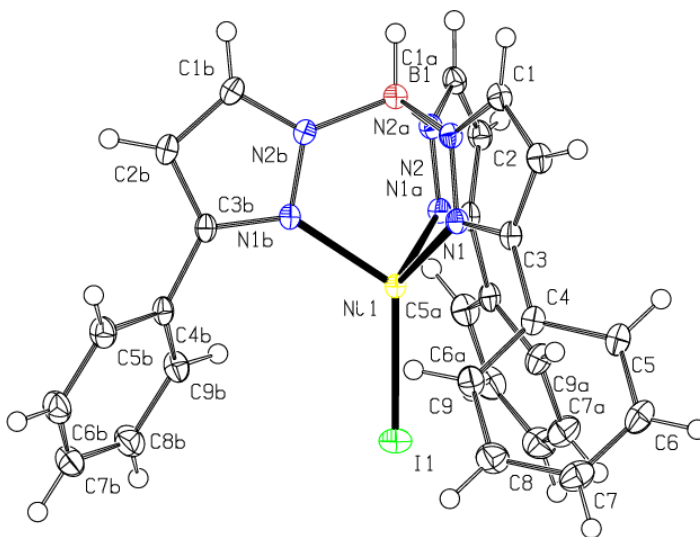


Figure 2.26. ORTEP of $(Tp^{Ph})NiI$ plotted at 50% probability with the numbering scheme depicted. Symmetry codes: (a) $1-y, 1+x, -y, z$; (b) $-x+y, 1-x, z$.

$(Tp^{Ph})ZnCl$. This compound crystallizes in the trigonal crystal system in the $P\bar{3}$ space group. The phenylpyrazole rings are also related by rotation about a principal axis defined by the B, Zn, and Cl atoms (Figure 2.27). The phenyl rings are rotated to fit the chlorine atom, precluding the existence of mirror planes, giving the monometallic complex C_3 symmetry in the solid state. With a Z of 2, the two molecules in the unit cell are related by an inversion center. The N1-Zn1 and Zn1-Cl1 bonds are 2.0350(12) and 2.1565(9) Å in length. For N1-Zn1-Cl1 $\angle = 123.02(3)^\circ$. This places the Cl ligand on the principal rotation axis and gives a τ_4 index of 0.81. Experimental details and results are recorded in Table A.34 - Table A.37.

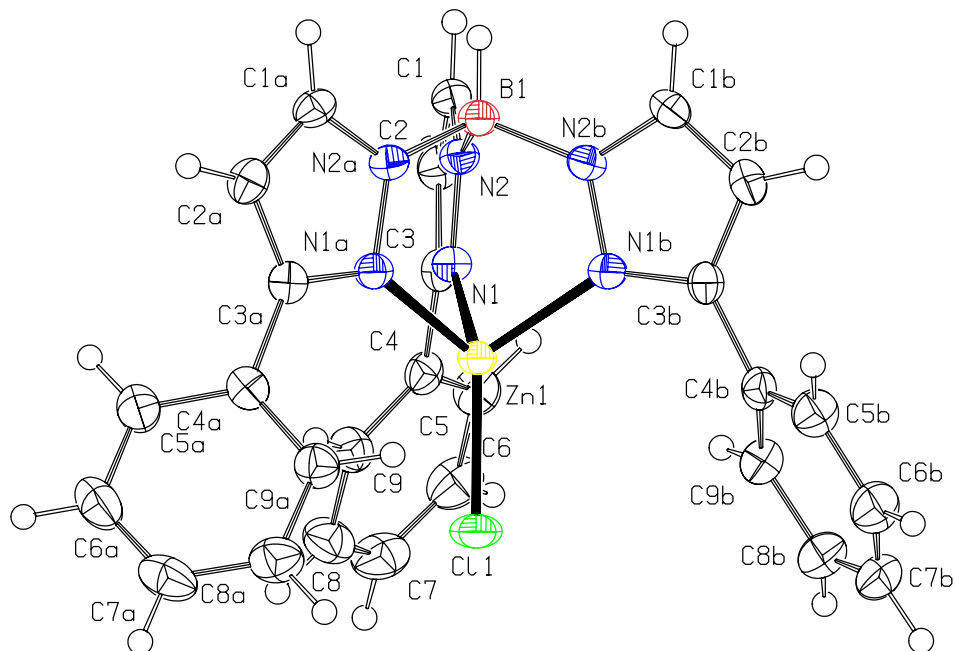


Figure 2.27. ORTEP of $(Tp^{Ph})ZnCl$ plotted at 50% probability with the numbering scheme depicted.

2.3.6. Magnetic Characterization

Four compounds have been magnetically characterized and show a range of behaviors with two being consistent with single molecule magnetism. Table 1.7 lists the compounds and their predicted or experimentally determined S values. Predicted values are italicized

Table 2.7. Monometallic complexes prepared and their spin ground states.

| Complex | S |
|-----------------|-----|
| $(Tp^{Ph})MnCl$ | 5/2 |
| $(Tp^{Ph})CoCl$ | 3/2 |
| $(Tp^{Ph})CoBr$ | 3/2 |

| | |
|-------------------------|-----|
| (Tp ^{Ph})CoI | 3/2 |
| (Tp ^{Ph})NiCl | 1 |
| (Tp ^{Ph})NiBr | 1 |
| (Tp ^{Ph})ZnCl | 0 |

Magnetic susceptibility experiments were conducted at a range of temperatures (1.8 K to room temperature) and field strengths (0 to 70000 Oe). In AC magnetic susceptibility experiments a range of frequencies were employed (0 to 10000 Hz). By collecting data as a function of several variables over 3-4 orders of magnitude, the robustness of the data is ensured, and the parameterization is over a large sample population. For HFEPR measurements a similar effort was made to cover a wide range. In all cases the physical limitations of the instrumentation provide the boundaries for the data sets.

(Tp^{Ph})MnCl. The magnetic characterization of this compound shows an isotropic, $S = 5/2$ complex with no barrier to magnetization reversal and minimal interaction between paramagnetic centers. Figure 2.28 depicts a plot of magnetization vs. field strength at room temperature. The linear fit ($R = 1$) indicates the absence of ferromagnetic impurities that could give spurious results in further magnetic measurements. To best characterize SMM behavior, measurements must be made at low temperature. Figure 2.29 depicts the magnetic susceptibility as a function of temperature in static magnetic fields from 1.85 to 300 K. At low temperatures, the magnetic susceptibility approaches zero as long-range order

sets in, but over much of the temperature domain the magnetic susceptibility remains constant at a value of $4.4 \text{ cm}^3 \text{ K mol}^{-1}$.

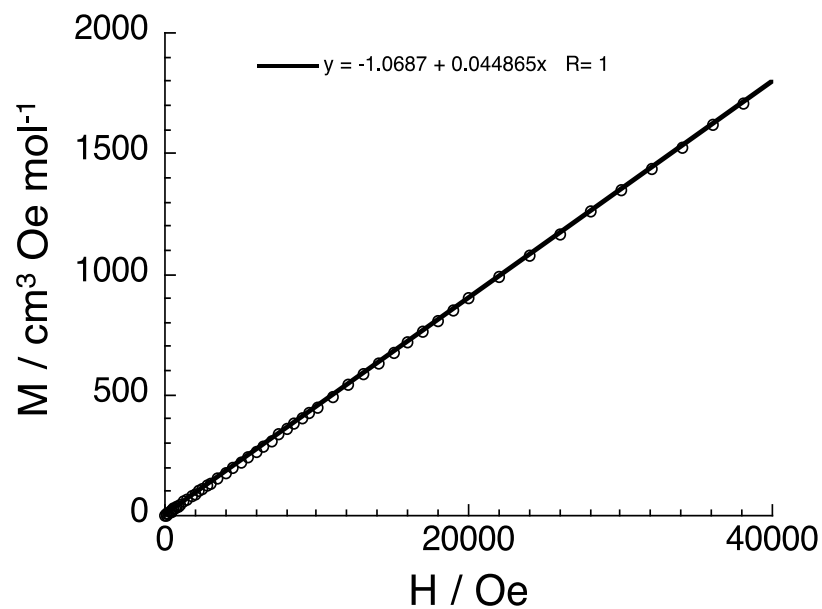


Figure 2.28. Magnetization versus field strength at room temperature for $(\text{Tp}^{\text{Ph}})\text{MnCl}$.

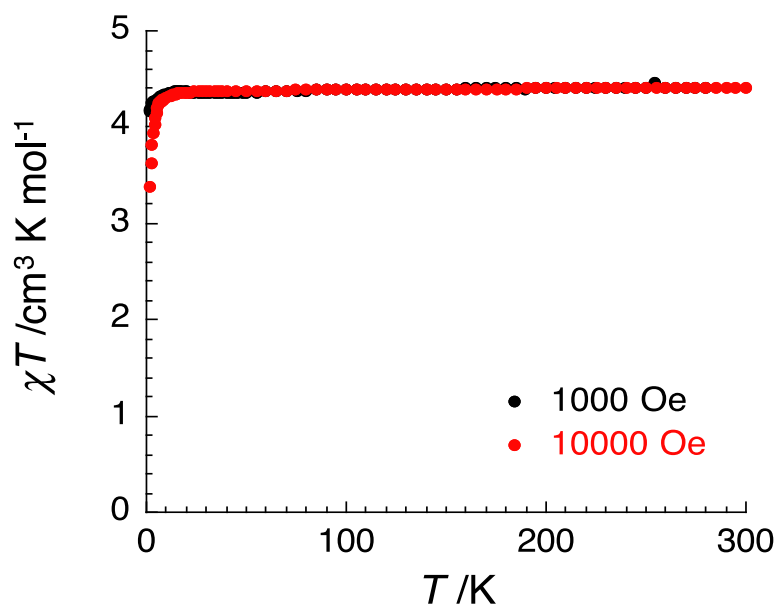


Figure 2.29. Magnetic susceptibility at 1000 and 10000 Oe as a function of temperature from 0-300 K for $(Tp^{Ph})MnCl$.

This saturation of the magnetization indicates a lack of anisotropy of the magnetic moment created by any process, either the formation of superparamagnetic domains or single molecule magnetism. By Equation 1.15 the saturation magnetization value gives $S = 5/2$ and $g = 2.00(5)$. A more accurate determination of the S and g values can be made by measuring the magnetization as a function of field strength divided by temperature and fitting a Brillouin function to the data. Figure 2.30 shows the plot of magnetization versus field strength divided by temperature. The plots become superimposed with each other and the fitted Brillouin function gives $g = 2.006 \pm 0.0017$. The plot shows a linear relationship at small field strengths. This indicates that the material is near the weak field limit where $(|\vec{H}| \ll k_B T)$, but as the field strength increases, saturation of the magnetization is approached where all the magnetic moments are in the ground state.

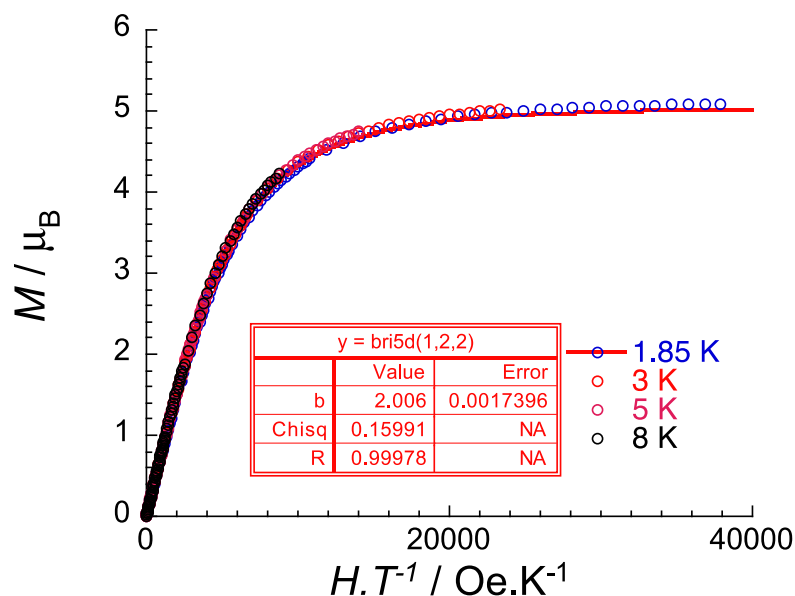


Figure 2.30. Magnetization vs field strength divided by temperature to enable fitting with a Brillouin function for $(\text{Tp}^{\text{Ph}})\text{MnCl}$. Results of curve fitting for the 1.85 K data set are included as a red inset. Experimental data are open circles and the fitted curve is plotted in red.

To restate the results of characterization of $(\text{Tp}^{\text{Ph}})\text{MnCl}$, the compound is pseudo C_3 symmetric in the solid state with small deviations from strict axial symmetry. It has no absorbance bands in the UV-visible region of the electromagnetic spectrum, and all magnetic measurements indicate a spin state of $S = 5/2$ and a Landé g equal to the spin-only value within experimental error, the result of an isotropic 6A ground state.

$(\text{Tp}^{\text{Ph}})\text{CoCl}$. The potential for in-state SOC in $(\text{Tp}^{\text{Ph}})\text{CoCl}$ makes it a promising candidate for exhibiting SMM behavior. At room temperature, the plot of magnetization versus magnetic field strength indicates that the compound contains no ferromagnetic impurities or ferromagnetic ordering (Figure 2.31).

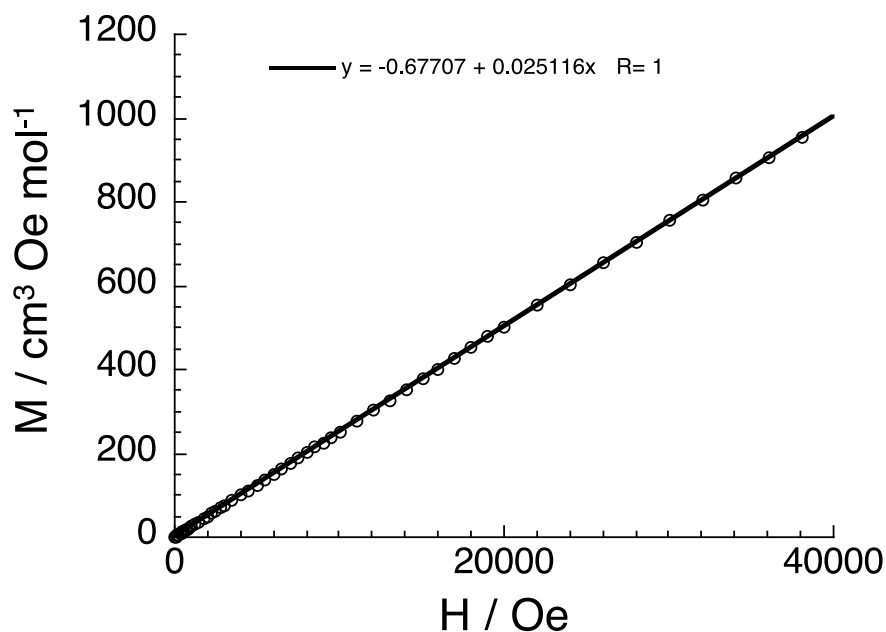


Figure 2.31. A plot of magnetization versus field strength at room temperature for $(Tp^{Ph})CoCl$ with a best fit line overlaid.

Figure 2.31 shows that up to 40000 Oe, the compound is at the weak field limit. Measurement of χT vs. T at 1000 and 10000 Oe from 0-300 K gives a saturation value of $2.45 \text{ cm}^3 \text{ K mol}^{-1}$ (Figure 2.32). From this a value of 2.3(1) for g can be calculated suggesting the presence of SOC as it deviates from the spin-only value of $g = 2.00$, consistent with a high spin Co^{II} center.

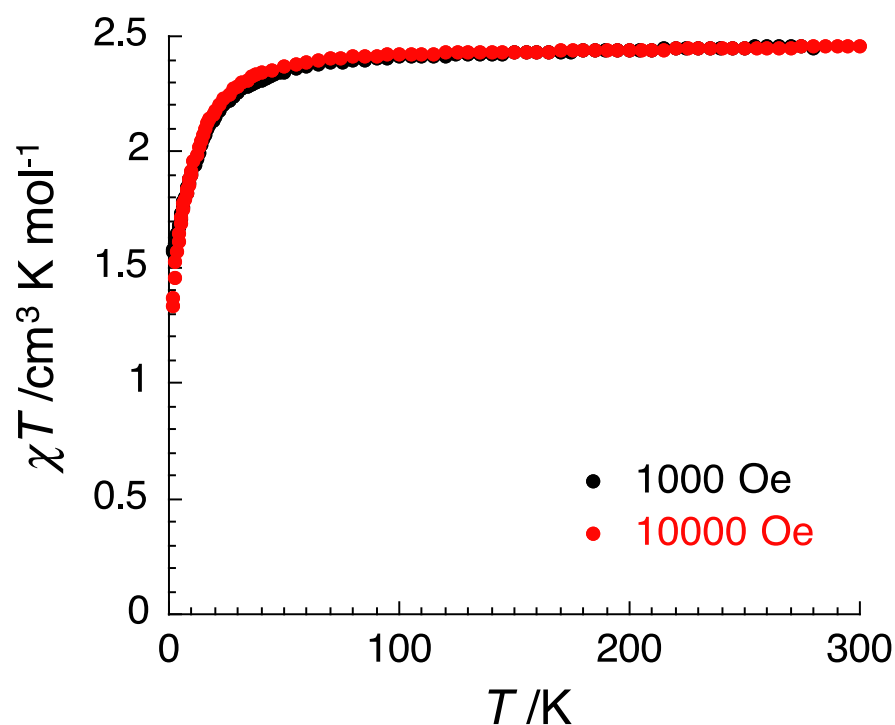


Figure 2.32. Magnetic susceptibility as a function of temperature at 1000 and 10000 Oe for $(Tp^{Ph})CoCl$.

At lower temperatures, measurement of the magnetization as a function of field strength show no apparent saturation of the magnetization at field strengths up to 40000 Oe at 1.85 K (Figure 2.33). The plot of magnetization versus HT^{-1} demonstrates that saturation of the magnetization is not achieved as accounting

for temperature does not make each isothermal superimposed on the others. Because there is no saturation, the fitting of a Brillouin function was not attempted. The deviation of g from the spin only value and the failure to reach saturation of the magnetization at low temperature and high magnetic field strength suggest that for $(\text{Tp}^{\text{Ph}})\text{CoCl}$, remnant magnetization may be observed under suitable conditions.

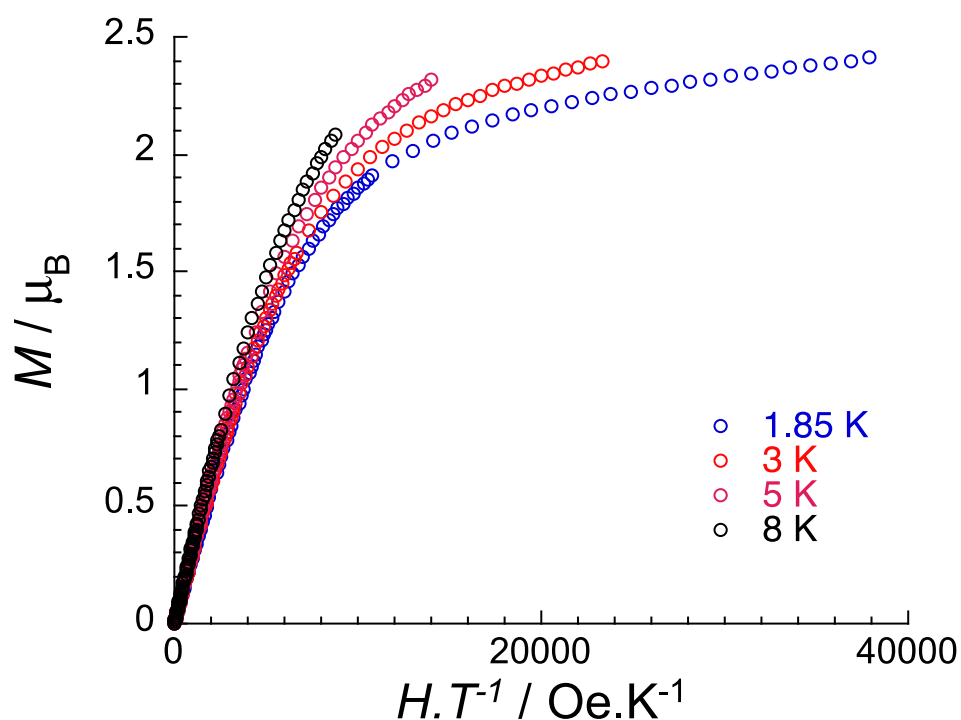


Figure 2.33. Magnetization versus magnetic field strength divided by temperature for $(\text{Tp}^{\text{Ph}})\text{CoCl}$ at temperatures between 1.85 and 8 K.

The characteristic frequency versus field strength was examined and shows a minimum around 500 Oe indicating that this is the optimum DC magnetic bias field to increase the out-of-phase magnetic susceptibility. Using this strength of DC bias magnetic field, AC magnetic susceptibility measurements were conducted on the temperature domain 1.85-8 K and AC frequency domain

10-10000 Hz. At low frequencies, χ' comprises most of the total susceptibility. As the frequency increases, χ'' increases to a maximum value that is frequency-dependent. In all cases, increasing temperature undermines the magnetization of the sample Figure 2.34 depicts the results. The lineshapes are clearer but exhibit the same trends.

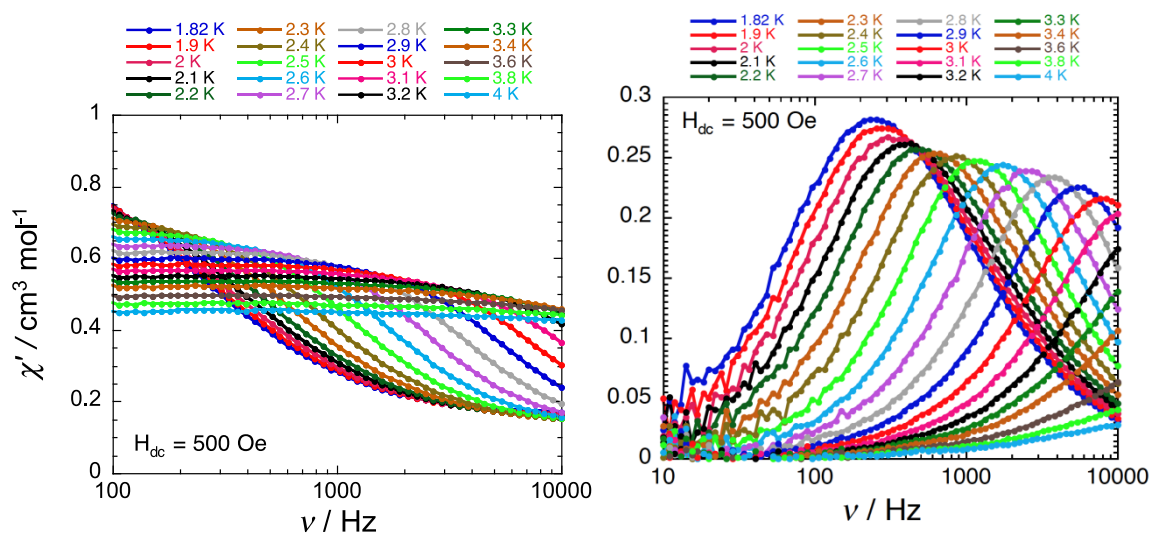


Figure 2.34. Left: Plots of χ' versus frequency for $(Tp^{Ph})CoCl$ in a bias field of 500 Oe at selected temperatures in the range of 1.8 to 4 K. The x axis has been plotted logarithmically to better present the lineshape. Right: Plots of χ' versus frequency for $(Tp^{Ph})CoCl$ in a bias field of 500 Oe at selected temperatures in the range of 1.8 to 4 K. The x axis has been plotted logarithmically to better present the lineshape.

The local maxima of χ'' can be made into an Arrhenius plot (Figure 2.35) from which a thermal barrier value and pre-exponential factor can be extracted.

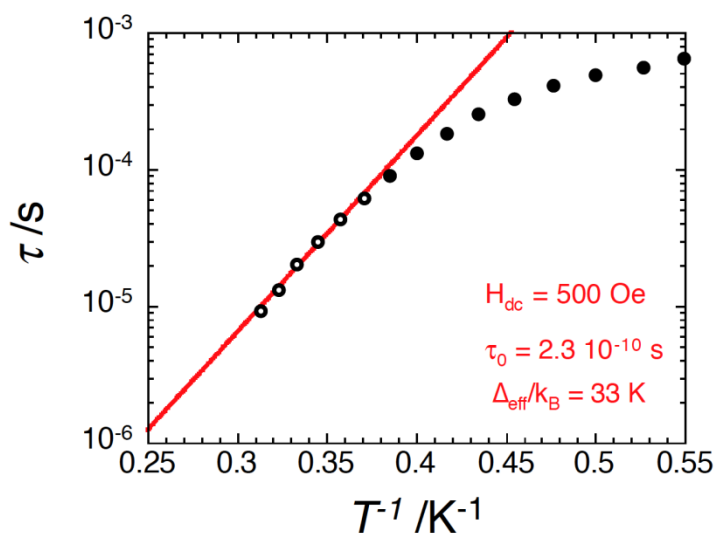


Figure 2.35. Arrhenius plot of the characteristic frequencies (ω) for the out-of-phase magnetic susceptibility of $(Tp^{Ph})CoCl$.

With an applied dc magnetic field of 500 Oe, an effective blocking temperature of 33 K is found with a pre-exponential factor of 2.3×10^{-10} s. The linear range of the Arrhenius plot extends up to roughly 0.375, above which there is a deviation.

This is attributable to relaxation pathways other than the Orbach process, which become dominant at lower temperatures and obey power laws other than $1/T$, specifically quantum tunneling of the magnetization. Via Equation 1.21 $|D| \cong 11.(5) \text{ cm}^{-1}$.

Other mononuclear SMMs with Co^{II} have been reported.^{34, 84, 86, 105, 125-126, 128, 130-131, 140, 144-145, 148} While many exhibit magnetic hysteresis only in an applied bias field, some examples are known that show magnetic hysteresis in zero bias field. Interestingly, these examples are tetrahedral or D_2 complexes that lack the rigid axial symmetry that has been considered a prerequisite for the suppression of quantum tunneling of the magnetization. This could be brought about by low-lying excited states that undermine the validity of quantum numbers and the

selection rules that govern them. The low symmetry and weak crystal field splitting can achieve this by eliminating the Laporte selection rule and increasing the density of states. It appears that a negative D value is necessary, but not sufficient, to observe SMM behavior in zero bias field. AC magnetic susceptibility is one method to determine the magnitude of D , but unequivocal assignment of the sign is more elusive, and other techniques are more suited to doing so. The magnetization dynamics suggest that the sign of D is positive, that easy plane anisotropy is present.

EPR measurements are a method by which the sign and magnitude of D can be measured. In comparison to other complexes $|D| \cong 11.(5) \text{ cm}^{-1}$ is typical and by no means approaches the highest values found to date. This leads to a calculated U_{eff} of roughly 26 K, but quantum tunneling decreases the observed lifetimes. The preexponential factor of $2.3 \times 10^{-10} \text{ s}$ is also comparable to literature values for monometallic Co complexes that show SMM behavior. These can range from $10^{-6} - 10^{-13}$.^{25, 125}

(Tp^{Ph})NiCl. While the lack of a degenerate ground state for Ni^{II} in C_3 symmetry precludes in-state SOC, out-of-state contributions to the SOC interaction may still introduce anisotropy to the magnetization. With a barrier to spin reversal, remnant magnetization may still be observed. These facts motivate the investigation of (Tp^{Ph})NiCl for SMM behavior.

A plot of the magnetization versus field strength at room temperature for (Tp^{Ph})NiCl (Figure 2.36) shows a linear relationship ($R = 1$), ruling out the

presence of ferromagnetic impurities or ferromagnetic ordering of the material. It is well-modeled by Equation 1.2 indicating that the material is at the weak field limit at fields up to 40000 Oe.

The magnetic susceptibility when plotted from 1.85 to 300 K shows a saturation at high temperature, deviating to lower values at low temperature (Figure 2.37).

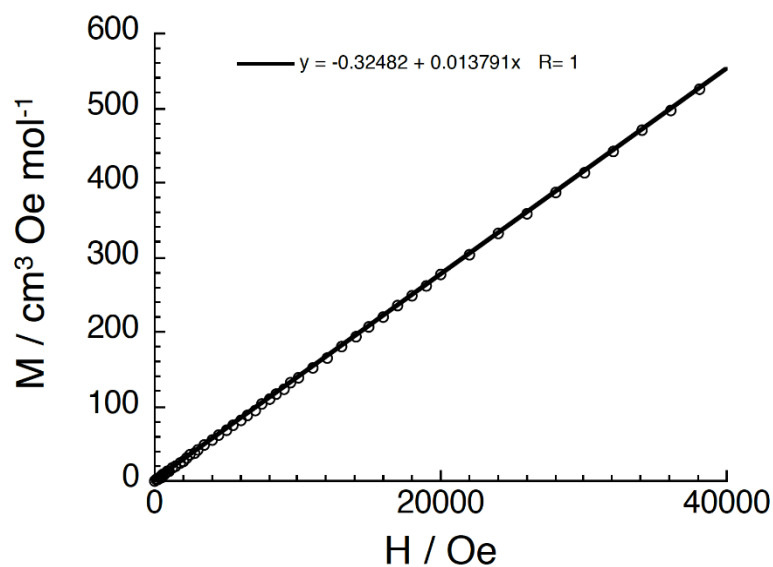


Figure 2.36. Magnetization versus field strength for $(Tp^{Ph})NiCl$ at room temperature with a linear fit overlaid.

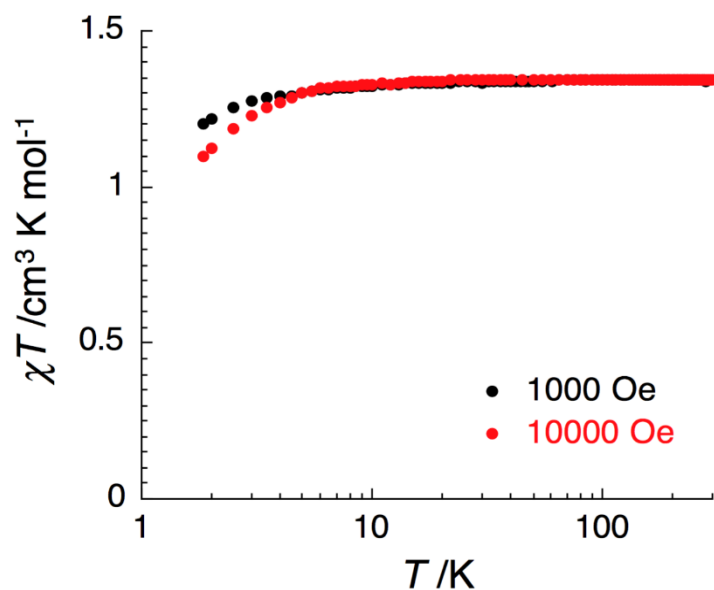


Figure 2.37. Magnetic susceptibility versus temperature at 1000 and 10000 Oe for $(\text{Tp}^{\text{Ph}})\text{NiCl}$. The x axis has been plotted logarithmically to include data over the entire temperature range from 1.8 K to room temperature while making the deviation at low temperature more visible.

The magnetic susceptibility at room temperature is $1.3 \text{ cm}^3 \text{ K/mol}$ which via Equation 1.15 gives $g = 2.3$, an agreement with the value from HFEP, $g = 2.3(1)$.

This deviation of g from the spin-only value prompted further investigation of the magnetic properties of $(\text{Tp}^{\text{Ph}})\text{NiCl}$. This was accomplished in a manner similar to the approach for $(\text{Tp}^{\text{Ph}})\text{CoCl}$ wherein the field and frequency dependencies were examined at low temperatures where the weak field limit no longer applies, and thermal disorder and field strength are comparable. Magnetization versus field strength, accounting for temperature, shows nearly superimposable traces that suggest weak magnetic anisotropy (Figure 2.38). Stronger magnetic anisotropy would manifest as a greater range of temperature-

adjust plots as in the case of $(\text{Tp}^{\text{Ph}})\text{CoCl}$. No attempt to fit the data with a Brillouin function was attempted.

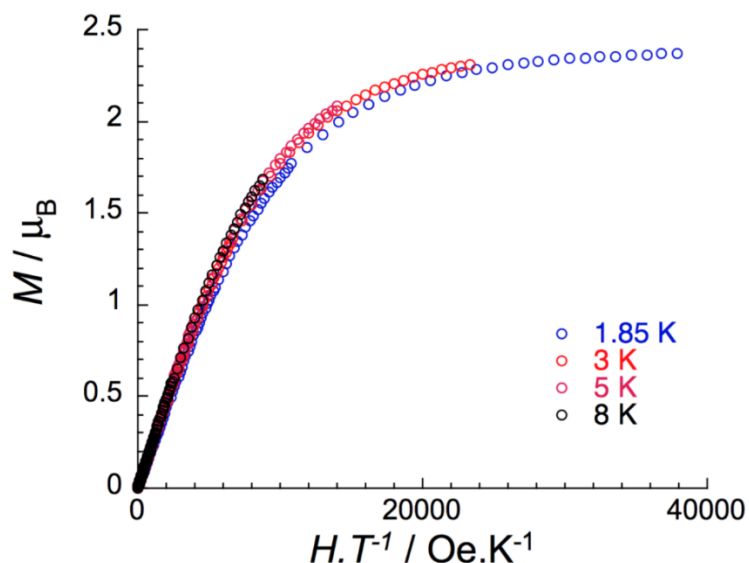


Figure 2.38. Magnetization versus field strength divided by temperature in the temperature range of 1.85 to 8 K for $(\text{Tp}^{\text{Ph}})\text{NiCl}$.

Next, the in-phase and out-of-phase magnetic susceptibility was surveyed at a range of DC bias fields to determine if hysteresis could be observed at zero bias field and the optimal conditions for making measurements to determine the characteristic frequency. Measurements were made at 1.9 K at ac field frequencies of 10 to 10000 Hz with applied bias fields in the range of 0 to 2500 Oe. At 0 Oe bias field, no hysteresis is observed. As a DC bias field is applied, frequency-dependent deviations appear as reductions in the magnetic moment. This strongly suggests that magnetic hysteresis can be observed with application of a bias field to suppress quantum tunneling of the magnetization. This is confirmed by examination of the out-of-phase data collected. Measurements were collected at 1.9 K, AC frequencies from 10 to 10000 Hz, and bias fields from 0 to 10000 Oe. Characteristic frequencies were extracted from the data and

when show an optimum bias field of 2500 Oe. The out-of-phase signal was measured by varying the temperature from 1.86 to 5 K. The results are shown in Figure 2.39.

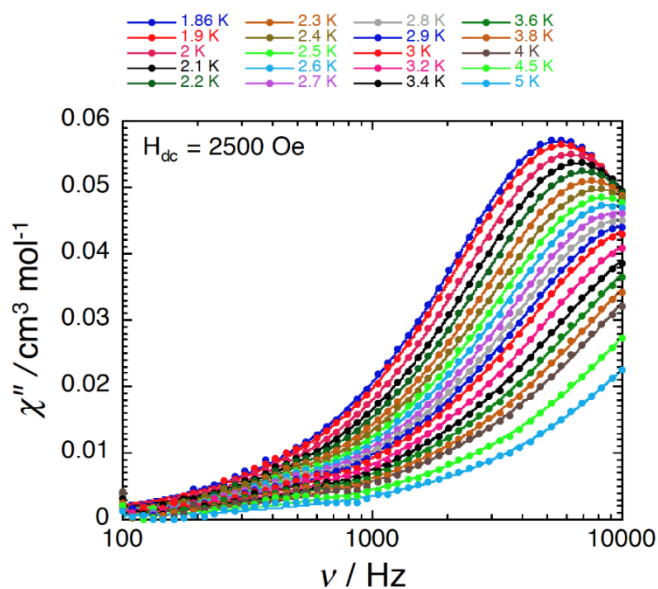


Figure 2.39. Out-of-phase susceptibility as a function of frequency at selected temperatures for $(\text{Tp}^{\text{Ph}})\text{NiCl}$.

The diminution of signal with increasing temperature is consistent with thermal energy overcoming hysteresis. From this data an Arrhenius plot was prepared (Figure 2.40). The extracted pre-exponential term is 4.6×10^{-6} s and $U_{\text{eff}} = 3.4$ K.

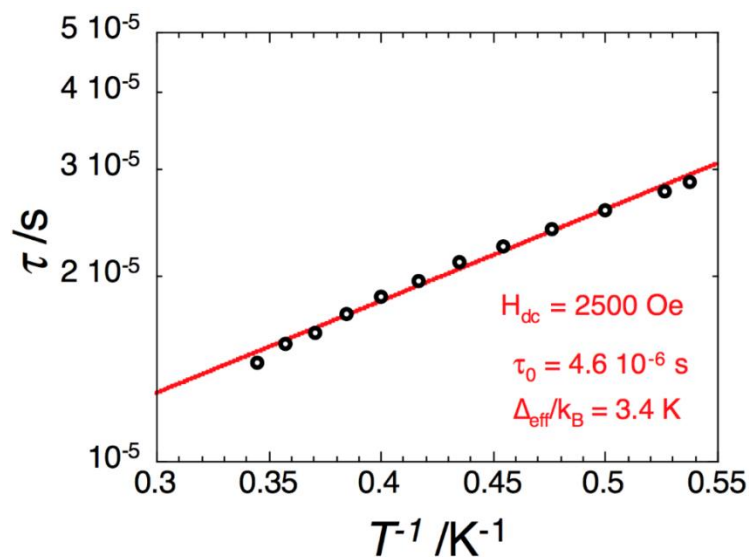


Figure 2.40. Arrhenius plot of magnetic data to determine the blocking temperature and pre-exponential term for $(\text{Tp}^{\text{Ph}})\text{NiCl}$.

$(\text{Tp}^{\text{Ph}})\text{Ni}(\text{phpy})\text{Cl}$. While this compound was not a synthetic target of this work, the low symmetry of the complex was thought to be interesting enough to examine the magnetic properties. The plot of magnetization versus field strength at 100 K (Figure 2.41) shows no long-range ordering or ferromagnetic impurities.

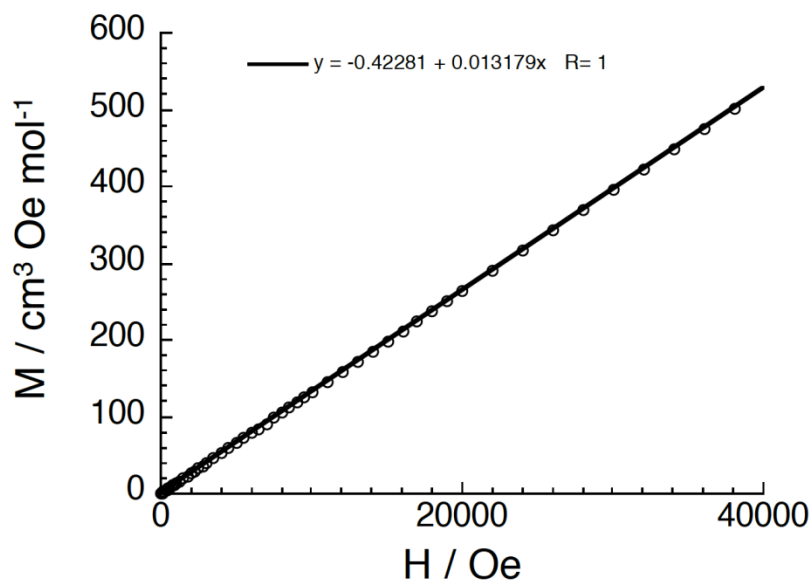


Figure 2.41. A plot of magnetization versus field strength at room temperature for $(Tp^{Ph})Ni(phpy)Cl$ with a best fit line overlaid.

The magnetic susceptibility was measured in two DC magnetic fields from the lower limit of the instrument to room temperature. The results are plotted in Figure 2.42.

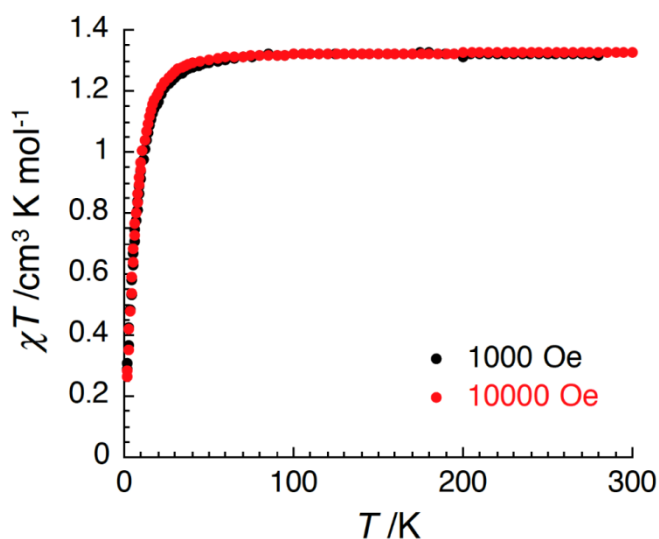


Figure 2.42. Magnetic susceptibility versus temperature at 1000 and 10000 Oe for $(Tp^{Ph})Ni(phpy)Cl$. The x axis has been plotted logarithmically to include data over the entire temperature range from 1.8 K to room temperature while making the deviation at low temperature more visible.

From this plot, the room temperature $\chi T = 1.32 \text{ cm}^3 \text{ K mol}^{-1}$, giving $g = 2.31$ which suggests a large degree of SOC, an assertion supported by further magnetic measurements. At 1.8 K there is no saturation of the magnetization up to 70000 Oe indicating a large magnetic anisotropy, and the fitting of data using the spin Hamiltonian formalism is poor. The χT vs. T data in Figure 2.42 can be fitted to give $g = 2.29(5)$ and $D = 22.5(5) \text{ K}$, but attempts to fit the M vs. H data failed. Each isothermal could be fitted with the g from the χT vs. T data, but each gave a different D value (Figure 2.43). The fitted D parameters for 1.85, 3, 5, and 8 K were 25.8(3), 25.9(7), 28.1(3), and 30.5(8) cm^{-1} . Superimposed isothermal plots will allow for a fit with acceptable residuals, but clearly this will not occur for this compound. One explanation is out-of-state contributions to SOC. This implies that excited states are present that are very low in energy, and as the temperature increases, these are quickly populated with each contributing to the resultant D value. This is a plausible explanation for the temperature-dependent ZFS. As the temperature increases, the population of states is altered, and each of these states has a different contribution to the ZFS. This causes the spin Hamiltonian formalism to fail.

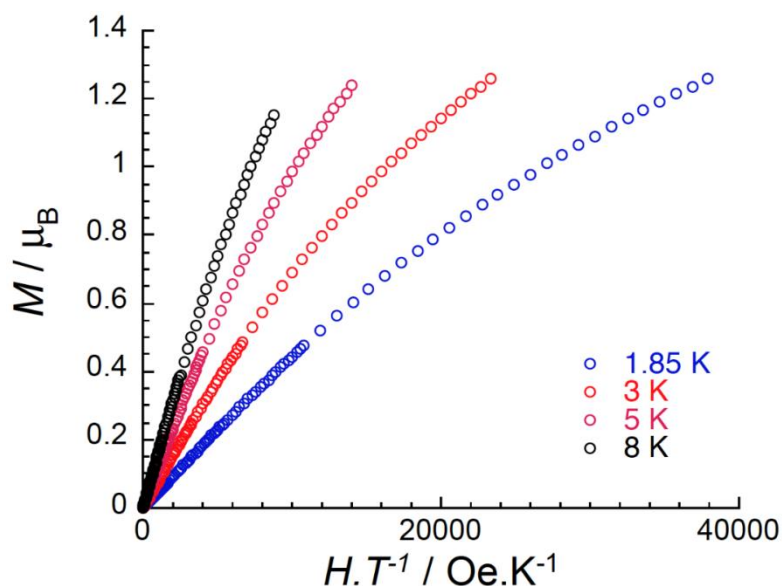


Figure 2.43. Magnetization versus field strength divided by temperature in the temperature range of 1.85 to 8 K for $(Tp^{Ph})Ni(phpy)Cl$.

Experiments at the range of the instrument to observe out-of-phase magnetic susceptibility found no evidence of this even with applied DC bias fields. For magnetic anisotropy to be present but no out-of-phase signal to be observed even with a DC bias field implies a density of states that makes suppression of QTM difficult. In the case where the compound is optimized for QTM, several processes can be operating in concert. These include spin-spin coupling, hyperfine interactions, and resonance QTM. ^{58}Ni (68%, $I = 0$) ^{60}Ni (26%, $I = 0$), ^{61}Ni (1%, $I = 3/2$), ^{62}Ni (4%, $I = 0$), and ^{64}Ni (1%, $I = 0$) are naturally occurring isotopes. Hyperfine interactions can split one M_s state into several, and this covers a wider range of energies, increasing the probability of quantum tunneling. Spin-spin coupling can provide a sink for $I = 0$ nuclei that have a lower probability of QTM by exchanging spin states such that the excited state is located on an $I = 3/2$ nucleus, i.e. ^{61}Ni , that can then engage in the enhanced

QTM discussed above. While this may seem daunting to unravel experimentally, there are techniques that could demonstrate what processes are occurring. Spin-spin coupling can be disrupted by increasing the mean distance between paramagnetic centers by magnetic dilution. While the compound $(\text{Tp}^{\text{Ph}})\text{Zn}(\text{phpy})\text{Cl}$ is not known to our knowledge, the preparation is likely to be accomplished by the addition of 1 equivalent of 3-phenylpyrazole to $(\text{Tp}^{\text{Ph}})\text{ZnCl}$. A small amount of $(\text{Tp}^{\text{Ph}})\text{Ni}(\text{phpy})\text{Cl}$ (ca. 1% mol:mol) could then be co-crystallized with $(\text{Tp}^{\text{Ph}})\text{Zn}(\text{phpy})\text{Cl}$. This would suppress spin-spin interactions, if present in pure $(\text{Tp}^{\text{Ph}})\text{Ni}(\text{phpy})\text{Cl}$. The preparation of crystals of $(\text{Tp}^{\text{Ph}})\text{Zn}(\text{phpy})\text{Cl}$ with evenly distributed $(\text{Tp}^{\text{Ph}})\text{Ni}(\text{phpy})\text{Cl}$ could be challenging. The two compounds may not mix evenly, and $(\text{Tp}^{\text{Ph}})\text{Zn}(\text{phpy})\text{Cl}$ might not be stable as the ionic radius of Zn^{II} is less than that of Ni^{II} . An alternate route would be to prepare $(\text{Tp}^{\text{Ph}})^{58}\text{Ni}(\text{phpy})\text{Cl}$ and $(\text{Tp}^{\text{Ph}})^{61}\text{Ni}(\text{phpy})\text{Cl}$. Due to its usefulness in radiomedicine, pure isotopes of Ni are commercially available. A given isotope of Ni metal can be reacted with HCl, isolated, and used as a reagent to prepare $(\text{Tp}^{\text{Ph}})^{58}\text{Ni}(\text{phpy})\text{Cl}$ or $(\text{Tp}^{\text{Ph}})^{61}\text{Ni}(\text{phpy})\text{Cl}$. Luckily, ^{58}Ni and ^{61}Ni are stable, avoiding the need for special equipment or precautions needed for radioactive isotopes.

2.4. Conclusions

For $(\text{Tp}^{\text{Ph}})\text{MnCl}$ it has been demonstrated that the complex is a simple paramagnetic material that exhibits no remnant magnetization. The ^6A ground state is isolated from any excited states that could contribute to out-of-state SOC

and create a barrier to magnetization reversal. Furthermore, although $(\text{Tp}^{\text{Ph}})\text{MnCl}$ has a non-degenerate ground state, a tilting of the Cl^- ligand away from collinearity with the $\text{M}\cdots\text{B}$ vector is observed in the solid state. This arises from crystal packing considerations and shows that this type of distortion is not necessarily from a Jahn-Teller effect.

The compound $(\text{Tp}^{\text{Ph}})\text{CoCl}$ has been spectroscopically and magnetically characterized and shows slow relaxation in the presence of a DC bias magnetic field. The AC magnetic susceptibility measurements show an $S = 3/2$ ground state and $U_{\text{eff}} = 33.4\text{K}$. $|D| \cong 11.5\text{ cm}^{-1}$ with the sign of D most likely being positive, as no slow relaxation is observed without a bias magnetic field.

Alteration of the halide from Cl to Br and I may increase the magnitude of D and change to easy axis anisotropy. Further characterization of $(\text{Tp}^{\text{Ph}})\text{CoBr}$ and $(\text{Tp}^{\text{Ph}})\text{CoI}$ are necessary. Magnetic measurements and EPR of both polymorphs of $(\text{Tp}^{\text{Ph}})\text{CoBr}$ could also be made to examine the role of the crystal lattice in magnetization.

$(\text{Tp}^{\text{Ph}})\text{NiCl}$ has been prepared and shows slow relaxation in a DC bias magnetic field. The lower barrier to magnetization reversal ($U_{\text{eff}} = 3.4\text{ K}$) can be ascribed to the smaller contribution of out-of-state mixing to generate SOC. Alteration of the axial ligand to heavier halides may increase the ZFS and potentially change the sign of D which is most likely positive. The addition of a ligand in $(\text{Tp}^{\text{Ph}})\text{Ni}(\text{phpy})\text{Cl}$ has a profound effect on the magnetic properties of the material, but they are unsuitable for investigation using the Spin Hamiltonian formalism. There is not one D value, but a temperature dependence. Either a

more detailed model needs to be employed or alternate characterization methods should be used like EPR.

Given the fruitful investigations of compounds $(\text{Tp}^{\text{Ph}})\text{CoCl}$, $(\text{Tp}^{\text{Ph}})\text{CoBr}$, $(\text{Tp}^{\text{Ph}})\text{NiCl}$, $(\text{Tp}^{\text{Ph}})\text{NiBr}$, and $(\text{Tp}^{\text{Ph}})\text{NiI}$, effort should be made to complete the characterizations of the halide series for both Co and Ni. The increased SOC and contribution to the ZFS of heavier halides may increase the observed blocking temperature, increase $|D|$ and render $D < 0$. This may increase the observed barrier to magnetization reversal and even make it observable under no DC bias magnetic field.

2.5. Experimental

All samples were prepared at the University of Missouri-Saint Louis using inorganic synthesis techniques including inert atmosphere methods. Schlenk lines and glove boxes were used to prepare and manipulate materials to produce samples and prepare them for further investigation. Argon gas (Airgas) was the inert atmosphere for Schlenk line manipulations and was used as received. A Vacuum Atmospheres Corporation glovebox was used with nitrogen gas (Airgas) as the inert atmosphere. When possible, nitrogen was provided from a high pressure boil off tank as these contain less water and oxygen. The VAC glovebox uses an adsorbent bed to remove oxygen and water from recirculated nitrogen gas, maintaining the concentration of oxygen below 0.3 ppm.

Potassium hydridotris(3-phenylpyrazolyl) borate was prepared according to literature procedure.¹⁶¹ Rinsing with toluene, hexanes, and heating *in vacuo*

removed residual 3(5)-phenylpyrazole. Anhydrous metal halides of Zn, Co, and Mn were prepared by heating hydrated salts *in vacuo*. FeCl₂·1.5thf was prepared according to literature procedure.²³³ The compounds (Tp^{Ph})NiCl, (Tp^{Ph})NiBr, and (Tp^{Ph})NiI were reported while this manuscript was in preparation by a different method than that reported here.¹⁷⁹

Pentane, hexane, diethyl ether, toluene, and tetrahydrofuran (Fisher) were refluxed with Na metal and benzophenone under a nitrogen atmosphere and distilled prior to use.²³⁴ Dichloromethane (Fisher) was refluxed over calcium hydride under a nitrogen atmosphere and distilled prior to use.²³⁴ Methanol (Fisher) was refluxed over magnesium turnings and iodine under a nitrogen atmosphere and distilled prior to use.²³⁴ Acetone was stirred over drierite™ (calcium sulfate) and distilled under reduced pressure prior to use.²³⁴

(Tp^{Ph})MnCl. This compound was synthesized by drying 0.172 g (0.869 mmol) MnCl₂·4OH₂ *in vacuo* at 150 °C after which 0.396 g (0.824 mmol) potassium hydridotris(3-phenylpyrazolyl) borate was added and the mixture stirred 16 hr with 15 mL dichloromethane. Filtering and reducing the volume to ca. 5 mL yielded a straw-colored solution. Upon layering with hexane tan crystals formed (0.212 g, 0.399 mmol). Yield: 48.4%. (M.W. = 531.71 g/mol). IR (Nujol, cm⁻¹): 3314 (m), 3119 (m), 3050 (m), 3031 (m), 2854 (vs), 2474 (m) 2334 (w), 2201 (w), 2136 (w), 1944 (w), 1877 (w), 1800 (w), 1771 (w), 1741 (w), 1677 (w), 1605 (w), 1581 (w), 1523 (m), 1493 (vs), 1467 (vs), 1365 (vs), 1279 (w), 1251 (m), 1182 (vs), 1118 (m), 1103 (m), 1089 (m), 1052 (vs), 1027 (m), 1007 (m), 957 (w), 914

(w), 887 (w), 872 (w), 840 (w), 789 (s), 759 (vs), 746 (m), 732 (s), 704 (s), 695 (vs), 676 (m), 651 (w), 527 (w), 518 (w), 453 (w), 439 (w).

(Tp^{Ph})CoCl. Anhydrous CoCl₂ (0.217 g, 1.67 mmol) and KTp^{Ph} (0.478 g, 0.995 mmol) were combined as solids and CH₂Cl₂ (40 mL) was added. The mixture was magnetically stirred for 16 h at room temperature. The following day the blue mixture was filtered, and the filtrate evacuated to dryness at 60 °C. The blue residue was dissolved in tetrahydrofuran (3 mL), layered with hexanes (15 mL), and allowed to stand for 2 d at -20 °C. The blue crystals were isolated via suction filtration and dried under vacuum at room temperature for 2 min. Yield: 0.270 g (51.5%). Anal. Calcd for C₂₇H₂₂BClCoN₆: C, 60.54; H, 4.14; N, 15.69. Found: C, 60.78; H, 3.97; N, 15.55. IR (Nujol/KBr, cm⁻¹): 3868 (w), 3814 (w), 3748 (w), 3742 (w), 3654 (w), 3646 (w), 3287 (m), 3139 (s), 3113 (s), 3050 (s), 3031 (s), 2854 (vs), 2495 (s), 2349 (w), 2285 (w), 2201 (w), 2133 (w), 1962 (w), 1942 (w), 1892 (w), 1877 (w), 1819 (w), 1798 (w), 1766 (w), 1743 (w), 1658 (w), 1600 (w), 1582 (w), 1524 (s), 1492 (vs), 1450 (vs), 1366 (vs), 1329 (m), 1181 (vs), 1118 (s), 1104 (s), 1089 (s), 1074 (vs), 1051 (vs), 1029 (vs), 1009 (s), 960 (m), 915 (m), 885 (m), 872 (m), 840 (m), 800 (vs), 790 (vs), 757 (vs), 741 (s), 728 (vs), 694 (vs), 676 (s), 648 (m), 633 (w), 619 (w), 569 (w), 528 (w), 517 (w), 458 (m), 440 (w). UV-vis (CH₂Cl₂): λ_{max}/nm (ε_M/M⁻¹ cm⁻¹): 595 (486), 632 (783), 668 (674), 930 (52), 1653 (70).

α/β-(Tp^{Ph})CoBr. CoBr₂ (0.219 g, 1.00 mmol) and KTp^{Ph} (0.459 g, 0.956 mmol) were added as solids to CH₂Cl₂ (10 mL) and allowed to magnetically stir for 2 d at room temperature. The mixture was filtered, and the filtrate evacuated to

dryness at 60 °C. The blue residue was dissolved in CH₂Cl₂ (ca. 3 mL), layered with 10 mL pentanes and allowed to stand for 2 d at -20 °C. The blue crystals were isolated via suction filtration and dried under vacuum at room temperature for 2 min. Yield: 0.237 g (42.7%). Two polymorphs (α -(Tp^{Ph})CoBr and β -(Tp^{Ph})CoBr) may be isolated via manual separation of crystals or extraction of the more soluble tetragonal polymorph (β -(Tp^{Ph})CoBr) into cold acetone. Anal. Calcd for C₂₇H₂₂BBrCoN₆ (mixture of α -(Tp^{Ph})CoBr and β -(Tp^{Ph})CoBr): C, 55.90; H, 3.82; N, 14.49. Found: C, 56.06; H, 3.89; N, 14.63. IR (Nujol, cm⁻¹): 3143 (m), 3114 (m), 2854 (vs), 2479 (m), 1943 (w), 1869 (w), 1792 (w), 1772 (w), 1749 (w), 1734 (w), 1717 (w), 1698 (w), 1684 (w), 1670 (w), 1653 (w), 1647 (w), 1636 (w), 1617 (w), 1576 (w), 1558 (w), 1541 (w), 1525 (m), 1493 (vs), 1468 (vs), 1249 (m), 1181 (vs), 1117 (m), 1087 (s), 1075 (s), 1048 (vs), 1005 (m), 962 (w), 912 (w), 872 (w), 793 (s), 762 (vs), 755 (vs), 727 (vs), 695 (vs), 674 (m), 648 (w), 618 (w), 524 (w), 452 (w), 419 (w). UV-vis (CH₂Cl₂): $\lambda_{\text{max}}/\text{nm}$ ($\epsilon_M/M^{-1} \text{ cm}^{-1}$): 561 (68), 598 (325), 643 (653), 673 (516), 942 (53), 1691 (80).

(Tp^{Ph})Col. In the absence of light, addition of an acetone (5 mL) solution of NaI (0.1545 g, 1.031 mmol) to a suspension of (Tp^{Ph})CoBr (0.4059 g, 0.7549 mmol) in acetone (15 mL) immediately gave a blue-green mixture that was magnetically stirred for 3 h at room temperature. The mixture was evacuated to dryness at room temperature and the residue was extracted into CH₂Cl₂ (8 mL). The mixture was filtered and pentane (30 mL) precipitated a blue-green powder.

Yield: 0.212 g (44.6%). Anal. Calcd for C₂₇H₂₂BrIN₆Co: C, 51.71; H, 3.54; N, 13.40. Found: C, 51.24; H, 3.31; N, 13.06. IR (Nujol, cm⁻¹): 3140 (w), 3114 (w),

2478 (m, sh), 1740 (w), 1650 (m), 1581 (w), 1524 (m), 1491 (vs), 1309 (m), 1216 (m), 1246 (s), 1216 (m), 1185 (vs), 1178 (vs), 1116 (m), 1089 (m), 1073 (s), 1046 (vs, sh), 910 (m), 871 (w), 792 (s), 761 (vs), 754 (vs), 730 (vs), 725 (vs), 692 (vs, sh), 646 (m), 519 (m), 499 (m), 440 (m).

(Tp^{Ph})NiCl. In methanol Ni(OH₂)₆Cl₂ (0.176g, 0.740 mmol) was dissolved and added to a slurry of 0.310g (0.645 mmol) KTp^{Ph} in tetrahydrofuran. The green and cloudy suspension was stirred for 16 hr to give a mustard yellow suspension. This gave a pink powder after evacuation to dryness. The solid was extracted with 20 mL dichloromethane and layered with 30 mL diethyl ether to give dark magenta X-ray quality crystals. A second crop was isolated with additional ether. Overall yield: 0.2256 g (65.4%). IR (Nujol, cm⁻¹): 3851 (w), 3139 (m), 3126 (s), 3074 (m), 3049 (m), 3023 (m), 2854 (vs), 2505 (m), 2314 (w), 2141 (w), 1993 (w), 1965 (w), 1939 (w), 1915 (w), 1887 (w), 1838 (w), 1812 (w), 1759 (w), 1671 (w), 1615 (w), 1580 (w), 1522 (m), 1494 (vs), 1404 (w), 1366 (s), 1278 (w), 1191 (vs), 1117 (m), 1093 (m), 1070 (s), 1053 (vs), 1028 (m), 955 (m), 919 (m), 883 (m), 843 (w), 821 (w), 797 (vs), 767 (vs), 741 (m), 730 (vs), 709 (s), 701 (vs), 676 (s), 638 (w), 617 (w), 530 (m). UV-vis (CH₂Cl₂): 486 (81), 524 (33), 805 (12), 950 (26) Anal. Calcd for C₂₇H₂₂BClN₆Ni (M.W. = 535.71 g/mol) C, 60.56; H, 4.14; N, 15.69. Found: C, 60.39; H, 3.89; N, 15.63.

(Tp^{Ph})NiBr. Solid NiBr₂ (0.744 g, 3.42 mmol) and KTp^{Ph} (1.63 g, 3.39 mmol) were suspended into CH₂Cl₂ (25 mL) and magnetically stirred for 48 h. The mixture was filtered, and the purple filtrate was evacuated to dryness at room temperature. The residue was re-dissolved in a minimum of CH₂Cl₂ (ca. 5 mL),

layered with pentane (10 mL), and allowed to stand for 7 d at -20 °C. Yield: 0.910 g (46.3%). Anal. Calcd for $C_{27}H_{22}BBrNiN_6$: C, 55.92; H, 3.82; N, 14.49. Found: C, 55.92; H, 3.91; N, 14.63. IR (Nujol, cm^{-1}): 3138 (m), 3125 (s), 3023 (s), 2504 (m), 1990 (w), 1963 (w), 1886 (w), 1837 (w), 1811 (w), 1759 (w), 1670 (w), 1580 (w), 1521 (m), 1493 (vs), 1467 (vs), 1366 (vs), 1190 (vs), 1117 (m), 1093 (m), 1071 (s), 1053 (vs), 1028 (m), 1013 (m), 970 (w), 954 (m), 918 (m), 883 (m), 842 (w), 796 (vs), 767 (vs), 741 (m), 730 (vs), 701 (vs), 676 (s), 617 (w), 530 (m), 445 (m). UV-vis (CH_2Cl_2): λ_{max}/nm ($\epsilon_M/M^1 cm^{-1}$): 497 (338), 532 (173), 817 (51), 951 (92). NIR (CCl_4): λ_{max}/nm ($\epsilon_M/M^1 cm^{-1}$): 1255 (10), 1391 (200), 1691 (80).

(Tp^{Ph})Ni(phpy)Cl. This compound was isolated as a side product from the synthesis of (Tp^{Ph})NiCl.

(Tp^{Ph})ZnCl. To prepare (Tp^{Ph})ZnCl, 0.160 g (1.17 mmol) $ZnCl_2$ and 0.403 g (0.834 mmol) KTp^{Ph} were dissolved in 10 mL dried MeOH and stirred 16 h. This mixture was evacuated to dryness and extracted with 15 mL dried dichloromethane. Filtering removed precipitated KCl and the clear supernatant was reduced in volume to ca. 5 mL. Layering with dry diethyl ether gave clear crystals (0.266 g, 0.491 mmol) Yield: 0.266 g (58.9%) Anal. Calcd for $C_{27}H_{22}BCIN_6Zn$ (M.W. = 542.15 g/mol) C, 59.82; H, 4.09; N, 15.50. Found: C, 59.58; H, 3.93; N, 15.20. IR (Nujol, cm^{-1}): 3139 (s), 3125 (s), 3075 (m), 3049 (s), 3024 (s), 2854 (vs), 2512 (m), 2503 (s), 1993 (w), 1966 (w), 1915 (w), 1888 (w), 1837 (w), 1813 (w), 1761 (w), 1687 (w), 1673 (w), 1580 (w), 1568 (w), 1523 (vs), 1494 (vs), 1468 (vs), 1447 (vs), 1420 (m), 1403 (m), 1380 (vs), 1370 (vs), 1277 (m), 1187 (vs), 1137 (m), 1117 (s), 1093 (s), 1071 (vs), 1053 (vs), 1027 (s), 1009

(s), 955 (s), 919 (s), 884 (s), 844 (s), 797 (vs), 768 (vs), 742 (vs), 730 (vs), 709 (vs), 701 (vs), 676 (vs), 648 (w), 638 (w), 617 (w), 530 (s), 444 (s), 436 (m).

2.6. References

25. Smolko, L.; Černák, J.; Dušek, M.; Miklovič, J.; Titiš, J.; Boča, R., Three Tetracoordinate Co(II) Complexes [Co(Biq)X₂](X = Cl, Br, I) with Easy-Plane Magnetic Anisotropy as Field-Induced Single-Molecule Magnets. *Dalton Transactions* **2015**, 44 (40), 17565-17571.
34. Gómez-Coca, S.; Aravena, D.; Morales, R.; Ruiz, E., Large Magnetic Anisotropy in Mononuclear Metal Complexes. *Coordination Chemistry Reviews* **2015**, 289, 379–392.
35. Neese, F.; Pantazis, D.A., What Is Not Required to Make a Single Molecule Magnet. *Faraday Discussions* **2011**, 148, 229-238.
38. Gatteschi, D.; Sessoli, R., Quantum Tunneling of Magnetization and Related Phenomena in Molecular Materials. *Angewandte Chemie International Edition* **2003**, 42 (3), 268-297.
50. Figgis, B.N.; Hitchman, M.A., Introduction. In *Ligand Field Theory and Its Applications*, Second Edition ed.; Wiley Interscience: New York, 1999; pp 1-26.
76. Huang, W.; Liu, T.; Wu, D.; Cheng, J.; Ouyang, Z.; Duan, C., Field-Induced Slow Relaxation of Magnetization in a Tetrahedral Co(II) Complex with Easy Plane Anisotropy. *Dalton Transactions* **2013**, 42 (43), 15326-15331.
84. Rechkemmer, Y.; Breitgoff, F.D.; van der Meer, M.; Atanasov, M.; Haki, M.; Orlita, M.; Neugebauer, P.; Neese, F.; Sarkar, B.; van Slageren, J., A Four-

Coordinate Cobalt(II) Single-Ion Magnet with Coercivity and a Very High Energy Barrier. *Nature Communications* **2016**, 7, 10467.

86. Herchel, R.; Váhovská, L.; Potočný, I.; Trávníček, Z.k., Slow Magnetic Relaxation in Octahedral Cobalt(II) Field-Induced Single-Ion Magnet with Positive Axial and Large Rhombic Anisotropy. *Inorganic Chemistry* **2014**, 53 (12), 5896-5898.

97. Perić, M.; García-Fuente, A.; Zlatar, M.; Daul, C.; Stepanović, S.; García-Fernández, P.; Gruden-Pavlović, M., Magnetic Anisotropy in “Scorpionate” First-Row Transition-Metal Complexes: A Theoretical Investigation. *Chemistry – A European Journal* **2015**, 21 (9), 3716-3726.

104. Zhang, Y.Z.; Mallik, U.P.; Clerac, R.; Rath, N.P.; Holmes, S.M., Irreversible Solvent-Driven Conversion in Cyanometalate $\{Fe_2Ni\}_N$ ($N=2, 3$) Single-Molecule Magnets. *Chemical Communications* **2011**, 47 (25), 7194-6.

105. Zhu, Y.-Y.; Cui, C.; Zhang, Y.-Q.; Jia, J.-H.; Guo, X.; Gao, C.; Qian, K.; Jiang, S.-D.; Wang, B.-W.; Wang, Z.-M., Zero-Field Slow Magnetic Relaxation from Single Co(II) Ion: A Transition Metal Single-Molecule Magnet with High Anisotropy Barrier. *Chemical Science* **2013**, 4 (4), 1802-1806.

110. Coutinho, J.T.; Antunes, M.A.; Pereira, L.C.; Bolvin, H.; Marcalo, J.; Mazzanti, M.; Almeida, M., Single-Ion Magnet Behaviour in $[U(Tp^{me2})_2]$. *Dalton Transactions* **2012**, 41 (44), 13568-71.

123. Park, K.; Holmes, S.M., Exchange Coupling and Contribution of Induced Orbital Angular Momentum of Low-Spin Fe^{3+} Ions to Magnetic Anisotropy in

Cyanide-Bridged Fe₂m₂ Molecular Magnets: Spin-Polarized Density-Functional Calculations. *Physical Review B* **2006**, *74* (22), 224440.

125. Zadrozny, J.M.; Telser, J.; Long, J.R., Slow Magnetic Relaxation in the Tetrahedral Cobalt(II) Complexes [Co (Eph)₄]²⁻ (E=O, S, Se). *Polyhedron* **2013**, *64*, 209-217.

126. Fataftah, M.S.; Zadrozny, J.M.; Rogers, D.M.; Freedman, D.E., A Mononuclear Transition Metal Single-Molecule Magnet in a Nuclear Spin-Free Ligand Environment. *Inorganic Chemistry* **2014**, *53* (19), 10716-10721.

128. Boča, R.; Miklovič, J.; Titiš, J.N., Simple Mononuclear Cobalt(II) Complex: A Single-Molecule Magnet Showing Two Slow Relaxation Processes. *Inorganic Chemistry* **2014**, *53* (5), 2367-2369.

130. Zadrozny, J.M.; Liu, J.; Piro, N.A.; Chang, C.J.; Hill, S.; Long, J.R., Slow Magnetic Relaxation in a Pseudotetrahedral Cobalt(II) Complex with Easy-Plane Anisotropy. *Chemical Communications* **2012**, *48* (33), 3927-9.

131. Zadrozny, J.M.; Long, J.R., Slow Magnetic Relaxation at Zero Field in the Tetrahedral Complex [Co(Sph)₄]²⁻. *Journal of the American Chemical Society* **2011**, *133* (51), 20732-4.

132. Titiš, J.; Miklovič, J.; Boča, R., Magnetostructural Study of Tetracoordinate Cobalt(II) Complexes. *Inorganic Chemistry Communications* **2013**, *35*, 72-75.

140. Vallejo, J.; Castro, I.; Ruiz-García, R.; Cano, J.; Julve, M.; Lloret, F.; De Munno, G.; Wernsdorfer, W.; Pardo, E., Field-Induced Slow Magnetic Relaxation in a Six-Coordinate Mononuclear Cobalt(II) Complex with a Positive Anisotropy. *Journal of the American Chemical Society* **2012**, *134* (38), 15704-15707.

141. Saber, M.R.; Dunbar, K.R., Ligands Effects on the Magnetic Anisotropy of Tetrahedral Cobalt Complexes. *Chemical Communications* **2014**, 50 (82), 12266-12269.
142. Chen, L.; Wang, J.; Wei, J.-M.; Wernsdorfer, W.; Chen, X.-T.; Zhang, Y.-Q.; Song, Y.; Xue, Z.-L., Slow Magnetic Relaxation in a Mononuclear Eight-Coordinate Cobalt(II) Complex. *Journal of the American Chemical Society* **2014**, 136 (35), 12213-12216.
144. Ziegenbalg, S.; Hornig, D.; Görls, H.; Plass, W., Cobalt(II)-Based Single-Ion Magnets with Distorted Pseudotetrahedral [N₂O₂] Coordination: Experimental and Theoretical Investigations. *Inorganic Chemistry* **2016**, 55, 4047-4058.
145. Buchholz, A.; Eseola, A.O.; Plass, W., Slow Magnetic Relaxation in Mononuclear Tetrahedral Cobalt(II) Complexes with 2-(1H-imidazol-2-yl) Phenol Based Ligands. *Comptes Rendus Chimie* **2012**, 15 (10), 929-936.
146. Cao, D.-K.; Feng, J.-Q.; Ren, M.; Gu, Y.-W.; Song, Y.; Ward, M.D., A Mononuclear Cobalt(II)-Dithienylethene Complex Showing Slow Magnetic Relaxation and Photochromic Behavior. *Chemical Communications* **2013**, 49 (78), 8863-8865.
147. Yang, F.; Zhou, Q.; Zhang, Y.; Zeng, G.; Li, G.; Shi, Z.; Wang, B.; Feng, S., Inspiration from Old Molecules: Field-Induced Slow Magnetic Relaxation in Three Air-Stable Tetrahedral Cobalt(II) Compounds. *Chemical Communications* **2013**, 49 (46), 5289-5291.
148. Eichhöfer, A.; Lan, Y.; Mereacre, V.; Bodenstein, T.; Weigend, F., Slow Magnetic Relaxation in Trigonal-Planar Mononuclear Fe(II) and Co(II)

Bis(Trimethylsilyl) Amido Complexes: A Comparative Study. *Inorganic Chemistry* **2014**, 53 (4), 1962-1974.

151. Poulten, R.C.; Page, M.J.; Algarra, A.s.G.; Le Roy, J.J.; López, I.; Carter, E.; Llobet, A.; Macgregor, S.A.; Mahon, M.F.; Murphy, D.M., Synthesis, Electronic Structure, and Magnetism of $[\text{Ni}(\text{6-Mes})_2]^+$: A Two-Coordinate Nickel(I) Complex Stabilized by Bulky N-Heterocyclic Carbenes. *Journal of the American Chemical Society* **2013**, 135 (37), 13640-13643.

155. Desrochers, P.J.; Telsler, J.; Zvyagin, S.A.; Ozarowski, A.; Krzystek, J.; Vivic, D.A., Electronic Structure of Four-Coordinate C_{3v} Nickel(II) Scorpionate Complexes: Investigation by High-Frequency and -Field Electron Paramagnetic Resonance and Electronic Absorption Spectroscopies. *Inorganic Chemistry* **2006**, 45, 8930-8941.

158. Tanabe, Y.; Sugano, S., On the Absorption Spectra of Complex Ions. I. *Journal of the Physical Society of Japan* **1954**, 9 (5), 753-766.

159. Trofimenko, S., Recent Advances in Poly(Pyrazolyl)Borate (Scorpionate) Chemistry. *Chemical Reviews* **1993**, 93 (3), 943-980.

160. Trofimenko, S., Scorpionates: Genesis, Milestones, Prognosis. *Polyhedron* **2004**, 23 (2-3), 197-203.

161. Trofimenko, S.; Calabrese, J.C.; Thompson, J.S., Novel Polypyrazolylborate Ligands: Coordination Control through 3-Substituents of the Pyrazole Ring. *Inorganic Chemistry* **1987**, 26 (10), 1507-1514.

162. Trofimenko, S., Boron-Pyrazole Chemistry. I. Pyrazaboles. *Journal of the American Chemical Society* **1967**, 89 (13), 3165-3170.

163. Trofimenko, S., Boron-Pyrazole Chemistry. II. Poly(1-Pyrazolyl)-Borates. *Journal of the American Chemical Society* **1967**, 89 (13), 3170-3177.
164. Trofimenko, S., Boron-Pyrazole Chemistry. Iv. Carbon- and Boron-Substituted Poly[(1-Pyrazolyl) Borates]. *Journal of the American Chemical Society* **1967**, 89 (24), 6288-6294.
165. Bortoluzzi, M.; Paolucci, G.; Polizzi, S.; Bellotto, L.; Enrichi, F.; Ciorba, S.; Richards, B.S., Photoluminescence Studies on Europium-Based Scorpionate-Complex. *Inorganic Chemistry Communications* **2011**, 14 (11), 1762-1766.
166. Silva, T.F.; Alegria, E.C.; Martins, L.M.; Pombeiro, A.J., Half-Sandwich Scorpionate Vanadium, Iron and Copper Complexes: Synthesis and Application in the Catalytic Peroxidative Oxidation of Cyclohexane under Mild Conditions. *Advanced Synthesis and Catalysis* **2008**, 350 (5), 706-716.
167. Tsoureas, N.; Owen, G.R.; Hamilton, A.; Orpen, A.G., Flexible Scorpionates for Transfer Hydrogenation: The First Example of Their Catalytic Application. *Dalton Transactions* **2008**, (43), 6039-6044.
168. Rocha, B.G.; Mac Leod, T.C.; da Silva, M.F.C.G.; Luzyanin, K.V.; Martins, L.M.; Pombeiro, A.J., Ni^{II}, Cu^{II} and Zn^{II} Complexes with a Sterically Hindered Scorpionate Ligand (Tpms^{Ph}) and Catalytic Application in the Diastereoselective Nitroaldol (Henry) Reaction. *Dalton Transactions* **2014**, 43 (40), 15192-15200.
169. Real, J.A.; Muñoz, M.C.; Faus, J.; Solans, X., Spin Crossover in Novel Dihydrobis(1-Pyrazolyl)Borate [H₂B(Pz)₂]-Containing Iron(II) Complexes. Synthesis, X-Ray Structure, and Magnetic Properties of [Fe{H₂B(Pz)₂}₂] (L =

1,10-Phenanthroline and 2,2'-Bipyridine). *Inorganic Chemistry* **1997**, 36 (14), 3008-3013.

170. Moubaraki, B.; Leita, B.A.; Halder, G.J.; Batten, S.R.; Jensen, P.; Smith, J.P.; Cashion, J.D.; Kepert, C.J.; Letard, J.F.; Murray, K.S., Structure, Magnetism and Photomagnetism of Mixed-Ligand Tris(Pyrazolyl)Methane Iron(II) Spin Crossover Compounds. *Dalton Transactions* **2007**, (39), 4413-26.

171. Ma, H.; Chattopadhyay, S.; Petersen, J.L.; Jensen, M.P., Harnessing Scorpionate Ligand Equilibria for Modeling Reduced Nickel Superoxide Dismutase Intermediates. *Inorganic Chemistry* **2008**, 47 (18), 7966-7968.

172. Krzystek, J.; Swenson, D.C.; Zvyagin, S.; Smirnov, D.; Ozarowski, A.; Telser, J., Cobalt(II) "Scorpionate" Complexes as Models for Cobalt-Substituted Zinc Enzymes: Electronic Structure Investigation by High-Frequency and-Field Electron Paramagnetic Resonance Spectroscopy. *Journal of the American Chemical Society* **2010**, 132 (14), 5241-5253.

173. Li, D.; Parkin, S.; Wang, G.; Yee, G.T.; Clérac, R.; Wernsdorfer, W.; Holmes, S.M., An S = 6 Cyanide-Bridged Octanuclear (Fe^{III})₄(N^{III})₄ Complex That Exhibits Slow Relaxation of the Magnetization. *Journal of the American Chemical Society* **2006**, 128 (13), 4214-4215.

174. Trofimenko, S.; Calabrese, J.C.; Kochi, J.K.; Wolowiec, S.; Hulsbergen, F.B.; Reedijk, J., Spectroscopic Analysis, Coordination Geometry, and X-Ray Structures of Nickel(II) Compounds with Sterically Demanding Tris(Pyrazolyl)Borate Ligands and Azide or (Thio)Cyanate Anions. Crystal and Molecular Structures of Bis[(μ -Thiocyanato-N,S)(Hydrotris(3-Isopropyl-4-

bromopyrazol-1-yl)borato) Nickel(II)]-3-Heptane and (Thiocyanato-N)(Hydrotris(3-Tert-Butyl-5-Methylpyrazol-1-yl)borato) Nickel(II). *Inorganic Chemistry* **1992**, 31 (19), 3943-3950.

175. Ye, S.; Neese, F., How Do Heavier Halide Ligands Affect the Signs and Magnitudes of the Zero-Field Splittings in Halogenonickel(II) Scorpionate Complexes? A Theoretical Investigation Coupled to Ligand-Field Analysis. *Journal of Chemical Theory and Computation* **2012**, 8 (7), 2344-2351.

176. Calabrese, J.C.; Domaille, P.J.; Thompson, J.S.; Trofimenko, S., Steric Effects in Polypyrazolylborates: Mixed Complexes $M(\text{HB}(3\text{-isopropyl-4-bromopyrazolyl})_3\text{L})$. *Inorganic Chemistry* **1990**, 29 (22), 4429-4437.

177. Zhang, Y.Z.; Mallik, U.P.; Rath, N.P.; Clerac, R.; Holmes, S.M., Pyrazolylborates and Their Importance in Tuning Single-Molecule Magnet Properties of $\{\text{Fe(III)}_2\text{Ni(II)}\}$ Complexes. *Inorganic Chemistry* **2011**, 50 (21), 10537-9.

178. Trofimenko, S.; Calabrese, J.C.; Domaille, P.J.; Thompson, J.S., Steric Effects in Polypyrazolylborate Ligands. Poly(3-isopropylpyrazolyl)borates: Ligands of Intermediate Steric Requirements. *Inorganic Chemistry* **1989**, 28 (6), 1091-1101.

179. Frampton, A.K.; Gartland, K.; Piro, N.A.; Kassel, W.S.; Dougherty, W.G., Structural Characterization and Electrochemical Properties of Nickel(II) Complexes Bearing Sterically Bulky Hydrotris(3-phenyl)- and Hydrotris(3-tert-butylpyrazol-1-yl) Borato Ligands. *Polyhedron* **2015**, 114, 172-178.

180. Trofimenko, S., Transition Metal Polypyrazolylborates Containing Other Ligands. *Journal of the American Chemical Society* **1969**, 91 (3), 588-595.
181. Renn, O.; Venanzi, L.M., High-Yield Syntheses of Sodium, Potassium, and Thallium Hydridotris[3,5-Bis(trifluoromethyl)pyrazolyl]borates and the X-Ray Crystal Structure of {Hydridotris[3,5-Bis(trifluoromethyl)pyrazolyl]borato}Thallium(I). *Helvetica Chimica Acta* **1995**, 78, 993-1000.
182. Deb, T.; Anderson, C.M.; Ma, H.; Petersen, J.L.; Young, V.G.; Jensen, M.P., Scorpionato Halide Complexes [(Tp^{ph,Me})Ni-X] [X = Cl, Br, I; Tp^{ph,Me} = Hydrotris(3-phenyl-5-methyl-1-pyrazolyl)borate]: Structures, Spectroscopy, and Pyrazole Adducts. *European Journal of Inorganic Chemistry* **2015**, 2015 (3), 458-467.
183. Martín, C.; Muñoz-Molina, J.M.; Locati, A.; Alvarez, E.; Maseras, F.; Belderrain, T.R.; Pérez, P.J., Copper(I)-Olefin Complexes: The Effect of the Trispyrazolylborate Ancillary Ligand in Structure and Reactivity. *Organometallics* **2010**, 29 (16), 3481-3489.
184. Cummins, D.C.; Yap, G.P.A.; Theopold, K.H., Scorpionates of the "Tetrahedral Enforcer" Variety as Ancillary Ligands for Dinitrogen Complexes of First Row Transition Metals (Cr-Co). *European Journal of Inorganic Chemistry* **2016**, 15-16, 2349-2356.
185. Abubekero, M.; Gianetti, T.L.; Kunishita, A.; Arnold, J., Synthesis and Characterization of Coordinatively Unsaturated Nickel(II) and Manganese(II)

Alkyl Complexes Supported by the Hydrotris(3-Phenyl-5-Methylpyrazolyl)Borate (Tp^{ph,Me}) Ligand. *Dalton Transactions* **2013**, 42 (29), 10525-10532.

186. Nieto, I.; Bontchev, R.P.; Ozarowski, A.; Smirnov, D.; Krzystek, J.; Telsler, J.; Smith, J.M., Synthesis and Spectroscopic Investigations of Four-Coordinate Nickel Complexes Supported by a Strongly Donating Scorpionate Ligand. *Inorganica Chimica Acta* **2009**, 362 (12), 4449-4460.

187. Gordon-Wylie, S.W.; Claus, B.L.; Horwitz, C.P.; Leychkis, Y.; Workman, J.M.; Marzec, A.J.; Clark, G.R.; Rickard, C.E.; Conklin, B.J.; Sellers, S., New Magnetically Coupled Bimetallic Complexes as Potential Building Blocks for Magnetic Materials. *Chemistry—A European Journal* **1998**, 4 (11), 2173-2181.

188. Stoian, S.A.; Vela, J.; Smith, J.M.; Sadique, A.R.; Holland, P.L.; Münck, E.; Bominaar, E.L., Mössbauer and Computational Study of an N₂-Bridged Diiron Diketiminato Complex: Parallel Alignment of the Iron Spins by Direct Antiferromagnetic Exchange with Activated Dinitrogen. *Journal of the American Chemical Society* **2006**, 128 (31), 10181-10192.

189. Jewson, J.D.; Liable-Sands, L.M.; Yap, G.P.A.; Rheingold, A.L.; Theopold, K.H., Paramagnetic Alkyl, Hydride, and Alkene Complexes of the Tp^{t-Bu,Me}Co Moiety. *Organometallics* **1999**, 18 (3), 300-305.

190. Jenkins, D.M.; Peters, J.C., Spin-State Tuning at Pseudotetrahedral *d*⁷ Ions: Examining the Structural and Magnetic Phenomena of Four-Coordinate [Bp₃]Co^{II}-X Systems. *Journal of the American Chemical Society* **2005**, 127 (19), 7148-7165.

191. Kremer-Aach, A.; Kläui, W.; Bell, R.; Strerath, A.; Wunderlich, H.; Mootz, D., Cobalt as a Probe for Zinc in Metalloenzyme Model Compounds? A Comparison of Spectroscopic Features and Coordination Geometry of Four- and Five-Coordinate Complexes. Crystal and Molecular Structures of $[\text{Co}(\text{H}^3\text{-Tp}^{\text{ph}})(\text{H}^2\text{-Tp}^{\text{ph}})]$, $[(\text{H}^3\text{-Tp}^{\text{ph}})\text{Zn}(\text{Anthranilate})]$, and $[(\text{H}^3\text{-Tp}^{\text{ph}})\text{M}(\text{H}^2\text{-Acac})]$ (Tp^{ph} = Hydrotris(3-Phenylpyrazol-1-yl)Borate, Acac = Pentane-2,4-Dionate, and $\text{M} = \text{Zn}, \text{Co}$). *Inorganic Chemistry* **1997**, 36 (8), 1552-1563.
192. Díaz-Requejo, M.M.; Caballero, A.; Belderraín, T.R.; Nicasio, M.C.; Trofimenko, S.; Pérez, P.J., Copper(I)–Homoscorpionate Catalysts for the Preferential, Kinetically Controlled Cis Cyclopropanation of α -Olefins with Ethyl Diazoacetate. *Journal of the American Chemical Society* **2002**, 124 (6), 978-983.
193. López-Linares, F.; Barrios, A.D.a.; Ortega, H.; Karam, A.m.; Agrifoglio, G.; González, E., Modification of Polyethylene Polydispersity by Blending a Ziegler-Natta Catalyst with a Group of Iv-Half Metallocene or Scorpionate Complexes. *Journal of Molecular Catalysis A: Chemical* **2002**, 179 (1), 87-92.
194. McKeown, B.A.; Lee, J.P.; Mei, J.; Cundari, T.R.; Gunnoe, T.B., Transition Metal Mediated C–H Activation and Functionalization: The Role of Poly(Pyrazolyl)Borate and Poly(Pyrazolyl)Alkane Ligands. *European Journal of Inorganic Chemistry* **2016**, 15-16, 2296-2311.
195. Jesson, J.P.; Trofimenko, S.; Eaton, D.R., Spin Equilibria in Octahedral Iron(II) Poly((1-Pyrazolyl)-Borates. *Journal of the American Chemical Society* **1967**, 89 (13), 3158-3164.

196. Liang, S.; Wang, H.; Deb, T.; Petersen, J.L.; Yee, G.T.; Jensen, M.P., Structural and Spectroscopic Trends in a Series of Half-Sandwich Scorpionate Complexes. *Inorganic Chemistry* **2012**, *51* (23), 12707-12719.
197. McGarvey, B.R.; Telsler, J., Simple Ligand-Field Theory of d^4 and d^6 Transition Metal Complexes with a C_3 Symmetry Axis. *Inorganic Chemistry* **2012**, *51* (11), 6000-6010.
198. Habib, F.; Luca, O.R.; Vieru, V.; Shiddiq, M.; Korobkov, I.; Gorelsky, S.I.; Takase, M.K.; Chibotaru, L.F.; Hill, S.; Crabtree, R.H.; Murugesu, M., Influence of the Ligand Field on Slow Magnetization Relaxation Versus Spin Crossover in Mononuclear Cobalt Complexes. *Angew. Chem., Int. Ed.* **2013**, *52* (43), 11290-3.
199. Habib, F.; Lin, P.H.; Long, J.; Korobkov, I.; Wernsdorfer, W.; Murugesu, M., The Use of Magnetic Dilution to Elucidate the Slow Magnetic Relaxation Effects of a Dy_2 Single-Molecule Magnet. *Journal of the American Chemical Society* **2011**, *133* (23), 8830-3.
200. Zhang, Y.Z.; Ferko, P.; Siretanu, D.; Ababei, R.; Rath, N.P.; Shaw, M.J.; Clerac, R.; Mathoniere, C.; Holmes, S.M., Thermochromic and Photoresponsive Cyanometalate Fe/Co Squares: Toward Control of the Electron Transfer Temperature. *Journal of the American Chemical Society* **2014**, *136* (48), 16854-64.
201. Brunker, T.J.; Hascall, T.; Cowley, A.R.; Rees, L.H.; O'Hare, D., Variable Coordination Modes of Hydrotris (3-Isopropyl-4-Bromopyrazolyl) Borate (Tp') in Fe(II), Mn(II), Cr(II), and Cr(III) Complexes: Formation of MTp'Cl (M = Fe and

- Mn), Structural Isomerism in CrTp₂, and the Observation of Tp⁻ as an Uncoordinated Anion. *Inorganic Chemistry* **2001**, 40 (13), 3170-3176.
202. Gorrell, I.B.; Parkin, G., (Tris-(3-Tert-Butylpyrazolyl) Hydroborato) Manganese(II),-Iron(II),-Cobalt(II), and-Nickel(II) Halide Derivatives: Facile Abstraction of Fluoride from (Bf₄)⁻. *Inorganic Chemistry* **1990**, 29 (13), 2452-2456.
203. Calabrese, J.C.; Trofimenko, S., Hydrotris(3-Neopentylpyrazol-1-Yl)Borates: A New Type of Sterically Hindered Poly(Pyrazolyl)Borates. *Inorganic Chemistry* **1992**, 31 (23), 4810-4814.
204. Trofimenko, S.; Calabrese, J.C.; Domaille, P.J.; Thompson, J.S., Steric Effects in Polypyrazolylborate Ligands. Poly (3-Isopropylpyrazolyl) Borates: Ligands of Intermediate Steric Requirements. *Inorganic Chemistry* **1989**, 28 (6), 1091-1101.
205. Detrich, J.L.; Konečný, R.; Vetter, W.M.; Doren, D.; Rheingold, A.L.; Theopold, K.H., Structural Distortion of the TpCo-L Fragment (Tp= Tris(Pyrazolyl)Borate). Analysis by X-Ray Diffraction and Density Functional Theory. *Journal of the American Chemical Society* **1996**, 118 (7), 1703-1712.
206. Figgis, B.N.; Hitchman, M.A., The Origin and Calculations of Delta. In *Ligand Field Theory and Its Applications*, Second Edition ed.; Wiley Interscience: New York, 1999; pp 83-91.
207. Figgis, B.N.; Hitchman, M.A., The Electronic Spectra of Complexes. In *Ligand Field Theory and Its Applications*, Second Edition ed.; Wiley Interscience: New York, 1999; pp 179-227.

208. Cotton, F.A.; Goodgame, D.M.L.; Goodgame, M., The Electronic Structures of Tetrahedral Cobalt(II) Complexes. *Journal of the American Chemical Society* **1961**, 83 (23), 4690-4699.
209. Garrett, B.B.; Goedken, V.; Quagliano, J.V., Electronic Spectra of Pseudotetrahedral Cobalt(II) and Nickel(II) Complexes of C_{3v} Symmetry. *Journal of the American Chemical Society* **1970**, 92 (3), 489-493.
210. Dzik, W.I.; van der Vlugt, J.I.; Reek, J.N.; de Bruin, B., Ligands That Store and Release Electrons During Catalysis. *Angewandte Chemie International Edition* **2011**, 50 (15), 3356-3358.
211. Ray, K.; Petrenko, T.; Wieghardt, K.; Neese, F., Joint Spectroscopic and Theoretical Investigations of Transition Metal Complexes Involving Non-Innocent Ligands. *Dalton Transactions* **2007**, (16), 1552-1566.
212. Jenkins, D.M.; Di Bilio, A.J.; Allen, M.J.; Betley, T.A.; Peters, J.C., Elucidation of a Low Spin Cobalt(II) System in a Distorted Tetrahedral Geometry. *Journal of the American Chemical Society* **2002**, 124 (51), 15336-15350.
213. Li, D.; Parkin, S.; Wang, G.; Yee, G.T.; Holmes, S.M., Synthesis and Spectroscopic and Magnetic Characterization of Tris(3,5-Dimethylpyrazol-1-yl) Borate Iron Tricyanide Building Blocks, a Cluster, and a One-Dimensional Chain of Squares. *Inorganic Chemistry* **2006**, 45 (5), 1951-1959.
214. Corwin Jr, D.T.; Fikar, R.; Koch, S.A., Four- and Five-Coordinate Cobalt(II) Thiolate Complexes: Models for the Catalytic Site of Alcohol Dehydrogenase. *Inorganic Chemistry* **1987**, 26 (19), 3079-3080.

215. Perumareddi, J.R., Ligand Field Theory of D^3 and D^7 Electronic Configurations in Noncubic Fields. I. Wave Functions and Energy Matrices. *The Journal of Physical Chemistry* **1967**, 71 (10), 3144-3154.
216. Jesson, J., Optical and Paramagnetic Resonance Spectra of Some Trigonal Co(II) Chelates. *The Journal of Chemical Physics* **1966**, 45 (3), 1049-1056.
217. Larrabee, J.A.; Alessi, C.M.; Asiedu, E.T.; Cook, J.O.; Hoerning, K.R.; Klingler, L.J.; Okin, G.S.; Santee, S.G.; Volkert, T.L., Magnetic Circular Dichroism Spectroscopy as a Probe of Geometric and Electronic Structure of Cobalt(II)-Substituted Proteins: Ground-State Zero-Field Splitting as a Coordination Number Indicator. *Journal of the American Chemical Society* **1997**, 119 (18), 4182-4196.
218. Jesson, J.; Trofimenko, S.; Eaton, D., Spectra and Structure of Some Transition Metal Poly (1-Pyrazolyl) Borates. *Journal of the American Chemical Society* **1967**, 89 (13), 3148-3158.
219. Schmidt, M.W.; Baldrige, K.K.; Boatz, J.A.; Elbert, S.T.; Gordon, M.S.; Jensen, J.H.; Koseki, S.; Matsunaga, N.; Nguyen, K.A.; Su, S., General Atomic and Molecular Electronic Structure System. *Journal of Computational Chemistry* **1993**, 14 (11), 1347-1363.
220. Pople, J.; Nesbet, R.K., Self-Consistent Orbitals for Radicals. *The Journal of Chemical Physics* **1954**, 22 (3), 571-572.
221. Fægri Jr, K.; Manne, R., A New Procedure for Roothaan's Symmetry-Restricted Open-Shell Scf Method. *Molecular Physics* **1976**, 31 (4), 1037-1049.

222. Rappe, A.K.; Smedley, T.A.; Goddard III, W.A., Flexible D Basis Sets for Scandium through Copper. *The Journal of Physical Chemistry* **1981**, *85* (18), 2607-2611.
223. Hsu, H.I.; Davidson, E.R.; Pitzer, R.M., An Scf Method for Hole States. *The Journal of Chemical Physics* **1976**, *65* (2), 609-613.
224. Perdew, J.P.; Chevary, J.A.; Vosko, S.H.; Jackson, K.A.; Pederson, M.R.; Singh, D.J.; Fiolhais, C., Atoms, Molecules, Solids, and Surfaces: Applications of the Generalized Gradient Approximation for Exchange and Correlation. *Physical Review B* **1992**, *46* (11), 6671.
225. Hassan, A.; Pardi, L.; Krzystek, J.; Sienkiewicz, A.; Goy, P.; Rohrer, M.; Brunel, L.-C., Ultrawide Band Multifrequency High-Field Emr Technique: A Methodology for Increasing Spectroscopic Information. *Journal of Magnetic Resonance* **2000**, *142* (2), 300-312.
226. Mola, M.; Hill, S.; Goy, P.; Gross, M., Instrumentation for Millimeter-Wave Magneto-electrodynamic Investigations of Low-Dimensional Conductors and Superconductors. *Review of Scientific Instruments* **2000**, *71* (1), 186-200.
227. Takahashi, S.; Hill, S., Rotating Cavity for High-Field Angle-Dependent Microwave Spectroscopy of Low-Dimensional Conductors and Magnets. *Review of Scientific Instruments* **2005**, *76* (2), 023114.
228. Krzystek, J.; Park, J.-H.; Meisel, M.W.; Hitchman, M.A.; Stratemeier, H.; Brunel, L.-C.; Telser, J., Epr Spectra from "Epr-Silent" Species: High-Frequency and High-Field Epr Spectroscopy of Pseudotetrahedral Complexes of Nickel(II). *Inorganic Chemistry* **2002**, *41* (17), 4478-4487.

229. Ebsworth, E.A.V.; Rankin, D.W.; Cradock, S., Electronic and Photoelectron Spectroscopy. In *Structural Methods in Inorganic Chemistry*, Blackwell Scientific Publications: 1987; pp 239-279.
230. Yang, L.; Powell, D.R.; Houser, R.P., Structural Variation in Copper(I) Complexes with Pyridylmethanamide Ligands: Structural Analysis with a New Four-Coordinate Geometry Index, T₄. *Dalton Transactions* **2007**, (9), 955-964.
231. Mantel, C.; Baffert, C.; Romero, I.; Deronzier, A.; Pécaut, J.; Collomb, M.-N.; Duboc, C., Structural Characterization and Electronic Properties Determination by High-Field and High-Frequency Epr of a Series of Five-Coordinated Mn(II) Complexes. *Inorganic Chemistry* **2004**, 43 (20), 6455-6463.
232. Li, D.P.; Zhang, X.P.; Wang, T.W.; Ma, B.B.; Li, C.H.; Li, Y.Z.; You, X.Z., Distinct Magnetic Dynamic Behavior for Two Polymorphs of the Same Dy(III) Complex. *Chemical Communications* **2011**, 47 (24), 6867-9.
233. Kern, R.J., Tetrahydrofuran Complexes of Transition Metal Chlorides. *Journal of Inorganic and Nuclear Chemistry* **1962**, 24, 1105-1109.
234. Amarego, W.L.F.; Perrin, D.D., *Purification of Laboratory Chemicals*. Butterworth and Heinemann: 1996.

Chapter 3. Chapter 3. Para-toluenesulfonates of Divalent First Row Transition Metals

3.1. Introduction

The results in this chapter were originally published in 2017 in *Polyhedron*.²³⁵ The author's contribution to the work was the confirmation of syntheses, yields, bulk magnetic susceptibilities, and collection of UV-vis spectra. Crystals suitable for X-ray diffraction were prepared and the unit cells measured to confirm crystal structures. Powder X-ray diffraction was not suitable for this as the compounds readily de-solvate when ground.

Weakly-coordinating anions (WCAs) can modulate the solid state, solution, and gas phase structure and reactivity of a wide range of compounds containing bonds with significant ionic character.²³⁶⁻²³⁸ In doing so, WCAs find applications in catalysis, electrochemistry, ionic liquids, non-aqueous battery electrolytes, and trivalent lanthanide extraction; they also stabilize reactive Lewis acids to a degree at which they can be isolated.^{236, 238-242} Notable successes of this approach are electrochemical measurements in low-polarity solvents, new catalytic materials, and shelf-stable electrophilic trifluoromethylation reagents.²⁴³⁻²⁴⁵ In low polarity solvents, the lack of a strong association with cations avoids ion pairing and oxidation by species generated *in situ* that can alter electrochemical measurements.²³⁶ In catalytic applications with metals, the absence of ligation allows for open coordination sites where substrates may bind. While sulfonates have long been known to participate in coordination to metal centers and hydrogen bonding, arenesulfonates offer some advantages over the

traditional WCAs like $[\text{NO}_3]^-$, $[\text{PF}_6]^-$, $[\text{SbF}_6]^-$, $[\text{BF}_4]^-$, and $[\text{ClO}_4]^-$. These anions can be redox-active, and hydrolysis creates reactive species that can readily destroy desired products. Perchlorates have been widely used as they form salts soluble in a wide range of solvents. Perchlorate salts are known for many group I and II metals, main group metals, *d* block metals, and inner transition metals.²⁴⁶ In anhydrous and organic solvate forms, perchlorate and nitrate salts can be friction and shock sensitive and strong oxidizers.²⁴⁶⁻²⁴⁹ Perchlorates are also harmful to the environment and inhibit iodine uptake in the thyroid.^{248, 250} While these shortcomings do not preclude their use, they make less hazardous alternatives desirable.²⁴⁷ Aryl sulfonates are electrochemically stable in a wide window and soluble in many organic solvents.²⁵¹⁻²⁵²

Hydrated *p*-toluenesulfonate salts of numerous metals are known, including Sc^{III} , Y^{III} , Ti^{III} , Mn^{II} , Fe^{II} , Ru^{III} , Co^{II} , Ni^{II} , Cu^{II} , Zn^{II} , La^{III} , Ce^{III} , Nd^{III} , Sm^{III} , Eu^{III} , Gd^{III} , Tb^{III} , Dy^{III} , Ho^{III} , Er^{III} , Yb^{III} , and Lu^{III} .^{238, 253-256} Related compounds such as benzenesulfonates and substituted naphthalenesulfonates are also known and share synthetic approaches.^{240, 242, 245} Multiple routes to these compounds have been used, including salt metathesis, acid/base neutralization reactions, and treatment of the metal powder with toluenesulfonic acid (Scheme 3.1).^{238-239, 242, 245, 257-258} Omitted from this scheme are the solvent molecules which often fill the coordination sphere.



*Scheme 3.1. Preparative routes to metal toluenesulfonates.*²⁵⁷⁻²⁵⁸

For transition metals, the inner coordination sphere is occupied solely by aquo ligands with the *p*-toluenesulfonate anions having no direct bonding interaction with the metal centers.²³⁸ This is attributed to weak dative bonding between sulfonate oxygens and transition metals. For group one and two metals and lanthanides, coordination of arenesulfonates is more common, with examples existing for Na^I, K^I, Rb^I, and Ba^{II}.²⁴⁰⁻²⁴¹ The presence of hydrated cations and relatively large organic anions causes layered materials to be a typical structural motif. This creates layers of charge-assisted hydrogen bonded tapes alternated with layers of stacked aromatic systems.²⁵⁹ This tendency has led some to observe that *cis* aquo ligands hydrogen bonding to deprotonated sulfonate groups can be considered a reliable synthon.²⁶⁰

Para-toluenesulfonate salts of various metals have been a subject of research attention for their potential as transition metal/organic hybrid materials and their similarity to layered metal oxide materials with the potential for ion exchange, shape and size exclusion catalysis, and intercalation behavior.^{245, 261} While sulfonate materials have not been extensively studied (with exceptions),

phosphonate materials have been examined and found to have certain characteristics which preclude application in tunable systems intended to replace metal oxide materials.^{245, 262} Phosphonates have a local C_{3v} symmetry and terminal oxygen atoms in common with sulfonates; the charge difference appears to break any other similarity. While phosphonates often have a charge of -2 that dictates a more specific stereochemistry, sulfonates carry a charge of -1, which leads to a more varied coordination chemistry.

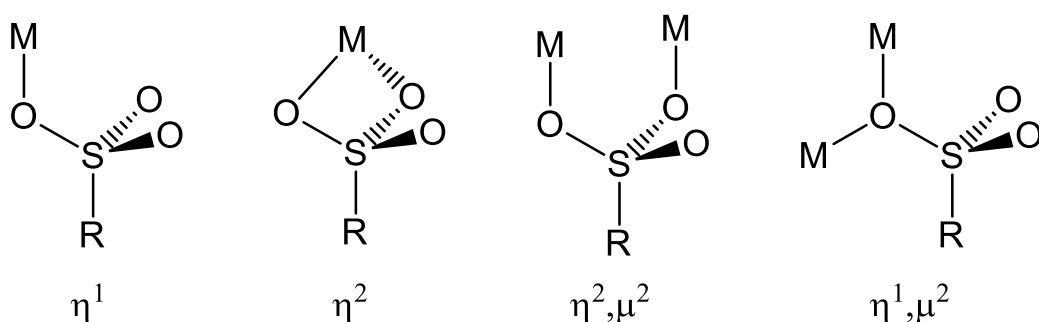


Figure 3.1 shows some of the possible coordination modes of the sulfonate group.²⁶³ Ag^I sulfonates have been studied more than most other metal types in terms of supramolecular structure, although they are still largely an unexplored class of compounds.^{262, 264-266}

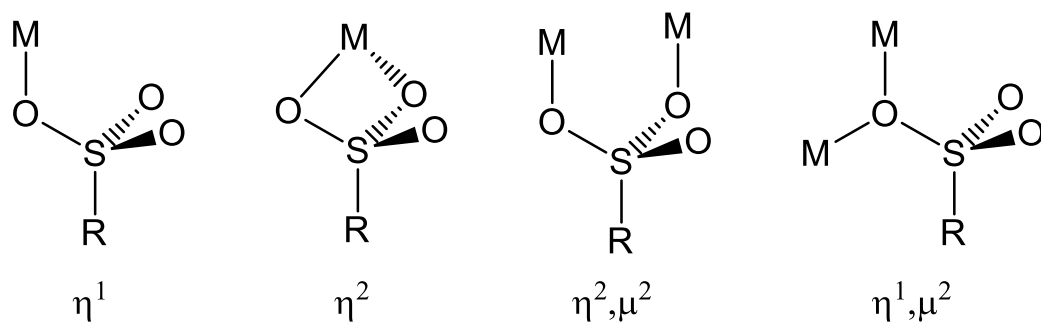


Figure 3.1. Coordination modes of sulfonate anions. Adapted from reference 29. A single SO_3 group can engage in multiple coordination modes with more than one metal.

Because of the thermal stability of the *p*-toluenesulfonate anion, these

salts can be dehydrated and the aquo ligands replaced by other ligands via recrystallization. The preparation of water-free solvated transition metal salts is a common route to preparing soluble transition metal reagents for non-aqueous coordination chemistry synthesis and more broadly a way to alter the electronic structure and reactivity.^{233, 267-270}

N,N-dimethylformamide (dmf) is a well-known organic liquid that is used as a polar solvent in laboratory and industrial settings, ligand, organic reagent, and model for peptide bonds.^{268, 271-272} Some of the characteristics that lead to this versatility are strong Lewis basicity of the carbonyl oxygen, high dipole moment of 3.91 Debye, a high permittivity of 36.7, and the presence of a peptide-like C-N bond.^{249, 271-273} Given this utility, the structure and vibrational spectroscopy of dmf has been extensively studied.^{249, 267, 272-275} dmf has C_s point group symmetry, which allows for significant mixing of vibrational modes such that assignment is not straightforward.²⁴⁹ Furthermore, the charge-separated resonance form has a significant contribution to the electronic structure of the molecule (Figure 3.2).²⁷³ This is reflected in the planarity or near planarity of all non-hydrogen atoms in the uncoordinated or coordinated molecule.^{273, 275} The Lewis basicity of the molecule is enhanced by the contribution of resonance form II (Figure 3.2).²⁷³

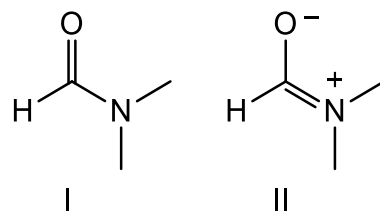


Figure 3.2. Resonance forms of N,N-dimethylformamide. Reproduced from reference 40.

The assignment of bands has a long and complicated history. Ab initio calculations, DFT calculations, gas phase and liquid phase infrared studies, and isotopic substitution have all been applied to the problem. However, some points are consistent between experiments. The infrared band at 1677 cm^{-1} is predominantly $\nu(\text{CO})$ in character and the band at 1507 cm^{-1} is predominantly $\nu(\text{CN})$ in character.²⁴⁹ Upon coordination, $\nu(\text{CO})$ decreases in energy and $\nu(\text{CN})$ often, but not always, increases in energy.^{249, 268} Coordination also often increases the energy of the NC_3 umbrella deformation.²⁴⁹ To prepare a water-free, soluble source of divalent metal *p*-toluenesulfonates, the aquo complexes were dehydrated and the resulting solids recrystallized from dmf.

3.2. Results and Discussion

3.2.1. Syntheses and Solubilities

Using Schlenk techniques to prevent oxidation by air, hydrated *p*-toluenesulfonate salts of Cr, Mn, Fe, Co, Ni can be synthesized by treatment of metal powders with toluenesulfonic acid in water (vide supra, Scheme 3.1, Top).^{238, 253-254, 256, 276} These salts crystallize readily, providing a well-characterized starting material for the subsequent transformations. Heating under vacuum removes the coordinated and lattice waters to give an anhydrous metal *p*-toluenesulfonate salt.²⁵⁸ These are then re-dissolved in dmf and crystallized to form a series of chains $\{\textit{trans}\text{-}[\text{Cr}^{\text{II}}(\text{OTs})_2(\text{dmf})_2]\}_n$, $\{\textit{trans}\text{-}[\text{Mn}^{\text{II}}(\text{OTs})_2(\text{dmf})_2]\}_n$ ($n \rightarrow \infty$) and monometallic complexes, $\textit{trans}\text{-}[\text{Fe}^{\text{II}}(\text{OTs})_2(\text{dmf})_4]$, $\textit{trans}\text{-}[\text{Co}^{\text{II}}(\text{OTs})_2(\text{dmf})_4]$, and $[\text{Ni}^{\text{II}}(\text{dmf})_6][\text{OTs}]_2$. Another compound, $\textit{trans}\text{-}$

$[\text{Fe}^{\text{II}}(\text{OTs})_2(\text{OH}_2)_2(\text{dmf})_2]$, can crystallize from wet dmf/diethyl ether solutions of *trans*- $[\text{Fe}^{\text{II}}(\text{OTs})_2(\text{dmf})_4]$. Attempts to prepare this complex in high yields were unsuccessful. { *Trans*- $[\text{Cr}^{\text{II}}(\text{OTs})_2(\text{dmf})_2]$ }_n, { *trans*- $[\text{Mn}^{\text{II}}(\text{OTs})_2(\text{dmf})_2]$ }_n, *trans*- $[\text{Fe}^{\text{II}}(\text{OTs})_2(\text{dmf})_4]$, *trans*- $[\text{Co}^{\text{II}}(\text{OTs})_2(\text{dmf})_4]$, and $[\text{Ni}^{\text{II}}(\text{dmf})_6][\text{OTs}]_2$ quickly dissolve in polar organic solvents including dmf, MeOH, nitromethane, and ethylenediamine, in addition to water. In contrast, solutions of { *Trans*- $[\text{Cr}^{\text{II}}(\text{OTs})_2(\text{dmf})_2]$ }_n, { *trans*- $[\text{Mn}^{\text{II}}(\text{OTs})_2(\text{dmf})_2]$ }_n, *trans*- $[\text{Fe}^{\text{II}}(\text{OTs})_2(\text{dmf})_4]$, *trans*- $[\text{Co}^{\text{II}}(\text{OTs})_2(\text{dmf})_4]$, and $[\text{Ni}^{\text{II}}(\text{dmf})_6][\text{OTs}]_2$ are unstable in acetone and dichloromethane, precipitating the anhydrous toluenesulfonate salts which indicates lability of the dmf ligands.²⁷⁷⁻²⁷⁹ The solubilities of *trans*- $[\text{Co}^{\text{II}}(\text{OTs})_2(\text{dmf})_4]$, and $[\text{Ni}^{\text{II}}(\text{dmf})_6][\text{OTs}]_2$ were examined in numerous solvents and the results presented in Table 3.1.

Table 3.1. Qualitative solubilities of *trans*- $[\text{Co}^{\text{II}}(\text{OTs})_2(\text{dmf})_4]$ and $[\text{Ni}^{\text{II}}(\text{dmf})_6][\text{OTs}]_2$ in selected organic solvents (dielectric constant, ϵ). Reproduced from reference 235.

| M ^{II} | benzene (2.3) | diethyl ether (4.3) | chloroform (4.8) | tetrahydrofuran (7.5) | ethyl acetate (6.0) | dichloromethane (9.1) | pyridine (12.3) | <i>tert</i> -butyl alcohol (12.5) | 1,2-diaminoethane | 2-propanol (18.3) | 1-propanol (20.1) | acetone (20.7) | ethanol (24.6) | 2,4-pentanedione | methanol (32.6) | nitromethane (35.8) | acetonitrile (37.5) | dimethylsulfoxide (47) |
|-----------------|---------------|---------------------|------------------|-----------------------|---------------------|-----------------------|-----------------|-----------------------------------|-------------------|-------------------|-------------------|----------------|----------------|------------------|-----------------|---------------------|---------------------|------------------------|
| Co | ■ | ■ | ■ | ■ | ■ | ■ | ■ | ■ | ■ | ■ | ■ | ■ | ■ | ■ | ■ | ■ | ■ | ■ |
| Ni | ■ | ■ | ■ | ■ | ■ | ■ | ■ | ■ | ■ | ■ | ■ | ■ | ■ | ■ | ■ | ■ | ■ | ■ |

■ = precipitation; ■ = insoluble; ■ = sparingly soluble; ■ = soluble.

3.2.2. Infrared Spectroscopy

The infrared spectrum of N,N-dimethylformamide as a thin film has previously been reported. The primary bands are 1685 (vs), 1512 (m), 1460 (w), 1450 (m), 1410 (s), 1395 (vs), 1268 (s), 1099 (vs), 1067 (m), 870 (m), 660 (s), 405 (m), and 319 (m).²⁸⁰ The low symmetry of the N,N-dimethylformamide molecule allows for strong coupling of modes that complicates band assignments, leading to a substantial body of literature on the topic.^{249, 273, 280-281} However, in the case of the band at 1685 cm^{-1} , the predominant contributor is the CO stretching mode, which is perturbed by coordination of the O lone pair to the metal center.²⁷³ Also potentially affected by shifting of electron density is the CN bond, which has significant double bond character as indicated by a barrier to rotation of ca. 89 kJ mol^{-1} and increased stretching frequency of 1268 cm^{-1} versus ca. 1100 cm^{-1} for single bond C-N.²⁸⁰ Finally, the aldehyde C-H stretch may show an effect from the altered electron density at aldehyde C, but the effect is likely to be less than the previous two bonds as it will be an inductive effect rather than a direct change in the bond order.

In assigning the origin of infrared absorption bands arising from dmf in the compounds, a few different factors must be taken into account: 1.) the mixed nature of free dmf vibrational modes, 2.) plausible σ and π interactions of the metal center with the dmf ligand, and 3.) the point group symmetry of the metal center.

Table 3.2 presents the sulfonate stretching frequencies for the anhydrous $\text{M}(\text{OTs})_2$ salts. The presence of two higher frequency S-O stretches and one

lower frequency stretch suggest that monodentate coordination is present in all cases. The two high frequency stretches arise from symmetric and antisymmetric S=O modes, assuming a low symmetry complex. The lower frequency stretch arises from the S-O bond where the O is coordinated to the metal. No rigid trends are observed in the frequencies, which fall in the range 1240-1216 cm^{-1} . These bands also show splitting, which may be a result of changing symmetry with respect to the metal center. These values provide a basis of comparison for the IR spectra of $\{\text{Cr}^{\text{II}}(\text{OTs})_2(\text{dmf})_2\}_n$, $\{\text{trans}[\text{Mn}^{\text{II}}(\text{OTs})_2(\text{dmf})_2]\}_n$, $\text{trans}[\text{Fe}^{\text{II}}(\text{OTs})_2(\text{dmf})_4]$, $\text{trans}[\text{Co}^{\text{II}}(\text{OTs})_2(\text{dmf})_4]$, and $[\text{Ni}^{\text{II}}(\text{dmf})_6][\text{OTs}]_2$.

Table 3.2. Infrared spectral data for anhydrous $M(\text{OTs})_2$ ($M = \text{Cr}, \text{Mn}, \text{Fe}, \text{Co}, \text{Ni}$) salts. Reproduced from reference 276.

| compd | $\nu(\text{CH})$ | $\nu_a(\text{SO}_2)$ | $\nu_s(\text{SO}_2)$ | $\delta(\text{CH})$ | $\delta(\text{CH})$ | $\delta(\text{CH})$ | $\nu(\text{SO})$ | $\delta(\text{CS})$ |
|----------------------|------------------|----------------------|----------------------|---------------------|---------------------|---------------------|------------------|---------------------|
| Cr(OTs) ₂ | 3060 | 1235 | 1161 | 1060 | 1015 | 817 | 688 | 575 |
| | 3039 | | | | | | | |
| Mn(OTs) ₂ | 3060 | 1200 | 1144 | 1065 | 1017 | 815 | 690 | 574 |
| | 3037 | | | | | | | |
| Fe(OTs) ₂ | 3061 | 1195 | 1143 | 1065 | 1018 | 815 | 688 | 576 |
| | 3039 | | | | | | | |
| Co(OTs) ₂ | 3061 | 1194 | 1142 | 1065 | 1018 | 819 | 686 | 576 |
| | 3039 | | | | | | | |
| Ni(OTs) ₂ | 3063 | 1201 | 1142 | 1067 | 1018 | 819 | 686 | 577 |
| | 3041 | | | | | | | |

The infrared spectra of $\{Trans-[Cr^{II}(OTs)_2(dmf)_2]\}_n$, $\{trans-[Mn^{II}(OTs)_2(dmf)_2]\}_n$, $trans-[Fe^{II}(OTs)_2(dmf)_4]$, $trans-[Co^{II}(OTs)_2(dmf)_4]$, and $[Ni^{II}(dmf)_6][OTs]_2$ contain absorptions that indicate dmf and para-toluenesulfonate anions are present.^{257, 276, 282} Aromatic CH bending modes are observed in the range of 1040 to 801 cm^{-1} , assignable to the aromatic tolyl rings on the para-toluenesulfonate anions. The CS bond is observed via the $\delta(CS)$ mode between 569 and 559 cm^{-1} . Antisymmetric and symmetric $\nu(SO_2)$ stretches are observed at 1170 and 1130-1119 cm^{-1} . In $\{Trans-[Cr^{II}(OTs)_2(dmf)_2]\}_n$ and $\{trans-[Mn^{II}(OTs)_2(dmf)_2]\}_n$, aromatic overtones are observed at 1919 and 1922 cm^{-1} , consistent with the presence of the toluenesulfonate anion. However, these absorptions are not observed in the other compounds.

Absorptions in the range 1657-1648 cm^{-1} are likely $\nu(CO)$ stretching modes shifted to lower energies as the coordination bond weakens the CO bond of dmf. The overall trend is that the frequency decreases across the period, consistent with a stronger metal-ligand bonding from left to right. This matches with the crystal structures, which show dmf replacing toluenesulfonate anions as ligands from left to right. Because the compounds are hygroscopic, spectral indicators of absorption of environmental water are present. For $\{Trans-[Cr^{II}(OTs)_2(dmf)_2]\}_n$, $\{trans-[Mn^{II}(OTs)_2(dmf)_2]\}_n$, and $trans-[Fe^{II}(OTs)_2(dmf)_4]$, $\nu(OH)$ and $\delta(HOH)$ bands are observed around 3300 and 1650 cm^{-1} , similar to the range for the related $[M^{II}(OH_2)_6][OTs]_2$ complexes.²⁷⁶

3.2.3. UV-vis Spectroscopy

The electronic spectra for $\{trans-[Cr^{II}(OTs)_2(dmf)_2]\}_n$, $\{trans-[Mn^{II}(OTs)_2(dmf)_2]\}_n$, $trans-[Fe^{II}(OTs)_2(dmf)_4]$, $trans-[Co^{II}(OTs)_2(dmf)_4]$, and $[Ni^{II}(dmf)_6][OTs]_2$ fulfill expectations for divalent metal ions in octahedral coordination environments.^{158, 283-285} $\{Trans-[Cr^{II}(OTs)_2(dmf)_2]\}_n$ exhibits a single band at 728 nm (${}^5T_{2g} \leftarrow {}^5E_g$) consistent with a high spin d^4 ion in an octahedral environment. An absorption at 408 nm is attributable to small amounts of a Cr^{III} impurity.^{50, 283-284, 286} $\{trans-[Mn^{II}(OTs)_2(dmf)_2]\}_n$ exhibits no absorptions in the UV-visible range as expected for an $S = 5/2$ ${}^6A_{1g}$ ground state with no spin- or Laporte-allowed transitions, supporting the presence of Mn^{II} .¹⁵⁸ Octahedral complexes of Fe^{II} typically exhibit a single ${}^5E_g \leftarrow {}^5T_{2g}$ transition. In $trans-[Fe^{II}(OTs)_2(dmf)_4]$, this transition is expected to be near 1000 nm based on comparison to the Fe^{II} aquo ion, outside the range of measurement.²⁰⁷ However, a shoulder is observed at the low energy end (850 nm) of the spectrum which fits with the presence of this peak.²⁸⁶

The electronic spectrum of $trans-[Co^{II}(OTs)_2(dmf)_4]$ is typical for a high spin d^7 Co^{II} ion ($S = 3/2$, ${}^4T_{1g}$ ground state), complicated by the presence of additional bands besides the three expected transitions. These expected transitions are ${}^4T_{2g} \leftarrow {}^4T_{1g} (v_1)$, ${}^4A_{2g} \leftarrow {}^4T_{1g} (v_2)$, ${}^4T_{1g} (P) \leftarrow {}^4T_{1g} (v_3)$, and the related hexaaqua Co^{II} complex exhibits them near 1235 nm, 625 nm, and 515 nm.^{50, 285-286} In $trans-[Co^{II}(OTs)_2(dmf)_4]$, v_1 falls in the near infrared, outside the UV-visible spectroscopy window of 350-850 nm. v_2 and v_3 fall at lower energies than the comparable hexaaqua complex, suggesting that dmf creates a larger

ligand field splitting. This suggests that dmf is a weaker field ligand as ligand strength is proportional to the energy difference between the t_{2g} and e_g orbital sets.⁵⁰ Solutions of $[\text{Ni}^{\text{II}}(\text{dmf})_6][\text{OTs}]_2$ in dmf exhibit the green color associated with solutions of divalent Ni. The Tanabe Sugano diagram for a d^8 ion in octahedral symmetry predicts three absorption bands, two of which typically fall in the UV-visible range.^{50, 158, 285} For $[\text{Ni}^{\text{II}}(\text{dmf})_6][\text{OTs}]_2$ absorptions are seen at 739, 679, and 402 nm. The absorptions at 679 and 739 nm are likely a splitting of the ${}^3\text{T}_{1g} \leftarrow {}^3\text{A}_{2g} ({}^3F)$ band due to spin orbit coupling. This leaves the ${}^3\text{T}_{1g} (\text{P}) \leftarrow {}^3\text{A}_{2g} (\nu_3)$ transition at 402 nm, with the third transition, ${}^3\text{T}_{2g} \leftarrow {}^3\text{A}_{2g} (\nu_1)$, falling outside the range of measurements making determination of Δ_0 impossible.

Table 3.3 summarizes the spectroscopic data collected in the UV-vis range.

Table 3.3. Spectroscopic data for $\{\text{trans}[\text{Cr}^{\text{II}}(\text{OTs})_2(\text{dmf})_2]\}_n$, $\text{trans}[\text{Co}^{\text{II}}(\text{OTs})_2(\text{dmf})_4]$, and $[\text{Ni}^{\text{II}}(\text{dmf})_6][\text{OTs}]_2$.

| Compound | λ (nm) | ϵ ($\text{M}^{-1}\text{cm}^{-1}$) | Assignment |
|---|----------------|--|---|
| $\{\text{trans}[\text{Cr}^{\text{II}}(\text{OTs})_2(\text{dmf})_2]\}_n$ | 725 | 19 | ${}^5\text{T}_{2g} \leftarrow {}^5\text{E}_g$ |
| $\text{trans}[\text{Co}^{\text{II}}(\text{OTs})_2(\text{dmf})_4]$ | 479 | 11 | ${}^4\text{T}_{1g} \leftarrow {}^4\text{T}_{1g}(\text{F})$ |
| | 497 | 14 | ${}^4\text{T}_{1g} \leftarrow {}^4\text{T}_{1g}(\text{F})$ |
| | 527 | 19 | ${}^4\text{T}_{1g} \leftarrow {}^4\text{T}_{1g}(\text{F})$ |
| $[\text{Ni}^{\text{II}}(\text{dmf})_6][\text{OTs}]_2$ | 402 | 11 | ${}^3\text{T}_{1g} (\text{P}) \leftarrow {}^3\text{A}_{2g}({}^3\text{F})$ |
| | 679 | 4.2 | ${}^3\text{T}_{1g} \leftarrow {}^3\text{A}_{2g}({}^3\text{F})$ |
| | 739 | 4.3 | ${}^3\text{T}_{1g} \leftarrow {}^3\text{A}_{2g}({}^3\text{F})$ |

3.2.4. Single Crystal X-Ray Diffraction Studies

$\{trans-[Cr^{II}(OTs)_2(dmf)_2]\}_n$. This compound crystallizes in the $P2_1/n$ space group with $Z = 2$ and Cr atoms situated at inversion centers (

Figure 3.3). Table B.1 - Table B.4 contain the experimental details, atomic coordinates, bond angles, and bond lengths. The Cr atoms form 1-D chains of corner-sharing squares with sulfonate groups bridging in an η^2, μ^2 fashion (Figure 3.4). Two molecules of dmf complete the inner coordination sphere for each metal ion. The SO bonds of the sulfonate functional group have two bond lengths, 1.444(2) Å (S1-O1 and S1-O3) and 1.482(2) Å (S1-O2) which indicates a degree of localization of the negative charge onto O2, which is bound to Cr. This is surprising as the SO bond lengths for the uncoordinated O1 and O3, coordinated to Cr, are identical within experimental error. The Cr-O2 bond length is 2.076(2) Å while the Cr-O3 bond length is 2.403(3) Å, a large difference of 14%. This lengthening of otherwise identical bonds is consistent with a Jahn-Teller distortion, which is expected for Cr^{II} ions in an octahedral environment. Another effect of this distortion may be observed in the SO stretches which are lower in energy overall for $\{trans-[Cr^{II}(OTs)_2(dmf)_2]\}_n$ versus $\{trans-[Mn^{II}(OTs)_2(dmf)_2]\}_n$. The aromatic rings of the toluenesulfonate anions are oriented roughly perpendicular to the squares. These rings are also relatively close to rings on adjacent chains (5.224(2) Å and 5.213(3) Å) which supports the idea that π interactions are present and in part influence the crystal structure. The tolyl rings are also parallel to the dmf ligands, which presumably allows for stabilizing interactions.

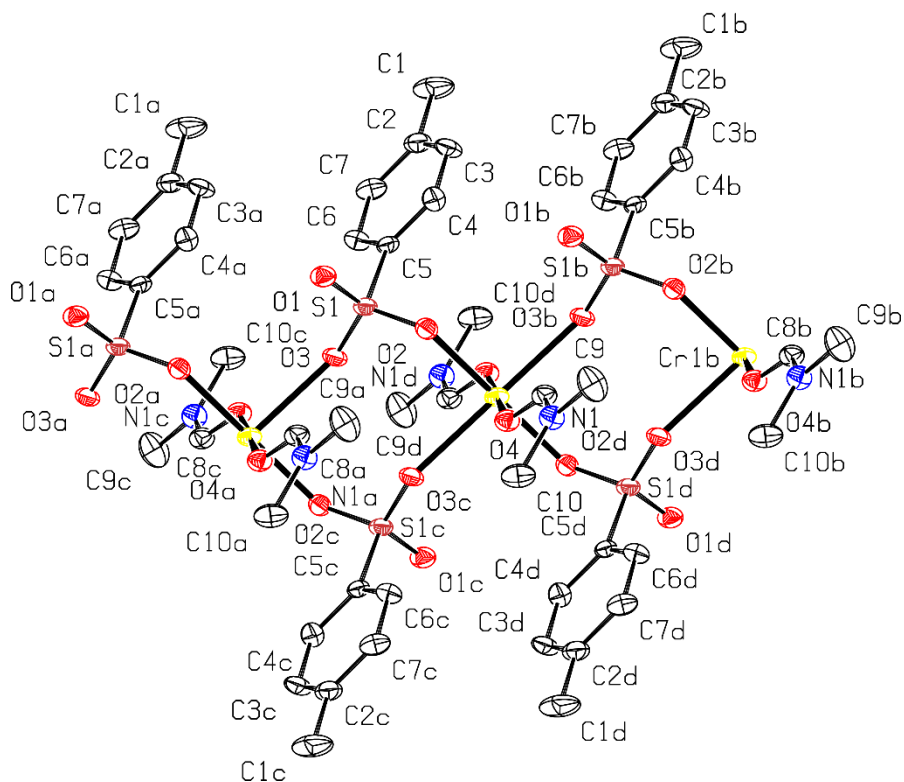


Figure 3.3. The numbering of atoms in $\{\text{trans-}[\text{Cr}^{\text{II}}(\text{OTs})_2(\text{dmf})_2]\}_n$. Non-hydrogen atoms are plotted at 50% probability and hydrogens have been omitted for clarity. Symmetry codes: (a) $x, -1 + y, z$; (b) $x, 1 + y, z$; (c) $1 - x, -y, -z$; (d) $1 - x, 1 - y, -z$.

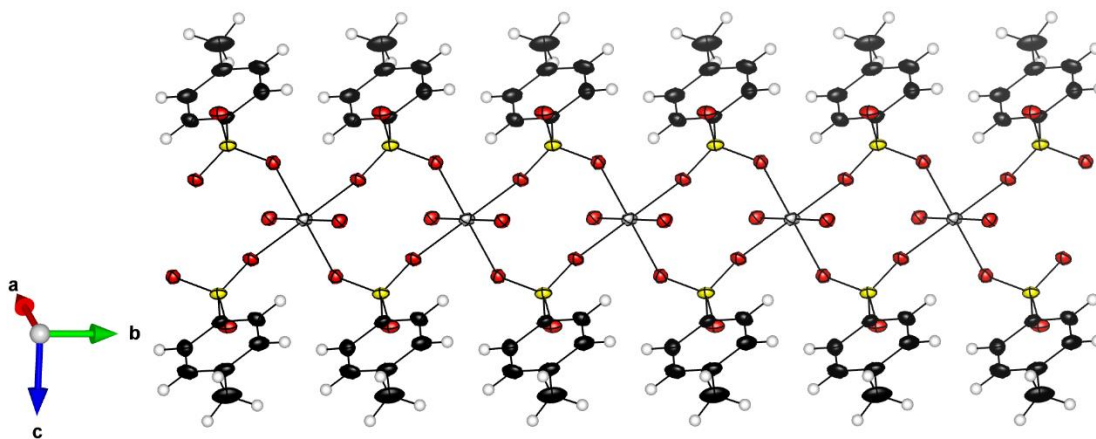


Figure 3.4. ORTEP of $\{\text{Trans-}[\text{Cr}^{\text{II}}(\text{OTs})_2(\text{dmf})_2]\}_n$ showing the polymeric structure. Chromium (gray), oxygen (light red), sulfur (yellow), and carbon (black) atoms are plotted at 50% probability. Hydrogen atoms are plotted at calculated distances as spheres with an arbitrary radius.

When viewed down the a-axis, the layered structure of the compound is

apparent with metal ions sandwiched between layers of coordinated solvent and anion (Figure 3.5). The anion and dmf ligands do not interdigitate but instead form two layers that take a herringbone-like arrangement with regards to each other.

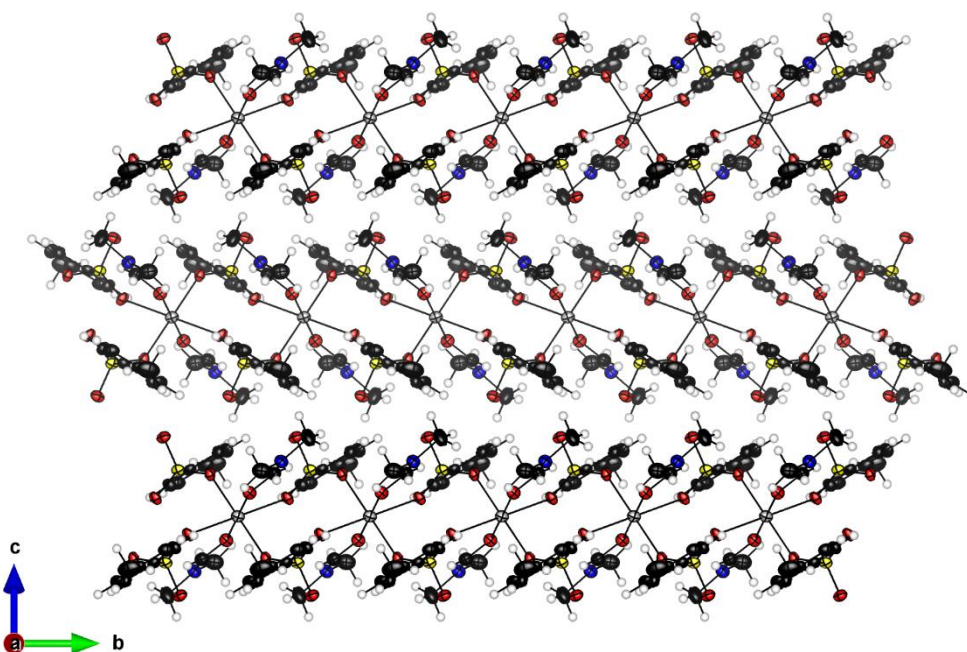


Figure 3.5. ORTEP of $\{\text{Trans-}[\text{Cr}^{\text{II}}(\text{OTs})_2(\text{dmf})_2]\}_n$ viewed down the *a* axis. Chromium (gray), oxygen (light red), sulfur (yellow), and carbon (black) atoms are plotted at 50% probability. Hydrogen atoms are plotted at calculated distances as spheres with an arbitrary radius.

Viewed down the *b*-axis, the Cr atoms and oxygen-containing functional groups form small polar columns largely isolated from each other by the less polar portions of the anion and solvent (Figure 3.6). No dmf is observed uncoordinated to the metal, a trend that is observed for all the compounds reported here. The Cr center is coplanar with the O atoms of the sulfonates because of the inversion center present at each Cr atom. Two Cr-O bonds to the tosylate are present, measuring 2.038(2) Å and 2.403(2) Å. The Cr-O bonds to

N,N-dimethylformamide are in the plane of the longer tosylate bond and tilted towards one tosylate with a distance of 2.076(2) Å. The presence of one Cr-O bond longer than the other two is consistent with a Jahn-Teller distortion, which is expected for a d^4 ion in a pseudo-octahedral environment. Similar differences in bond length have been observed in related compounds, including $[\text{Cr}^{\text{II}}(\text{OH}_2)_6][\text{OTs}]_2$ and $[\text{NH}_4]_2[\text{Cr}^{\text{II}}(\text{OH}_2)_6][\text{SO}_4]_2 \cdot \text{H}_2\text{O}$. The Cr-O bonds in the former range between 2.035(1) and 2.487(1) Å and 2.052(1) and 2.327(1) Å in the latter, and the difference is attributed to J-T distortions.²⁵⁷ Viewed down the a^* axis the tolyl rings appear to be somewhat herringbone in packing, but the methyl groups appear to preclude a closer packing arrangement. The tolyl rings, planar N,N'-dimethylformamide ligands, and S=O bonds are all parallel to each other.

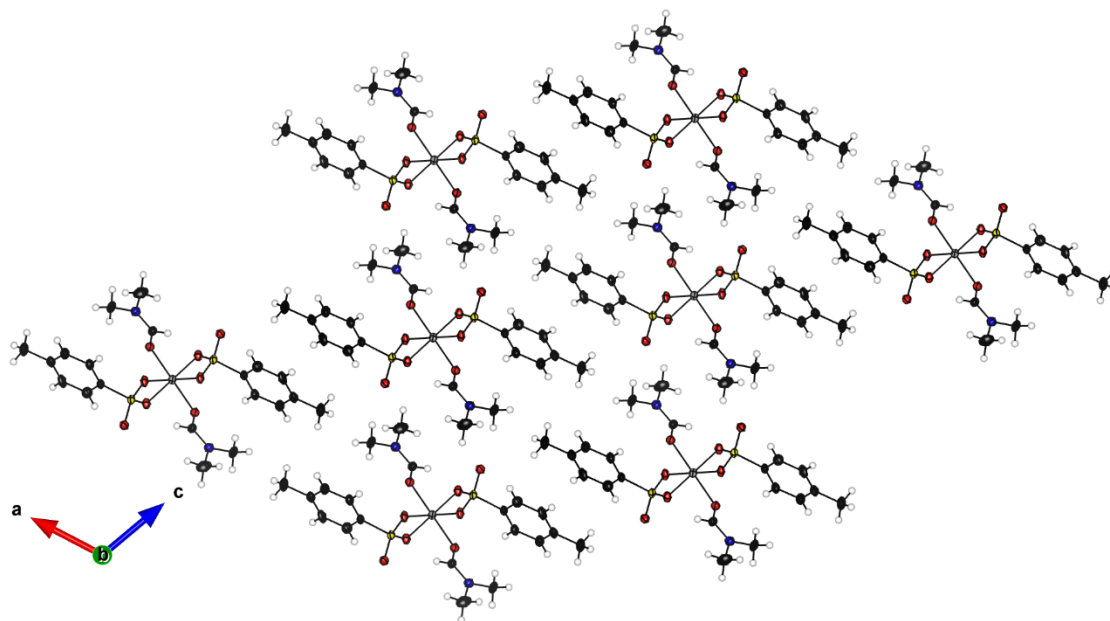


Figure 3.6. ORTEP of $\{\text{Trans}[\text{Cr}^{\text{II}}(\text{OTs})_2(\text{dmf})_2]\}_n$ viewed down the b axis. Chromium (gray), oxygen (light red), sulfur (yellow), and carbon (black) atoms are plotted at 50% probability. Hydrogen atoms are plotted at calculated distances as spheres with an arbitrary radius.

$\{trans-[Mn^{II}(OTs)_2(dmf)_2]\}_n$. The crystal structure of $\{trans-[Mn^{II}(OTs)_2(dmf)_2]\}_n$ is similar to the Cr analogue, again crystallizing in the monoclinic crystal system and $P2_1/n$ space group with $Z = 2$. Figure 3.7 displays the atom numbering scheme. Two bridging sulfonates coordinating in η^2, μ^2 fashion between adjacent metal centers form corner-sharing squares built into 1-D chains. Two distinct Mn-O bonds are present that include the p-toluenesulfonate anion, Mn1-O2 and Mn1-O3. They measure 2.1935(11) Å and 2.1564(12) Å respectively. One unique S atom is present in the asymmetric unit, with three different SO bonds of 1.4646(12) Å (S1-O1), 1.4484(12) Å (S1-O2), and 1.4558(11) Å (S1-O3) in the sulfonate functional group. The shortest of the three bonds, corresponds to the unbound O3. A similar packing of the tolyl substituents as in the case of Cr is observed. The chains are formed by the metal ions and polar sulfonate groups being surrounded by the less polar tolyl groups. Table B.5 - Table B.8 record the atom coordinates, bond angles, and bond lengths for $\{trans-[Mn^{II}(OTs)_2(dmf)_2]\}_n$.

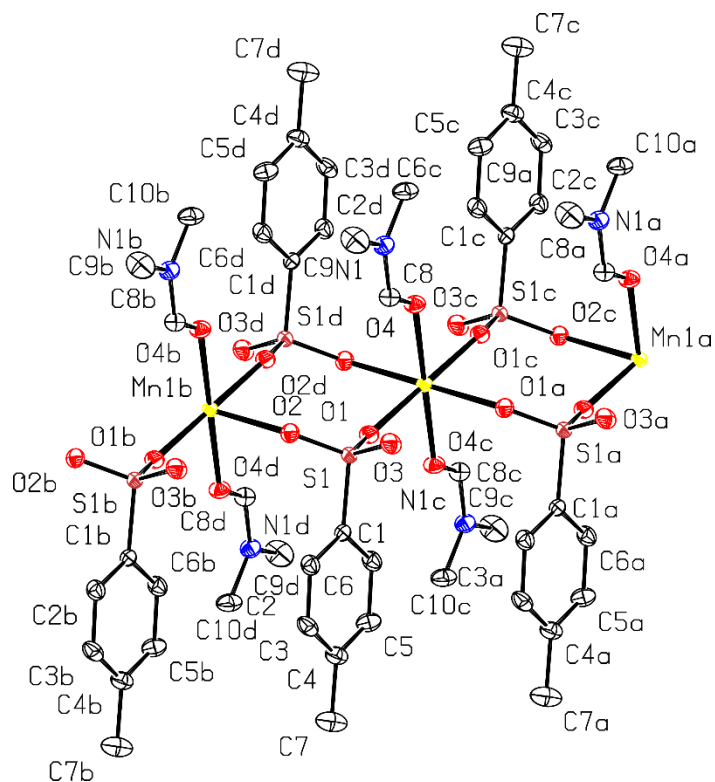


Figure 3.7. Atom numbering scheme for $\{trans-[Mn^{II}(OTs)_2(dmf)_2]\}_n$. Non-hydrogen atoms are plotted at 50% probability and hydrogens are plotted at calculated distances as spheres with an arbitrary radius. Symmetry codes: (a) $x, -1 + y, z$; (b) $x, 1 + y, z$; (c) $-x, -y, -z$; (d) $-x, 1 - y, -z$.

$trans-[Fe^{II}(OTs)_2(dmf)_4]$. The compound $trans-[Fe^{II}(OTs)_2(dmf)_4]$ is a departure from the pattern set by the crystal structures of $[trans-Cr^{II}(dmf)_2(OTs)_2]_n$ and $\{trans-[Mn^{II}(OTs)_2(dmf)_2]\}_n$. The neutral mononuclear complex crystallizes in the $P2_1/n$ space group with $Z = 2$. Four dmf ligands occupy equatorial positions with monodentate tosylates coordinating axially (Figure 3.8). Table B.9 - Table B.12 detail experimental conditions, atom coordinates, bond angles, and bond lengths. The $Fe^{II}-O_{dmf}$ bonds are close in length at 2.1574(7) (Fe1-O2) and 2.1237(7) Å (Fe1-O1). The $Fe^{II}-OTs$ bond is shorter than the $Fe^{II}-O_{dmf}$ bonds at 2.0958(7) Å (Fe1-O3), which can be rationalized as follows. The bond to the OTs is more

electrostatic in character allowing for a closer interaction than in the case of the dmf ligand. The S1-O3 bond is 1.4793(8) Å compared to 1.4466(8) Å and 1.4532(8) Å for S1-O4 and S1-O5 suggesting some charge localization. These Fe^{II}-O bonds are comparable in length to {Fe^{II}(OH₂)₆}²⁺ cations in [NH₄]₂[Fe^{II}(OH₂)₆][SO₄]₂ and [Fe^{II}(OH₂)₆][SiF₆]₂. In contrast, differences in bond angles exist comparing these three compounds compared to *trans*-[Fe^{II}(OTs)₂(dmf)₄]. No lattice solvent is present, and a herringbone-type pattern is observed in the aromatic rings and dimethylamino groups of the dmf. The bond angles are all less than one degree from 90°, similar to those observed in hexaquoiron (II) complexes. Since J-T distortions can occur through changes in bond angle or length, it may be that energy minimization occurs through the presence of different bond lengths rather than angular distortion.

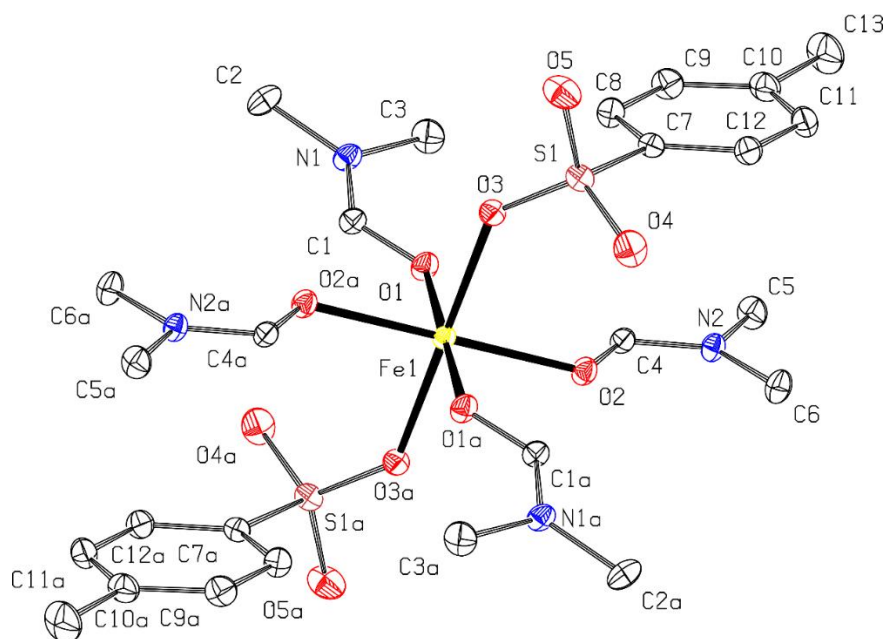


Figure 3.8. Atom numbering scheme for [Fe(dmf)₄(OTs)₂]. Non-hydrogen atoms are plotted at 50% probability. Symmetry code: (a) 1 - x, -y, -z.

***trans*-[Fe(dmf)₂(OTs)₂(OH₂)₂]**. In *trans*-[Fe(dmf)₂(OTs)₂(OH₂)₂] (Figure 3.9), the symmetry is reduced in comparison to the remainder of the series as it crystallizes in the $P\bar{1}$ space group. The experimental details, atom coordinates, bond angles, and bond lengths are recorded in Table B.13 - Table B.16. The Fe-O bond angles are all within 4° of 90°, and the deviation is likely a result of crystal packing. Since the metal center has pseudo D_{2h} symmetry, the rigorous degeneracy of the e orbitals that would be present in O_h is broken, rendering a Jahn-Teller distortion less likely. The Fe-OH₂ (Fe1-O1) bond length is 2.1498(9) Å, the Fe-O_{dmf} bond (Fe1-O2) 2.0804(7) Å, and the Fe-OTs bond (Fe1-O3) is 2.1428(8) Å. The aryl rings are disordered with 50% occupancy in two positions.

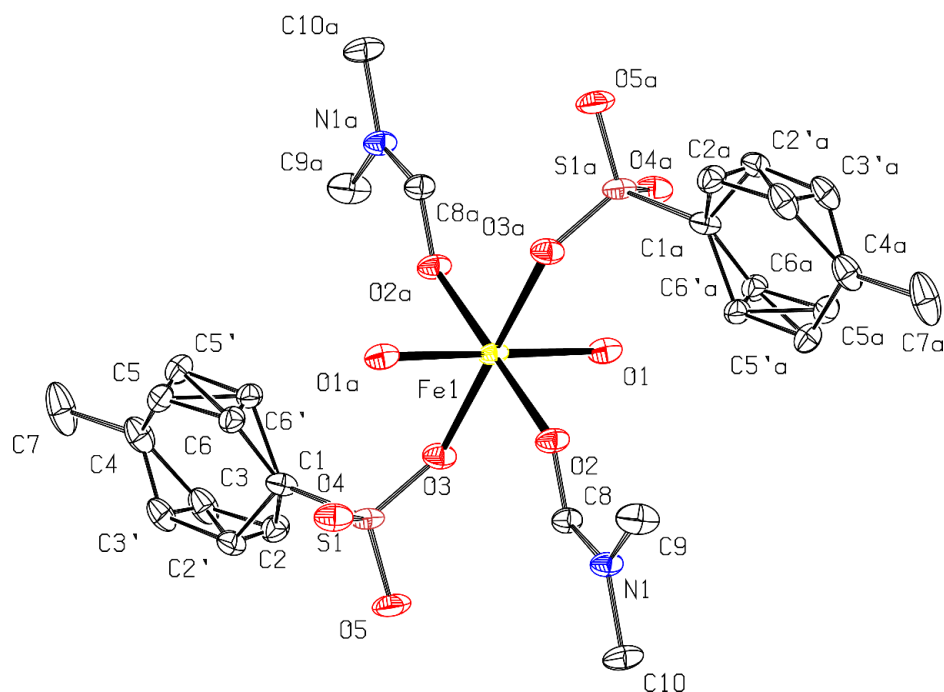


Figure 3.9. Atom numbering scheme for *trans*-[Fe(dmf)₂(OTs)₂(OH₂)₂]. Non-hydrogen atoms are plotted at 50% probability and hydrogens are omitted for clarity. Symmetry code: (a) $-x, -y, 2 - z$.

Two hydrogen bonds are also observed, as shown in Figure 3.10. The first is intramolecular hydrogen bonding between the O-H of water and the sulfonate. The O-H \cdots O angle is 159.4(7) $^\circ$ and the OH bond length in the aquo ligand is 0.819(17) Å. The distance between the H and sulfonate O is 1.969(15) Å. The interaction is likely limited by strain within the ring formed by this potential interaction.

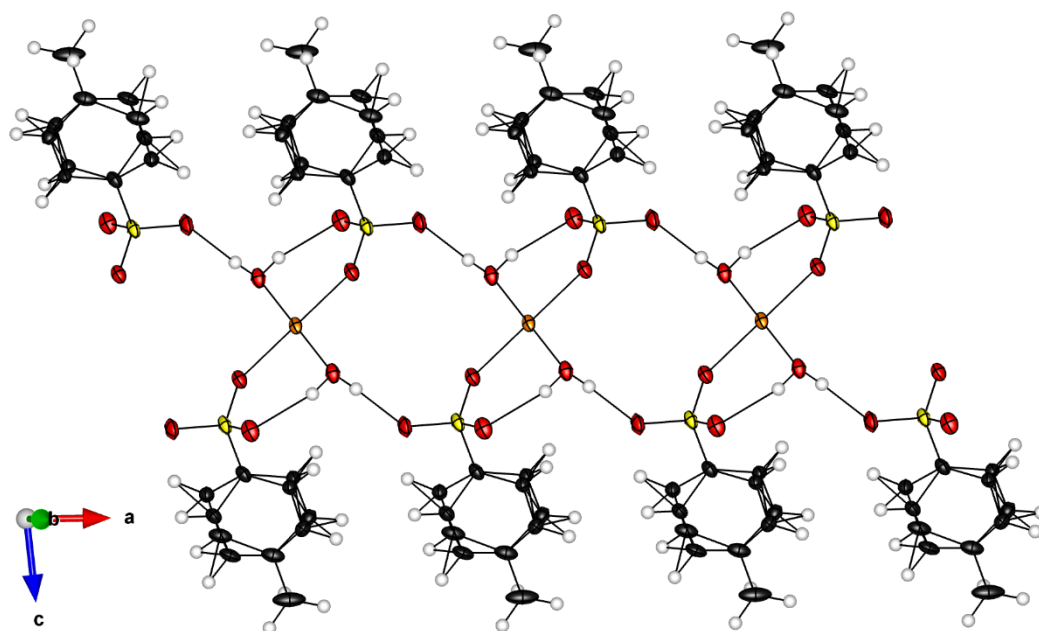


Figure 3.10. Hydrogen bonding in trans-[Fe(dmf)₂(OTs)₂(OH₂)₂]. Iron (orange), oxygen (light red), sulfur (yellow), and carbon (black) atoms are plotted at 50% probability. Hydrogen atoms are plotted at calculated distances as spheres with an arbitrary radius. The dmf ligands have been removed to clearly show the ribbon motif created by hydrogen bonding.

The intermolecular hydrogen bonding shows lengths and angles suggesting a stronger interaction. The O-H \cdots O angle is 174.4(8) $^\circ$ and the distance is 1.87(2) Å. The O-H bond length in the aquo ligand is 0.818(19) Å. These intermolecular hydrogen bonds create ribbons in the crystal structure and

may be the reason the herringbone arrangement of tolyl groups is no longer observed (Figure 3.10).

***Trans*-[Co(dmf)₄(OTs)₂]**. The compound crystallizes with $Z = 2$ in the $P2_1/c$ space group. Each monometallic complex contains four equatorial dmf ligands with the two toluenesulfonate anions occupying the axial positions (Figure 3.11). Experiment data, atom coordinates, bond angles, and bonds lengths are detailed in Table B.17 - Table B.20. The Co-OTS bond is 2.0282(14) Å in length and the Co-O_{dmf} bonds show two different lengths of 2.0487(14) Å and 2.2310(16) Å with bonds of the same length in the trans positions. All O-Co-O bond angles deviate no more than 4° from 90° expected for an octahedral configuration. The packing of these complexes into the crystal lattice forms a herringbone pattern of dmf and tolyl rings (Figure 3.12). In comparison to the earlier metals of the series, the dmf ligands are becoming competitive in strength, disrupting the chain motif observed in Cr and Mn.

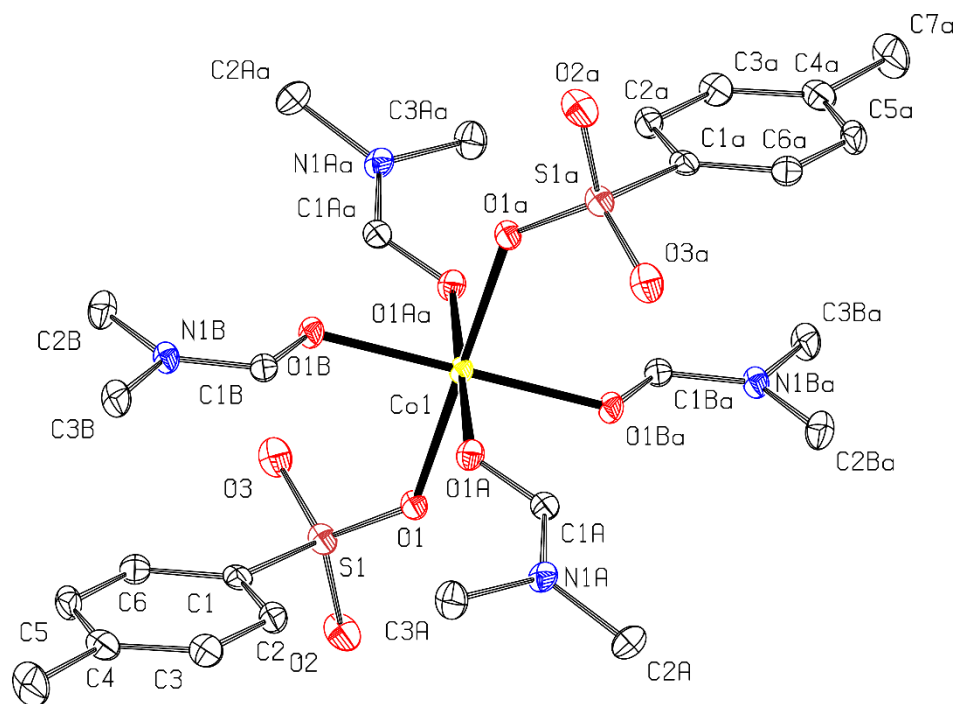


Figure 3.11. Atom numbering scheme for *trans*-[Co(dmf)₄(OTs)₂]. Non-hydrogen atoms are plotted at 50% probability. Hydrogens are omitted for clarity. Symmetry code: (a) - x, -y, -z.

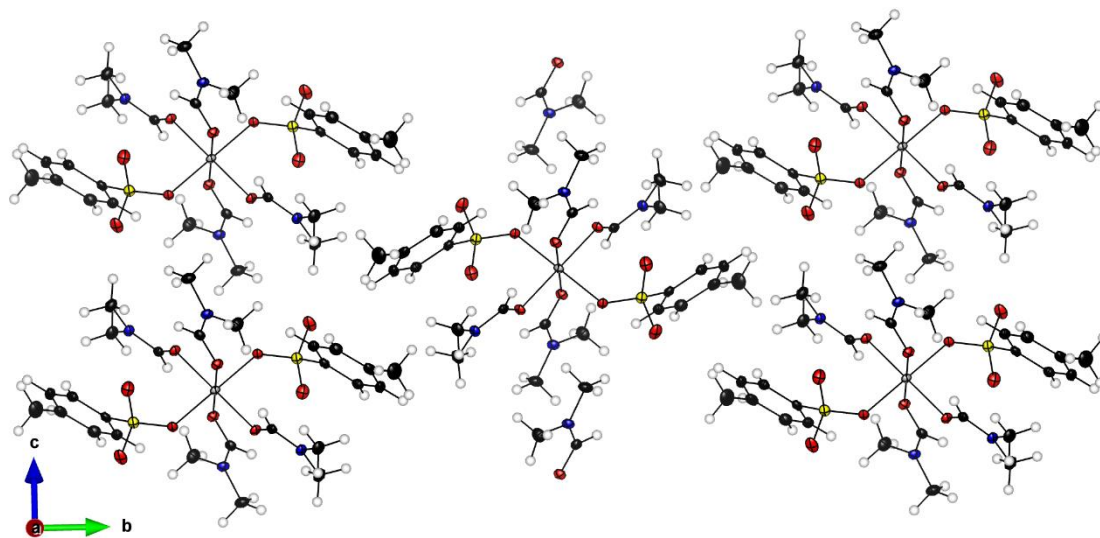


Figure 3.12. *Trans*-[Co(dmf)₄(OTs)₂]. Cobalt (gray), oxygen (red), sulfur (yellow), and carbon (black) atoms are plotted at 50% probability. Hydrogen atoms are plotted at calculated distances as spheres with an arbitrary radius.

[Ni(dmf)₆][OTs]₂. This compound crystallizes in the $P2_1/n$ space group with $Z = 2$. Table B.21 - Table B.24 document the experimental details, atom coordinates, bond angles, and bond lengths. The tosylate anions no longer directly bind to the metal center, and instead the Ni is ligated by six N,N-dimethylformamide molecules (Figure 3.12). Three unique Ni-O bonds are present, measuring 2.0620(13) Å, 2.0510(12) Å, and 2.0422(12) Å. The bond angles are all within 3° of 90°, close to the ideal octahedral arrangement of the ligands. The S1-O bond lengths are very close in value which indicates the negative charge is delocalized across the SO₃⁻ moiety in contrast to the other structures where bond lengths indicate that the charge is largely on the coordinating O atom. This is further supported by a longer S1-C7 bond.

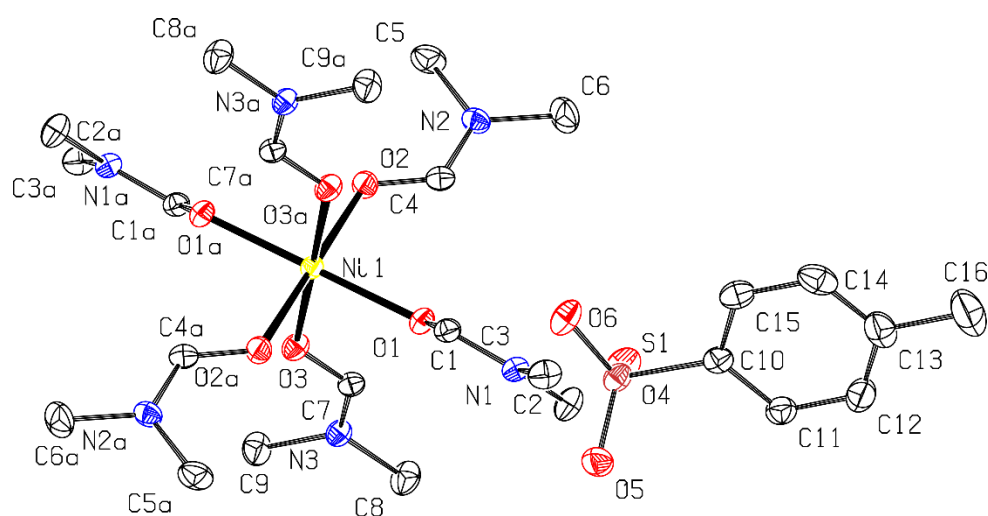


Figure 3.13. Atom numbering scheme for [Ni(dmf)₆][OTs]₂. Non-hydrogen atoms are plotted at 50% probability. Hydrogen atoms and the second tosylate anion, symmetric about the inversion center, have been omitted for clarity. Symmetry code: (a) $-x, -y, -z$.

3.2.5. Bulk Magnetic Measurements

Since the first-row transition metal complexes under discussion here can be paramagnetic, the measurement of the bulk magnetic susceptibility was undertaken to fully characterize the compounds. From the bulk susceptibility the magnetic momenta of the compounds were calculated, and the results are presented in Table 3.4.

Table 3.4. Experimental magnetic momenta and spin only values for {trans-[Cr^{II}(OTs)₂(dmf)₂]}_n, {trans-[Mn^{II}(OTs)₂(dmf)₂]}_n, trans-[Fe^{II}(OTs)₂(dmf)₄], trans-[Co^{II}(OTs)₂(dmf)₄], and [Ni(dmf)₆][OTs]₂.

| Compound | μ_{eff} (exp., BM) | μ_{eff} (calc. spin-only, BM) ²⁸⁷ |
|--|-------------------------------|--|
| {trans-[Cr ^{II} (OTs) ₂ (dmf) ₂]} _n | 5.02 | 4.90 |
| {trans-[Mn ^{II} (OTs) ₂ (dmf) ₂]} _n | 5.92 | 5.92 |
| trans-[Fe ^{II} (OTs) ₂ (dmf) ₄] | 4.82 | 4.90 |
| trans-[Co ^{II} (OTs) ₂ (dmf) ₄] | 3.87 | 3.87 |
| [Ni(dmf) ₆][OTs] ₂ | 2.71 | 2.83 |

These measurements show the complexes to be paramagnetic, high spin compounds of divalent metals.²⁸⁷ The charges determined from them are consistent with the presence of two tosylate anions per metal. The SOC is largely quenched by the crystal field, giving all complexes a magnetic moment at or near the spin only value.

3.3. Conclusions

Five compounds, {trans-[Cr^{II}(OTs)₂(dmf)₂]}_n, {trans-[Mn^{II}(OTs)₂(dmf)₂]}_n, trans-[Fe^{II}(OTs)₂(dmf)₄], trans-[Co^{II}(OTs)₂(dmf)₄], [Ni(dmf)₆][OTs]₂ have been

synthesized and spectroscopically characterized. Another compound, $[\text{Fe}^{\text{II}}(\text{OTs})_2(\text{OH}_2)_2(\text{dmf})_2]$, was isolated in the preparation of crystals suitable for single crystal X-ray diffraction. The UV-visible spectra show that no oxidation or reduction of the transition metal cation takes place if air sensitive techniques are used, and the compounds are soluble in a range of solvents. Combined, these show that the complexes could have use as sources of divalent Cr, Mn, Fe, Co, and Ni for inorganic and organometallic syntheses. The magnetic characterization shows minimal deviation from the expected spin-only values, so these complexes are unlikely to show magnetically interesting phenomena.

Structural variety is provided in the series of compounds due to the similar donor strengths of the dmf and toluenesulfonate ligands as well as the variable denticity of the sulfonate functional group. The Cr^{II} and Mn^{II} compounds form chains with sulfonate bridging ligands, the remainder of the coordination sphere being filled with dmf ligands. On moving to Fe^{II} , the bridging motif is no longer the most stable and instead the *p*-toluenesulfonates occupy axial positions with the remainder filled with dmf. The same type of structure is observed for Co^{II} . With Ni^{II} the shift of ligand strength is complete; dmf fills all coordination sites with the toluenesulfonate present as an unbound anion.

3.4. Experimental

All syntheses and manipulations were carried out under an Ar atmosphere using Schlenk techniques or a nitrogen-filled glovebox. Stainless steel cannulae, needles, and ground glass syringes were used to transfer solutions and solvents.

The anhydrous *para*-toluenesulfonate salts were prepared by dehydrating the hydrates under heat (160 °C) and vacuum for at least 1 hr. N,N'-dimethylformamide was purified and dried using a Vacuum Atmospheres Corporation solvent purification system. Diethyl ether was dried by distillation over sodium and benzophenone in a nitrogen atmosphere, and all solvents were sparged before use. Elemental analyses were performed by Robertson Microlit laboratories. For some compounds the calculated value includes lattice solvent not observed in the single crystal X-ray structures. It is likely that the solvent was included on the surface of microanalysis samples as exposure to dynamic vacuum can de-solvate compounds and this was deliberately avoided by short drying times at room temperature.

Measurements of the bulk magnetic susceptibility at room temperature were conducted with a Johnston Matthey bulk magnetic susceptibility balance Mk. 1. The instrument was calibrated using $\text{HgCo}(\text{NCS})_4$.²⁸⁸ Pascal's corrections were applied to the samples.²⁸⁹

In the present work two instrumental setups were used to collect single crystal X-ray diffraction data. Both used Mo $K\alpha$ radiation to avoid excessive absorption by the crystal samples. For $\{\textit{trans}\text{-}[\text{Cr}^{\text{II}}(\text{OTs})_2(\text{dmf})_2]\}_n$ and $[\text{Fe}^{\text{II}}(\text{OTs})_2(\text{OH}_2)_2(\text{dmf})_2]$, a Nonius kappa CCD diffractometer was used to collect data. The initial cell parameters were determined from ten frames 1° apart (DENZO) and subsequently refined using the full data set.²⁹⁰ Lorentz and polarization corrections were applied as part of the data reduction. The solution and refinement of the data was completed using SHELXS97 (direct methods)

and SHELXL97 (F^2 by weighted full-matrix least-squares refinement).²⁹¹⁻²⁹²

Empirical absorption corrections were applied using SCALEPACK.²⁹⁰

For the structures of $\{trans-[Mn^{II}(OTs)_2(dmf)_2]\}_n$, $trans-[Fe^{II}(OTs)_2(dmf)_4]$, $trans-[Co^{II}(OTs)_2(dmf)_4]$ and $[Ni^{II}(dmf)_6][OTs]_2$ a Bruker Apex-II CCD diffractometer was used to collect the data. Preliminary unit cell determinations were made from 36 10 s frames and refined using Bruker SAINT. The data was integrated using Bruker SAINT and absorption correction models were determined using SADABS. The solution and refinement of the data was completed using SHELXS97 (direct methods) and SHELXL97 (least squares refinement).²⁹¹⁻²⁹² In both cases Lorentz and polarization corrections were applied as part of the data reduction. The data were integrated using Bruker SAINT, and absorption correction models were determined using SADABS.²⁹³ The solution and refinement of the data were completed using SHELXS97 (direct methods) and SHELXL97 (least squares refinement).²⁹¹⁻²⁹²

For $\{trans-[Cr^{II}(OTs)_2(dmf)_2]\}_n$, $\{trans-[Mn^{II}(OTs)_2(dmf)_2]\}_n$, $trans-[Fe^{II}(OTs)_2(dmf)_4]$, $[Fe^{II}(OTs)_2(OH_2)_2(dmf)_2]$, $trans-[Co^{II}(OTs)_2(dmf)_4]$, and $[Ni^{II}(dmf)_6][OTs]_2$ hydrogen atoms were located using difference maps, placed at calculated positions using riding models, and isotropically refined. All non-hydrogen atoms were anisotropically refined. Atomic scattering factors were taken from the International Tables for Crystallography Vol. C. 82.²⁹⁴ Figures were generated using VESTA.²⁹⁵

The infrared spectra were recorded from Nujol mulls pressed between KBr plates on a Thermo-Fisher 6700 FTIR spectrometer on the domain of 4000-400

cm^{-1} . The UV-visible spectra were recorded as N,N-dimethylformamide solutions using an Ocean Optics Flame S-UV-VIS-ES spectrophotometer from 200-850 nm using a DH-2000-BAL deuterium tungsten source.

{*trans*-[Cr^{II}(OTs)₂(dmf)₂]}_n. Solid Cr(OTs)₂ (2.00 g, 5.07 mmol) was dissolved into N,N-dimethylformamide (10 mL) with stirring, and the pale blue-green solution was layered with diethyl ether (30 mL). After 7 days the pale blue crystals were isolated via filtration, washed with diethyl ether (2 × 5 mL), and dried under vacuum for 2 min. at room temperature. Yield: 1.68 g (59.4%). Anal Calcd. for CrC₂₀H₃₀O₉N₂S₂ ({*trans*-[Cr^{II}(OTs)₂(dmf)₂]}+H₂O): C, 43.00; H, 5.42; N, 5.01. Found: C, 42.67; H, 5.22; N, 4.67. IR (Nujol, cm^{-1}): 3304 (w), 3148 (w), 1919 (w), 1655 (vs), 1497 (s), 1419 (s), 1240 (vs), 1164 (vs), 1120 (vs), 1039 (vs), 1015 (vs), 950 (m), 819 (vs), 801 (s), 703 (vs), 685 (vs), 588 (s), 559 (vs), 420 (m). UV-vis (DMF): $\lambda_{\text{max}} / \text{nm}$ ($\epsilon_{\text{M}} / \text{M}^{-1} \text{cm}^{-1}$) 728 nm (19). $\mu_{\text{eff}} = 5.02 \text{ BM}$.

{*trans*-[Mn^{II}(OTs)₂(dmf)₂]}_n. Anhydrous N,N-dimethylformamide (10 mL) was added to Mn(OTs)₂ to form a colorless solution. Upon layering with diethyl ether (40 mL) and allowing to stand 7 days, colorless crystals were isolated and washed with diethyl ether (3 × 10 mL) and dried for 2 min. under vacuum. Yield: 1.19 g (49.3%). Anal Calcd. for MnC₂₀H₃₀O₉N₂S₂ ({*trans*-[Mn^{II}(OTs)₂(dmf)₂]}_n+H₂O): C, 42.78; H, 5.38; N, 4.98. Found: C, 42.11; H, 5.37; N, 4.50. IR (Nujol, cm^{-1}): 3300 (w), 3147 (w), 3062 (m), 3024 (m), 2954 (vs), 2923 (vs), 2855 (vs), 2734 (w), 1922 (w), 1657 (vs), 1620 (vs, sh), 1599 (s), 1573 (m), 1497 (s), 1457 (s), 1444 (s), 1438 (s), 1416 (s), 1392 (s), 1379 (s, sh), 1364 (m, sh), 1311 (w), 1288 (w, sh), 1253 (vs), 1234 (vs), 1176 (vs), 1130 (vs), 1114 (vs),

1107 (vs), 1058 (s, sh), 1049 (vs), 1017 (vs), 974 (w), 951 (w), 870 (m), 851 (w), 847 (w), 819 (vs), 801 (s), 709 (s), 688 (vs), 683 (vs), 580 (vs), 565 (vs), 557 (vs), 413 (m), 409 (m), 401 (s). $\mu_{\text{eff}} = 5.92$ BM.

***trans*-[Fe^{II}(OTs)₂(dmf)₄]**. Dissolving Fe(OTs)₂ (2.00 g, 5.02 mmol) into N,N-dimethylformamide (10 mL) created a pale green solution. Layering with diethyl ether (40 mL) initiated crystallization of the pale green product. Collection of crystals after 7 days, washing with diethyl ether (3 × 10 mL), and drying in vacuo for two minutes yielded 1.90 g of pale green crystals (68.8%). Anal Calcd. for FeC₂₆H₄₄O₁₁N₄S₂ (*trans*-[Fe^{II}(OTs)₂(dmf)₄]+H₂O): C, 44.06; H, 5.91; N, 7.21. Found: C, 44.07; H, 6.26; N, 7.91. IR (Nujol, cm⁻¹): 3291(m, br), 3012 (m), 3000 (m), 2951 (vs), 2923 (vs), 2854 (vs), 1693(m), 1648 (vs, br), 1616 (s, sh), 1600 (m, sh), 1497 (s), 1457 (s), 1440 (s), 1411 (s), 1376 (vs), 1285 (w), 1248 (vs), 1216 (s), 1169 (vs), 1119 (s), 1106 (s), 1097 (s), 1063 (m), 1047 (m), 1011 (vs), 865 (w), 854 (w), 825 (s), 815 (m), 799 (w), 714 (w), 682 (s), 575(m), 567 (s), 560 (s), 492 (w), 411 (m), 401 (m). $\mu_{\text{eff}} = 4.82$ BM.

***trans*-[Co^{II}(OTs)₂(dmf)₄]** Co(OTs)₂ was dissolved (3.2927 g, 8.2049 mmol) into N,N-dimethylformamide (15 mL), and the pink solution was layered with diethyl ether (30 mL). After four days pink crystals were collected by decanting and rinsed with 2x10 mL diethyl ether before drying under vacuum for 2 min. Yield: 4.997 g (7.204 mmol, 87.8 %). Anal Calcd. for CoC₂₆H₄₂O₁₀N₄S₂: C, 45.02; H, 6.10; N, 8.08. Found: C, 44.45; H, 5.70; N, 7.74. IR (Nujol, cm⁻¹): 3013 (m), 3001 (s), 2952 (vs), 2923 (vs), 2867 (vs), 2854 (vs), 1693 (m), 1648 (vs, br), 1613 (s, sh), 1602 (s), 1497 (s), 1457 (s), 1439 (s), 1416 (s), 1411 (s), 1375 (vs), 1284

(w), 1245 (vs), 1228 (s), 1183 (s), 1169 (vs), 1120 (vs), 1107 (vs), 1096 (vs), 1063 (w), 1039 (s), 1011 (vs), 866 (vs), 854 (vs), 826 (s), 815 (m), 800 (w), 713 (w), 689 (vs), 682 (vs), 576 (s), 656 (vs), 559 (vs), 414 (m), 401 (m). UV-vis (DMF): λ_{\max} /nm (ϵ_M /M⁻¹ cm⁻¹) 479 (11), 497 (14), 527 (19). $\mu_{\text{eff}} = 3.87$ BM

[Ni(dmf)₆][OTs]₂. Solid Ni(OTs)₂ (2.00g, 4.98 mmol) was dissolved into N,N-dimethylformamide (10 mL) to give a green solution. This was layered with diethyl ether (30 mL). Green crystals formed within 1 hour. After 7 days, crystals were isolated via cannulation, washed with diethyl ether (2 × 10 mL) and dried under vacuum for 2 min. Yield: 2.10 g (2.2629 mmol, 60.7%). Anal Calcd. for NiC₂₆H₄₂O₁₀N₄S₂ ([Ni(dmf)₆][OTs]₂ – 2dmf): C, 45.03; H, 6.10; N, 8.08. Found: C, 44.75; H, 6.06; N, 7.91. IR (Nujol, cm⁻¹): 3143 (m), 3083 (m), 3062 (m), 3048 (m), 3015 (s), 3003 (s), 2955 (vs), 2924 (vs), 2867 (vs), 2855 (vs), 1690 (s, sh), 1653 (vs, br), 1611 (vs, sh), 1601 (s, sh), 1497 (vs), 1455 (vs), 1439 (vs), 1417 (s), 1410 (vs), 1402 (vs), 1372 (vs), 1283 (s), 1244 (vs), 1227 (vs), 1213 (vs), 1170 (vs), 1119 (vs), 1108 (vs), 1098 (vs), 1063 (s), 1048 (s), 1035 (vs), 1012 (vs), 868 (m), 855 (m), 849 (m), 825 (vs), 800 (s), 713 (s), 691 (vs), 681 (vs), 636 (w), 578 (s), 565 (vs), 558 (vs), 498 (w). UV-vis (DMF): λ_{\max} /nm (ϵ_M /M⁻¹ cm⁻¹) 402 (11), 679 (4.2), 739 (4.3). $\mu_{\text{eff}} = 2.71$ BM.

3.5. References

50. Figgis, B.N.; Hitchman, M.A., Introduction. In *Ligand Field Theory and Its Applications*, Second Edition ed.; Wiley Interscience: New York, 1999; pp 1-26.

158. Tanabe, Y.; Sugano, S., On the Absorption Spectra of Complex Ions. I. *Journal of the Physical Society of Japan* **1954**, 9 (5), 753-766.
207. Figgis, B.N.; Hitchman, M.A., The Electronic Spectra of Complexes. In *Ligand Field Theory and Its Applications*, Second Edition ed.; Wiley Interscience: New York, 1999; pp 179-227.
233. Kern, R.J., Tetrahydrofuran Complexes of Transition Metal Chlorides. *Journal of Inorganic and Nuclear Chemistry* **1962**, 24, 1105-1109.
235. Ferko, P.J.; Withers, J.R.; Nguyen, H.; Allison, C.; Ema, J.; Ema, T.; Rath, N.P.; Zhang, Y.-Z.; Holmes, S.M., Synthesis and Characterization of First Row Transition Metal P-Toluenesulfonate Complexes and Chains. *Polyhedron* **2017**, 123, 344-352.
236. Krossing, I.; Raabe, I., Noncoordinating Anions—Fact or Fiction? A Survey of Likely Candidates. *Angewandte Chemie International Edition* **2004**, 43 (16), 2066-2090.
237. Shelly, K.; Reed, C.A.; Lee, Y.J.; Scheidt, W.R., The Least Coordinating Anion. *Journal of the American Chemical Society* **1986**, 108 (11), 3117-3118.
238. Batsanov, A.S.; Howard, J.A.K.; Moore, N.S.; Kilner, M., Hexaaquanickel(II) Bis(P-Tolylsulfonate). *Acta Crystallographica Section E* **2001**, 57 (10), m485-m487.
239. Matsumoto, F.; Ohki, Y.; Suzuki, Y.; Ouchi, A., The Crystal and Molecular Structure of Di- μ -Hydroxo-Bis[Pentaaquascandium(III)] Benzenesulfonate Tetrahydrate, $\{[(\text{H}_2\text{O})_5\text{Sc}(\text{OH})_2\{\text{Sc}(\text{H}_2\text{O})_5\}](\text{C}_6\text{H}_5\text{SO}_3)_4 \cdot 4\text{H}_2\text{O}\}$: A Dimeric Complex

- in Pentagonal-Bipyramidal Hepta-Coordination. *Bulletin of the Chemical Society of Japan* **1989**, 62 (6), 2081-2083.
240. Gunderman, B.J.; Kabell, I.D.; Squattrito, P.J.; Dubey, S.N., Structural Chemistry of Naphthalenedisulfonate Salts. *Inorganica Chimica Acta* **1997**, 258 (2), 237-246.
241. Gunderman, B.J.; Squattrito, P.J., Synthesis and Structures of Potassium and Rubidium Arenesulfonates. *Inorganic Chemistry* **1994**, 33 (13), 2924-2931.
242. Gunderman, B.J.; Squattrito, P.J., Structural Variations in Layered Alkali Metal Naphthalenesulfonates. *Inorganic Chemistry* **1995**, 34 (9), 2399-2406.
243. Ma, J.-A.; Cahard, D., Strategies for Nucleophilic, Electrophilic, and Radical Trifluoromethylations. *Journal of Fluorine Chemistry* **2007**, 128 (9), 975-996.
244. LeSuer, R.J.; Buttolph, C.; Geiger, W.E., Comparison of the Conductivity Properties of the Tetrabutylammonium Salt of Tetrakis(Pentafluorophenyl) Borate Anion with Those of Traditional Supporting Electrolyte Anions in Nonaqueous Solvents. *Analytical Chemistry* **2004**, 76 (21), 6395-6401.
245. Shubnell, A.J.; Kosnic, E.J.; Squattrito, P.J., Structures of Layered Metal Sulfonate Salts: Trends in Coordination Behavior of Alkali, Alkaline Earth and Transition Metals. *Inorganica Chimica Acta* **1994**, 216 (1), 101-112.
246. Schumacher, J.C., *Perchlorates: Their Properties, Manufacture, and Uses*. Reinhold Publishing Corporation: 1960; Vol. 146.
247. Wolsey, W.C., Perchlorate Salts, Their Uses and Alternatives. *Journal of Chemical Education* **1973**, 50 (6), A335.

248. Srinivasan, A.; Viraraghavan, T., Perchlorate: Health Effects and Technologies for Its Removal from Water Resources. *International Journal of Environmental Research and Public Health* **2009**, *6* (4), 1418-1442.
249. Ståkhandske, C.M.; Mink, J.; Sandström, M.; Pápai, I.; Johansson, P., Vibrational Spectroscopic and Force Field Studies of N,N-Dimethylthioformamide, N,N-Dimethylformamide, Their Deuterated Analogues and Bis(N,N-Dimethylthioformamide) Mercury(II) Perchlorate. *Vibrational Spectroscopy* **1997**, *14* (2), 207-227.
250. Cunniff, S.; Cramer, R.; Maupin, H., Perchlorate: Challenges and Lessons. In *Perchlorate*, Springer: 2006; pp 1-15.
251. Fujinaga, T.; Sakamoto, I., Electrochemical Studies of Sulfonates in Non-Aqueous Solvents: Part I. Polarographic Reductions of Alkali Metal Ions with Sulfonate Supporting Electrolyte in N, N-Dimethylformamide and Acetonitrile. *Journal of Electroanalytical Chemistry and Interfacial Electrochemistry* **1976**, *67* (2), 201-213.
252. Xu, K.; Angell, C., Synthesis and Characterization of Lithium Sulfonates as Components of Molten Salt Electrolytes. *Electrochimica Acta* **1995**, *40* (13), 2401-2403.
253. Aquino, M.A.; Clegg, W.; Liu, Q.-T.; Sykes, A.G., Hexaaquatitanium (III) Tris (P-Toluenesulfonate) Trihydrate. *Acta Crystallographica Section C: Crystal Structure Communications* **1995**, *51* (4), 560-562.

254. Cabaleiro-Martinez, S.; Castro, J.; Romero, J.; Garcia-Vazquez, J.A.; Sousa, A., Hexaaquacobalt(II) Bis(4-Toluenesulfonate). *Acta Crystallographica Section C* **2000**, *56* (6), e249-e250.
255. Faithfull, D.L.; Harrowfield, J.M.; Ogden, M.I.; Skelton, B.W.; Third, K.; White, A.H., Synthetic and Structural Studies in the Lanthanide Toluene-4-Sulfonate Hydrates. *Australian Journal of Chemistry* **1992**, *45* (3), 583-594.
256. Fewings, K.R.; Junk, P.C.; Georganopoulou, D.; Prince, P.D.; Steed, J.W., Supramolecular Interactions in Metal Tosylate Complexes. *Polyhedron* **2001**, *20* (7), 643-649.
257. Holmes, S.M. Molecule-Based Magnets Constructed from Hexacyanometalates. University of Illinois at Urbana-Champaign, Urbana, 1999.
258. Arduini, A.L.; Garnett, M.; Thompson, R.C.; Wong, T.C.T., Magnetic and Spectral Studies on Cobalt(II) and Copper(II) Salts of Methylsulfuric, Trifluoromethylsulfuric, and Paratolylsulfuric Acids. *Canadian Journal of Chemistry* **1975**, *53* (24), 3812-3819.
259. Lie, S.; Maris, T.; Wuest, J.D., Molecular Networks Created by Charge-Assisted Hydrogen Bonding in Phosphonate, Phosphate, and Sulfonate Salts of Bis(Amidines). *Crystal Growth & Design* **2014**, *14* (7), 3658-3666.
260. Dalrymple, S.A.; Shimizu, G.K., Exploiting Complementary Second-Sphere Effects in Supramolecular Coordination Solids. *Supramolecular Chemistry* **2003**, *15* (7-8), 591-606.

261. Kosnic, E.J.; McClymont, E.L.; Hodder, R.A.; Squattrito, P.J., Synthesis and Structures of Layered Metal Sulfonate Salts. *Inorganica Chimica Acta* **1992**, *210*, 143-151.
262. Shimizu, G.K.; Enright, G.D.; Ratcliffe, C.I.; Rego, G.S.; Reid, J.L.; Ripmeester, J.A., Silver Sulfonates: An Unexplored Class of Layered Solids. *Chemistry of Materials* **1998**, *10* (11), 3282-3283.
263. Côté, A.P.; Shimizu, G.K., The Supramolecular Chemistry of the Sulfonate Group in Extended Solids. *Coordination Chemistry Reviews* **2003**, *245* (1), 49-64.
264. Smith, G.; Cloutt, B.A.; Lynch, D.E.; Byriel, K.A.; Kennard, C.H., Nitrogen Base Adducts with Silver(I) P-Toluenesulfonate: Syntheses and Single Crystal X-Ray Characterizations of the Adducts with Pyridine (1:1), 2-Aminopyridine (1: 2), 2-Aminopyrimidine (1:1), 4,6-Dimethyl-2-Aminopyrimidine (2:3), and 3-Aminobenzoic Acid (1: 2) and the Crystal Structure of the Parent Silver(I) P-Toluenesulfonate. *Inorganic Chemistry* **1998**, *37* (13), 3236-3242.
265. Hoffart, D.J.; Dalrymple, S.A.; Shimizu, G.K., Structural Constraints in the Design of Silver Sulfonate Coordination Networks: Three New Polysulfonate Open Frameworks. *Inorganic Chemistry* **2005**, *44* (24), 8868-8875.
266. Côté, A.P.; Ferguson, M.J.; Khan, K.A.; Enright, G.D.; Kulynych, A.D.; Dalrymple, S.A.; Shimizu, G.K., Intercalation of Alcohols in Ag Sulfonates: Topotactic Behavior Despite Flexible Layers. *Inorganic Chemistry* **2002**, *41* (2), 287-292.

267. De Oliveira, O.A.; Chagas, A.P.; Airoidi, C., Synthesis, Characterization, and Thermochemistry of Adducts of Zinc, Cadmium and Mercury Halides with N, N-Dimethylformamide. *Inorganic Chemistry* **1983**, *22* (1), 136-140.
268. Yilmaz, V.; Topcu, Y., Preparation, Characterization and Thermal Reactivity of N, N-Dimethylformamide Complexes of Some Transition Metal Chlorides. *Thermochimica Acta* **1997**, *307* (2), 143-147.
269. Archambault, J.; Rivest, R., Donor Acceptor Reactions of Titanium Tetrachloride with Formamide and N,N-Dimethyl Formamide. *Canadian Journal of Chemistry* **1958**, *36* (11), 1461-1466.
270. Berthet, J.-C.; Thuéry, P.; Ephritikhine, M., New Efficient Synthesis of $[U_4(\text{MeCN})_4]$. X-Ray Crystal Structures of $[U_2(\text{MecCN})_7][U_6]$, $[U_4(\text{Py})_3]$, and $[U(\text{DMF})_9]_4$. *Inorganic Chemistry* **2005**, *44* (4), 1142-1146.
271. Muzart, J., N,N-Dimethylformamide: Much More Than a Solvent. *Tetrahedron* **2009**, *65* (40), 8313-8323.
272. Lei, Y.; Li, H.; Pan, H.; Han, S., Structures and Hydrogen Bonding Analysis of N, N-Dimethylformamide and N,N-Dimethylformamide-Water Mixtures by Molecular Dynamics Simulations. *The Journal of Physical Chemistry A* **2003**, *107* (10), 1574-1583.
273. Zhou, X.; Krauser, J.A.; Tate, D.R.; VanBuren, A.S.; Clark, J.A.; Moody, P.R.; Liu, R., Theoretical Study of the Structure and Vibrational Spectrum of N, N-Dimethylformamide. *The Journal of Physical Chemistry* **1996**, *100* (42), 16822-16827.

274. Steele, D.; Quatermain, A., The Vibrational Spectra of Amides—II. The Force Field and Isotopic Shifts of N, N-Dimethyl Formamide. *Spectrochimica Acta Part A: Molecular Spectroscopy* **1987**, *43* (6), 781-789.
275. Schultz, G.; Hargittai, I., Molecular Structure of N, N-Dimethylformamide from Gas-Phase Electron Diffraction. *The Journal of Physical Chemistry* **1993**, *97* (19), 4966-4969.
276. Holmes, S.; McKinley, S.; Girolami, G., Transition Metal P-Toluenesulfonates. *Inorganic Synthesis, Vol. 33* **2002**, *33*, 91-103.
277. Kumar, S.; Gupta, S.K.; Sharma, S., Thermal Analyses of Mn (RSO₃)₂ Hydrates and Pyridine Complexes (R = CH₃, P-CH₃C₆H₄, P-ClC₆H₄). *Thermochimica Acta* **1983**, *71* (1-2), 193-197.
278. Aquino, M.A.S.; Clegg, W.; Liu, Q.-T.; Sykes, A.G., Hexaaquatitanium(III) Tris(*p*-Toluenesulfonate) Trihydrate. *Acta Crystallographica Section C* **1995**, *51* (4), 560-562.
279. Debevc, K.O.; Pohar, C.; Vlachy, V., Enthalpies of Dilution of Alkaline and Alkaline Earth *p*-Toluenesulfonates. *Journal of Solution Chemistry* **1996**, *25* (8), 787-795.
280. Durgaprasad, G.; Sathyanarayana, D.; Patel, C., Infrared Spectra and Normal Vibrations of N, N-Dimethylformamide and N, N-Dimethylthioformamide. *Bulletin of the Chemical Society of Japan* **1971**, *44* (2), 316-322.
281. Torii, H.; Tasumi, M., Low-Wavenumber Vibrational Dynamics of Liquid Formamide and N-Methylformamide: Molecular Dynamics and Instantaneous

- Normal Mode Analysis. *The Journal of Physical Chemistry A* **2000**, 104 (18), 4174-4181.
282. Nakamoto, K., *Infrared and Raman Spectra of Inorganic and Coordination Compounds, Part B, Applications in Coordination, Organometallic, and Bioinorganic Chemistry*. Wiley: Hoboken, 2009.
283. Fackler Jr, J.P.; Holah, D.G., Properties of Chromium(II) Complexes. I. Electronic Spectra of the Simple Salt Hydrates. *Inorganic Chemistry* **1965**, 4 (7), 954-958.
284. Cotton, F.A.; Daniels, L.M.; Murillo, C.A.; Quesada, J.F., Hexaaqua Dipositive Ions of the First Transition Series: New and Accurate Structures; Expected and Unexpected Trends. *Inorganic Chemistry* **1993**, 32 (22), 4861-4867.
285. Lever, A.B.P., *Inorganic Electronic Spectroscopy*. CVH: New York, 1999.
286. Jørgenson, C.K., *Absorption Spectra and Chemical Bonding in Complexes*. Pergamon Press: New York, 1964.
287. Figgis, B.N.; Hitchman, M.A., Magnetic Properties of Complexes. In *Ligand Field Theory and Its Applications*, Second Edition ed.; Wiley Interscience: New York, 1999; pp 228-281.
288. Jeffery, J.; Rose, K., The Structure of Cobalt Mercury Thiocyanate, $\text{Co}(\text{Ncs})_4\text{hg}$. *Acta Crystallographica Section B: Structural Crystallography and Crystal Chemistry* **1968**, 24 (5), 653-662.
289. Bain, G.A.; Berry, J.F., Diamagnetic Corrections and Pascal's Constants. *Journal of Chemical Education* **2008**, 85, 532-536.

290. Otwinowski, Z.; Minor, W., Processing of X-Ray Diffraction Data Collected in Oscillation Mode. *Methods in Enzymology* **1997**, *276*, 307-326.
291. Sheldrick, G.M., A Short History of Shelx. *Acta Crystallographica Section A: Foundations of Crystallography* **2008**, *64* (1), 112-122.
292. Dolomanov, O.V.; Blake, A.J.; Champness, N.R.; Schröder, M., Olex: New Software for Visualization and Analysis of Extended Crystal Structures. *Journal of Applied Crystallography* **2003**, *36* (5), 1283-1284.
293. Sheldrick, G.I., Sadabs, Program for Empirical Absorption Correction of Area Detector Data. *University of Göttingen, Germany* **1996**.
294. Allen, F.; Kennard, O.; Watson, D.; Brammer, L.; Orpen, A.; Taylor, R., International Tables for Crystallography, Vol. C. Dordrecht: Kluwer Academic Publishers: 1995.
295. Momma, K.; Izumi, F., Vesta: A Three-Dimensional Visualization System for Electronic and Structural Analysis. *Journal of Applied Crystallography* **2008**, *41* (3), 653-658.

Chapter 4. Partially Completed Work

4.1. Introduction

Novel compounds were pursued as part of the work documented in chapter 2. Incomplete characterizations from these efforts are a starting point for future work. The goal of all the compounds presented below was the preparation and study of magnetically interesting compounds. They can be divided into monometallic and bimetallic complexes. The monometallic complexes were prepared to examine in greater detail the role of the axial ligand in determining the electronic structure. Additional monometallic complexes with weak field ligands were prepared. These were made to examine the effect of small changes in the ligand strength and symmetry on the magnetic properties. Monometallic complexes with stronger ligands were also attempted. It remains an open question as to whether a sufficiently strong ligand is available to change the ground state in $(\text{Tp}^{\text{Ph}})^-$ complexes by shifts in the molecular orbital predominantly z^2 in character.

The partial characterization of compounds in this chapter often includes single crystal X-ray diffraction.²⁹⁶⁻²⁹⁹ While the method is robust, and valid structures can be provided even with significantly flawed datasets, it is possible to solve and refine incorrect structures. The production of a valid, quality crystal structure, that is, one with correctly assigned Laue group, space group, accurate bond lengths and angles, and correct identification of atoms, depends on the collection of a quality dataset. A quality dataset includes diffraction data from low to high angles with the intensities exhibiting a large signal to noise ratio, collected

from a small number of highly crystalline domains. Most of the crystal structures presented in this chapter are based on preliminary data that is not of a quality suitable for publishing. Nevertheless, they have been included as they provide a starting point for further research efforts.

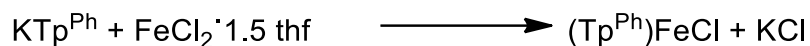
4.2. Results and Discussion

(Tp^{Ph})FeCl. Experiences with Co and Ni indicated that use of anhydrous metal chlorides was the preferred synthetic route to avoid hydrolysis of the scorpionate ligand. Attempts to prepare (Tp^{Ph})FeCl were made using FeCl₂•1.5thf as a source of anhydrous, divalent Fe.²³³ In principle, a one-step synthesis is possible since the metal chloride is being combined with the ligand in the same reagent.

K(Tp^{Ph}) was stirred with FeCl₂•1.5thf in CH₂Cl₂ or toluene in an inert atmosphere. The irreversible formation of KCl was to drive the reaction. In the case of toluene, no reaction occurred after 72 hours. In CH₂Cl₂, the reaction proceeded slowly, and due to ambient temperature fluctuations and the softening of vacuum grease by CH₂Cl₂, air and water typically began reacting and forming undesirable side products at more than 48 hours stirring. FeCl₂•1.5thf has low solubility in toluene, CH₂Cl₂, and thf and this appears to slow the reaction. For the crystal structure presented, the reaction mixture in CH₂Cl₂ was filtered, reduced in volume to give a pale green solution, and layered with diethyl ether. Preparation of larger quantities will be necessary for a complete characterization. Some possible methods include vacuum line synthesis by the procedure here, or synthesis of a solvated five or six coordinate precursor followed by vacuum desolvation and

recrystallization. A more polar solvent like acetonitrile or thf may work.

Alternately, the synthesis of an Fe^{II} complex with a more weakly coordinating anion followed by anion substitution may be preferable. Fe(OTs)₂ or Fe(OTf)₂ could be reacted with K(Tp^{Ph}), purified, and the anion substituted with Cl⁻ by salt metathesis. The OTs⁻ or OTf⁻ anion could also be substituted by Br⁻ and I⁻ to complete the halide series. The full characterization, including magnetic data, is desirable as low coordinate Fe^{II} in axial coordination modes has been shown to have significant magnetic anisotropy.³⁰⁰⁻³⁰²



Scheme 4.1. Synthesis of (Tp^{Ph})FeCl.

The preliminary crystal structure (Figure 4.1) supports the synthesis of (Tp^{Ph})FeCl in showing the connectivity of the compound and unit cell parameters and data in line with other (Tp^{Ph})MCl complexes.

Magnetically, Fe^{II} in the C_{3v} or pseudo-C_{3v} environment could show in-state SOC. If the z² orbital is lowest in energy as in the case of Co^{II}, the six d electrons of Fe^{II} will form a ⁵E ground state, which would create in-state SOC. (Tp^{Ph})FeCl could also be used as a reagent for the preparation of bimetallics, similar to (Tp^{Ph})CoCl and (Tp^{Ph})NiCl, as discussed below.

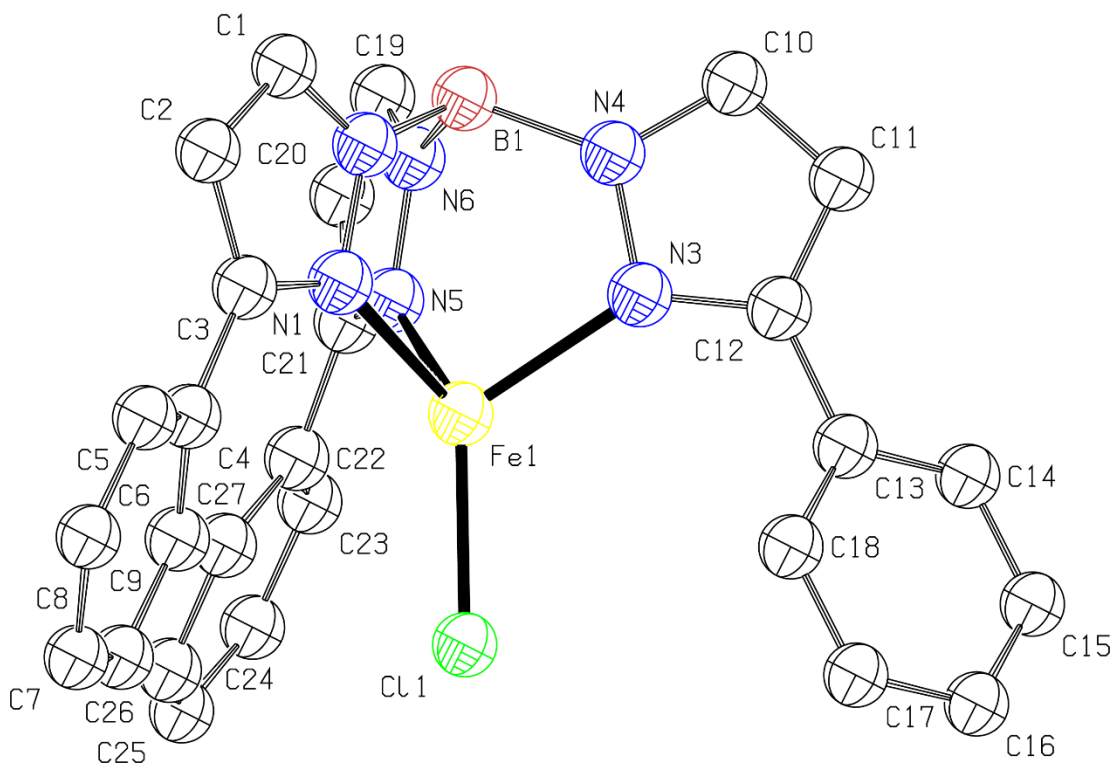


Figure 4.1. ORTEP from tentative XRD structure for $(\text{Tp}^{\text{Ph}})\text{FeCl}$ with isotropic ellipsoids plotted at 50% level.

$(\text{Tp}^{\text{Ph}})\text{Fe}(\text{thf})\text{Cl}$. In altering solvents to produce $(\text{Tp}^{\text{Ph}})\text{FeCl}$, thf was used and resulted in the formation of a small amount of a crystalline material tentatively identified by XRD crystallography as $(\text{Tp}^{\text{Ph}})\text{Fe}(\text{thf})\text{Cl}$. The conjectured compound crystallizes in the $C2/c$ space group with 8 molecules occupying the unit cell. Each molecule is a monometallic, five coordinate complex with distorted trigonal bipyramidal symmetry. Further characterization to confirm the identity and purity of the compound followed by magnetic characterization are desirable, as it is structurally similar to $(\text{Tp}^{\text{Ph}})\text{Ni}(\text{phpy})\text{Cl}$, and the low symmetry of the complex may increase the magnetic anisotropy through SOC allowed by the relaxation of selection rules.

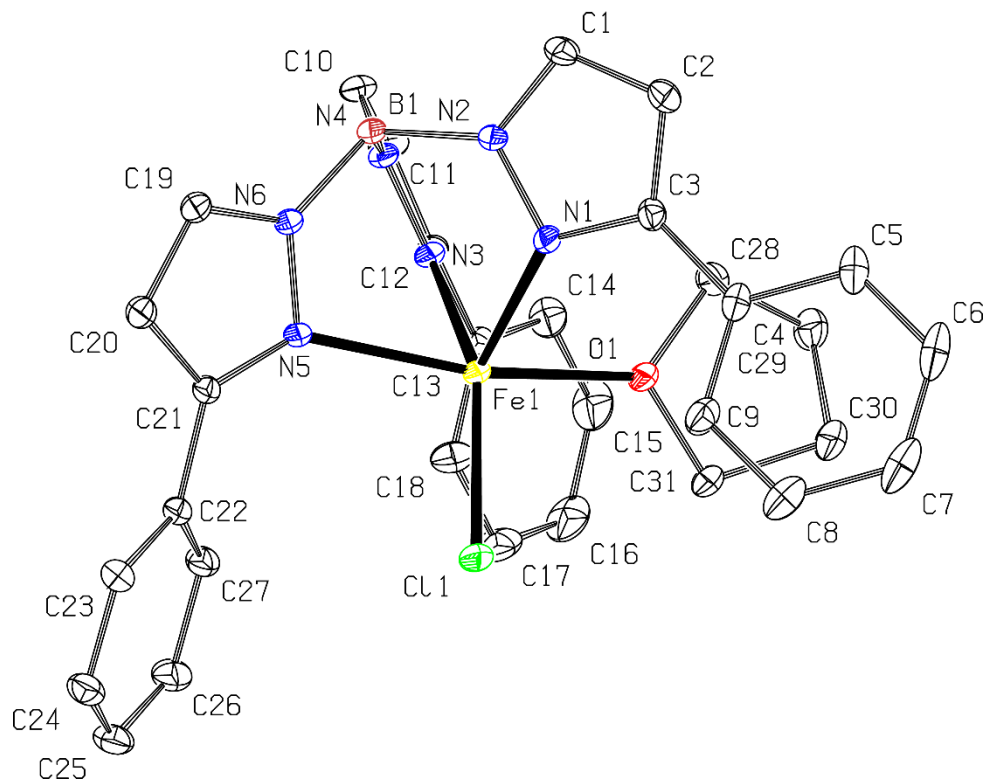


Figure 4.2. Atom numbering scheme for $(\text{Tp}^{\text{Ph}})\text{Fe}(\text{thf})\text{Cl}$ plotted at 50% probability. Hydrogens have been omitted for clarity.

$(\text{Tp}^{\text{Ph}})\text{Fe}(\text{phpy})\text{Cl}\cdot\text{solvent}$. As in the case of $(\text{Tp}^{\text{Ph}})\text{NiCl}$ synthesis, hydrolysis appears to generate 3-phenylpyrazole, which allows for the formation of $(\text{Tp}^{\text{Ph}})\text{Fe}(\text{phpy})\text{Cl}$. A crystal of the compound was isolated from a CH_2Cl_2 solution layered with diethyl ether. The tentative crystal structure shows the presence of solvent, but due to the poor diffraction of the sample crystal, the location and identity of the solvent cannot be positively determined (*vide infra*). A complete synthesis and characterization may be made from treatment of $(\text{Tp}^{\text{Ph}})\text{FeCl}$ with 3-phenylpyrazole and crystallization from the same solvents, or altering the solvents to prepare different materials. This is dependent on the discovery of a

high-yield synthesis of $(\text{Tp}^{\text{Ph}})\text{FeCl}$. The compound crystallizes in the P-1 space group.

Attempts to complete refinement with solvent disorder modeled using atomistic methods resulted in numerous fragments and overall poor fit. The use of SQUEEZE is further justified because the solvents are diethyl ether and dichloromethane, both of which will interact weakly with the complex, if at all. The fit finds 85.4 electrons in 278.8 \AA^3 , which corresponds to roughly two CH_2Cl_2 molecule per $(\text{Tp}^{\text{Ph}})\text{Fe}(\text{phpy})\text{Cl}$. Examination of the crystal lattice in this tentative X-ray structure reveals relatively large pores that could contain solvent without limiting the position and orientation. This, combined with weak intermolecular interactions between CH_2Cl_2 and the complex, could explain the observed disorder. It is possible that better data sets will reveal intrinsic solvent disorder.

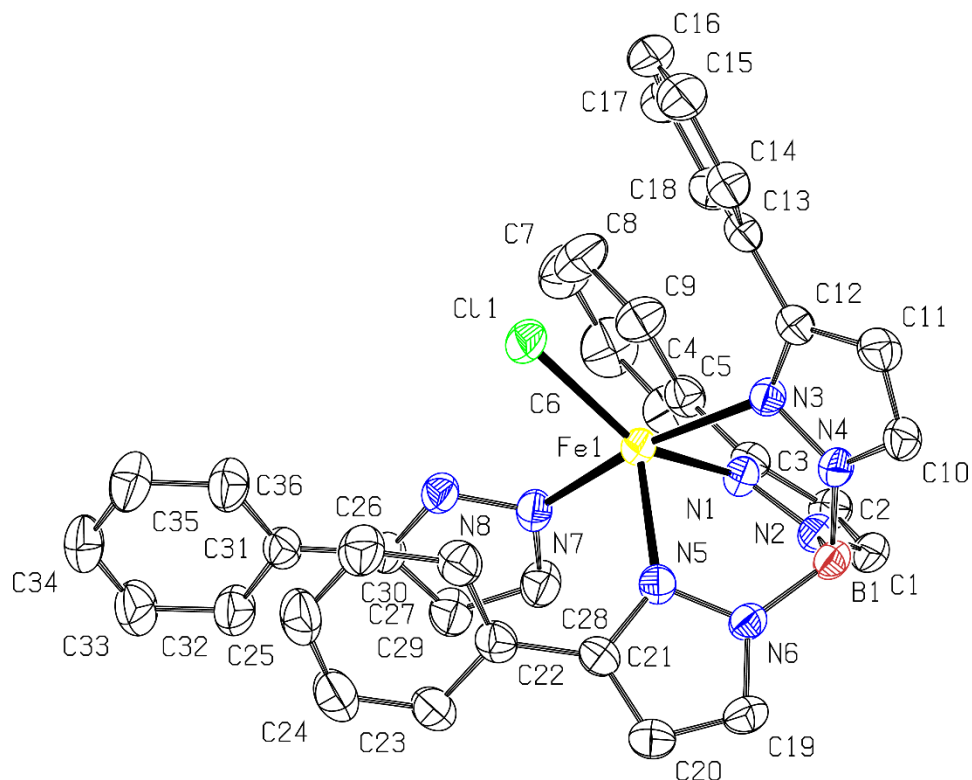


Figure 4.3. ORTEP from tentative XRD structure for $(Tp^{Ph})Fe(phpy)Cl \cdot \text{solvent}$ with ellipsoids plotted at 50% level. Hydrogens and solvent have been omitted for clarity.

The possibility of intriguing magnetic properties for low-symmetry, five-coordinate Fe^{II} complexes has been outlined previously and supports the thorough investigation of such compounds. A more efficient synthetic strategy could increase the yield and purity, providing a larger amount of material to be used to grow better crystals. A quality X-ray structure is essential for the interpretation of any magnetic data collected. Having two crystal types of the same compound could allow for the examination of effects of interatomic distances between paramagnetic centers.

(Tp^{Ph})Fe(phpy)Br•CH₂Cl₂. during the synthesis or crystallization of (Tp^{Ph})FeBr hydrolysis appears to generate 3-phenylpyrazole which coordinates to the Fe center to form (Tp^{Ph})Fe(phpy)Br. The compound was crystallized from CH₂Cl₂ layered with diethyl ether as in the case of the chloride, but the crystal quality was higher, indicating the presence of CH₂Cl₂ in the lattice.

This compound crystallizes in the *P*-1 space group, the same as for (Tp^{Ph})Fe(phpy)Cl and (Tp^{Ph})Ni(phpy)Cl. An intrinsically disordered data set was collected (Rint = 0.1940), solved and refined with a Goof = 1.018 and for [I>2σ(I)] R₁ = 0.0656, indicating the poor refinement of the structure.

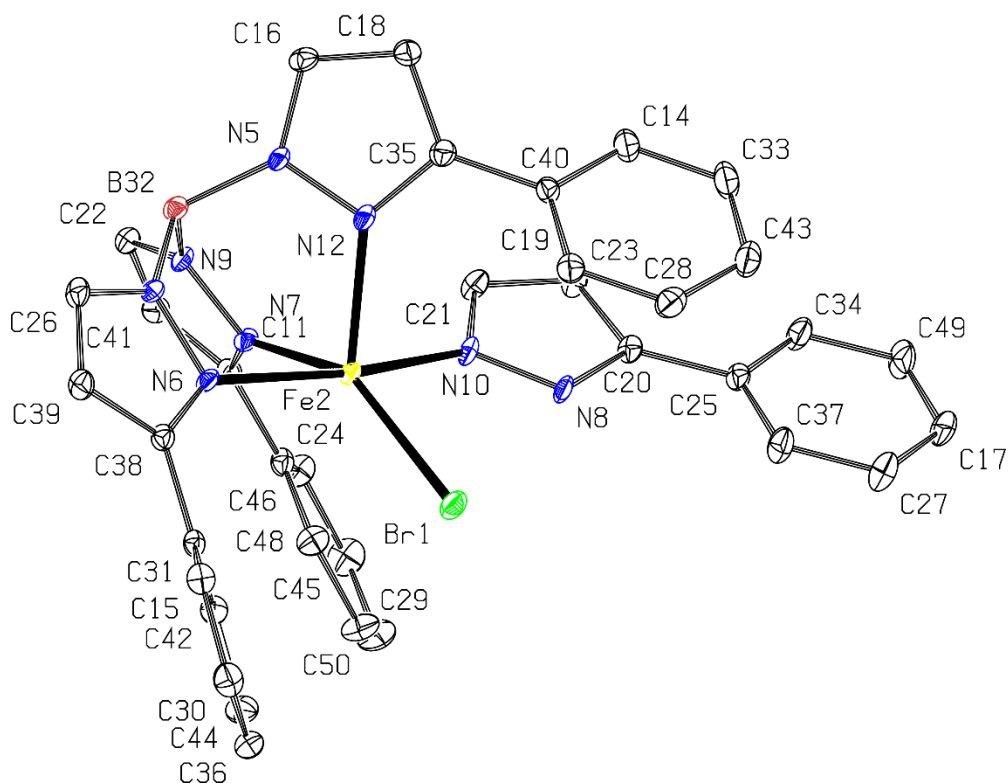
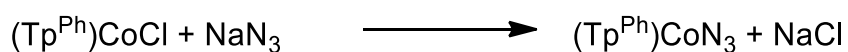


Figure 4.4. A view of the ORTEP of (Tp^{Ph})Fe(phpy)Br•CH₂Cl₂ depicting the numbering scheme. The hydrogens and lattice solvent have been omitted for clarity.

(Tp^{Ph})CoN₃. The synthesis of (Tp^{Ph})CoN₃ and (Tp^{Ph})NiN₃ was attempted by treatment of the corresponding halide complexes with NaN₃, a synthetic strategy employed by other workers to prepare azide derivatives of scorpionate complexes.¹⁸⁵ These compounds must be synthesized and handled carefully as they may be friction or shock sensitive.³⁰³ (Tp^{Ph})CoN₃ was isolated in low yields, but the isolation procedure could be optimized to improve the yield, and the reaction run on a larger scale, taking care to not generate too much potentially shock or friction sensitive material. The experimental procedure and infrared data are presented in the experimental section.



Scheme 4.2. The synthesis of (Tp^{Ph})CoN₃ by salt metathesis.

X-ray diffraction data were collected, solved, and refined. The numbering scheme is presented in Scheme 4.2 **Error! Reference source not found.**

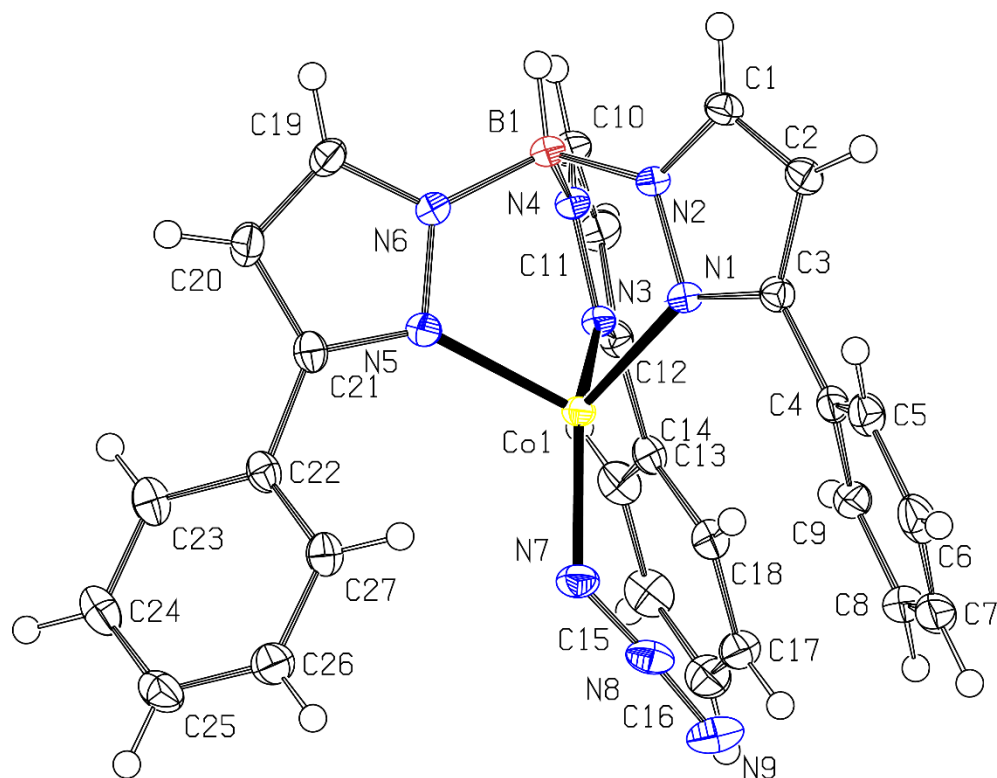


Figure 4.5. A view of the structure of $(Tp^{Ph})CoN_3$, showing the atom-labelling scheme. Displacement ellipsoids are drawn at the 50% probability level.

$(Tp^{Ph})Co(thf)Cl$. This compound can be formed by the crystallization of $(Tp^{Ph})CoCl$ from tetrahydrofuran and pentanes. For complete characterization, more material should be prepared.

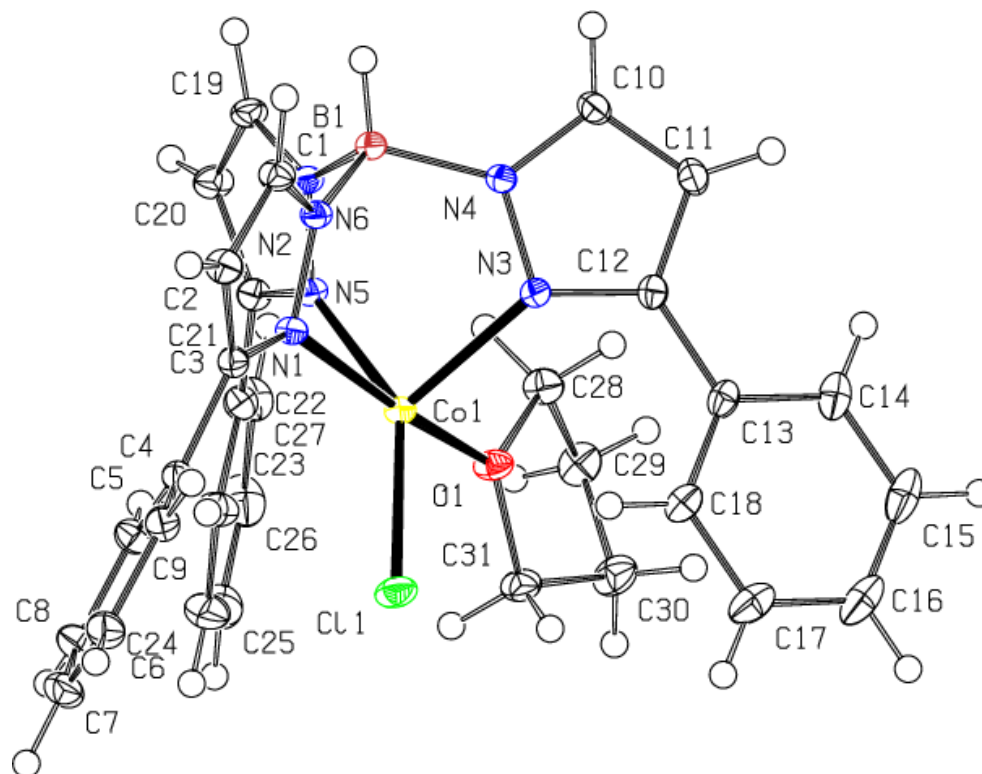
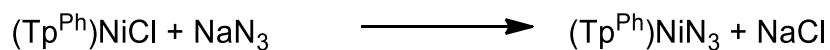


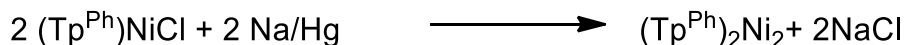
Figure 4.6. Numbering scheme and ORTEP for $(\text{Tp}^{\text{Ph}})\text{Co}(\text{thf})\text{Cl}$. Ellipsoids plotted at 50% probability.

$(\text{Tp}^{\text{Ph}})\text{NiN}_3$. The synthesis of $(\text{Tp}^{\text{Ph}})\text{NiN}_3$ was attempted by treatment of the corresponding halide complexes with NaN_3 , a synthetic strategy employed by other workers to prepare azide derivatives of scorpionate complexes.¹⁸⁵ Green crystals were isolated but characterization has not been completed. A procedure and limited data are presented in the experimental section along with UV/vis data.



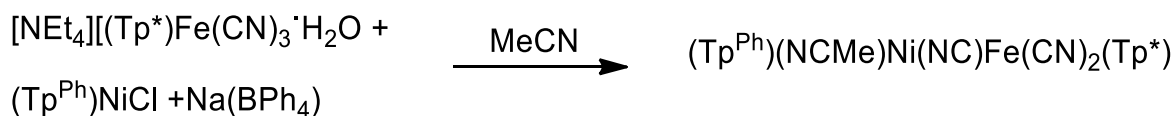
Scheme 4.3. The synthesis of $(\text{Tp}^{\text{Ph}})\text{NiN}_3$ by salt metathesis.

(Tp^{Ph})₂Ni₂•thf. Attempted one electron reduction of (Tp^{Ph})NiCl with a Na/Hg amalgam resulted in the formation of a bimetallic cluster (Scheme 4.4). A full characterization may find interesting magnetic results, but the structure shown in Figure 4.7 shows a Ni-Ni bond which will likely result in a diamagnetic complex similar to paddlewheel complexes.⁶⁵



Scheme 4.4. The synthesis of (Tp^{Ph})₂Ni₂ by one electron reduction.

This compound crystallizes in the triclinic $P\bar{1}$ space group with a Z of one and one disordered thf molecule present as lattice solvent. Based on the charge balance, the Ni centers can be assigned a formal oxidation state of one. The Ni1-Ni1a distance is 2.7121(5) Å, longer than the Ni-Ni bond in metallic Ni of 2.49(4) Å.³⁰⁴ It is possible that reaction of this compound with a ligand may generate a monometallic Ni^I complex which in a C_3 environment could show strong SOC and magnetic anisotropy.



Scheme 4.5. Synthesis of $[(\text{Tp}^*)\text{Fe}(\text{CN})_2-\mu\text{CN}-\text{Ni}(\text{NCMe})(\text{Tp}^{\text{Ph}})]$.

The atom numbering for the X-ray structure is shown in Figure 4.8.

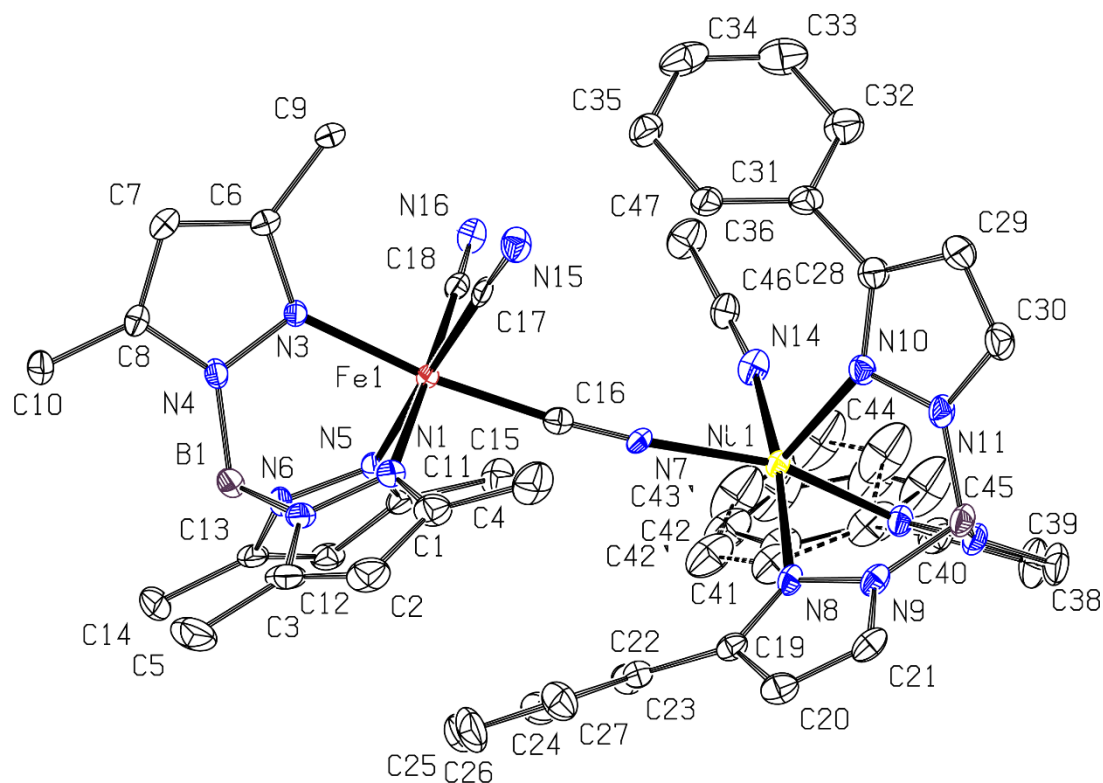


Figure 4.8. ORTEP and numbering scheme for $[(\text{Tp}^*)\text{Fe}(\text{CN})_2-\mu\text{CN}-\text{Ni}(\text{NCMe})(\text{Tp}^{\text{Ph}})]$. Ellipsoids plotted at 50% probability. Hydrogen atoms and lattice solvent molecules have been omitted for clarity.

$[(\text{Tp}^*)\text{Fe}(\text{CN})_2-\mu\text{CN}-\text{Co}(\text{dmf})(\text{Tp}^{\text{Ph}})]\cdot 2\text{dmf}$. Treatment of $[\text{NEt}_4][$

$(\text{Tp}^*)\text{Fe}(\text{CN})_3]\cdot\text{H}_2\text{O}$ in dmf with $(\text{Tp}^{\text{Ph}})\text{CoCl}$ in MeCN in air yields a dark red solution that is more intense than either of the starting material solutions, indicative of a charge transfer band for the cyanide-bridged Fe/Co compounds.

Slow evaporation in air yielded the crystalline product, and the preliminary X-ray

structure shown in Figure 4.9 was determined. However, the crystal weakly diffracted and the isotropic structure is below the standards for publication.

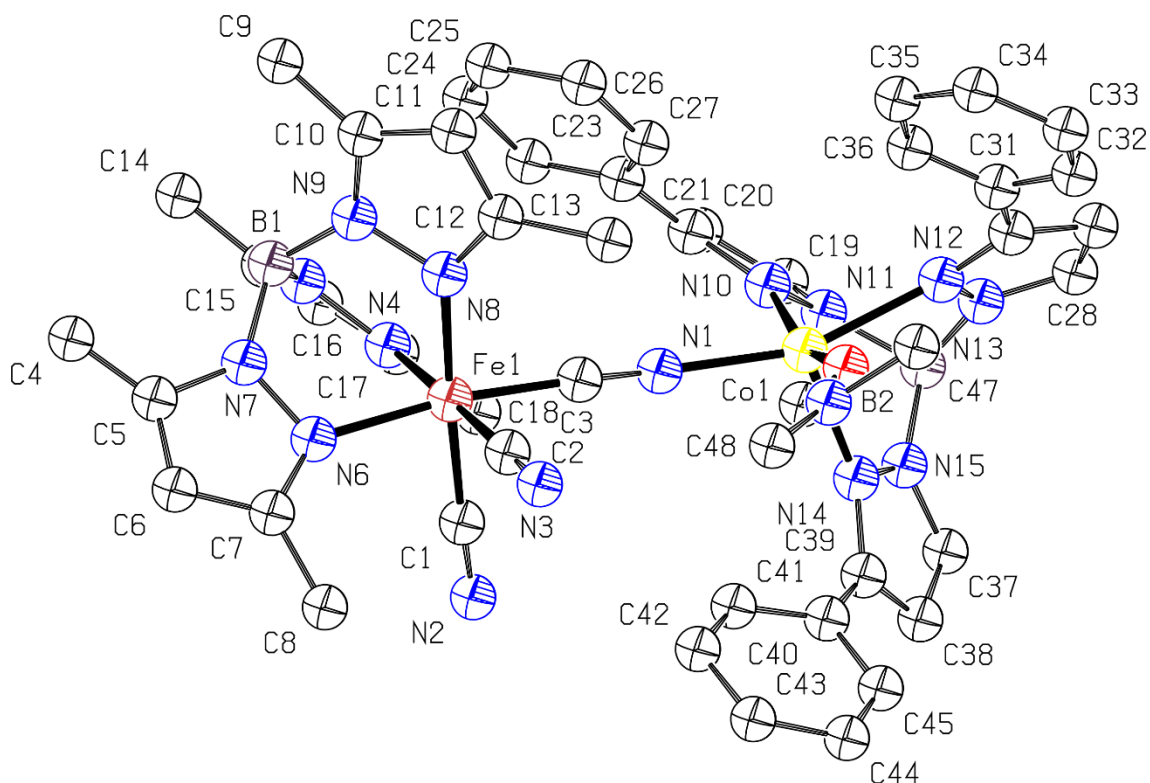


Figure 4.9. ORTEP and numbering scheme for $[(Tp^)Fe(CN)_2-\mu CN-Co(dmf)(Tp^{Ph})]\cdot 2dmf$. The solvent molecules have been omitted for clarity. Hydrogen positions were not solved. Displacement spheres plotted at 50% probability.*

4.3. Conclusions

The progress towards synthesis and characterization of several compounds has been summarized here with the intent of providing a starting point for future work. Optimization of reaction and crystallization conditions will provide crystalline compounds of purity necessary for characterization. These compounds, especially the monometallic and homobimetallic ones, can also

undergo further transformations to generate novel, magnetically interesting, compounds.

4.4. Experimental

Unless otherwise noted, all syntheses and manipulations were carried out under an Ar atmosphere using Schlenk techniques or a nitrogen-filled glovebox. Stainless steel cannulae, needles, and ground glass syringes were used to transfer solutions and solvents. The anhydrous *para*-toluenesulfonate salts were prepared by dehydrating the hydrates under heat (160 °C) and vacuum for at least 1 hr. N,N'-dimethylformamide was purified and dried using a Vacuum Atmospheres Corporation solvent purification system. Diethyl ether was dried by distillation over sodium and benzophenone in a nitrogen atmosphere, and all solvents were sparged before use. Elemental analyses were performed by Robertson Microlit laboratories.

(Tp^{Ph})CoN₃. 0.2346 g (0.4363 mmol) (Tp^{Ph})CoCl was dissolved in 15 mL dichloromethane. With Ar counterflow 0.0462 g (0.711 mmol) was added as a solid. The mixture was stirred overnight and filtered to isolate a blue solution. The volume was reduced *in vacuo* to 5 mL and 20 mL of pentanes were added. Storing at -20 °C for one week yielded 0.0736 g blue crystals. Yield: 30.9%. IR (nujol, cm⁻¹): 3394 (w), 3142 (w), 3117 (w), 2503 (m), 2073 (s), 1649 (w), 1525 (w), 1491 (m), 1344 (m), 1183 (s), 1090 (m), 1048 (s), 909 (w), 876 (w), 839 (W), 792 (m), 756 (s), 694 (m), 675 (m), 646 (w), 630 (w), 595 (w), 528 (w), 5145 (w), 457 (w), 418 (s).

(Tp^{Ph})NiN₃. Dissolved 0.2452 g (0.4579 mmol) (Tp^{Ph})NiCl in 15 mL dichloromethane. Suspended 0.0436 g (0.6708 mmol) NaN₃ in 5 mL dichloromethane and transferred via cannula into (Tp^{Ph})NiCl solution. Stirred overnight and evacuated to dryness. Extracted with 8 mL dichloromethane and added 40 mL pentanes while stirring. Storing at -20 °C overnight yielded 0.0520 g dark green needles Yield: 20.9%. UV/vis dichloromethane (nm, M⁻¹cm⁻¹): 376 (1820), 473 (836), 578 (128).

(Tp^{Ph})(NCMe)Ni(NC)Fe(CN)₂(Tp^{*}). In air, 0.3570 g (0.6162 mmol) [NEt₄][(Tp^{*})Fe(CN)₃].H₂O was dissolved in 10 mL acetonitrile. A slurry of 0.3303 g (0.6168 mmol) (Tp^{Ph})NiCl in 20 mL acetonitrile was prepared and added dropwise to the first solution. Stirring for 1 hour gave a dark red solution. 0.2111 g (0.6169 mmol) NaBPh₄ was dissolved in 3 mL acetonitrile and added dropwise to the dark red solution. After stirring 15 minutes the solution was evacuated to dryness and extracted with 10 mL dichloromethane and 1 mL acetonitrile. After filtering the solution was layered with 20 mL diethyl ether and standing overnight at -20 °C gave 0.6346g (0.5780 mmol) of dark red crystals. 93% yield. IR (nujol, cm⁻¹): 3095 (m), 3052 (s), 2539 (m), 2312 (w), 2285 (w), 2250 (w), 2149 (s), 2119 (m), 1942 (w), 1885 (w), 1809 (w), 1648 (w), 1581 (w), 1544 (s), 1523 (m), 1488 (vs), 1415 (vs), 1268 (m), 1193 (vs), 1182 (vs), 1117 (m), 1094 (w), 1064 (vs), 1047 (vs), 996 (m, br), 908 (w), 867 (m), 846 (w), 815 (w), 800 (m), 784 (s), 759

(vs), 745 (s), 734 (vs), 709 (vs), 696 (vs), 674 (w), 652 (w), 642 (w), 627 (w), 613 (w), 604 (m), 538 (w), 498 (w), 480 (w), 462 (w), 437 (w).

[(Tp^{Ph})Ni]₂. 0.130 g (Tp^{Ph})NiCl was dissolved in 20 mL tetrahydrofuran and cannulated onto 1.255g 0.699% Na/Hg. Stirring for one hour resulted in a color change from magenta to red passing through an orange color. The tetrahydrofuran was decanted off and filtered. The resulting solution was reduced to 5 mL in volume and layered with 10 mL of hexane. 0.0556 g red solid.

4.5. References

65. Cotton, F.A.; Daniels, L.M.; Murillo, C.A.; Pascual, I.; Zhou, H.-C., Remarkable Effects of Axial Π^* Coordination on the Cr–Cr Quadruple Bond in Dichromium Paddlewheel Complexes. *Journal of the American Chemical Society* **1999**, *121* (29), 6856-6861.
185. Abubekеров, M.; Gianetti, T.L.; Kunishita, A.; Arnold, J., Synthesis and Characterization of Coordinatively Unsaturated Nickel(II) and Manganese(II) Alkyl Complexes Supported by the Hydrotris(3-Phenyl-5-Methylpyrazolyl)Borate (Tp^{ph,Me}) Ligand. *Dalton Transactions* **2013**, *42* (29), 10525-10532.
213. Li, D.; Parkin, S.; Wang, G.; Yee, G.T.; Holmes, S.M., Synthesis and Spectroscopic and Magnetic Characterization of Tris(3,5-Dimethylpyrazol-1-Yl) Borate Iron Tricyanide Building Blocks, a Cluster, and a One-Dimensional Chain of Squares. *Inorganic Chemistry* **2006**, *45* (5), 1951-1959.

233. Kern, R.J., Tetrahydrofuran Complexes of Transition Metal Chlorides. *Journal of Inorganic and Nuclear Chemistry* **1962**, *24*, 1105-1109.
296. Jones, P., Crystal Structure Determination: A Critical View. *Chemical Society Reviews* **1984**, *13* (2), 157-172.
297. Kuchta, M.C.; Parkin, G., Incorrect Atom Connectivity in X-Ray Structure Solutions Associated with a "Partial Polar Ambiguity": A Non-Macrocyclic Structure for the Macrocyclic Lead Complex, $[H^4-Me_8taa]Pb$. *New Journal of Chemistry* **1998**, *22* (5), 523-530.
298. Harlow, R.L., Troublesome Crystal Structures: Prevention, Detection, and Resolution. *Journal of research of the National Institute of Standards and Technology* **1996**, *101* (3), 327.
299. Spek, A.L., Single-Crystal Structure Validation with the Program Platon. *Journal of Applied Crystallography* **2003**, *36* (1), 7-13.
300. Holland, P.L., Electronic Structure and Reactivity of Three-Coordinate Iron Complexes. *Accounts of Chemical Research* **2008**, *41* (8), 905-14.
301. Holland, P.L., Low-Coordinate Iron Complexes as Synthetic Models of Nitrogenase. *Canadian Journal of Chemistry* **2005**, *83* (4), 296-301.
302. Andres, H.; Bominaar, E.L.; Smith, J.M.; Eckert, N.A.; Holland, P.L.; Münck, E., Planar Three-Coordinate High-Spin Fe(II) Complexes with Large Orbital Angular Momentum: Mössbauer, Electron Paramagnetic Resonance, and Electronic Structure Studies. *Journal of the American Chemical Society* **2002**, *124* (12), 3012-3025.

303. Churchill, D.G., Chemical Structure and Accidental Explosion Risk in the Research Laboratory. *Journal of Chemical Education* **2006**, 83 (12), 1798.
304. Bonamico, M.; Dessy, G.; Fares, V., Mixed Nickel Co-Ordination in a Binuclear Complex with a Short Nickel–Nickel Bond. *Journal of the Chemical Society D: Chemical Communications* **1969**, (13), 697-698.

Chapter 5. Conclusions

5.1. The Limitations of the Spin Hamiltonian Formalism in Single Molecule Magnetism

In Chapter 1 the context of this work in single molecule magnetism is summarized with the approaches to description and prediction from chemistry and physics being presented. The general concepts of magnetic phenomena are described from the unpaired electron to the cooperativity between spin centers in extended lattices. Physics provides the underlying theory and descriptions from over 100 years of concerted research. This includes the spin Hamiltonian formalism, the approach applied to the compounds in this work.^{59-60, 64, 74, 83} More recently, chemistry has provided, via molecular orbital theory, a method to explain, predict, and possibly design magnetic materials.^{60, 64, 305-310} The chapter concludes with an explanation of AC magnetic susceptibility,^{38, 121, 149, 311} which is a specialized technique that provides important information about magnetic dynamics and physical parameters like g , D , and E can be determined.

The important hypothesis put forth by others^{35, 70, 100-101} and discussed in the introduction is the role of axial symmetry in suppressing QTM in single molecule magnets. Based on mathematical arguments, a perfectly axial complex should have orthogonal microstates, suppressing QTM.³⁸ The axial symmetry and lack of higher symmetry elements in the complexes should also relax selection rules, allowing for greater state mixing, increasing SOC.^{61, 96, 123} These hypotheses are examined in Chapter 2, which documents the preparation and

characterization of eight compounds. The general synthetic route to scorpionate complexes is discussed and their application in many areas of research briefly mentioned. Fruitful efforts have been made and described to systematically alter the identity of the metal ion and the axial ligand. This generates a related set of compounds for magnetic study which, to date, has been partially completed. While none show zero-field remnant magnetization, magnetic hysteresis can be observed in three of them ((Tp^{Ph})CoCl, (Tp^{Ph})NiCl, and (Tp^{Ph})Ni(phpy)Cl) with several others awaiting full magnetic characterization. For these compounds, axial symmetry predicts magnetic hysteresis, but the presence of remnant magnetization in zero field depends on the sign of D . Axial symmetry is low enough to allow mixing of states by relaxing selection rules, and this increases SOC, giving rise to ZFS. This supports the hypothesis that axially symmetric complexes allow greater mixing of states, leading to SOC.

The larger magnitude of in-state SOC versus out-of-state SOC is shown in (Tp^{Ph})CoCl and (Tp^{Ph})NiCl, but the latter compound shows that even out-of-state SOC can give rise to magnetic hysteresis. The contribution rapidly drops off as the energy difference increases between the two states that are mixing, but if they are close in energy, they can mix without being strictly degenerate. The compound (Tp^{Ph})Ni(phpy)Cl shows the limitations of the spin Hamiltonian approach to magnetic characterization. Instead of a single D value that quantifies the ZFS, a temperature dependence is observed. This suggests that the density of states is higher than in (Tp^{Ph})NiCl and that a more detailed model

is necessary to describe the magnetic behavior. Computational methods may better explain the observations, and this is a route many in the field are taking.

In Chapter 3 the preparation of five divalent transition metal paratoluenesulfonates with coordinated dmf ligands was reported. The characterization of the compounds showed a variety of structural motifs from 1-D ribbons to monomolecular complexes. The spectroscopic data is consistent with a weaker ligand field, making these complexes substitutionally labile and promising sources of M^{II} ions for inorganic synthesis. The reported complexes show solubility in solvents with low polarity. The paratoluenesulfonate anion is more environmentally benign than other weakly coordinating anions and less expensive. These compounds also avoid the hazardous nature of anions like perchlorate and nitrate, which can be shock and friction sensitive.

Chapter 4 documents the partially completed work related to the objectives and efforts towards single molecule magnets presented in Chapter 3. Some of the compounds are magnetically interesting, while others may be useful intermediates in the preparation of novel magnetic materials. Completion of this work will allow for examination of a larger set of compounds with further trends perhaps being observed. It may also aid answering the questions above.

5.2. References

35. Neese, F.; Pantazis, D.A., What Is Not Required to Make a Single Molecule Magnet. *Faraday Discussions* **2011**, *148*, 229-238.

38. Gatteschi, D.; Sessoli, R., Quantum Tunneling of Magnetization and Related Phenomena in Molecular Materials. *Angewandte Chemie International Edition* **2003**, *42* (3), 268-297.
59. Moriya, T., Anisotropic Superexchange Interaction and Weak Ferromagnetism. *Physical Review* **1960**, *120* (1), 91.
60. Curély, J., Magnetic Orbitals and Mechanisms of Exchange II. Superexchange. *Monatshefte für Chemie - Chemical Monthly* **2005**, *136* (6), 1013-1036.
61. Dai, D.; Xiang, H.; Whangbo, M.-H., Effects of Spin-Orbit Coupling on Magnetic Properties of Discrete and Extended Magnetic Systems. *Journal of Computational Chemistry* **2008**, *29* (13), 2187-2209.
64. Curély, J., Magnetic Orbitals and Mechanisms of Exchange I. Direct Exchange. *Monatshefte für Chemie - Chemical Monthly* **2005**, *136* (6), 987-1011.
70. Zadrozny, J.M.; Atanasov, M.; Bryan, A.M.; Lin, C.-Y.; Rekken, B.D.; Power, P.P.; Neese, F.; Long, J.R., Slow Magnetization Dynamics in a Series of Two-Coordinate Iron(II) Complexes. *Chemical Science* **2013**, *4* (1), 125-138.
74. Orbach, R., Spin-Lattice Relaxation in Rare-Earth Salts. *Proceedings of the Royal Society of London Series A* **1961**, *264* (1319), 458-484.
83. Orbach, R., On the Theory of Spin-Lattice Relaxation in Paramagnetic Salts. *Proceedings of the Physical Society* **1961**, *77* (4), 821.
96. Lin, P.H.; Smythe, N.C.; Gorelsky, S.I.; Maguire, S.; Henson, N.J.; Korobkov, I.; Scott, B.L.; Gordon, J.C.; Baker, R.T.; Murugesu, M., Importance of out-of-State Spin-Orbit Coupling for Slow Magnetic Relaxation in Mononuclear

Fe(II) Complexes. *Journal of the American Chemical Society* **2011**, 133 (40), 15806-9.

100. Zadrozny, J.M.; Xiao, D.J.; Atanasov, M.; Long, G.J.; Grandjean, F.; Neese, F.; Long, J.R., Magnetic Blocking in a Linear Iron(I) Complex. *Nat Chem* **2013**, 5 (7), 577-81.

101. Zadrozny, J.M.; Xiao, D.J.; Long, J.R.; Atanasov, M.; Neese, F.; Grandjean, F.; Long, G.J., Mossbauer Spectroscopy as a Probe of Magnetization Dynamics in the Linear Iron(I) and Iron(II) Complexes $[\text{Fe}(\text{C}(\text{SiMe}_3)_2)]^{1-/0}$. *Inorganic Chemistry* **2013**, 52 (22), 13123-31.

121. Jurca, T.; Farghal, A.; Lin, P.-H.; Korobkov, I.; Murugesu, M.; Richeson, D.S., Single-Molecule Magnet Behavior with a Single Metal Center Enhanced through Peripheral Ligand Modifications. *Journal of the American Chemical Society* **2011**, 133 (40), 15814-15817.

123. Park, K.; Holmes, S.M., Exchange Coupling and Contribution of Induced Orbital Angular Momentum of Low-Spin Fe^{3+} Ions to Magnetic Anisotropy in Cyanide-Bridged Fe_2m_2 Molecular Magnets: Spin-Polarized Density-Functional Calculations. *Physical Review B* **2006**, 74 (22), 224440.

149. Vaidya, S.; Upadhyay, A.; Singh, S.K.; Gupta, T.; Tewary, S.; Langley, S.K.; Walsh, J.P.; Murray, K.S.; Rajaraman, G.; Shanmugam, M., A Synthetic Strategy for Switching the Single Ion Anisotropy in Tetrahedral Co (II) Complexes. *Chemical Communications* **2015**, 51 (18), 3739-3742.

305. Ditchfield, R., Molecular Orbital Theory of Magnetic Shielding and Magnetic Susceptibility. *The Journal of Chemical Physics* **1972**, 56 (11), 5688-5691.
306. Yoshizawa, K.; Hoffmann, R., The Role of Orbital Interactions in Determining Ferromagnetic Coupling in Organic Molecular Assemblies. *Journal of the American Chemical Society* **1995**, 117 (26), 6921-6926.
307. Journaux, Y.; Kahn, O.; Zarembowitch, J.; Galy, J.; Jaud, J., Symmetry of the Magnetic Orbitals and Exchange Interaction in Copper Iron (Cu^{II}Fe^{III}) and Copper Chromium (Cu^{II}Cr^{III}) Heterobinuclear Complexes. Crystal Structure of CuFe [(Fsa)₂en]Cl(H₂O)(CH₃OH)·CH₃OH. *Journal of the American Chemical Society* **1983**, 105 (26), 7585-7591.
308. Kahn, O., Molecular Engineering of Coupled Polynuclear Systems: Orbital Mechanism of the Interaction between Metallic Centers. *Inorganica Chimica Acta* **1982**, 62, 3-14.
309. Kollmar, C.; Kahn, O., Ferromagnetic Spin Alignment in Molecular Systems: An Orbital Approach. *Accounts of Chemical Research* **1993**, 26 (5), 259-265.
310. Verdaguer, M., Rational Synthesis of Molecular Magnetic Materials: A Tribute to Olivier Kahn. *Polyhedron* **2001**, 20 (11), 1115-1128.
311. Hein, R., Ac Magnetic Susceptibility, Meissner Effect, and Bulk Superconductivity. *Physical Review B* **1986**, 33 (11), 7539.

Appendix A. Supplemental Data for Chapter 2

Table A.1. Peak fitting results for $(Tp^{Ph})CoCl$, $(Tp^{Ph})CoBr$, $(Tp^{Ph})NiCl$, $(Tp^{Ph})NiBr$, $(Tp^{Ph})NiI$.

| cmpd | peak | (nm) | w (nm) | A | σ (nm) | FWHM (nm) |
|---------------------|------|-----------------|-----------------|-----------------|-----------------|----------------|
| $(Tp^{Ph})Co$ Cl | 1 | 557 ± 1.6 | 44 ± 2 | 4100 ± 300 | 22 ± 1.1 | 52 ± 3 |
| | 2 | 594 ± 0.3 | 25.7 ± 0.5 | 12300 ± 600 | 12.9 ± 0.3 | 30.2 ± 0.6 |
| | 3 | 628 ± 0 | 31.2 ± 0.7 | 27400 ± 900 | 15.6 ± 0.3 | 36.8 ± 0.8 |
| | 4 | 665.0 ± 0.3 | 34.2 ± 0.3 | 27400 ± 500 | 17.1 ± 0.14 | 40.3 ± 0.3 |
| | 5 | 930 ± 0.9 | 137.9 ± 1.9 | 8700 ± 100 | 69.0 ± 0.9 | 162 ± 2 |
| $(Tp^{Ph})Co$ Br | 1 | 558 ± 0.8 | 35 ± 1 | 2600 ± 100 | 17.7 ± 0.5 | 42 ± 1.2 |
| | 2 | 604 ± 0.5 | 32.4 ± 0.8 | 13100 ± 600 | 16.2 ± 0.4 | 38.1 ± 0.9 |
| | 3 | 634 ± 0.3 | 28.7 ± 0.6 | 14900 ± 900 | 14.4 ± 0.3 | 33.8 ± 0.7 |
| | 4 | 664 ± 0.3 | 37.1 ± 0.3 | 26100 ± 400 | 18.5 ± 0.12 | 43.6 ± 0.3 |

| | | | | | | |
|------------------------|---|-----------|-----------|------------|------------|------------|
| | | | 137.9 ± | | | 162.3 ± |
| | 5 | 942 ± 0.4 | 0.8 | 9090 ± 40 | 68.9 ± 0.4 | 0.9 |
| (Tp ^{Ph})Ni | | 486.15 ± | 33.5 ± | | 16.8 ± | |
| Cl | 1 | 0.09 | 0.3 | 52.0 ± 0.8 | 0.14 | 39.5 ± 0.3 |
| | 2 | 525.1 ± | 90.9 ± | 63 ± 1 | 45.5 ± 0.4 | 107 ± 1.0 |
| | | 0.8 | 0.9 | | | |
| | 3 | 805.2 ± | 27 ± 1.5 | 4.0 ± 0.3 | 13.6 ± 0.8 | 32 ± 1.8 |
| | | 0.7 | | | | |
| | 4 | 950.5 ± | 172 ± 1.2 | 105.8 ± | 85.8 ± 0.6 | 202 ± 1.4 |
| | | 0.5 | | 0.6 | | |
| (Tp ^{Ph})Ni | | 197.21 ± | 35.3 ± | | 17.64 ± | 41.5 ± |
| Br | 1 | 0.05 | 0.15 | 70.0 ± 0.6 | 0.08 | 0.18 |
| | 2 | 532.0 ± | 84.7 ± | 89.4 ± 0.7 | 42.3 ± | 99.7 ± 0.4 |
| | | 0.4 | 0.3 | | 0.17 | |
| | 3 | 820.5426 | 34.2 ± | 7.5 ± 0.3 | 17.1 ± 0.4 | 311 ± 8 |
| | | | 0.8 | | | |
| | 4 | 940.6 ± | 95 ± 2 | 37 ± 2 | 47 ± 1.1 | 112 ± 3 |
| | | 0.4 | | | | |
| | 5 | 980 ± 4 | 264 ± 7 | 103 ± 1.4 | 132 ± 3 | 311 ± 8 |
| (Tp ^{Ph})NiI | | 386.8 ± | 72.9 ± | | | |
| | 1 | 0.2 | 0.6 | 66.8 ± 0.6 | 36.5 ± 0.3 | 85.8 ± 0.7 |
| | 2 | 443.3 ± | 35.6 ± | 15.8 ± 0.4 | 17.8 ± | 41.9 ± 0.4 |
| | | 0.13 | 0.4 | | 0.18 | |

| | | | | | |
|---|---------|--------|--------|------------|------------|
| 3 | 516.8 ± | 43.9 ± | 25.7 ± | 22.0 ± | 51.7 ± 0.3 |
| | 0.11 | 0.2 | 0.18 | 0.11 | |
| 4 | 583.9 ± | 63.9 ± | 11.2 ± | 32.0 ± 0.5 | 75 ± 1.1 |
| | 0.6 | 0.9 | 0.18 | | |

Table A.2. Single crystal X-ray diffraction experimental details for $(Tp^{Ph})MnCl$.

| | |
|---|------------------------------------|
| Chemical formula | $C_{27}H_{22}BCIMnN_6$ |
| M_r | 531.73 |
| Crystal system, space group | Monoclinic, $P2_1/n$ |
| Temperature (K) | 100 |
| a, b, c (Å) | 9.6804(17), 15.691(3), 16.811(3) |
| β (°) | 96.555(11) |
| V (Å ³) | 2536.8(8) |
| Z | 1 |
| Radiation type | Mo $K\alpha$ $\lambda = 0.71073$ Å |
| μ (mm ⁻¹) | 0.65 |
| Crystal size (mm) | 0.25 x 0.22 x 0.18 |
| Diffractometer | Bruker APEX II CCD |
| Absorption correction | none |
| No. of measured, independent, and observed [$I > 2\sigma(I)$] reflections | 36573, 7455, 4565 |
| R_{int} | 0.133 |
| $(\sin \theta/\lambda)_{max}$ (Å ⁻¹) | 0.716 |

| | |
|--|--|
| $R[F^2 > 2s(F^2)], wR(F^2), S$ | 0.058, 0.169, 1.02 |
| No. of reflections | 7455 |
| No. of parameters | 328 |
| H-atom treatment | H atoms treated by a mixture of independent and constrained refinement |
| Largest diff. peak/hole ($e \text{ \AA}^{-3}$) | 0.94, -1.24 |

Table A.3. Atom Coordinates for $(Tp^{Ph})MnCl$.

| Atom | x | y | z | Occupancy |
|------|---------|----------|---------|-----------|
| Mn1 | 0.24992 | 0.24315 | 0.26064 | 1.000 |
| Cl1 | 0.47087 | 0.28742 | 0.30099 | 1.000 |
| N6 | 0.04070 | 0.10366 | 0.24676 | 1.000 |
| N3 | 0.15600 | 0.23898 | 0.13869 | 1.000 |
| N1 | 0.06510 | 0.29090 | 0.30269 | 1.000 |
| N5 | 0.18030 | 0.11347 | 0.27063 | 1.000 |
| N4 | 0.02220 | 0.20906 | 0.13236 | 1.000 |
| C21 | 0.22550 | 0.03920 | 0.30461 | 1.000 |
| C3 | 0.02450 | 0.34150 | 0.36028 | 1.000 |
| C9 | 0.23220 | 0.43770 | 0.38118 | 1.000 |
| H9 | 0.24840 | 0.42900 | 0.32710 | 1.000 |
| C22 | 0.37450 | 0.02180 | 0.32625 | 1.000 |
| C20 | 0.11440 | -0.01850 | 0.30425 | 1.000 |

| | | | | |
|-----|----------|----------|----------|-------|
| H20 | 0.11650 | -0.07470 | 0.32520 | 1.000 |
| C12 | 0.18320 | 0.25760 | 0.06399 | 1.000 |
| C4 | 0.12120 | 0.39590 | 0.41079 | 1.000 |
| C13 | 0.31760 | 0.29180 | 0.04593 | 1.000 |
| N2 | -0.05270 | 0.25015 | 0.26732 | 1.000 |
| C19 | 0.00190 | 0.02510 | 0.26655 | 1.000 |
| H19 | -0.08970 | 0.00290 | 0.25610 | 1.000 |
| C2 | -0.11950 | 0.33360 | 0.36212 | 1.000 |
| H2 | -0.17500 | 0.36180 | 0.39710 | 1.000 |
| C7 | 0.29830 | 0.50450 | 0.50746 | 1.000 |
| H7 | 0.35830 | 0.54140 | 0.54020 | 1.000 |
| C8 | 0.31880 | 0.49130 | 0.42898 | 1.000 |
| H8 | 0.39310 | 0.51930 | 0.40740 | 1.000 |
| C5 | 0.10130 | 0.41000 | 0.49087 | 1.000 |
| H5 | 0.02680 | 0.38260 | 0.51280 | 1.000 |
| B1 | -0.04620 | 0.17830 | 0.20618 | 1.000 |
| H1 | -0.14260 | 0.15780 | 0.18830 | 1.000 |
| C11 | 0.06570 | 0.23930 | 0.00972 | 1.000 |
| H11 | 0.05610 | 0.24660 | -0.04670 | 1.000 |
| C1 | -0.16300 | 0.27670 | 0.30289 | 1.000 |
| H1A | -0.25630 | 0.25870 | 0.28900 | 1.000 |
| C6 | 0.18940 | 0.46370 | 0.53856 | 1.000 |
| H6 | 0.17510 | 0.47250 | 0.59290 | 1.000 |

| | | | | |
|-----|----------|----------|----------|-------|
| C18 | 0.44250 | 0.26840 | 0.08960 | 1.000 |
| H18 | 0.44180 | 0.22950 | 0.13290 | 1.000 |
| C27 | 0.47340 | 0.05510 | 0.28069 | 1.000 |
| H27 | 0.44520 | 0.09300 | 0.23790 | 1.000 |
| C24 | 0.55810 | -0.05480 | 0.40440 | 1.000 |
| H24 | 0.58710 | -0.09240 | 0.44730 | 1.000 |
| C14 | 0.32230 | 0.34790 | -0.01822 | 1.000 |
| H14 | 0.23860 | 0.36420 | -0.04950 | 1.000 |
| C10 | -0.03190 | 0.20860 | 0.05523 | 1.000 |
| H10 | -0.12290 | 0.19020 | 0.03550 | 1.000 |
| C25 | 0.65530 | -0.02160 | 0.35800 | 1.000 |
| H25 | 0.75050 | -0.03710 | 0.36830 | 1.000 |
| C15 | 0.44880 | 0.37980 | -0.03654 | 1.000 |
| H15 | 0.45080 | 0.41860 | -0.07980 | 1.000 |
| C17 | 0.56870 | 0.30110 | 0.07088 | 1.000 |
| H17 | 0.65310 | 0.28550 | 0.10190 | 1.000 |
| C26 | 0.61210 | 0.03330 | 0.29720 | 1.000 |
| H26 | 0.67820 | 0.05690 | 0.26590 | 1.000 |
| C16 | 0.57040 | 0.35590 | 0.00730 | 1.000 |
| H16 | 0.65650 | 0.37730 | -0.00630 | 1.000 |
| C23 | 0.41960 | -0.03310 | 0.38849 | 1.000 |
| H23 | 0.35420 | -0.05620 | 0.42060 | 1.000 |

Table A.4. Bond angles for $(Tp^{Ph})MnCl$ (°).

| | | | |
|------------|------------|-------------|----------|
| N3—Mn1—Cl1 | 125.08(6) | N3—C12—C11 | 109.4(3) |
| N3—Mn1—N5 | 86.77(9) | C11—C12—C13 | 127.6(3) |
| N1—Mn1—Cl1 | 126.07(7) | C9—C4—C3 | 122.2(2) |
| N1—Mn1—N3 | 92.72(8) | C9—C4—C5 | 117.6(3) |
| N1—Mn1—N5 | 91.40(9) | C5—C4—C3 | 120.1(2) |
| N5—Mn1—Cl1 | 123.77(6) | C18—C13—C12 | 122.1(3) |
| N5—N6—B1 | 120.6(2) | C18—C13—C14 | 118.1(3) |
| C19—N6—N5 | 109.0(2) | C14—C13—C12 | 119.8(3) |
| C19—N6—B1 | 130.4(2) | N1—N2—B1 | 122.3(2) |
| N4—N3—Mn1 | 112.22(15) | C1—N2—N1 | 108.8(2) |
| C12—N3—Mn1 | 141.15(19) | C1—N2—B1 | 128.4(2) |
| C12—N3—N4 | 106.6(2) | N6—C19—C20 | 109.9(3) |
| C3—N1—Mn1 | 140.45(18) | C1—C2—C3 | 105.4(2) |
| C3—N1—N2 | 106.7(2) | C8—C7—C6 | 119.5(3) |
| N2—N1—Mn1 | 112.17(17) | C7—C8—C9 | 120.5(3) |
| N6—N5—Mn1 | 112.87(18) | C6—C5—C4 | 120.7(3) |
| C21—N5—Mn1 | 139.43(19) | N4—B1—N6 | 109.1(2) |
| C21—N5—N6 | 106.7(2) | N2—B1—N6 | 108.8(2) |
| N3—N4—B1 | 122.1(2) | N2—B1—N4 | 111.2(3) |
| C10—N4—N3 | 109.8(2) | C10—C11—C12 | 105.6(3) |
| C10—N4—B1 | 128.1(2) | N2—C1—C2 | 109.4(2) |
| N5—C21—C22 | 121.7(3) | C7—C6—C5 | 120.4(3) |

| | | | |
|-------------|----------|-------------|----------|
| N5—C21—C20 | 110.1(3) | C13—C18—C17 | 121.0(3) |
| C20—C21—C22 | 127.5(3) | C26—C27—C22 | 120.6(3) |
| N1—C3—C4 | 122.8(2) | C23—C24—C25 | 120.3(3) |
| N1—C3—C2 | 109.7(3) | C15—C14—C13 | 120.4(3) |
| C2—C3—C4 | 127.6(3) | N4—C10—C11 | 108.6(3) |
| C8—C9—C4 | 121.3(3) | C26—C25—C24 | 119.1(3) |
| C27—C22—C21 | 120.7(3) | C16—C15—C14 | 120.4(3) |
| C23—C22—C21 | 121.1(3) | C16—C17—C18 | 119.7(3) |
| C23—C22—C27 | 118.0(3) | C25—C26—C27 | 120.9(3) |
| C19—C20—C21 | 104.3(3) | C15—C16—C17 | 120.4(3) |
| N3—C12—C13 | 123.0(2) | C24—C23—C22 | 121.0(3) |

Table A.5. Bond lengths for (Tp^{Ph})MnCl (Å).

| | | | |
|---------|-----------|---------|----------|
| Mn1—Cl1 | 2.2774(8) | C20—C19 | 1.378(4) |
| Mn1—N1 | 2.133(2) | C12—C13 | 1.471(4) |
| Mn1—N3 | 2.147(2) | C12—C11 | 1.404(4) |
| Mn1—N5 | 2.156(3) | C4—C5 | 1.399(4) |
| N6—N5 | 1.374(3) | C13—C18 | 1.390(4) |
| N6—C19 | 1.341(4) | C13—C14 | 1.397(4) |
| N6—B1 | 1.554(4) | N2—B1 | 1.532(4) |
| N3—N4 | 1.370(3) | N2—C1 | 1.347(3) |
| N3—C12 | 1.344(3) | C2—C1 | 1.367(4) |

| | | | |
|---------|----------|---------|----------|
| N1—C3 | 1.345(4) | C7—C8 | 1.372(4) |
| N1—N2 | 1.382(3) | C7—C6 | 1.385(5) |
| N5—C21 | 1.348(4) | C5—C6 | 1.387(4) |
| N4—B1 | 1.549(4) | C11—C10 | 1.370(4) |
| N4—C10 | 1.342(3) | C18—C17 | 1.394(4) |
| C21—C22 | 1.473(4) | C27—C26 | 1.383(4) |
| C21—C20 | 1.405(4) | C24—C25 | 1.390(5) |
| C3—C4 | 1.464(4) | C24—C23 | 1.379(4) |
| C3—C2 | 1.404(4) | C14—C15 | 1.389(5) |
| C9—C4 | 1.399(4) | C25—C26 | 1.364(5) |
| C9—C8 | 1.379(4) | C15—C16 | 1.369(5) |
| C22—C27 | 1.393(4) | C17—C16 | 1.373(5) |
| C22—C23 | 1.388(4) | | |

Table A.6. Single crystal X-ray diffraction experimental details for $(Tp^{Ph})CoCl$.

| | |
|-----------------------------|------------------------------------|
| Chemical formula | $C_{27}H_{22}BClCoN_6$ |
| M_r | 535.69 |
| Crystal system, space group | Trigonal, $P-3$ |
| Temperature (K) | 100 |
| a, c (Å) | 11.4035(6), 11.3047(5) |
| V (Å ³) | 1273.11(15) |
| Z | 2 |
| Radiation type | Mo $K\alpha$ $\lambda = 0.71073$ Å |

| | |
|---|---|
| μ (mm ⁻¹) | 0.81 |
| Crystal size (mm) | 0.17 × 0.17 × 0.13 |
| Diffractometer | Bruker <i>APEX-II</i> CCD diffractometer |
| Absorption correction | Multi-scan <i>SADABS2012/1</i> (Bruker, 2012) |
| T_{\min} , T_{\max} | 0.651, 0.745 |
| No. of measured, independent, and observed [$I > 2\sigma(I)$] reflections | 7135, 1576, 1247 |
| R_{int} | 0.055 |
| $(\sin \theta/\lambda)_{\text{max}}$ (Å ⁻¹) | 0.602 |
| $R[F^2 > 2\sigma(F^2)]$, $wR(F^2)$, S | 0.035, 0.078, 1.05 |
| No. of reflections | 1576 |
| No. of parameters | 109 |
| H-atom treatment | H-atom parameters constrained |
| Largest diff. peak/hole (e Å ⁻³) | 0.24, -0.27 |

Table A.7. Atom Coordinates for $(Tp^{Ph})CoCl$.

| Atom | x | y | z | Occupancy |
|------|---------|---------|---------|-----------|
| Co1 | 0.66667 | 0.33333 | 0.30816 | 1.000 |
| Cl1 | 0.66667 | 0.33333 | 0.11558 | 1.000 |
| N1 | 0.67014 | 0.48585 | 0.40350 | 1.000 |
| N2 | 0.67266 | 0.46324 | 0.52284 | 1.000 |
| C3 | 0.68200 | 0.60880 | 0.39311 | 1.000 |

| | | | | |
|-----|---------|---------|---------|-------|
| C2 | 0.69270 | 0.66490 | 0.50530 | 1.000 |
| H4 | 0.70230 | 0.75070 | 0.52340 | 1.000 |
| C1 | 0.68620 | 0.57060 | 0.58333 | 1.000 |
| H5 | 0.69070 | 0.57950 | 0.66710 | 1.000 |
| C4 | 0.67860 | 0.66880 | 0.27823 | 1.000 |
| C9 | 0.57940 | 0.59390 | 0.19480 | 1.000 |
| H8 | 0.51920 | 0.50010 | 0.20740 | 1.000 |
| C5 | 0.76910 | 0.80450 | 0.25470 | 1.000 |
| H10 | 0.83920 | 0.85630 | 0.30980 | 1.000 |
| B1 | 0.66667 | 0.33333 | 0.56970 | 1.000 |
| H15 | 0.66667 | 0.33333 | 0.65810 | 1.000 |
| C6 | 0.75880 | 0.86520 | 0.15230 | 1.000 |
| H1 | 0.82160 | 0.95780 | 0.13710 | 1.000 |
| C7 | 0.65680 | 0.79050 | 0.07240 | 1.000 |
| H2 | 0.64820 | 0.83250 | 0.00300 | 1.000 |
| C8 | 0.56770 | 0.65590 | 0.09280 | 1.000 |
| H7 | 0.49790 | 0.60480 | 0.03730 | 1.000 |

Table A.8. Bond angles for (Tp^{Ph})CoCl (°)

| | | | |
|---------------------------------------|-----------|----------|----------|
| N1 ⁱⁱ —Co1—Cl1 | 122.07(5) | C4—C3—C6 | 127.0(2) |
| N1—Co1—Cl1 | 122.07(5) | C5—C4—C3 | 105.5(2) |
| N1 ⁱ —Co1—Cl1 | 122.07(5) | N2—C5—C4 | 109.0(2) |
| N1 ⁱ —Co1—N1 ⁱⁱ | 94.42(7) | C8—C6—C3 | 120.9(2) |

| | | | |
|--------------------------|------------|---------------------------------------|------------|
| N1 ⁱ —Co1—N1 | 94.42(7) | C10—C6—C3 | 120.4(2) |
| N1 ⁱⁱ —Co1—N1 | 94.42(7) | C10—C6—C8 | 118.5(2) |
| N2—N1—Co1 | 110.69(13) | C6—C8—C7 | 120.3(2) |
| C3—N1—Co1 | 142.73(15) | C1—C10—C6 | 121.0(3) |
| C3—N1—N2 | 106.27(17) | N2 ⁱ —B15—N2 ⁱⁱ | 108.86(17) |
| N1—N2—B15 | 121.4(2) | N2 ⁱ —B15—N2 | 108.86(17) |
| C5—N2—N1 | 109.44(18) | N2 ⁱⁱ —B15—N2 | 108.86(17) |
| C5—N2—B15 | 129.1(2) | C2—C1—C10 | 119.7(3) |
| N1—C3—C4 | 109.8(2) | C7—C2—C1 | 120.3(3) |
| N1—C3—C6 | 123.2(2) | C2—C7—C8 | 120.1(3) |

Symmetry codes: (i) - $x + y + 1, -x + 1, z$, (ii) - $y + 1, x - y, z$.

Table A.9. Bond lengths for (Tp^{Ph})CoCl (Å)

| | | | |
|----------------------|------------|----------------------|----------|
| Co1—Cl1 | 2.1771(11) | C4—C5 | 1.365(3) |
| Co1—N1 | 2.0296(19) | C6—C8 | 1.391(3) |
| Co1—N1 ⁱ | 2.0296(19) | C6—C10 | 1.390(3) |
| Co1—N1 ⁱⁱ | 2.0296(19) | C8—C7 | 1.393(3) |
| N1—N2 | 1.377(2) | C10—C1 | 1.384(3) |
| N1—C3 | 1.345(3) | B15—N2 ⁱ | 1.542(2) |
| N2—C5 | 1.343(3) | B15—N2 ⁱⁱ | 1.542(2) |
| N2—B15 | 1.542(2) | C1—C2 | 1.379(4) |
| C3—C4 | 1.398(3) | C2—C7 | 1.372(4) |
| C3—C6 | 1.477(3) | | |

Symmetry codes: (i) - $x + y + 1, -x + 1, z$, (ii) - $y + 1, x - y, z$.

Table A.10. Single crystal X-ray diffraction experimental details for α -(Tp^{Ph})CoBr.

| | |
|--|---|
| Chemical formula | C ₂₇ H ₂₂ BBrCoN ₆ |
| M_r | 580.15 |
| Crystal system, space group | Trigonal, <i>P</i> -3 |
| Temperature (K) | 100 |
| a, c (Å) | 11.4026(19), 11.485(2) |
| V (Å ³) | 1293.2(5) |
| Z | 2 |
| Radiation type | Mo K α λ = 0.71073 Å |
| μ (mm ⁻¹) | 2.24 |
| Crystal size (mm) | 0.29 × 0.28 × 0.28 |
| Diffractometer | Bruker APEX-II CCD diffractometer |
| Absorption correction | Multi-scan SADABS2014/3 (Bruker,2014) |
| T_{\min}, T_{\max} | 0.659, 0.747 |
| No. of measured, independent, and observed [$I > 2\sigma(I)$] reflections | 34662, 3470, 3043 |
| R_{int} | 0.040 |
| $(\sin \theta/\lambda)_{\text{max}}$ (Å ⁻¹) | 0.790 |
| $R[F^2 > 2\sigma(F^2)], wR(F^2), S$ | 0.025, 0.064, 1.04 |
| No. of reflections | 3470 |

| | |
|--|-------------------------------|
| No. of parameters | 110 |
| H-atom treatment | H-atom parameters constrained |
| Largest diff. peak/hole ($e \text{ \AA}^{-3}$) | 0.53, -0.32 |

Table A.11. Atom Coordinates for α -(Tp^{Ph})CoBr.

| Atom | x | y | z | Occupancy |
|------|---------|---------|---------|-----------|
| Br1 | 0.33333 | 0.66667 | 0.88837 | 1.000 |
| Co2 | 0.33333 | 0.66667 | 0.68606 | 1.000 |
| B14 | 0.33333 | 0.66667 | 0.42840 | 1.000 |
| N1 | 0.32916 | 0.81607 | 0.59229 | 1.000 |
| C1 | 0.30735 | 0.97443 | 0.49237 | 1.000 |
| N3 | 0.32732 | 0.79139 | 0.47469 | 1.000 |
| C2 | 0.31947 | 0.98957 | 0.71671 | 1.000 |
| C6 | 0.31430 | 0.88501 | 0.41436 | 1.000 |
| C5 | 0.31799 | 0.92766 | 0.60309 | 1.000 |
| C3 | 0.41790 | 1.01194 | 0.80070 | 1.000 |
| C4 | 0.22810 | 1.03520 | 0.73879 | 1.000 |
| C7 | 0.23650 | 1.10440 | 0.84168 | 1.000 |
| C8 | 0.33730 | 1.12950 | 0.92279 | 1.000 |
| C9 | 0.42740 | 1.08333 | 0.90277 | 1.000 |
| H14 | 0.33333 | 0.66667 | 0.33400 | 1.000 |
| H4 | 0.15980 | 1.01900 | 0.68337 | 1.000 |
| H7 | 0.17350 | 1.13420 | 0.85627 | 1.000 |

| | | | | |
|----|---------|---------|---------|-------|
| H8 | 0.34430 | 1.17830 | 0.99186 | 1.000 |
| H9 | 0.49570 | 1.10000 | 0.95839 | 1.000 |
| H3 | 0.47840 | 0.97853 | 0.78827 | 1.000 |
| H1 | 0.29756 | 1.05056 | 0.47486 | 1.000 |
| H6 | 0.31048 | 0.88943 | 0.33207 | 1.000 |

Table A.12. Bond angles for α -(Tp^{Ph})CoBr (°).

| | | | |
|---------------------------------------|------------|--------------------------------------|------------|
| N1 ⁱ —Co1—Br1 | 121.97(2) | C9—C4—C3 | 121.17(9) |
| N1—Co1—Br1 | 121.97(2) | C9—C4—C5 | 118.86(9) |
| N1 ⁱⁱ —Co1—Br1 | 121.97(2) | C5—C4—C3 | 119.82(9) |
| N1 ⁱⁱ —Co1—N1 ⁱ | 94.55(3) | N1—C3—C2 | 109.81(8) |
| N1 ⁱⁱ —Co1—N1 | 94.55(3) | N1—C3—C4 | 123.00(9) |
| N1 ⁱ —Co1—N1 | 94.55(3) | C2—C3—C4 | 127.16(9) |
| N2—N1—Co1 | 110.57(6) | C8—C9—C4 | 120.45(10) |
| C3—N1—Co1 | 142.55(7) | C7—C8—C9 | 120.18(11) |
| C3—N1—N2 | 106.60(8) | C6—C5—C4 | 120.57(10) |
| N1—N2—B1 | 121.57(9) | C6—C7—C8 | 119.91(10) |
| C1—N2—N1 | 109.82(8) | C7—C6—C5 | 120.00(10) |
| C1—N2—B1 | 128.57(10) | N2 ⁱⁱ —B1—N2 ⁱ | 108.73(7) |
| C1—C2—C3 | 105.11(8) | N2 ⁱⁱ —B1—N2 | 108.73(7) |
| N2—C1—C2 | 108.66(9) | N2 ⁱ —B1—N2 | 108.74(7) |

Symmetry codes: (i) - y + 1, x - y + 1, z, (ii) - x + y, - x + 1, z.

Table A.13. Bond lengths for α -(Tp^{Ph})CoBr (Å).

| | | | |
|---------------------|------------|---------------------|------------|
| Br1-Co1 | 2.3229(5) | C4-C9 | 1.4012(14) |
| Co1-N1 ⁱ | 2.0361(9) | C4-C5 | 1.4029(14) |
| N1-N2 | 1.3735(12) | C9-C8 | 1.3961(15) |
| N1-C3 | 1.3513(12) | C8-C7 | 1.3938(17) |
| N2-C1 | 1.3464(12) | C5-C6 | 1.3970(16) |
| N2-B1 | 1.5514(10) | C7-C6 | 1.3926(18) |
| C2-C1 | 1.3859(14) | B1-N2 ⁱⁱ | 1.5514(11) |
| C2-C3 | 1.4055(14) | B1-N2 ⁱ | 1.5514(11) |
| C4-C3 | 1.4779(14) | | |

Symmetry codes: (i) $-y + 1, x - y + 1, z$; (ii) $-x + y, -x + 1, z$.

Table A.14. Single crystal X-ray diffraction experimental details for β -(Tp^{Ph})CoBr.

| | |
|-----------------------------|---|
| Chemical formula | C ₂₇ H ₂₂ BBrCoN ₆ |
| <i>M_r</i> | 580.15 |
| Crystal system, space group | Tetragonal, <i>P4₂/n</i> |
| Temperature (K) | 100 |
| <i>a</i> , <i>c</i> (Å) | 22.4801(17), 9.8562(8) |
| <i>V</i> (Å ³) | 4980.9(9) |
| <i>Z</i> | 8 |
| Radiation type | Mo K α λ = 0.71073 Å |

| | |
|---|--|
| μ (mm ⁻¹) | 2.32 |
| Crystal size (mm) | 0.39 × 0.37 × 0.22 |
| Diffractometer | Bruker APEX-II CCD diffractometer |
| Absorption correction | Multi-scan SADABS2014/3 (Bruker, 2014) |
| T_{\min} , T_{\max} | 0.560, 0.745 |
| No. of measured, independent, and observed [$I > 2\sigma(I)$] reflections | 86883, 5126, 4869 |
| R_{int} | 0.052 |
| $(\sin \theta/\lambda)_{\text{max}}$ (Å ⁻¹) | 0.626 |
| $R[F^2 > 2\sigma(F^2)]$, $wR(F^2)$, S | 0.021, 0.048, 1.03 |
| No. of reflections | 5126 |
| No. of parameters | 326 |
| H-atom treatment | H-atom parameters constrained |
| Largest diff. peak/hole (e Å ⁻³) | 0.32, -0.22 |

Table A. 15. Atom Coordinates for β -(Tp^{Ph})CoBr.

| Atom | x | y | z | Occupancy |
|------|---------|---------|---------|-----------|
| Br1 | 0.80118 | 0.50102 | 0.51086 | 1.000 |
| Co1 | 0.75079 | 0.49748 | 0.30165 | 1.000 |
| N1 | 0.79696 | 0.49428 | 0.12347 | 1.000 |
| N5 | 0.69213 | 0.56176 | 0.24098 | 1.000 |
| C27 | 0.67578 | 0.60408 | 0.52900 | 1.000 |

| | | | | |
|-----|---------|---------|----------|-------|
| H27 | 0.67960 | 0.56220 | 0.51930 | 1.000 |
| C18 | 0.67392 | 0.40400 | 0.55530 | 1.000 |
| H18 | 0.67360 | 0.44550 | 0.53750 | 1.000 |
| N2 | 0.75826 | 0.49347 | 0.01542 | 1.000 |
| N3 | 0.69109 | 0.43225 | 0.25636 | 1.000 |
| C1 | 0.78802 | 0.50158 | -0.10042 | 1.000 |
| H1 | 0.77090 | 0.50270 | -0.18860 | 1.000 |
| B1 | 0.69031 | 0.49234 | 0.03710 | 1.000 |
| H1A | 0.66980 | 0.49050 | -0.05280 | 1.000 |
| N4 | 0.67231 | 0.43792 | 0.12376 | 1.000 |
| C13 | 0.67136 | 0.36380 | 0.44810 | 1.000 |
| N6 | 0.67158 | 0.54952 | 0.11266 | 1.000 |
| C22 | 0.67312 | 0.63989 | 0.41380 | 1.000 |
| C2 | 0.84745 | 0.50811 | -0.07100 | 1.000 |
| H2 | 0.87890 | 0.51470 | -0.13360 | 1.000 |
| C10 | 0.63532 | 0.39274 | 0.09400 | 1.000 |
| H10 | 0.61630 | 0.38660 | 0.00900 | 1.000 |
| C19 | 0.63664 | 0.59471 | 0.07020 | 1.000 |
| H19 | 0.61710 | 0.59680 | -0.01520 | 1.000 |
| C6 | 1.00651 | 0.54412 | 0.17920 | 1.000 |
| H6 | 1.03770 | 0.56950 | 0.14930 | 1.000 |
| C7 | 1.01391 | 0.50952 | 0.29500 | 1.000 |
| H7 | 1.05020 | 0.51100 | 0.34420 | 1.000 |

| | | | | |
|-----|---------|---------|---------|-------|
| C21 | 0.66832 | 0.61443 | 0.27690 | 1.000 |
| C4 | 0.90687 | 0.50546 | 0.15060 | 1.000 |
| C16 | 0.67727 | 0.32325 | 0.71580 | 1.000 |
| H16 | 0.67880 | 0.30950 | 0.80680 | 1.000 |
| C17 | 0.67700 | 0.38369 | 0.68860 | 1.000 |
| H17 | 0.67890 | 0.41140 | 0.76120 | 1.000 |
| C12 | 0.66483 | 0.38306 | 0.30630 | 1.000 |
| C20 | 0.63386 | 0.63693 | 0.16990 | 1.000 |
| H20 | 0.61300 | 0.67370 | 0.16730 | 1.000 |
| C11 | 0.62952 | 0.35695 | 0.20570 | 1.000 |
| H11 | 0.60640 | 0.32170 | 0.21320 | 1.000 |
| C5 | 0.95354 | 0.54152 | 0.10740 | 1.000 |
| H5 | 0.94900 | 0.56470 | 0.02750 | 1.000 |
| C26 | 0.67288 | 0.62866 | 0.65650 | 1.000 |
| H26 | 0.67460 | 0.60350 | 0.73390 | 1.000 |
| C23 | 0.66891 | 0.70198 | 0.43160 | 1.000 |
| H23 | 0.66800 | 0.72750 | 0.35480 | 1.000 |
| C3 | 0.85196 | 0.50298 | 0.06980 | 1.000 |
| C14 | 0.67208 | 0.30304 | 0.47740 | 1.000 |
| H14 | 0.67040 | 0.27500 | 0.40540 | 1.000 |
| C8 | 0.96810 | 0.47301 | 0.33830 | 1.000 |
| H8 | 0.97310 | 0.44930 | 0.41720 | 1.000 |
| C9 | 0.91477 | 0.47082 | 0.26700 | 1.000 |

| | | | | |
|-----|---------|---------|---------|-------|
| H9 | 0.88360 | 0.44570 | 0.29750 | 1.000 |
| C25 | 0.66753 | 0.68955 | 0.67360 | 1.000 |
| H25 | 0.66490 | 0.70630 | 0.76190 | 1.000 |
| C15 | 0.67526 | 0.28327 | 0.61020 | 1.000 |
| H15 | 0.67610 | 0.24180 | 0.62850 | 1.000 |
| C24 | 0.66613 | 0.72555 | 0.56020 | 1.000 |
| H24 | 0.66320 | 0.76740 | 0.57110 | 1.000 |

Table A. 16. Bond angles for β -(Tp^{Ph})CoBr (°).

| | | | |
|-------------|------------|-------------|------------|
| N1—Co1—Br1 | 120.68(5) | C27—C22—C21 | 121.8(2) |
| N1—Co1—N5 | 95.81(7) | C27—C22—C23 | 118.2(2) |
| N5—Co1—Br1 | 122.85(5) | C23—C22—C21 | 119.7(2) |
| N3—Co1—Br1 | 122.23(5) | C1—C2—C3 | 105.73(18) |
| N3—Co1—N1 | 96.95(7) | N4—C10—C11 | 109.07(19) |
| N3—Co1—N5 | 91.13(6) | N6—C19—C20 | 109.0(2) |
| N2—N1—Co1 | 110.19(11) | C5—C6—C7 | 119.9(2) |
| C3—N1—Co1 | 142.40(13) | C8—C7—C6 | 119.7(2) |
| C3—N1—N2 | 106.03(15) | N5—C21—C22 | 123.7(2) |
| N6—N5—Co1 | 110.13(13) | N5—C21—C20 | 109.8(2) |
| C21—N5—Co1 | 143.18(15) | C20—C21—C22 | 126.2(2) |
| C21—N5—N6 | 106.51(17) | C5—C4—C3 | 119.29(19) |
| C26—C27—C22 | 120.7(2) | C5—C4—C9 | 118.65(18) |
| C13—C18—C17 | 120.4(2) | C9—C4—C3 | 122.02(19) |

| | | | |
|-------------|------------|-------------|------------|
| N1—N2—B1 | 121.29(15) | C15—C16—C17 | 119.6(2) |
| C1—N2—N1 | 110.08(14) | C16—C17—C18 | 120.3(2) |
| C1—N2—B1 | 128.06(17) | N3—C12—C13 | 123.08(19) |
| N4—N3—Co1 | 110.05(12) | N3—C12—C11 | 109.48(19) |
| C12—N3—Co1 | 143.08(15) | C11—C12—C13 | 127.4(2) |
| C12—N3—N4 | 106.76(17) | C19—C20—C21 | 105.3(2) |
| N2—C1—C2 | 108.73(18) | C10—C11—C12 | 105.64(19) |
| N2—B1—N4 | 110.41(17) | C6—C5—C4 | 121.0(2) |
| N2—B1—N6 | 108.85(17) | C27—C26—C25 | 120.9(2) |
| N6—B1—N4 | 108.71(16) | C24—C23—C22 | 120.0(2) |
| N3—N4—B1 | 121.10(16) | N1—C3—C2 | 109.43(18) |
| C10—N4—N3 | 109.05(17) | N1—C3—C4 | 123.97(18) |
| C10—N4—B1 | 129.69(18) | C2—C3—C4 | 126.60(18) |
| C18—C13—C12 | 122.3(2) | C15—C14—C13 | 120.7(2) |
| C18—C13—C14 | 118.5(2) | C7—C8—C9 | 120.4(2) |
| C14—C13—C12 | 119.1(2) | C8—C9—C4 | 120.32(19) |
| N5—N6—B1 | 121.26(16) | C24—C25—C26 | 118.9(2) |
| C19—N6—N5 | 109.27(18) | C16—C15—C14 | 120.5(2) |
| C19—N6—B1 | 129.44(18) | C23—C24—C25 | 121.3(2) |

Table A. 17. Bond lengths for β -(Tp^{Ph})CoBr (Å).

| | | | |
|---------|------------|---------|----------|
| Br1—Co1 | 2.3539(3) | N6—C19 | 1.351(3) |
| Co1—N1 | 2.0413(16) | C22—C21 | 1.470(3) |

| | | | |
|---------|------------|---------|----------|
| Co1—N5 | 2.0457(18) | C22—C23 | 1.410(3) |
| Co1—N3 | 2.0373(17) | C2—C3 | 1.397(3) |
| N1—N2 | 1.375(2) | C10—C11 | 1.370(3) |
| N1—C3 | 1.359(2) | C19—C20 | 1.367(3) |
| N5—N6 | 1.374(2) | C6—C7 | 1.391(3) |
| N5—C21 | 1.347(3) | C6—C5 | 1.386(3) |
| C27—C22 | 1.393(3) | C7—C8 | 1.384(3) |
| C27—C26 | 1.375(3) | C21—C20 | 1.403(3) |
| C18—C13 | 1.392(3) | C4—C5 | 1.393(3) |
| C18—C17 | 1.392(3) | C4—C3 | 1.470(3) |
| N2—C1 | 1.336(2) | C4—C9 | 1.398(3) |
| N2—B1 | 1.543(3) | C16—C17 | 1.385(3) |
| N3—N4 | 1.379(2) | C16—C15 | 1.376(4) |
| N3—C12 | 1.347(3) | C12—C11 | 1.400(3) |
| C1—C2 | 1.375(3) | C26—C25 | 1.384(4) |
| B1—N4 | 1.546(3) | C23—C24 | 1.375(4) |
| B1—N6 | 1.544(3) | C14—C15 | 1.384(3) |
| N4—C10 | 1.345(3) | C8—C9 | 1.391(3) |
| C13—C12 | 1.470(3) | C25—C24 | 1.381(4) |
| C13—C14 | 1.396(3) | | |

Table A.18. Single crystal X-ray diffraction experimental details for (Tp^{Ph})NiCl.

Chemical formula

C₂₇H₂₂BCIN₆Ni

| | |
|--|------------------------------------|
| M_r | 535.48 |
| Crystal system, space group | Trigonal, $P-3$ |
| Temperature (K) | 143 |
| a, c (Å) | 11.3577(2), 11.2575(3) |
| V (Å ³) | 1257.63(5) |
| Z | 2 |
| Radiation type | Mo $K\alpha$ $\lambda = 0.71073$ Å |
| μ (mm ⁻¹) | 0.91 |
| Crystal size (mm) | 0.25 × 0.25 × 0.15 |
| Diffractometer | Bruker APEX-II CCD diffractometer |
| Absorption correction | Multi-scan SADABS v2008/1 |
| T_{\min}, T_{\max} | 0.805, 0.876 |
| No. of measured, independent, and observed [$I > 2\sigma(I)$] reflections | 41082, 3264, 2867 |
| R_{int} | 0.047 |
| $(\sin \theta/\lambda)_{\text{max}}$ (Å ⁻¹) | 0.785 |
| $R[F^2 > 2\sigma(F^2)], wR(F^2), S$ | 0.029, 0.079, 1.02 |
| No. of reflections | 3264 |
| No. of parameters | 109 |
| H-atom treatment | H-atom parameters constrained |
| Largest diff. peak/hole (e Å ⁻³) | 0.44, -0.52 |

Table A.19. Atom Coordinates for $(Tp^{Ph})NiCl$.

| Atom | x | y | z | Occupancy |
|------|---------|---------|---------|-----------|
| Ni1 | 0.66667 | 0.33333 | 0.69040 | 1.000 |
| Cl1 | 0.66667 | 0.33333 | 0.88241 | 1.000 |
| B1 | 0.66667 | 0.33333 | 0.42327 | 1.000 |
| H1 | 0.66667 | 0.33333 | 0.33440 | 1.000 |
| N2 | 0.78944 | 0.32552 | 0.47214 | 1.000 |
| N1 | 0.81154 | 0.32886 | 0.59180 | 1.000 |
| C3 | 0.92285 | 0.31680 | 0.60651 | 1.000 |
| C2 | 0.97195 | 0.30538 | 0.49508 | 1.000 |
| H2A | 1.04880 | 0.29550 | 0.47940 | 1.000 |
| C1 | 0.88459 | 0.31158 | 0.41314 | 1.000 |
| H3A | 0.89080 | 0.30680 | 0.32930 | 1.000 |
| C4 | 0.98478 | 0.32085 | 0.72280 | 1.000 |
| C5 | 1.02839 | 0.22773 | 0.74721 | 1.000 |
| H5A | 1.00860 | 0.15630 | 0.69270 | 1.000 |
| C6 | 1.10054 | 0.23900 | 0.85073 | 1.000 |
| H6A | 1.12860 | 0.17470 | 0.86710 | 1.000 |
| C7 | 1.13144 | 0.34412 | 0.93007 | 1.000 |
| H7A | 1.18290 | 0.35330 | 0.99950 | 1.000 |
| C8 | 1.08692 | 0.43578 | 0.90771 | 1.000 |

| | | | | |
|-----|---------|---------|---------|-------|
| H8A | 1.10730 | 0.50720 | 0.96240 | 1.000 |
| C9 | 1.01239 | 0.42334 | 0.80540 | 1.000 |
| H9A | 0.98020 | 0.48490 | 0.79170 | 1.000 |

Table A.20. Bond angles in $(Tp^{Ph})NiCl$ ($^{\circ}$).

| | | | |
|---------------------------------------|-----------|-----------|------------|
| N1 ⁱ —Ni1—N1 | 92.34(3) | N2—N1—Ni1 | 113.85(6) |
| N1 ⁱ —Ni1—N1 ⁱⁱ | 92.34(3) | N1—C1—C2 | 109.60(8) |
| N1—Ni1—N1 ⁱⁱ | 92.34(3) | N1—C1—C4 | 124.21(8) |
| N1 ⁱ —Ni1—Cl1 | 123.59(2) | C2—C1—C4 | 126.15(9) |
| N1—Ni1—Cl1 | 123.59(2) | C3—C2—C1 | 105.25(8) |
| N1 ⁱⁱ —Ni1—Cl1 | 123.59(2) | N2—C3—C2 | 108.44(8) |
| N2—B1—N2 ⁱ | 108.00(7) | C9—C4—C5 | 118.78(9) |
| N2—B1—N2 ⁱⁱ | 108.00(7) | C9—C4—C1 | 121.41(9) |
| N2 ⁱ —B1—N2 ⁱⁱ | 108.00(7) | C5—C4—C1 | 119.55(9) |
| C3—N2—N1 | 110.06(8) | C6—C5—C4 | 120.55(11) |
| C3—N1—B1 | 129.35(9) | C7—C6—C5 | 120.08(11) |
| N1—N2—B1 | 120.57(9) | C6—C7—C8 | 119.85(11) |
| C1—N1—N2 | 106.66(8) | C7—C8—C9 | 120.26(11) |
| C1—N1—Ni1 | 139.21(7) | C8—C9—C4 | 120.41(10) |

Symmetry code(s): (i) $-x+y+1, -x+1, z$, (ii) $-y+1, x-y, z$.

Table A.21. Bond lengths in $(Tp^{Ph})NiCl$ (\AA).

| | | | |
|---------------------|-----------|-------|------------|
| Ni1—N1 ⁱ | 2.0064(8) | C1—C2 | 1.4049(14) |
|---------------------|-----------|-------|------------|

| | | | |
|----------------------|------------|-------|------------|
| Ni1—N1 | 2.0064(8) | C1—C4 | 1.4759(13) |
| Ni1—N1 ⁱⁱ | 2.0064(8) | C2—C3 | 1.3821(14) |
| Ni1—Cl1 | 2.1615(5) | C4—C9 | 1.3974(14) |
| B1—N2 | 1.5423(10) | C4—C5 | 1.4012(14) |
| B1—N2 ⁱ | 1.5423(10) | C5—C6 | 1.3933(16) |
| B1—N2 ⁱⁱ | 1.5423(10) | C6—C7 | 1.3882(19) |
| N2—C3 | 1.3436(12) | C7—C8 | 1.3889(17) |
| N2—N1 | 1.3673(11) | C8—C9 | 1.3941(15) |
| N1—C1 | 1.3482(12) | | |

Symmetry codes: (i) $-x + y + 1, -x + 1, z$, (ii) $-y + 1, x - y, z$.

Table A.22. Single crystal X-ray diffraction experimental details for (Tp^{Ph})Ni(phpy)Cl.

| | |
|-----------------------------|--|
| Chemical formula | C ₃₆ H ₃₀ BCIN ₈ Ni |
| <i>Mr</i> | 679.66 |
| Crystal system, space group | Triclinic, <i>P</i> -1 |
| Temperature (K) | 100 |
| <i>a, b, c</i> (Å) | 9.0933(4), 12.2962(5), 14.3846(6) |
| α, β, γ (°) | 93.5735(17), 95.4836(14), 93.6953(14) |
| <i>V</i> (Å ³) | 1593.89(12) |
| <i>Z</i> | 2 |
| Radiation type | Mo K α λ = 0.71073 Å |

| | |
|---|---|
| μ (mm ⁻¹) | 0.73 |
| Crystal size (mm) | 0.31 × 0.24 × 0.21 |
| Diffractometer | Bruker Apex II |
| Absorption correction | none |
| No. of measured, independent, and observed | 34257, 13056, 9255 |
| $[I > 2\sigma(I)]$ reflections | |
| R_{int} | 0.051 |
| $(\sin \theta/\lambda)_{\text{max}}$ (Å ⁻¹) | 0.795 |
| $R[F^2 > 2\sigma(F^2)]$, $wR(F^2)$, S | 0.039, 0.096, 0.92 |
| No. of reflections | 13056 |
| No. of parameters | 431 |
| H-atom treatment | H atoms treated by a mixture of independent and constrained refinement |
| Largest diff. peak/hole (e Å ⁻³) | 0.55, -0.81 |

Table A.23. Atom Coordinates for (TpPh)Ni(phpy)Cl.

| Atom | x | y | z | Occupancy |
|------|---------|---------|---------|-----------|
| Ni1 | 0.40952 | 0.68098 | 0.73941 | 1.000 |
| Cl2 | 0.15861 | 0.65710 | 0.68940 | 1.000 |
| N2 | 0.59809 | 0.53492 | 0.64733 | 1.000 |

| | | | | |
|-----|----------|---------|---------|-------|
| N1 | 0.45593 | 0.53539 | 0.67085 | 1.000 |
| N5 | 0.37014 | 0.81990 | 0.81954 | 1.000 |
| N3 | 0.53273 | 0.77047 | 0.65609 | 1.000 |
| N5 | 0.59227 | 0.65592 | 0.83074 | 1.000 |
| N8 | 0.23273 | 0.85483 | 0.81627 | 1.000 |
| N9 | 0.71918 | 0.64268 | 0.78995 | 1.000 |
| N4 | 0.66864 | 0.73499 | 0.64315 | 1.000 |
| C11 | 0.53033 | 0.87022 | 0.62247 | 1.000 |
| C12 | 0.23111 | 0.40662 | 0.64495 | 1.000 |
| C13 | -0.03825 | 0.96618 | 0.81126 | 1.000 |
| C14 | 0.38437 | 0.44256 | 0.63074 | 1.000 |
| C15 | 0.22830 | 0.95301 | 0.86234 | 1.000 |
| C16 | 0.08850 | 1.00496 | 0.86770 | 1.000 |
| C17 | 0.39998 | 0.93511 | 0.62273 | 1.000 |
| C18 | 0.26945 | 0.61063 | 1.02925 | 1.000 |
| C19 | 0.48058 | 0.38347 | 0.58019 | 1.000 |
| C20 | 0.74899 | 0.81027 | 0.60268 | 1.000 |
| C21 | 0.37212 | 0.98299 | 0.89886 | 1.000 |
| C22 | 0.78158 | 0.65393 | 0.94203 | 1.000 |
| C23 | 0.66547 | 0.89768 | 0.58828 | 1.000 |
| C24 | 0.18978 | 0.39273 | 0.73414 | 1.000 |
| C25 | 0.37090 | 0.61907 | 0.96397 | 1.000 |
| C26 | 0.62818 | 0.66084 | 0.92362 | 1.000 |

| | | | | |
|-----|----------|---------|---------|-------|
| C27 | 0.12764 | 0.37901 | 0.56828 | 1.000 |
| C28 | 0.26151 | 0.89055 | 0.58620 | 1.000 |
| C29 | -0.17222 | 1.01213 | 0.81958 | 1.000 |
| C30 | 0.83450 | 0.64192 | 0.85598 | 1.000 |
| C31 | 0.04969 | 0.34922 | 0.74645 | 1.000 |
| C32 | 0.31220 | 0.64058 | 1.12261 | 1.000 |
| C33 | 0.07997 | 1.09283 | 0.93241 | 1.000 |
| C34 | 0.51603 | 0.66087 | 0.99049 | 1.000 |
| C35 | -0.05200 | 0.32082 | 0.66953 | 1.000 |
| C36 | 0.45470 | 0.68377 | 1.14972 | 1.000 |
| C37 | 0.45569 | 0.89775 | 0.87029 | 1.000 |
| B38 | 0.71529 | 0.62729 | 0.68248 | 1.000 |
| C39 | 0.55544 | 0.69469 | 1.08438 | 1.000 |
| C40 | -0.01330 | 0.33709 | 0.58067 | 1.000 |
| C41 | -0.05332 | 1.13923 | 0.94043 | 1.000 |
| C42 | 0.61341 | 0.44492 | 0.59262 | 1.000 |
| C43 | 0.41590 | 1.04396 | 0.65749 | 1.000 |
| C44 | 0.15580 | 1.05976 | 0.62257 | 1.000 |
| C45 | -0.17958 | 1.09848 | 0.88503 | 1.000 |
| C46 | 0.29270 | 1.10498 | 0.65762 | 1.000 |
| C47 | 0.13984 | 0.95299 | 0.58620 | 1.000 |
| H38 | 0.82280 | 0.61040 | 0.66130 | 1.000 |
| H27 | 0.15397 | 0.38903 | 0.50689 | 1.000 |

| | | | | |
|-----|----------|---------|---------|-------|
| H40 | -0.08376 | 0.31942 | 0.52789 | 1.000 |
| H35 | -0.14809 | 0.29024 | 0.67785 | 1.000 |
| H31 | 0.02311 | 0.33878 | 0.80772 | 1.000 |
| H24 | 0.25854 | 0.41335 | 0.78722 | 1.000 |
| H43 | 0.51090 | 1.07637 | 0.68106 | 1.000 |
| H46 | 0.30360 | 1.17886 | 0.68229 | 1.000 |
| H44 | 0.07190 | 1.10192 | 0.62333 | 1.000 |
| H47 | 0.04498 | 0.92189 | 0.56095 | 1.000 |
| H28 | 0.24964 | 0.81688 | 0.56101 | 1.000 |
| H39 | 0.65285 | 0.72564 | 1.10362 | 1.000 |
| H36 | 0.48370 | 0.70609 | 1.21362 | 1.000 |
| H32 | 0.24370 | 0.63147 | 1.16790 | 1.000 |
| H18 | 0.17008 | 0.58418 | 1.00992 | 1.000 |
| H25 | 0.34140 | 0.59611 | 0.90026 | 1.000 |
| H33 | 0.16606 | 1.12106 | 0.97123 | 1.000 |
| H41 | -0.05796 | 1.19956 | 0.98439 | 1.000 |
| H45 | -0.27122 | 1.12962 | 0.89181 | 1.000 |
| H29 | -0.25839 | 0.98446 | 0.78057 | 1.000 |
| H13 | -0.03343 | 0.90712 | 0.76608 | 1.000 |
| H19 | 0.45869 | 0.31549 | 0.54489 | 1.000 |
| H20 | 0.84722 | 0.80415 | 0.58666 | 1.000 |
| H21 | 0.40702 | 1.04797 | 0.93572 | 1.000 |
| H22 | 0.83719 | 0.65694 | 1.00162 | 1.000 |

| | | | | |
|-----|---------|---------|---------|-------|
| H23 | 0.69361 | 0.96318 | 0.56082 | 1.000 |
| H30 | 0.93482 | 0.63439 | 0.84496 | 1.000 |
| H37 | 0.55951 | 0.89579 | 0.88515 | 1.000 |
| H42 | 0.70160 | 0.42663 | 0.56671 | 1.000 |
| H8 | 0.16570 | 0.81200 | 0.78430 | 1.000 |

Table A.24. Bond angles for $(Tp^{Ph})Ni(phpy)Cl$ ($^{\circ}$).

| | | | |
|------------|------------|-------------|------------|
| C11—Ni1—N1 | 93.18(3) | C21—C15—C16 | 132.98(12) |
| C11—Ni1—N7 | 89.34(3) | C15—C16—C13 | 121.20(12) |
| C11—Ni1—N3 | 114.87(3) | C33—C16—C13 | 118.66(13) |
| C11—Ni1—N5 | 152.26(3) | C33—C16—C15 | 120.11(12) |
| N7—Ni1—N1 | 174.55(4) | C28—C17—C11 | 120.88(13) |
| N3—Ni1—N1 | 91.73(4) | C43—C17—C11 | 120.00(13) |
| N3—Ni1—N7 | 91.59(4) | C43—C17—C28 | 119.09(14) |
| N5—Ni1—N1 | 84.81(4) | C32—C18—C25 | 120.16(15) |
| N5—Ni1—N7 | 90.71(4) | C42—C19—C14 | 105.17(12) |
| N5—Ni1—N3 | 92.86(4) | C23—C20—N4 | 108.39(12) |
| B38—N2—N1 | 121.71(10) | C37—C21—C15 | 105.61(12) |
| C42—N2—N1 | 109.88(11) | C30—C22—C26 | 105.66(12) |
| C42—N2—B38 | 128.41(11) | C20—C23—C11 | 105.50(12) |
| N2—N1—Ni1 | 113.59(8) | C31—C24—C12 | 120.65(13) |
| C14—N1—Ni1 | 139.40(9) | C34—C25—C18 | 120.78(14) |
| C14—N1—N2 | 106.37(10) | C22—C26—N5 | 109.24(12) |

| | | | |
|-------------|------------|-------------|------------|
| N8—N7—Ni1 | 119.82(8) | C34—C26—N5 | 122.33(12) |
| C37—N7—Ni1 | 134.51(9) | C34—C26—C22 | 128.09(12) |
| C37—N7—N8 | 105.12(11) | C40—C27—C12 | 120.49(14) |
| N4—N3—Ni1 | 115.87(8) | C47—C28—C17 | 120.24(16) |
| C11—N3—Ni1 | 136.44(9) | C45—C29—C13 | 119.62(14) |
| C11—N3—N4 | 106.22(11) | C22—C30—N6 | 107.98(12) |
| N6—N5—Ni1 | 115.00(8) | C35—C31—C24 | 120.01(15) |
| C26—N5—Ni1 | 137.52(9) | C36—C32—C18 | 119.70(16) |
| C26—N5—N6 | 106.96(10) | C41—C33—C16 | 120.32(14) |
| C15—N8—N7 | 112.79(11) | C26—C34—C25 | 121.21(12) |
| C30—N6—N5 | 110.13(11) | C39—C34—C25 | 118.19(14) |
| B38—N6—N5 | 120.30(10) | C39—C34—C26 | 120.39(13) |
| B38—N6—C30 | 129.53(12) | C40—C35—C31 | 119.78(15) |
| C20—N4—N3 | 110.25(11) | C39—C36—C32 | 120.27(15) |
| B38—N4—N3 | 120.18(11) | C21—C37—N7 | 110.72(12) |
| B38—N4—C20 | 129.26(12) | N6—B38—N2 | 108.34(11) |
| C17—C11—N3 | 122.57(12) | N4—B38—N2 | 109.34(10) |
| C23—C11—N3 | 109.64(12) | N4—B38—N6 | 106.96(11) |
| C23—C11—C17 | 127.79(12) | C36—C39—C34 | 120.82(15) |
| C24—C12—C14 | 120.97(12) | C35—C40—C27 | 120.18(14) |
| C27—C12—C14 | 120.05(12) | C45—C41—C33 | 120.48(14) |
| C27—C12—C24 | 118.84(13) | C19—C42—N2 | 108.74(12) |
| C29—C13—C16 | 121.12(14) | C46—C43—C17 | 119.86(16) |

| | | | |
|-------------|------------|-------------|------------|
| C12—C14—N1 | 123.99(11) | C47—C44—C46 | 119.80(16) |
| C19—C14—N1 | 109.83(12) | C41—C45—C29 | 119.78(14) |
| C19—C14—C12 | 126.03(12) | C44—C46—C43 | 120.62(17) |
| C16—C15—N8 | 121.25(12) | C44—C47—C28 | 120.35(17) |
| C21—C15—N8 | 105.75(11) | | |

Table A.25. Bond lengths for $(Tp^{Ph})Ni(phpy)Cl$ (Å).

| | | | |
|---------|------------|---------|------------|
| Ni1—Cl1 | 2.3201(4) | C15—C16 | 1.4653(18) |
| Ni1—N1 | 2.0767(11) | C15—C16 | 1.4653(18) |
| Ni1—N7 | 2.0705(11) | C15—C21 | 1.3801(19) |
| Ni1—N3 | 2.0407(11) | C16—C33 | 1.3925(19) |
| Ni1—N5 | 2.0693(10) | C17—C28 | 1.382(2) |
| N2—N1 | 1.3674(15) | C17—C43 | 1.393(2) |
| N2—B38 | 1.5332(19) | C18—C25 | 1.382(2) |
| N2—C42 | 1.3401(17) | C18—C32 | 1.382(2) |
| N1—C14 | 1.3452(16) | C19—C42 | 1.373(2) |
| N7—N8 | 1.3447(15) | C20—C23 | 1.370(2) |
| N7—C37 | 1.3278(16) | C21—C37 | 1.3977(19) |
| N3—N4 | 1.3623(15) | C22—C26 | 1.4038(19) |
| N3—C11 | 1.3470(16) | C22—C30 | 1.373(2) |
| N5—N6 | 1.3580(15) | C24—C31 | 1.381(2) |
| N5—C26 | 1.3413(16) | C25—C34 | 1.394(2) |
| N8—C15 | 1.3454(17) | C26—C34 | 1.467(2) |

| | | | |
|---------|------------|---------|------------|
| N6—C30 | 1.3468(16) | C27—C40 | 1.382(2) |
| N6—B38 | 1.5425(19) | C28—C47 | 1.387(2) |
| N4—C20 | 1.3382(17) | C29—C45 | 1.384(2) |
| N4—B38 | 1.5407(18) | C31—C35 | 1.384(2) |
| C11—C17 | 1.4709(19) | C32—C36 | 1.379(2) |
| C11—C23 | 1.396(2) | C33—C41 | 1.384(2) |
| C12—C14 | 1.4716(18) | C34—C39 | 1.3942(19) |
| C12—C24 | 1.3884(19) | C35—C40 | 1.381(2) |
| C12—C27 | 1.3895(18) | C36—C39 | 1.380(2) |
| C13—C16 | 1.3845(19) | C41—C45 | 1.380(2) |
| C13—C29 | 1.388(2) | C43—C46 | 1.388(2) |
| C14—C19 | 1.3998(18) | C44—C46 | 1.367(3) |

Table A.26. Single crystal X-ray diffraction experimental details for $(Tp^{Ph})NiBr$.

| | |
|-----------------------------|------------------------------------|
| Chemical formula | $C_{27}H_{22}BBrN_6Ni$ |
| M_r | 579.93 |
| Crystal system, space group | Trigonal, $P-3$ |
| Temperature (K) | 100 |
| a, c (Å) | 11.3592(8), 11.3914(9) |
| V (Å ³) | 1272.9(2) |
| Z | 2 |
| Radiation type | Mo $K\alpha$ $\lambda = 0.71073$ Å |
| μ (mm ⁻¹) | 2.36 |

| | |
|--|---|
| Crystal size (mm) | 0.29 × 0.26 × 0.19 |
| Diffractometer | Bruker P4 |
| Absorption correction | Multi-scan <i>SADABS2012/1</i> (Bruker,2012) |
| T_{\min} , T_{\max} | 0.629, 0.748 |
| No. of measured, independent, and observed [$I > 2\sigma(I)$] reflections | 22639, 5625, 4420 |
| R_{int} | 0.024 |
| $(\sin \theta/\lambda)_{\text{max}}$ (\AA^{-1}) | 0.949 |
| $R[F^2 > 2s(F^2)]$, $wR(F^2)$, S | 0.027, 0.071, 1.04 |
| No. of reflections | 5625 |
| No. of parameters | 109 |
| H-atom treatment | H-atom parameters constrained |
| Largest diff. peak/hole ($e \text{\AA}^{-3}$) | 0.60, -0.76 |

Table A.27. Atom Coordinates for $(\text{Tp}^{\text{Ph}})\text{NiBr}$.

| Atom | x | y | z | Occupancy |
|------|---------|---------|----------|-----------|
| Br1 | 0.33333 | 0.66667 | 0.38592 | 1.000 |
| Ni1 | 0.33333 | 0.66667 | 0.18465 | 1.000 |
| N2 | 0.46419 | 0.67506 | -0.03054 | 1.000 |
| N1 | 0.48294 | 0.67162 | 0.08758 | 1.000 |
| C3 | 0.60627 | 0.68400 | 0.10223 | 1.000 |
| C4 | 0.66421 | 0.68094 | 0.21736 | 1.000 |

| | | | | |
|-----|---------|---------|----------|-------|
| C1 | 0.57327 | 0.68937 | -0.08878 | 1.000 |
| H1 | 0.58420 | 0.69421 | -0.17164 | 1.000 |
| C2 | 0.66712 | 0.69588 | -0.00786 | 1.000 |
| H2 | 0.75395 | 0.70616 | -0.02335 | 1.000 |
| C9 | 0.58895 | 0.57946 | 0.29969 | 1.000 |
| H9 | 0.49538 | 0.51734 | 0.28584 | 1.000 |
| C5 | 0.80066 | 0.77458 | 0.24157 | 1.000 |
| H5 | 0.85245 | 0.84522 | 0.18714 | 1.000 |
| B1 | 0.33333 | 0.66667 | -0.07879 | 1.000 |
| H1a | 0.33333 | 0.66667 | -0.16667 | 1.000 |
| C6 | 0.86122 | 0.76499 | 0.34503 | 1.000 |
| H6 | 0.95361 | 0.82944 | 0.36108 | 1.000 |
| C7 | 0.78636 | 0.66117 | 0.42453 | 1.000 |
| H7 | 0.82804 | 0.65331 | 0.49410 | 1.000 |
| C8 | 0.65035 | 0.56886 | 0.40201 | 1.000 |
| H8 | 0.59901 | 0.49822 | 0.45658 | 1.000 |

Table A.28. Bond angles for $(Tp^{Ph})NiBr$ ($^{\circ}$).

| | | | |
|---------------------------------------|-------------|----------|-----------|
| N1 ⁱ —Ni1—Br1 | 123.479(19) | C2—C3—C4 | 126.27(7) |
| N1—Ni1—Br1 | 123.479(19) | C9—C4—C3 | 121.31(7) |
| N1 ⁱⁱ —Ni1—Br1 | 123.479(19) | C5—C4—C3 | 119.64(7) |
| N1 ⁱⁱ —Ni1—N1 ⁱ | 92.50(3) | C5—C4—C9 | 118.85(7) |
| N1—Ni1—N1 ⁱ | 92.50(3) | C2—C1—N2 | 108.50(7) |

| | | | |
|--------------------------|-----------|--------------------------------------|-----------|
| N1 ⁱⁱ —Ni1—N1 | 92.50(3) | C1—C2—C3 | 105.11(7) |
| C1—N2—N1 | 110.04(6) | C8—C9—C4 | 120.40(8) |
| B1—N2—N1 | 120.57(7) | C6—C5—C4 | 120.56(8) |
| B1—N2—C1 | 129.37(7) | N2 ⁱⁱ —B1—N2 | 108.03(6) |
| N2—N1—Ni1 ⁱⁱ | 113.71(5) | N2 ⁱ —B1—N2 | 108.03(6) |
| C3—N1—Ni1 ⁱⁱ | 139.26(5) | N2 ⁱ —B1—N2 ⁱⁱ | 108.03(6) |
| C3—N1—N2 | 106.75(6) | C7—C6—C5 | 120.01(8) |
| C4—C3—N1 | 124.11(7) | C8—C7—C6 | 119.84(8) |
| C2—C3—N1 | 109.60(7) | C7—C8—C9 | 120.30(8) |

Symmetry codes: (i) $-x + y, -x + 1, z$, (ii) $-y + 1, x - y + 1, z$.

Table A.29. Bond lengths for $(Tp^{Ph})NiBr$ (Å).

| | | | |
|----------------------|------------|-------|------------|
| Br1—Ni1 | 2.2927(3) | C3—C2 | 1.4055(11) |
| Ni1—N1 ⁱ | 2.0046(7) | C4—C9 | 1.3978(11) |
| Ni1—N1 ⁱⁱ | 2.0046(7) | C4—C5 | 1.4004(11) |
| Ni1—N1 | 2.0046(7) | C1—C2 | 1.3830(11) |
| N2—N1 | 1.3659(9) | C9—C8 | 1.3941(12) |
| N2—C1 | 1.3419(10) | C5—C6 | 1.3960(12) |
| N2—B1 | 1.5424(8) | C6—C7 | 1.3897(14) |
| N1—C3 | 1.3466(10) | C7—C8 | 1.3901(13) |
| C3—C4 | 1.4755(11) | | |

Symmetry codes: (i) $-x + y, -x + 1, z$, (ii) $-y + 1, x - y + 1, z$.

Table A.30. Single crystal X-ray diffraction experimental details for (Tp^{Ph})NiI.

| | |
|---|---|
| Chemical formula | C ₂₇ H ₂₂ BiN ₆ Ni |
| <i>M</i> _r | 626.92 |
| Crystal system, space group | Trigonal, <i>P</i> -3 |
| Temperature (K) | 100 |
| <i>a</i> , <i>c</i> (Å) | 11.395(3), 11.661(3) |
| <i>V</i> (Å ³) | 1311.2(5) |
| <i>Z</i> | 1 |
| Radiation type | Mo Kα λ = 0.71073 Å |
| μ (mm ⁻¹) | 1.94 |
| Crystal size (mm) | 0.52 × 0.45 × 0.24 |
| Diffractometer | Bruker APEX-II CCD |
| | Multi-scan |
| Absorption correction | SADABS2014/5 (Bruker,2014/5) was used for absorption correction |
| <i>T</i> _{min} , <i>T</i> _{max} | 0.578, 0.747 |
| No. of measured, independent, and observed | 35172, 3544, 3240 |
| [<i>I</i> > 2σ(<i>I</i>)] reflections | |

| | |
|--|-------------------------------|
| R_{int} | 0.041 |
| $(\sin \theta/\lambda)_{\text{max}}$ (\AA^{-1}) | 0.795 |
| $R[F^2 > 2\sigma(F^2)]$, $wR(F^2)$, S | 0.031, 0.098, 1.02 |
| No. of reflections | 3544 |
| No. of parameters | 108 |
| H-atom treatment | H-atom parameters constrained |
| Largest diff. peak/hole ($e \text{\AA}^{-3}$) | 2.02, -1.55 |

Table A.31. Atom Coordinates for $(\text{Tp}^{\text{Ph}})\text{Ni}$.

| Atom | x | y | z | Occupancy |
|------|---------|---------|---------|-----------|
| I1 | 0.33333 | 0.66667 | 0.11209 | 1.000 |
| Ni1 | 0.33333 | 0.66667 | 0.32188 | 1.000 |
| C2 | 0.66667 | 0.69676 | 0.50976 | 1.000 |
| H2 | 0.75331 | 0.70734 | 0.52504 | 1.000 |
| C4 | 0.66376 | 0.68181 | 0.29010 | 1.000 |
| N2 | 0.46396 | 0.67541 | 0.53165 | 1.000 |
| N1 | 0.48249 | 0.67151 | 0.41667 | 1.000 |
| C3 | 0.60599 | 0.68414 | 0.40249 | 1.000 |
| C5 | 0.79970 | 0.77590 | 0.26599 | 1.000 |
| H5 | 0.85160 | 0.84550 | 0.31976 | 1.000 |
| C9 | 0.58900 | 0.58100 | 0.20955 | 1.000 |
| H9 | 0.49630 | 0.51770 | 0.22380 | 1.000 |

| | | | | |
|-----|---------|---------|---------|-------|
| C6 | 0.85920 | 0.76850 | 0.16420 | 1.000 |
| H6 | 0.95100 | 0.83333 | 0.14830 | 1.000 |
| B1 | 0.33333 | 0.66667 | 0.57880 | 1.000 |
| H1 | 0.33333 | 0.66667 | 0.66460 | 1.000 |
| C8 | 0.64940 | 0.57260 | 0.10850 | 1.000 |
| H8 | 0.59820 | 0.50280 | 0.05470 | 1.000 |
| C7 | 0.78440 | 0.66610 | 0.08600 | 1.000 |
| H7 | 0.82550 | 0.65990 | 0.01710 | 1.000 |
| C1 | 0.57301 | 0.69046 | 0.58851 | 1.000 |
| H1a | 0.58404 | 0.69589 | 0.66944 | 1.000 |

Table A.32. Bond angles in $(Tp^{Ph})NiII$ ($^{\circ}$).

| | | | |
|---------------------------------------|------------|--------------------------------------|------------|
| N1 ⁱ —Ni1—I1 | 123.42(4) | C3—N1—Ni1 ⁱⁱ | 139.45(13) |
| N1—Ni1—I1 | 123.42(4) | C3—N1—N2 | 106.63(14) |
| N1 ⁱⁱ —Ni1—I1 | 123.42(4) | C4—C3—C2 | 126.46(16) |
| N1 ⁱⁱ —Ni1—N1 ⁱ | 92.57(6) | N1—C3—C2 | 109.67(16) |
| N1—Ni1—N1 ⁱ | 92.57(6) | N1—C3—C4 | 123.86(16) |
| N1 ⁱⁱ —Ni1—N1 | 92.57(6) | C6—C5—C4 | 120.70(19) |
| C1—C2—C3 | 105.04(15) | C8—C9—C4 | 120.44(18) |
| C5—C4—C3 | 119.82(17) | C7—C6—C5 | 119.93(19) |
| C9—C4—C3 | 121.28(16) | N2 ⁱⁱ —B1—N2 | 108.01(14) |
| C9—C4—C5 | 118.72(17) | N2 ⁱ —B1—N2 | 108.01(14) |
| B1—N2—N1 | 120.62(17) | N2 ⁱ —B1—N2 ⁱⁱ | 108.01(14) |

| | | | |
|-------------------------|------------|----------|------------|
| C1—N2—N1 | 110.01(15) | C7—C8—C9 | 120.2(2) |
| C1—N2—B1 | 129.35(18) | C8—C7—C6 | 120.0(2) |
| N2—N1—Ni1 ⁱⁱ | 113.59(11) | N2—C1—C2 | 108.65(16) |

Symmetry codes: (i) $-x + y, -x + 1, z$, (ii) $-y + 1, x - y + 1, z$.

Table A.33. Bond lengths in $(Tp^{Ph})NiI$ (Å).

| | | | |
|----------------------|------------|-------|----------|
| I1—Ni1 | 2.4463(8) | N2—N1 | 1.363(2) |
| Ni1—N1 ⁱ | 2.0041(15) | N2—B1 | 1.543(2) |
| Ni1—N1 ⁱⁱ | 2.0041(15) | N2—C1 | 1.342(2) |
| Ni1—N1 | 2.0041(15) | N1—C3 | 1.351(2) |
| C2—C3 | 1.401(3) | C5—C6 | 1.390(3) |
| C2—C1 | 1.382(3) | C9—C8 | 1.392(3) |
| C4—C3 | 1.473(3) | C6—C7 | 1.388(3) |
| C4—C5 | 1.402(3) | C8—C7 | 1.390(3) |
| C4—C9 | 1.396(3) | | |

Symmetry codes: (i) $-x + y, -x + 1, z$, (ii) $-y + 1, x - y + 1, z$.

Table A.34. Single crystal X-ray diffraction experimental details for $(Tp^{Ph})ZnCl$.

| | |
|-----------------------------|------------------------|
| Chemical formula | $C_{27}H_{22}BClN_6Zn$ |
| M_r | 542.19 |
| Crystal system, space group | Trigonal, $P-3$ |
| Temperature (K) | 100 |

| | |
|--|--|
| a, c (Å) | 11.326(3), 11.335(3) |
| V (Å ³) | 1259.3(5) |
| Z | 2 |
| Radiation type | Mo K α $\lambda = 0.71073$ Å |
| μ (mm ⁻¹) | 1.11 |
| Crystal size (mm) | 0.28 × 0.18 × 0.17 |
| Data collection | |
| Diffractometer | Bruker APEX-II CCD diffractometer |
| Absorption correction | Multi-scan SADABS v2008/1 |
| No. of measured, independent, and observed [$I > 2\sigma(I)$] reflections | 12667, 2620, 2162 |
| R_{int} | 0.096 |
| $(\sin \theta/\lambda)_{\text{max}}$ (Å ⁻¹) | 0.720 |
| $R[F^2 > 2\sigma(F^2)], wR(F^2), S$ | 0.033, 0.088, 0.99 |
| No. of reflections | 2620 |
| No. of parameters | 110 |
| H-atom treatment | H atoms treated by a mixture of independent and constrained refinement |
| Largest diff. peak/hole (e Å ⁻³) | 0.41, -0.62 |

Table A.35. Atom Coordinates for $(Tp^{Ph})ZnCl$.

| Atom | x | y | z | Occupancy |
|------|---------|---------|---------|-----------|
| Zn1 | 0.66667 | 0.33333 | 0.30592 | 1.000 |
| Cl1 | 0.66667 | 0.33333 | 0.11567 | 1.000 |
| N1 | 0.67013 | 0.48569 | 0.40375 | 1.000 |
| C3 | 0.68208 | 0.60851 | 0.39296 | 1.000 |
| N2 | 0.67319 | 0.46339 | 0.52252 | 1.000 |
| C4 | 0.67860 | 0.66787 | 0.27801 | 1.000 |
| C9 | 0.57861 | 0.59321 | 0.19470 | 1.000 |
| H9 | 0.51730 | 0.49890 | 0.20750 | 1.000 |
| C2 | 0.69309 | 0.66503 | 0.50477 | 1.000 |
| H2 | 0.70290 | 0.75140 | 0.52260 | 1.000 |
| C1 | 0.68682 | 0.56999 | 0.58333 | 1.000 |
| H1 | 0.69140 | 0.57870 | 0.66700 | 1.000 |
| B1 | 0.66667 | 0.33333 | 0.56930 | 1.000 |
| H1A | 0.66667 | 0.33333 | 0.65760 | 1.000 |
| C5 | 0.76953 | 0.80379 | 0.25491 | 1.000 |
| H5 | 0.84010 | 0.85610 | 0.30970 | 1.000 |
| C6 | 0.75840 | 0.86455 | 0.15205 | 1.000 |
| H6 | 0.82160 | 0.95790 | 0.13680 | 1.000 |
| C7 | 0.65650 | 0.79020 | 0.07246 | 1.000 |
| H7 | 0.64790 | 0.83270 | 0.00330 | 1.000 |
| C8 | 0.56730 | 0.65520 | 0.09279 | 1.000 |

H8 0.49750 0.60350 0.03720 1.000

Table A.36. Bond angles in $(Tp^{Ph})ZnCl$ ($^{\circ}$).

| | | | |
|---------------------------------------|------------|--------------------------------------|------------|
| N1—Zn1—Cl1 | 123.02(3) | C1—N2—B1 | 128.29(14) |
| N1 ⁱⁱ —Zn1—Cl1 | 123.02(3) | C9—C4—C3 | 121.47(14) |
| N1 ⁱ —Zn1—Cl1 | 123.02(3) | C5—C4—C3 | 119.97(14) |
| N1 ⁱⁱ —Zn1—N1 | 93.13(5) | C5—C4—C9 | 118.37(14) |
| N1 ⁱ —Zn1—N1 | 93.13(5) | C4—C9—C8 | 120.66(16) |
| N1 ⁱ —Zn1—N1 ⁱⁱ | 93.13(5) | C1—C2—C3 | 105.84(13) |
| C3—N1—Zn1 | 141.54(10) | N2—C1—C2 | 108.07(13) |
| C3—N1—N2 | 106.43(11) | N2 ⁱ —B1—N2 ⁱⁱ | 108.67(11) |
| N2—N1—Zn1 | 111.71(9) | N2 ⁱ —B1—N2 | 108.66(11) |
| N1—C3—C4 | 122.96(13) | N2 ⁱⁱ —B1—N2 | 108.67(11) |
| N1—C3—C2 | 109.50(13) | C4—C5—C6 | 120.53(17) |
| C2—C3—C4 | 127.51(14) | C7—C6—C5 | 120.27(17) |
| N1—N2—B1 | 121.52(14) | C8—C7—C6 | 119.99(17) |
| C1—N2—N1 | 110.15(12) | C7—C8—C9 | 120.14(18) |

Symmetry codes: (i) $-x + y + 1, -x + 1, z$, (ii) $-y + 1, x - y, z$.

Table A.37. Bond lengths in $(Tp^{Ph})ZnCl$ (\AA).

| | | | |
|----------------------|------------|-------|----------|
| Zn1—Cl1 | 2.1565(9) | C4—C9 | 1.390(2) |
| Zn1—N1 ⁱ | 2.0350(12) | C4—C5 | 1.383(2) |
| Zn1—N1 ⁱⁱ | 2.0350(12) | C9—C8 | 1.390(2) |

| | | | |
|--------|------------|---------------------|------------|
| Zn1—N1 | 2.0350(12) | C2—C1 | 1.373(2) |
| N1—C3 | 1.3343(18) | B1—N2 ⁱ | 1.5324(16) |
| N1—N2 | 1.3734(17) | B1—N2 ⁱⁱ | 1.5324(16) |
| C3—C4 | 1.476(2) | C5—C6 | 1.391(2) |
| C3—C2 | 1.397(2) | C6—C7 | 1.372(3) |
| N2—C1 | 1.3317(18) | C7—C8 | 1.367(3) |
| N2—B1 | 1.5324(16) | | |

Symmetry codes: (i) $-x + y + 1, -x + 1, z$, (ii) $-y + 1, x - y, z$.

Appendix B. Supplemental Data for Chapter 3

Table B.1. Single crystal X-ray diffraction experimental details for {trans-[Cr^{II}(OTs)₂(dmf)₂]}_n.

| | |
|---|--|
| Chemical formula | C ₂₀ H ₂₈ CrN ₂ O ₈ S ₂ |
| <i>M</i> _r | 540.56 |
| Crystal system, space group | Monoclinic, <i>P</i> 2 ₁ / <i>n</i> |
| Temperature (K) | 90 |
| <i>a</i> , <i>b</i> , <i>c</i> (Å) | 14.5952(5), 5.2241(2), 17.0215(8) |
| β (°) | 112.454(2) |
| <i>V</i> (Å ³) | 1199.44(8) |
| <i>Z</i> | 2 |
| Radiation type | Mo K α λ = 0.71073 Å |
| μ (mm ⁻¹) | 0.70 |
| Crystal size (mm) | 0.30 × 0.25 × 0.10 |
| Diffractometer | Nonius Kappa CCD diffractometer |
| Absorption correction | Multi-scan SCALEPACK (Otwinowski & Minor, 1997) |
| No. of measured, independent, and observed [<i>I</i> > 2 σ (<i>I</i>)] reflections | 0.818, 0.933 |
| <i>R</i> _{int} | 4520, 2492, 1661 |
| (sin θ / λ) _{max} (Å ⁻¹) | 0.058 |

| | |
|--|-------------------------------|
| $R[F^2 > 2\sigma(F^2)], wR(F^2), S$ | 0.052, 0.140, 1.05 |
| No. of reflections | 2492 |
| No. of parameters | 154 |
| H-atom treatment | H-atom parameters constrained |
| Largest diff. peak/hole ($e \text{ \AA}^{-3}$) | 0.68, -0.50 |

Table B.2. Atom Coordinates for $\{trans-[Cr^I(OTs)_2(dmf)_2]\}_n$.

| Atom | x | y | z | Occupancy |
|------|---------|----------|---------|-----------|
| Cr1 | 0.50000 | 0.50000 | 0.00000 | 1.000 |
| C1 | 0.06210 | 0.32130 | 0.13190 | 1.000 |
| H1A | 0.02160 | 0.41680 | 0.08090 | 1.000 |
| H1B | 0.07270 | 0.42600 | 0.18240 | 1.000 |
| H1C | 0.02790 | 0.16280 | 0.13530 | 1.000 |
| C2 | 0.16140 | 0.25690 | 0.12750 | 1.000 |
| C3 | 0.24320 | 0.41070 | 0.16580 | 1.000 |
| H3 | 0.23740 | 0.55930 | 0.19580 | 1.000 |
| C4 | 0.33480 | 0.35180 | 0.16140 | 1.000 |
| H4 | 0.39080 | 0.45830 | 0.18840 | 1.000 |
| C5 | 0.34230 | 0.13580 | 0.11720 | 1.000 |
| C6 | 0.26150 | -0.01810 | 0.07860 | 1.000 |
| H6 | 0.26720 | -0.16510 | 0.04790 | 1.000 |
| C7 | 0.17130 | 0.03990 | 0.08420 | 1.000 |
| H7 | 0.11600 | -0.06960 | 0.05820 | 1.000 |

| | | | | |
|------|---------|----------|---------|-------|
| C8 | 0.68450 | 0.77350 | 0.10760 | 1.000 |
| H8 | 0.64200 | 0.88150 | 0.12340 | 1.000 |
| C9 | 0.82080 | 1.03470 | 0.19790 | 1.000 |
| H9A | 0.76680 | 1.12640 | 0.20660 | 1.000 |
| H9B | 0.85700 | 1.15310 | 0.17560 | 1.000 |
| H9C | 0.86600 | 0.96410 | 0.25220 | 1.000 |
| C10 | 0.85020 | 0.67910 | 0.11460 | 1.000 |
| H10A | 0.81430 | 0.55020 | 0.07220 | 1.000 |
| H10B | 0.89720 | 0.59390 | 0.16520 | 1.000 |
| H10C | 0.88630 | 0.79310 | 0.09070 | 1.000 |
| O1 | 0.51511 | -0.06270 | 0.19868 | 1.000 |
| O2 | 0.50648 | 0.28940 | 0.10545 | 1.000 |
| O3 | 0.43858 | -0.12510 | 0.04557 | 1.000 |
| O4 | 0.64647 | 0.58810 | 0.05949 | 1.000 |
| N1 | 0.77995 | 0.82820 | 0.13777 | 1.000 |
| S1 | 0.45934 | 0.04804 | 0.11644 | 1.000 |

Table B.3. Bond angles in $\{trans-[Cr^{II}(OTs)_2(dmf)_2]\}$ ($^{\circ}$).

| | | | |
|--------------------------------------|----------|-----------|------------|
| O4—Cr1—O4 ⁱ | 180.0 | C5—C6—C7 | 120.2(3) |
| O4—Cr1—O2 | 89.85(8) | C6—C7—C2 | 120.5(3) |
| O4 ⁱ —Cr1—O2 | 90.15(8) | O4—C8—N1 | 124.1(3) |
| O4—Cr1—O2 ⁱ | 90.15(8) | S1—O2—Cr1 | 133.61(13) |
| O4 ⁱ —Cr1—O2 ⁱ | 89.85(8) | C8—O4—Cr1 | 128.2(2) |

| | | | |
|------------------------|----------|-----------|------------|
| O2—Cr1—O2 ⁱ | 180.0 | C8—N1—C9 | 121.6(3) |
| C3—C2—C7 | 118.7(3) | C8—N1—C10 | 121.8(3) |
| C3—C2—C1 | 121.2(4) | C9—N1—C10 | 116.6(3) |
| C7—C2—C1 | 120.1(4) | O1—S1—O3 | 114.80(14) |
| C2—C3—C4 | 121.2(3) | O1—S1—O2 | 110.25(14) |
| C5—C4—C3 | 118.9(3) | O3—S1—O2 | 112.76(13) |
| C6—C5—C4 | 120.5(3) | O1—S1—C5 | 106.53(14) |
| C6—C5—S1 | 120.0(3) | O3—S1—C5 | 105.81(14) |
| C4—C5—S1 | 119.4(3) | O2—S1—C5 | 106.00(15) |

Symmetry code: (i) $-x + 1, -y + 1, -z$.

Table B.4. Bond lengths in {trans-[Cr^{II}(OTs)₂(dmf)₂]} (Å).

| | | | |
|---------------------|----------|--------|----------|
| Cr1—O4 | 2.038(2) | C5—S1 | 1.773(3) |
| Cr1—O4 ⁱ | 2.038(2) | C6—C7 | 1.389(5) |
| Cr1—O2 | 2.076(2) | C8—O4 | 1.253(4) |
| Cr1—O2 ⁱ | 2.076(2) | C8—N1 | 1.318(4) |
| C1—C2 | 1.518(5) | C9—N1 | 1.449(4) |
| C2—C3 | 1.379(5) | C10—N1 | 1.457(4) |
| C2—C7 | 1.390(5) | O1—S1 | 1.444(2) |
| C3—C4 | 1.402(5) | O2—S1 | 1.482(2) |
| C4—C5 | 1.384(5) | O3—S1 | 1.444(2) |
| C5—C6 | 1.370(5) | | |

Symmetry code: (i) $-x + 1, -y + 1, -z$.

Table B.5. Single crystal X-ray diffraction experimental details for [trans-Mn(dmf)₂(OTs)₂]_n.

| | |
|---|--|
| Chemical formula | C ₂₀ H ₂₈ MnN ₂ O ₈ S ₂ |
| <i>M</i> _r | 543.50 |
| Crystal system, space group | Monoclinic, <i>P</i> 2 ₁ / <i>n</i> |
| Temperature (K) | 100 |
| <i>a</i> , <i>b</i> , <i>c</i> (Å) | 14.8262 (8), 5.2111 (3), 16.2554 (9) |
| <i>β</i> (°) | 107.948 (3) |
| <i>V</i> (Å ³) | 1194.79 (12) |
| <i>Z</i> | 2 |
| Radiation type | Mo K α λ = 0.71073 Å |
| μ (mm ⁻¹) | 0.78 |
| Crystal size (mm) | 0.30 × 0.08 × 0.05 |
| Diffractometer | Bruker APEX-II CCD |
| Absorption correction | Multi-scan SADABS v2008/1 |
| <i>T</i> _{min} , <i>T</i> _{max} | 0.800, 0.965 |
| No. of measured, independent, and observed [<i>I</i> > 2 σ (<i>I</i>)] reflections | 16816, 3769, 2838 |
| <i>R</i> _{int} | 0.045 |
| (sin θ / λ) _{max} (Å ⁻¹) | 0.722 |
| <i>R</i> [<i>F</i> ² > 2 σ (<i>F</i> ²)], <i>wR</i> (<i>F</i> ²), <i>S</i> | 0.036, 0.097, 1.02 |

| | |
|--|-------------------------------|
| No. of reflections | 3769 |
| No. of parameters | 154 |
| H-atom treatment | H-atom parameters constrained |
| Largest diff. peak/hole ($e \text{ \AA}^{-3}$) | 0.59, -0.48 |

Table B.6. Atom Coordinates for $[\text{trans-Mn}(\text{dmf})_2(\text{OTs})_2]_n$.

| Atom | x | y | z | Occupancy |
|------|---------|----------|---------|-----------|
| Mn1 | 0.50000 | 0.00000 | 0.00000 | 1.000 |
| S1 | 0.46608 | 0.48378 | 0.12785 | 1.000 |
| O1 | 0.64976 | -0.07980 | 0.05335 | 1.000 |
| O2 | 0.50351 | 0.23370 | 0.11318 | 1.000 |
| O3 | 0.51630 | 0.58380 | 0.21276 | 1.000 |
| O4 | 0.46036 | 0.66300 | 0.05771 | 1.000 |
| N1 | 0.78168 | -0.29200 | 0.13173 | 1.000 |
| C1 | 0.68910 | -0.25240 | 0.10467 | 1.000 |
| H1 | 0.65020 | -0.36270 | 0.12580 | 1.000 |
| C2 | 0.82449 | -0.49240 | 0.19400 | 1.000 |
| H2A | 0.77450 | -0.59060 | 0.20760 | 1.000 |
| H2B | 0.86600 | -0.41410 | 0.24700 | 1.000 |
| H2C | 0.86170 | -0.60720 | 0.16930 | 1.000 |
| C3 | 0.84565 | -0.13910 | 0.09971 | 1.000 |
| H3A | 0.87060 | -0.24450 | 0.06170 | 1.000 |
| H3B | 0.89830 | -0.07770 | 0.14860 | 1.000 |

| | | | | |
|------|---------|---------|---------|-------|
| H3C | 0.81130 | 0.00800 | 0.06720 | 1.000 |
| C4 | 0.34712 | 0.43270 | 0.12434 | 1.000 |
| C5 | 0.32396 | 0.22340 | 0.16704 | 1.000 |
| H5 | 0.37150 | 0.10420 | 0.19640 | 1.000 |
| C6 | 0.23076 | 0.19020 | 0.16641 | 1.000 |
| H6 | 0.21490 | 0.04770 | 0.19570 | 1.000 |
| C7 | 0.16037 | 0.36290 | 0.12346 | 1.000 |
| C8 | 0.18491 | 0.57090 | 0.08179 | 1.000 |
| H8 | 0.13750 | 0.69090 | 0.05290 | 1.000 |
| C9 | 0.27790 | 0.60700 | 0.08146 | 1.000 |
| H9 | 0.29370 | 0.74960 | 0.05220 | 1.000 |
| C10 | 0.05871 | 0.31940 | 0.12115 | 1.000 |
| H10A | 0.02450 | 0.48320 | 0.11100 | 1.000 |
| H10B | 0.05760 | 0.24730 | 0.17650 | 1.000 |
| H10C | 0.02820 | 0.19960 | 0.07440 | 1.000 |

Table B.7. Bond angles in $[trans-Mn(dmf)_2(OTs)_2]_n$ ($^\circ$)

| | | | |
|---|-----------|---------------------------|------------|
| O4 ⁱ —Mn1—O4 ⁱⁱ | 180.00(7) | O4 ⁱ —Mn1—O2 | 88.49(4) |
| O4 ⁱ —Mn1—O1 | 86.98(5) | O4 ⁱⁱ —Mn1—O2 | 91.51(4) |
| O4 ⁱⁱ —Mn1—O1 | 93.02(5) | O1—Mn1—O2 | 90.82(4) |
| O4 ⁱ —Mn1—O1 ⁱⁱⁱ | 93.02(5) | O1 ⁱⁱⁱ —Mn1—O2 | 89.18(4) |
| O4 ⁱⁱ —Mn1—O1 ⁱⁱⁱ | 86.98(5) | O2 ⁱⁱⁱ —Mn1—O2 | 180.0 |
| O1—Mn1—O1 ⁱⁱⁱ | 180.0 | C9—C4—C5 | 120.39(15) |

| | | | |
|--|----------|----------|------------|
| O4 ⁱ —Mn1—O2 ⁱⁱⁱ | 91.51(4) | C9—C4—S1 | 119.62(13) |
| O4 ⁱⁱ —Mn1—O2 ⁱⁱⁱ | 88.49(4) | C5—C4—S1 | 119.95(13) |
| O1—Mn1—O2 ⁱⁱⁱ | 89.18(4) | C6—C5—C4 | 119.45(16) |
| O1 ⁱⁱⁱ —Mn1—O2 ⁱⁱⁱ | 90.82(4) | | |

Symmetry codes: (i) $-x+1, -y+1, -z$; (ii) $x, y-1, z$; (iii) $-x+1, -y, -z$; (iv) $x, y+1, z$.

Table B.8. Bond lengths in [trans-Mn(dmf)₂(OTs)₂]_n.

| | | | |
|-----------------------|------------|----------------------|------------|
| Mn1—O4 ⁱ | 2.1564(12) | O4—Mn1 ^{iv} | 2.1564(12) |
| Mn1—O4 ⁱⁱ | 2.1564(12) | N1—C1 | 1.322(2) |
| Mn1—O1 | 2.1606(11) | N1—C3 | 1.452(2) |
| Mn1—O1 ⁱⁱⁱ | 2.1606(11) | N1—C2 | 1.457(2) |
| Mn1—O2 ⁱⁱⁱ | 2.1935(11) | C4—C9 | 1.387(2) |
| Mn1—O2 | 2.1935(11) | C4—C5 | 1.391(2) |
| S1—O3 | 1.4484(12) | C5—C6 | 1.389(2) |
| S1—O4 | 1.4558(12) | C6—C7 | 1.392(3) |
| S1—O2 | 1.4646(12) | C7—C8 | 1.385(3) |
| S1—C4 | 1.7672(15) | C7—C10 | 1.513(2) |
| O1—C1 | 1.243(2) | C8—C9 | 1.393(2) |

Symmetry codes: (i) $-x + 1, -y + 1, -z$; (ii) $x, y - 1, z$; (iii) $-x + 1, -y, -z$; (iv) $x, y + 1,$

z .

Table B.9. Single crystal X-ray diffraction experimental details for trans-[Fe^{II}(OTs)₂(dmf)₄].

| | |
|---|---|
| Chemical formula | C ₂₀ H ₃₂ FeN ₂ O ₁₀ S ₂ |
| <i>M</i> _r | 580.45 |
| Crystal system, space group | Triclinic, <i>P</i> -1 |
| Temperature (K) | 100 |
| <i>a</i> , <i>b</i> , <i>c</i> (Å) | 6.3485(1), 8.6866(2), 12.1192(2) |
| <i>α</i> , <i>β</i> , <i>γ</i> (°) | 87.850(1), 84.329(1), 76.859(1) |
| <i>V</i> (Å ³) | 647.57(2) |
| <i>Z</i> | 1 |
| Radiation type | Mo K α λ = 0.71073 Å |
| μ (mm ⁻¹) | 0.80 |
| Crystal size (mm) | 0.23 × 0.12 × 0.07 |
| Diffractometer | Bruker APEX-II CCD |
| Absorption correction | Multi-scan SADABS v2008/1 |
| <i>T</i> _{min} , <i>T</i> _{max} | 0.838, 0.946 |
| No. of measured, independent, and observed [<i>I</i> > 2 σ (<i>I</i>)] reflections | 21481, 4885, 4271 |
| <i>R</i> _{int} | 0.032 |
| (sin θ / λ) _{max} (Å ⁻¹) | 0.781 |
| <i>R</i> [<i>F</i> ² > 2 σ (<i>F</i> ²)], <i>wR</i> (<i>F</i> ²), <i>S</i> | 0.031, 0.084, 1.03 |
| No. of reflections | 4885 |

| | |
|--|--|
| No. of parameters | 202 |
| No. of restraints | 3 |
| H-atom treatment | H atoms treated by a mixture of independent and constrained refinement |
| Largest diff. peak/hole ($e \text{ \AA}^{-3}$) | 0.47, -0.59 |

Table B.10. Atom Coordinates for trans-[Fe^{II}(OTs)₂(dmf)₄].

| Atom | x | y | z | Occupancy |
|------|---------|----------|----------|-----------|
| Fe1 | 0.50000 | 0.00000 | 0.00000 | 1.000 |
| S1 | 0.69326 | 0.11985 | 0.13282 | 1.000 |
| O1 | 0.29965 | 0.00290 | 0.10930 | 1.000 |
| O2 | 0.33872 | 0.05767 | -0.17766 | 1.000 |
| O3 | 0.63983 | 0.06348 | 0.15187 | 1.000 |
| O4 | 0.73648 | 0.12782 | -0.01161 | 1.000 |
| O5 | 0.83256 | 0.13859 | 0.28238 | 1.000 |
| N1 | 0.22219 | -0.00950 | 0.33063 | 1.000 |
| N2 | 0.12175 | 0.12349 | -0.26452 | 1.000 |
| C1 | 0.31772 | -0.02118 | 0.23793 | 1.000 |
| H1 | 0.40500 | -0.04960 | 0.27180 | 1.000 |
| C2 | 0.25894 | -0.03560 | 0.48701 | 1.000 |
| H2A | 0.35940 | -0.06150 | 0.50740 | 1.000 |
| H2B | 0.14940 | -0.05480 | 0.48610 | 1.000 |

| | | | | |
|-----|----------|----------|----------|-------|
| H2C | 0.29280 | -0.00810 | 0.57290 | 1.000 |
| C3 | 0.08460 | 0.03329 | 0.28541 | 1.000 |
| H3A | 0.12830 | 0.06420 | 0.35910 | 1.000 |
| H3B | -0.02900 | 0.01950 | 0.29310 | 1.000 |
| H3C | 0.06220 | 0.04490 | 0.17370 | 1.000 |
| C4 | 0.19993 | 0.08129 | -0.17337 | 1.000 |
| H4 | 0.14680 | 0.06800 | -0.09950 | 1.000 |
| C5 | -0.04415 | 0.14781 | -0.25627 | 1.000 |
| H5A | -0.07920 | 0.12880 | -0.17450 | 1.000 |
| H5B | -0.14280 | 0.14480 | -0.36240 | 1.000 |
| H5C | -0.02180 | 0.18610 | -0.22640 | 1.000 |
| C6 | 0.20042 | 0.14909 | -0.37274 | 1.000 |
| H6A | 0.31480 | 0.13080 | -0.36260 | 1.000 |
| H6B | 0.22480 | 0.18740 | -0.34340 | 1.000 |
| H6C | 0.11460 | 0.14630 | -0.48510 | 1.000 |
| C7 | 0.49620 | 0.15922 | 0.10846 | 1.000 |
| C8 | 0.37571 | 0.14338 | 0.18373 | 1.000 |
| H8 | 0.39630 | 0.11070 | 0.24470 | 1.000 |
| C9 | 0.22513 | 0.17563 | 0.16910 | 1.000 |
| H9 | 0.14280 | 0.16470 | 0.21990 | 1.000 |
| C10 | 0.19362 | 0.22393 | 0.08063 | 1.000 |
| C11 | 0.31324 | 0.23863 | 0.00291 | 1.000 |
| H11 | 0.29120 | 0.27080 | -0.06040 | 1.000 |

| | | | | |
|------|----------|---------|----------|-------|
| C12 | 0.46460 | 0.20665 | 0.01704 | 1.000 |
| H12 | 0.54580 | 0.21720 | -0.03550 | 1.000 |
| C13 | 0.03224 | 0.25904 | 0.06938 | 1.000 |
| H13A | 0.06900 | 0.28570 | 0.15760 | 1.000 |
| H13B | -0.06590 | 0.23630 | 0.07860 | 1.000 |
| H13C | -0.01120 | 0.27790 | -0.03530 | 1.000 |

Table B.11. Bond angles in *trans*-[Fe^{II}(OTs)₂(dmf)₄] (°).

| | | | |
|--|----------|-------------|------------|
| O1—Fe1—O1 ⁱ | 180.0 | O1B—C1B—N1B | 124.72(12) |
| O1—Fe1—O1A ⁱ | 90.73(3) | C1B—N1B—C3B | 121.90(11) |
| O1 ⁱ —Fe1—O1A ⁱ | 89.27(3) | C1B—N1B—C2B | 121.37(11) |
| O1—Fe1—O1A | 89.27(3) | C3B—N1B—C2B | 116.68(10) |
| O1 ⁱ —Fe1—O1A | 90.73(3) | S1—O1—Fe1 | 137.01(6) |
| O1A ⁱ —Fe1—O1A | 180.0 | O3—S1—O2 | 114.76(6) |
| O1—Fe1—O1B ⁱ | 89.46(3) | O3—S1—O1 | 113.25(6) |
| O1 ⁱ —Fe1—O1B ⁱ | 90.54(3) | O2—S1—O1 | 110.24(6) |
| O1A ⁱ —Fe1—O1B ⁱ | 88.36(3) | O3—S1—C1 | 106.83(6) |
| O1A—Fe1—O1B ⁱ | 91.65(3) | O2—S1—C1 | 106.02(6) |
| O1—Fe1—O1B | 90.54(3) | O1—S1—C1 | 104.93(6) |
| O1 ⁱ —Fe1—O1B | 89.47(3) | C6—C1—C2 | 120.15(12) |
| O1A ⁱ —Fe1—O1B | 91.64(3) | C6—C1—S1 | 119.85(10) |
| O1A—Fe1—O1B | 88.35(3) | C2—C1—S1 | 119.99(10) |
| O1B ⁱ —Fe1—O1B | 180.0 | C3—C2—C1 | 119.72(12) |

| | | | |
|-------------|------------|----------|------------|
| C1A—O1A—Fe1 | 122.63(8) | C2—C3—C4 | 120.80(12) |
| O1A—C1A—N1A | 123.80(12) | C5—C4—C3 | 118.73(12) |
| C1A—N1A—C2A | 121.78(11) | C5—C4—C7 | 121.12(13) |
| C1A—N1A—C3A | 121.10(11) | C3—C4—C7 | 120.15(13) |
| C2A—N1A—C3A | 116.95(11) | C6—C5—C4 | 120.78(13) |
| C1B—O1B—Fe1 | 125.20(8) | C1—C6—C5 | 119.80(12) |

Symmetry code: (i) -x, -y, -z.

Table B.12. Bond lengths in trans-[Fe^{II}(OTs)₂(dmf)₄] (Å).

| | | | |
|---------------------|-------------|---------|-------------|
| Fe1—O3 | 2.0958 (7) | N1—C2 | 1.4547 (13) |
| Fe1—O3 ⁱ | 2.0958 (7) | N1—C3 | 1.4595 (14) |
| Fe1—O1 | 2.1237 (7) | N2—C4 | 1.3233 (12) |
| Fe1—O1 ⁱ | 2.1237 (7) | N2—C6 | 1.4560 (13) |
| Fe1—O2 ⁱ | 2.1574 (7) | N2—C5 | 1.4603 (13) |
| Fe1—O2 | 2.1574 (7) | C7—C12 | 1.3917 (14) |
| S1—O4 | 1.4466 (8) | C7—C8 | 1.3944 (14) |
| S1—O5 | 1.4532 (8) | C8—C9 | 1.3923 (14) |
| S1—O3 | 1.4793 (8) | C9—C10 | 1.3967 (15) |
| S1—C7 | 1.7736 (10) | C10—C11 | 1.3966 (16) |
| O1—C1 | 1.2434 (11) | C10—C13 | 1.5087 (15) |
| O2—C4 | 1.2487 (12) | C11—C12 | 1.3944 (15) |

N1—C1 1.3265 (12)

Symmetry code: (i) $-x, -y, -z$.Table B.13. Single crystal X-ray diffraction experimental details for *trans*-[Fe^{II}(dmf)₂(OTs)₂(OH₂)₂].

| | |
|---|---|
| Chemical formula | C ₂₀ H ₃₂ FeN ₂ O ₁₀ S ₂ |
| <i>M</i> _r | 580.45 |
| Crystal system, space group | Triclinic, <i>P</i> -1 |
| Temperature (K) | 100 |
| <i>a</i> , <i>b</i> , <i>c</i> (Å) | 6.3485(1), 8.6866(2), 12.1192(2) |
| α , β , γ (°) | 87.850(1), 84.329(1), 76.859(1) |
| <i>V</i> (Å ³) | 647.57(2) |
| <i>Z</i> | 1 |
| Radiation type | Mo K α λ = 0.71073 Å |
| μ (mm ⁻¹) | 0.80 |
| Crystal size (mm) | 0.23 × 0.12 × 0.07 |
| Diffractometer | Bruker APEX-II CCD |
| Absorption correction | Multi-scan SADABS v2008/1 |
| <i>T</i> _{min} , <i>T</i> _{max} | 0.838, 0.946 |
| No. of measured, independent, and observed [<i>I</i> > 2 σ (<i>I</i>)] reflections | 21481, 4885, 4271 |
| <i>R</i> _{int} | 0.032 |

| | |
|--|--|
| $(\sin \theta/\lambda)_{\max}$ (\AA^{-1}) | 0.781 |
| $R[F^2 > 2\sigma(F^2)]$, $wR(F^2)$, S | 0.031, 0.084, 1.03 |
| No. of reflections | 4885 |
| No. of parameters | 202 |
| No. of restraints | 3 |
| H-atom treatment | H atoms treated by a mixture of independent and constrained refinement |
| Largest diff. peak/hole / $e \text{\AA}^{-3}$ | 0.47, -0.59 |

Table B.14. Atom Coordinates for *trans*-[Fe^{II}(dmf)₂(OTs)₂(OH₂)₂].

| Atom | x | y | z | Occupancy |
|------|----------|----------|---------|-----------|
| Fe1 | 0.00000 | 0.00000 | 1.00000 | 1.000 |
| S1 | 0.36202 | -0.03332 | 0.77737 | 1.000 |
| O1 | 0.07855 | 0.16632 | 1.10724 | 1.000 |
| H1A | -0.02700 | 0.19000 | 1.15300 | 1.000 |
| H1B | 0.18200 | 0.13300 | 1.14350 | 1.000 |
| O2 | 0.20647 | -0.19187 | 1.06963 | 1.000 |
| O3 | 0.24984 | 0.04521 | 0.87929 | 1.000 |
| O4 | 0.30936 | -0.18620 | 0.76489 | 1.000 |
| O5 | 0.59378 | -0.03996 | 0.76946 | 1.000 |
| N1 | 0.50936 | -0.36677 | 1.11363 | 1.000 |
| C1 | 0.26249 | 0.08717 | 0.66470 | 1.000 |

| | | | | |
|------|----------|----------|---------|-------|
| C4 | 0.11260 | 0.26257 | 0.47898 | 1.000 |
| C7 | 0.03190 | 0.35467 | 0.37762 | 1.000 |
| H7A | 0.00810 | 0.46810 | 0.39110 | 1.000 |
| H7B | -0.10510 | 0.32980 | 0.36190 | 1.000 |
| H7C | 0.14020 | 0.32590 | 0.31400 | 1.000 |
| C8 | 0.40782 | -0.23953 | 1.06081 | 1.000 |
| H8 | 0.49240 | -0.18180 | 1.01400 | 1.000 |
| C9 | 0.38640 | -0.45598 | 1.18867 | 1.000 |
| H9A | 0.23130 | -0.40580 | 1.19090 | 1.000 |
| H9B | 0.43430 | -0.45770 | 1.26320 | 1.000 |
| H9C | 0.41070 | -0.56450 | 1.16240 | 1.000 |
| C10 | 0.74517 | -0.41962 | 1.10187 | 1.000 |
| H10A | 0.80740 | -0.34910 | 1.04980 | 1.000 |
| H10B | 0.78580 | -0.52760 | 1.07360 | 1.000 |
| H10C | 0.80100 | -0.41760 | 1.17420 | 1.000 |
| C2 | 0.39540 | 0.18630 | 0.61830 | 0.500 |
| H2 | 0.52450 | 0.19420 | 0.64900 | 0.500 |
| C3 | 0.32580 | 0.27210 | 0.52440 | 0.500 |
| H3 | 0.41220 | 0.33800 | 0.48770 | 0.500 |
| C5 | 0.00570 | 0.16770 | 0.53920 | 0.500 |
| H5 | -0.12900 | 0.15840 | 0.51550 | 0.500 |
| C6 | 0.07310 | 0.08090 | 0.63370 | 0.500 |
| H6 | -0.01540 | 0.01940 | 0.67400 | 0.500 |

| | | | | |
|-----|----------|---------|---------|-------|
| C2' | 0.39870 | 0.11970 | 0.57046 | 0.500 |
| H2' | 0.55100 | 0.07870 | 0.56880 | 0.500 |
| C3' | 0.31550 | 0.20990 | 0.48041 | 0.500 |
| H3' | 0.41160 | 0.23190 | 0.41980 | 0.500 |
| C5' | -0.04690 | 0.22660 | 0.56380 | 0.500 |
| H5' | -0.19830 | 0.26140 | 0.55740 | 0.500 |
| C6' | 0.03240 | 0.13840 | 0.65520 | 0.500 |
| H6' | -0.06700 | 0.11150 | 0.71240 | 0.500 |

Table B.15. Bond angles in *trans*-[Fe^{II}(dmf)₂(OTs)₂(OH₂)₂] (°).

| | | | |
|--------------------------------------|----------|------------|------------|
| O2—Fe1—O2 ⁱ | 180.0 | C6—C1—C2 | 125.73(17) |
| O2—Fe1—O3 | 93.18(3) | C6—C1—C2' | 109.20(17) |
| O2 ⁱ —Fe1—O3 | 86.82(3) | C2—C1—C6' | 117.27(16) |
| O2—Fe1—O3 ⁱ | 86.82(3) | C2'—C1—C6' | 115.32(16) |
| O2 ⁱ —Fe1—O3 ⁱ | 93.18(3) | C6—C1—S1 | 118.73(14) |
| O3—Fe1—O3 ⁱ | 180.0 | C2—C1—S1 | 115.51(11) |
| O2—Fe1—O1 ⁱ | 86.90(3) | C2'—C1—S1 | 123.02(11) |
| O2 ⁱ —Fe1—O1 ⁱ | 93.10(3) | C6'—C1—S1 | 120.98(12) |
| O3—Fe1—O1 ⁱ | 91.17(3) | C3'—C4—C5 | 109.90(18) |
| O3 ⁱ —Fe1—O1 ⁱ | 88.83(3) | C3'—C4—C5' | 123.74(17) |
| O2—Fe1—O1 | 93.10(3) | C3'—C4—C7 | 117.93(15) |
| O2 ⁱ —Fe1—O1 | 86.90(3) | C5—C4—C7 | 124.16(16) |
| O3—Fe1—O1 | 88.83(3) | C5'—C4—C7 | 118.04(15) |

| | | | |
|-------------------------|------------|------------|------------|
| O3 ⁱ —Fe1—O1 | 91.17(3) | C5—C4—C3 | 113.16(15) |
| O1 ⁱ —Fe1—O1 | 180.0 | C5'—C4—C3 | 113.01(15) |
| O5—S1—O4 | 113.79(5) | C7—C4—C3 | 122.67(14) |
| O5—S1—O3 | 111.59(5) | O2—C8—N1 | 123.07(10) |
| O4—S1—O3 | 111.52(5) | C3—C2—C1 | 115.56(19) |
| O5—S1—C1 | 105.69(5) | C2—C3—C4 | 121.4(2) |
| O4—S1—C1 | 106.79(5) | C4—C5—C6 | 126.2(2) |
| O3—S1—C1 | 106.94(5) | C1—C6—C5 | 117.6(2) |
| C8—O2—Fe1 | 132.58(7) | C3'—C2'—C1 | 122.05(19) |
| S1—O3—Fe1 | 134.45(5) | C4—C3'—C2' | 120.38(19) |
| C8—N1—C9 | 120.23(9) | C6'—C5'—C4 | 116.8(2) |
| C8—N1—C10 | 121.88(10) | C5'—C6'—C1 | 121.3(2) |
| C9—N1—C10 | 117.86(9) | | |

Symmetry code(s): (i) -x, -y, -z + 2.

Table B.16. Bond lengths in *trans*-[Fe^{II}(dmf)₂(OTs)₂(OH₂)₂] (Å).

| | | | |
|---------------------|-----------|--------|----------|
| Fe1—O2 | 2.0804(7) | C1—C6 | 1.308(3) |
| Fe1—O2 ⁱ | 2.0804(7) | C1—C2 | 1.404(2) |
| Fe1—O3 | 2.1428(8) | C1—C2' | 1.423(2) |
| Fe1—O3 ⁱ | 2.1428(8) | C1—C6' | 1.442(3) |
| Fe1—O1 ⁱ | 2.1498(9) | C4—C3' | 1.267(3) |
| Fe1—O1 | 2.1498(9) | C4—C5 | 1.336(3) |
| S1—O5 | 1.4530(9) | C4—C5' | 1.447(3) |

| | | | |
|--------|------------|---------|------------|
| S1—O4 | 1.4578(9) | C4—C7 | 1.5085(18) |
| S1—O3 | 1.4720(9) | C4—C3 | 1.531(3) |
| S1—C1 | 1.7668(11) | C2—C3 | 1.390(3) |
| O2—C8 | 1.2460(13) | C5—C6 | 1.396(4) |
| N1—C8 | 1.3234(13) | C2'—C3' | 1.395(3) |
| N1—C9 | 1.4558(15) | C5'—C6' | 1.392(3) |
| N1—C10 | 1.4568(14) | | |

Symmetry code: (i) -x, -y, -z + 2.

Table B.17. Single crystal X-ray diffraction experimental details for trans-[Co^{II}(dmf)₄(OTs)₂].

| | |
|------------------------------------|---|
| Chemical formula | C ₂₆ H ₄₂ CoN ₄ O ₁₀ S ₂ |
| <i>M_r</i> | 693.69 |
| Crystal system, space group | Monoclinic, <i>P</i> 2 ₁ / <i>c</i> |
| Temperature (K) | 90 |
| <i>a</i> , <i>b</i> , <i>c</i> (Å) | 7.84650(10), 24.5324(3), 8.79750(10) |
| β (°) | 110.926(6) |
| <i>V</i> (Å ³) | 1581.76(3) |
| <i>Z</i> | 2 |
| Radiation type | Mo K α λ = 0.71073 Å |
| μ (mm ⁻¹) | 0.73 |
| Crystal size (mm) | 0.20 × 0.20 × 0.20 |

| | |
|--|---|
| Diffractometer | Nonius Kappa CCD diffractometer |
| Absorption correction | Multi-scan SCALEPACK (Otwinowski & Minor, 1997) |
| No. of measured, independent, and observed [$I > 2\sigma(I)$] reflections | 7142, 3644, 2817 |
| R_{int} | 0.056 |
| $(\sin \theta/\lambda)_{\text{max}}$ (\AA^{-1}) | 0.778 |
| $R[F^2 > 2\sigma(F^2)]$, $wR(F^2)$, S | 0.037, 0.103, 1.052 |
| No. of reflections | 3644 |
| No. of parameters | 201 |
| H-atom treatment | H-atom parameters constrained |
| Largest diff. peak/hole ($e \text{\AA}^{-3}$) | 0.59, -0.58 |

Table B.18. Atom coordinates for *trans*-[Co^{II}(dmf)₄(OTs)₂].

| | x | y | z | Occupancy |
|-----|---------|----------|---------|-----------|
| Co1 | 0.00000 | 0.00000 | 0.00000 | 1.000 |
| O1A | 0.30360 | 0.00363 | 0.11202 | 1.000 |
| C1A | 0.41730 | -0.02108 | 0.23930 | 1.000 |
| H1A | 0.36780 | -0.05100 | 0.27830 | 1.000 |
| N1A | 0.60610 | -0.00974 | 0.32890 | 1.000 |

| | | | | |
|------|----------|----------|----------|-------|
| C2A | 0.72840 | -0.03587 | 0.48530 | 1.000 |
| H2A1 | 0.83270 | -0.05300 | 0.46770 | 1.000 |
| H2A2 | 0.65960 | -0.06360 | 0.51950 | 1.000 |
| H2A3 | 0.77240 | -0.00800 | 0.57010 | 1.000 |
| C3A | 0.69720 | 0.03325 | 0.28230 | 1.000 |
| H3A1 | 0.62290 | 0.04580 | 0.17280 | 1.000 |
| H3A2 | 0.81540 | 0.02030 | 0.28240 | 1.000 |
| H3A3 | 0.71640 | 0.06350 | 0.35940 | 1.000 |
| O1B | -0.01860 | 0.05729 | -0.17464 | 1.000 |
| C1B | 0.12430 | 0.08102 | -0.17100 | 1.000 |
| H1B | 0.24060 | 0.06850 | -0.10160 | 1.000 |
| N1B | 0.10990 | 0.12298 | -0.26390 | 1.000 |
| C2B | -0.07820 | 0.14852 | -0.37390 | 1.000 |
| H2B1 | -0.17810 | 0.12930 | -0.35430 | 1.000 |
| H2B2 | -0.09250 | 0.14490 | -0.48870 | 1.000 |
| H2B3 | -0.08110 | 0.18720 | -0.34690 | 1.000 |
| C3B | 0.28400 | 0.14770 | -0.25600 | 1.000 |
| H3B1 | 0.38550 | 0.12750 | -0.17830 | 1.000 |
| H3B2 | 0.28830 | 0.18570 | -0.22060 | 1.000 |
| H3B3 | 0.29380 | 0.14640 | -0.36390 | 1.000 |
| O1 | 0.01090 | 0.06250 | 0.15411 | 1.000 |
| O2 | -0.05490 | 0.13839 | 0.28063 | 1.000 |
| O3 | -0.25150 | 0.12646 | -0.01280 | 1.000 |

| | | | | |
|-----|----------|---------|----------|-------|
| S1 | -0.06359 | 0.11902 | 0.13233 | 1.000 |
| C1 | 0.10890 | 0.15885 | 0.10810 | 1.000 |
| C2 | 0.30470 | 0.14334 | 0.18380 | 1.000 |
| H2 | 0.33650 | 0.11030 | 0.24370 | 1.000 |
| C3 | 0.43990 | 0.17579 | 0.16880 | 1.000 |
| H3 | 0.56520 | 0.16610 | 0.21540 | 1.000 |
| C4 | 0.38180 | 0.22417 | 0.08010 | 1.000 |
| C5 | 0.18480 | 0.23873 | 0.00260 | 1.000 |
| H5 | 0.15270 | 0.27150 | -0.05860 | 1.000 |
| C6 | 0.04850 | 0.20644 | 0.01650 | 1.000 |
| H6 | -0.07700 | 0.21560 | -0.03210 | 1.000 |
| C7 | 0.53250 | 0.25979 | 0.06900 | 1.000 |
| H7A | 0.56990 | 0.28550 | 0.16030 | 1.000 |
| H7B | 0.48910 | 0.28010 | -0.03370 | 1.000 |
| H7C | 0.63680 | 0.23710 | 0.07320 | 1.000 |

Table B.19. Bond angles in trans-[Co^{II}(dmf)₄(OTs)₂] (°).

| | | | |
|---------------------------------------|----------|-------------|------------|
| O1 ⁱ —Co1—O1 | 180.0 | O1B—C1B—N1B | 118.6(2) |
| O1 ⁱ —Co1—O1B | 92.44(6) | C1B—N1B—C3B | 115.32(19) |
| O1—Co1—O1B | 87.56(6) | C1B—N1B—C2B | 123.70(18) |
| O1 ⁱ —Co1—O1B ⁱ | 87.56(6) | C3B—N1B—C2B | 120.94(16) |
| O1—Co1—O1B ⁱ | 92.44(6) | S1—O1—Co1 | 134.14(9) |
| O1B—Co1—O1B ⁱ | 180.0 | O2—S1—O1 | 108.48(9) |

| | | | |
|--|------------|----------|------------|
| O1 ⁱ —Co1—O1A | 96.26(6) | O2—S1—O3 | 116.47(10) |
| O1—Co1—O1A | 83.74(6) | O1—S1—O3 | 114.94(9) |
| O1B—Co1—O1A | 94.74(6) | O2—S1—C1 | 98.36(10) |
| O1B ⁱ —Co1—O1A | 85.26(6) | O1—S1—C1 | 104.55(9) |
| O1 ⁱ —Co1—O1A ⁱ | 83.74(6) | O3—S1—C1 | 112.21(10) |
| O1—Co1—O1A ⁱ | 96.26(6) | C6—C1—C2 | 123.55(19) |
| O1B—Co1—O1A ⁱ | 85.26(6) | C6—C1—S1 | 114.81(17) |
| O1B ⁱ —Co1—O1A ⁱ | 94.74(6) | C2—C1—S1 | 121.62(16) |
| O1A—Co1—O1A ⁱ | 180.0 | C3—C2—C1 | 121.3(2) |
| C1A—O1A—Co1 | 130.95(13) | C2—C3—C4 | 115.8(2) |
| O1A—C1A—N1A | 129.54(18) | C3—C4—C5 | 122.3(2) |
| C3A—N1A—C1A | 120.97(18) | C3—C4—C7 | 114.9(2) |
| C3A—N1A—C2A | 110.98(18) | C5—C4—C7 | 122.8(2) |
| C1A—N1A—C2A | 127.85(17) | C6—C5—C4 | 122.3(2) |
| C1B—O1B—Co1 | 118.44(14) | C5—C6—C1 | 114.8(2) |

Symmetry code: (i) -x, -y, -z.

Table B.20. Bond lengths in trans-[Co^{II}(dmf)₄(OTs)₂] (Å).

| | | | |
|----------------------|------------|---------|------------|
| Co1—O1 ⁱ | 2.0281(14) | N1B—C2B | 1.578(3) |
| Co1—O1 | 2.0282(14) | O1—S1 | 1.4903(15) |
| Co1—O1B | 2.0487(14) | O2—S1 | 1.3670(15) |
| Co1—O1B ⁱ | 2.0487(14) | O3—S1 | 1.5790(18) |
| Co1—O1A | 2.2310(16) | S1—C1 | 1.743(2) |
| Co1—O1A ⁱ | 2.2310(16) | C1—C6 | 1.401(3) |

| | | | |
|---------|----------|-------|----------|
| O1A—C1A | 1.305(3) | C1—C2 | 1.489(3) |
| C1A—N1A | 1.435(3) | C2—C3 | 1.370(3) |
| N1A—C3A | 1.414(3) | C3—C4 | 1.404(3) |
| N1A—C2A | 1.510(3) | C4—C5 | 1.493(3) |
| O1B—C1B | 1.254(3) | C4—C7 | 1.501(3) |
| C1B—N1B | 1.294(3) | C5—C6 | 1.371(3) |
| N1B—C3B | 1.473(3) | | |

Symmetry code: (i) -x, -y, -z.

Table B.21. Single crystal X-ray diffraction experimental details for [Ni^{II}(dmf)₆][OTs]₂.

| | |
|-----------------------------|---|
| Chemical formula | C ₃₂ H ₅₆ N ₆ NiO ₁₂ S ₂ |
| M_r | 839.66 |
| Crystal system, space group | Monoclinic, $P2_1/c$ |
| Temperature (K) | 100 |
| a, b, c (Å) | 9.5355(7), 22.6964(14), 9.3886(6) |
| β (°) | 94.884(4) |
| V (Å ³) | 2024.5(2) |
| Z | 2 |
| Radiation type | Mo K α $\lambda = 0.71073$ Å |
| μ (mm ⁻¹) | 0.65 |
| Crystal size (mm) | 0.20 × 0.17 × 0.08 |

| | |
|--|-------------------------------|
| Diffractometer | Bruker APEX-II CCD |
| Absorption correction | Multi-scan SADABS v2008/1 |
| T_{\min} , T_{\max} | 0.882, 0.948 |
| No. of measured, independent, and observed [$I > 2\sigma(I)$] reflections | 29822, 4168, 3307 |
| R_{int} | 0.061 |
| $(\sin \theta/\lambda)_{\text{max}}$ (\AA^{-1}) | 0.627 |
| $R[F^2 > 2\sigma(F^2)]$, $wR(F^2)$, S | 0.032, 0.077, 1.02 |
| No. of reflections | 4168 |
| No. of parameters | 248 |
| H-atom treatment | H-atom parameters constrained |
| Largest diff. peak/hole ($e \text{\AA}^{-3}$) | 0.27, -0.48 |

Table B.22. Atom Coordinates for $[\text{Ni}^{\text{II}}(\text{dmf})_6][\text{OTs}]_2$.

| Atom | x | y | z | Occupancy |
|------|---------|---------|---------|-----------|
| Ni1 | 0.50000 | 1.00000 | 0.50000 | 1.000 |
| O1 | 0.38052 | 0.92500 | 0.50490 | 1.000 |
| O2 | 0.35190 | 1.05043 | 0.59165 | 1.000 |
| O3 | 0.59374 | 0.98217 | 0.69904 | 1.000 |
| N1 | 0.28005 | 0.84326 | 0.40125 | 1.000 |

| | | | | |
|-----|----------|---------|---------|-------|
| N2 | 0.13254 | 1.06424 | 0.66240 | 1.000 |
| N3 | 0.60389 | 0.94149 | 0.91979 | 1.000 |
| C1 | 0.34890 | 0.89348 | 0.39800 | 1.000 |
| H1 | 0.37640 | 0.90660 | 0.30840 | 1.000 |
| C2 | 0.23120 | 0.82042 | 0.53310 | 1.000 |
| H2A | 0.27610 | 0.84230 | 0.61460 | 1.000 |
| H2B | 0.25570 | 0.77860 | 0.54280 | 1.000 |
| H2C | 0.12880 | 0.82500 | 0.53070 | 1.000 |
| C3 | 0.23910 | 0.80972 | 0.27120 | 1.000 |
| H3A | 0.28370 | 0.82700 | 0.19070 | 1.000 |
| H3B | 0.13660 | 0.81100 | 0.25150 | 1.000 |
| H3C | 0.26960 | 0.76870 | 0.28450 | 1.000 |
| C4 | 0.23410 | 1.03128 | 0.61654 | 1.000 |
| H4 | 0.21590 | 0.99050 | 0.60170 | 1.000 |
| C5 | 0.15230 | 1.12690 | 0.68940 | 1.000 |
| H5A | 0.25110 | 1.13730 | 0.68160 | 1.000 |
| H5B | 0.12670 | 1.13620 | 0.78580 | 1.000 |
| H5C | 0.09230 | 1.14940 | 0.61900 | 1.000 |
| C6 | -0.00450 | 1.03953 | 0.68530 | 1.000 |
| H6A | -0.00070 | 0.99650 | 0.67720 | 1.000 |
| H6B | -0.07520 | 1.05510 | 0.61320 | 1.000 |
| H6C | -0.02980 | 1.05030 | 0.78090 | 1.000 |
| C7 | 0.54270 | 0.95064 | 0.79059 | 1.000 |

| | | | | |
|-----|----------|---------|---------|-------|
| H7 | 0.45460 | 0.93220 | 0.76560 | 1.000 |
| C8 | 0.54300 | 0.90239 | 1.02060 | 1.000 |
| H8A | 0.45090 | 0.88860 | 0.97950 | 1.000 |
| H8B | 0.53180 | 0.92370 | 1.10970 | 1.000 |
| H8C | 0.60540 | 0.86850 | 1.04040 | 1.000 |
| C9 | 0.74050 | 0.96744 | 0.96580 | 1.000 |
| H9A | 0.76780 | 0.99500 | 0.89270 | 1.000 |
| H9B | 0.81120 | 0.93620 | 0.97950 | 1.000 |
| H9C | 0.73410 | 0.98860 | 1.05610 | 1.000 |
| S1 | 0.13959 | 0.87511 | 0.89540 | 1.000 |
| O4 | 0.12234 | 0.90205 | 1.03325 | 1.000 |
| O5 | 0.24047 | 0.82679 | 0.90508 | 1.000 |
| O6 | 0.16511 | 0.91755 | 0.78467 | 1.000 |
| C10 | -0.02680 | 0.84278 | 0.84350 | 1.000 |
| C11 | -0.07730 | 0.79888 | 0.92930 | 1.000 |
| H11 | -0.02040 | 0.78480 | 1.01010 | 1.000 |
| C12 | -0.21020 | 0.77585 | 0.89670 | 1.000 |
| H12 | -0.24380 | 0.74610 | 0.95630 | 1.000 |
| C13 | -0.29600 | 0.79512 | 0.77900 | 1.000 |
| C14 | -0.24470 | 0.83887 | 0.69400 | 1.000 |
| H14 | -0.30160 | 0.85290 | 0.61320 | 1.000 |
| C15 | -0.11120 | 0.86235 | 0.72580 | 1.000 |
| H15 | -0.07760 | 0.89210 | 0.66620 | 1.000 |

| | | | | |
|------|----------|---------|---------|-------|
| C16 | -0.44220 | 0.77005 | 0.74660 | 1.000 |
| H16A | -0.46790 | 0.77160 | 0.64340 | 1.000 |
| H16B | -0.50970 | 0.79320 | 0.79640 | 1.000 |
| H16C | -0.44380 | 0.72900 | 0.77910 | 1.000 |

Table B.23. Bond angles in $[\text{Ni}^{\text{II}}(\text{dmf})_6][\text{OTs}]_2$ (°).

| | | | |
|--------------------------------------|------------|-------------|------------|
| O3—Ni1—O3 ⁱ | 180.000(1) | C5—N2—C6 | 117.13(17) |
| O3—Ni1—O1 ⁱ | 89.10(5) | C7—N3—C8 | 121.70(17) |
| O3 ⁱ —Ni1—O1 ⁱ | 90.90(5) | C7—N3—C9 | 121.53(17) |
| O3—Ni1—O1 | 90.90(5) | C8—N3—C9 | 116.67(16) |
| O3 ⁱ —Ni1—O1 | 89.10(5) | O1—C1—N1 | 124.36(17) |
| O1 ⁱ —Ni1—O1 | 180.000(1) | O2—C4—N2 | 124.07(18) |
| O3—Ni1—O2 | 89.43(5) | O3—C7—N3 | 123.78(18) |
| O3 ⁱ —Ni1—O2 | 90.57(5) | O6—S1—O4 | 113.38(9) |
| O1 ⁱ —Ni1—O2 | 87.14(5) | O6—S1—O5 | 113.20(9) |
| O1—Ni1—O2 | 92.86(5) | O4—S1—O5 | 112.67(9) |
| O3—Ni1—O2 ⁱ | 90.57(5) | O6—S1—C10 | 106.10(9) |
| O3 ⁱ —Ni1—O2 ⁱ | 89.43(5) | O4—S1—C10 | 104.58(9) |
| O1 ⁱ —Ni1—O2 ⁱ | 92.86(5) | O5—S1—C10 | 105.99(9) |
| O1—Ni1—O2 ⁱ | 87.14(5) | C15—C10—C11 | 119.01(19) |
| O2—Ni1—O2 ⁱ | 180.00(6) | C15—C10—S1 | 122.10(16) |

| | | | |
|-----------|------------|-------------|------------|
| C1—O1—Ni1 | 123.66(12) | C11—C10—S1 | 118.76(15) |
| C4—O2—Ni1 | 123.06(12) | C12—C11—C10 | 119.9(2) |
| C7—O3—Ni1 | 125.27(13) | C11—C12—C13 | 121.6(2) |
| C1—N1—C2 | 121.63(16) | C12—C13—C14 | 118.0(2) |
| C1—N1—C3 | 121.96(16) | C12—C13—C16 | 120.8(2) |
| C2—N1—C3 | 116.26(16) | C14—C13—C16 | 121.1(2) |
| C4—N2—C5 | 121.45(17) | C15—C14—C13 | 120.8(2) |
| C4—N2—C6 | 121.41(17) | C10—C15—C14 | 120.6(2) |

Symmetry code: (i) $-x + 1, -y + 2, -z + 1$.

Table B.24. Bond lengths in $[\text{Ni}^{\text{II}}(\text{dmf})_6][\text{OTs}]_2$ (Å).

| | | | |
|---------------------|------------|---------|------------|
| Ni1—O3 | 2.0422(13) | N3—C7 | 1.317(2) |
| Ni1—O3 ⁱ | 2.0422(13) | N3—C8 | 1.454(2) |
| Ni1—O1 ⁱ | 2.0510(13) | N3—C9 | 1.461(2) |
| Ni1—O1 | 2.0511(13) | S1—O6 | 1.4529(15) |
| Ni1—O2 | 2.0619(13) | S1—O4 | 1.4534(14) |
| Ni1—O2 ⁱ | 2.0619(13) | S1—O5 | 1.4564(15) |
| O1—C1 | 1.248(2) | S1—C10 | 1.778(2) |
| O2—C4 | 1.245(2) | C10—C15 | 1.384(3) |
| O3—C7 | 1.249(2) | C10—C11 | 1.393(3) |

| | | | |
|-------|----------|---------|----------|
| N1—C1 | 1.317(2) | C11—C12 | 1.381(3) |
| N1—C2 | 1.455(2) | C12—C13 | 1.388(3) |
| N1—C3 | 1.463(2) | C13—C14 | 1.389(3) |
| N2—C4 | 1.324(2) | C13—C16 | 1.513(3) |
| N2—C5 | 1.454(3) | C14—C15 | 1.389(3) |
| N2—C6 | 1.454(3) | | |

Symmetry code: (i) $-x + 1, -y + 2, -z + 1$.

Appendix C. Supplemental Data for Chapter 4.

Table C.1. Single crystal X-ray diffraction experimental details for $(Tp^{Ph})FeCl$.

| | |
|--|------------------------------------|
| Chemical formula | $C_{27}H_{22}BClFeN_6$ |
| M_r | 2130.55 |
| Crystal system, space group | Monoclinic, $P2_1/n$ |
| Temperature (K) | 100 K |
| a, b, c (Å) | 9.5304(15), 15.733(3), 16.641(2) |
| β (°) | 94.281(5) |
| V (Å ³) | 2488.2(7) |
| Z | 1 |
| $F(000)$ | 1098.3109 |
| Radiation type | Mo $K\alpha$ $\lambda = 0.71073$ Å |
| μ (mm ⁻¹) | 0.74 |
| Crystal size (mm) | 0.2x0.2 x0.1 |
| Diffractometer | Bruker APEX-II CCD |
| Absorption correction | none |
| No. of measured, independent and observed [$I > 2\sigma(I)$] reflections | 10399, 1879, 1631 |
| R_{int} | 0.107 |
| θ_{max} (°) | 18.7 |
| $(\sin \theta/\lambda)_{max}$ (Å ⁻¹) | 0.451 |

| | |
|--|--|
| $R[F^2 > 2\sigma(F^2)], wR(F^2), S$ | 0.059, 0.106, 1.11 |
| No. of reflections | 1879 |
| No. of parameters | 328 |
| No. of restraints | 0 |
| No. of constraints | 42 |
| H-atom treatment | H atoms treated by a mixture of independent and constrained refinement |
| Weighting scheme | $w = 1/[\sigma^2(F_o^2) + (0.0223P)^2 + 11.2201P]$ where $P = (F_o^2 + 2F_c^2)/3$ |
| $(\Delta/\sigma)_{\max}$ | < 0.001 |
| Largest diff. peak/hole ($e \text{ \AA}^{-3}$) | 0.65, -0.65 |

Table C.2. Atom Coordinates for $(Tp^{Ph})FeCl$.

| Atom | x | y | z | Occupancy |
|------|---------|---------|---------|-----------|
| Fe1 | 0.26534 | 0.25691 | 0.73936 | 1.000 |
| N3 | 0.56820 | 0.24640 | 0.73430 | 1.000 |
| N4 | 0.47500 | 0.39340 | 0.75680 | 1.000 |
| N6 | 0.47970 | 0.28620 | 0.86890 | 1.000 |
| N7 | 0.44850 | 0.20750 | 0.69840 | 1.000 |
| N11 | 0.34390 | 0.25790 | 0.86010 | 1.000 |
| N30 | 0.33500 | 0.38250 | 0.73160 | 1.000 |
| Cl1 | 0.05382 | 0.21534 | 0.69077 | 1.000 |

| | | | | |
|-----|----------|---------|---------|-------|
| C4 | 0.30610 | 0.23770 | 0.93470 | 1.000 |
| C5 | 0.29080 | 0.45790 | 0.70000 | 1.000 |
| C16 | 0.02390 | 0.12310 | 1.03490 | 1.000 |
| H16 | 0.01690 | 0.08730 | 1.08030 | 1.000 |
| C8 | 0.68110 | 0.21920 | 0.69810 | 1.000 |
| H8 | 0.77570 | 0.23580 | 0.71170 | 1.000 |
| C1 | -0.09620 | 0.14510 | 0.98740 | 1.000 |
| H1 | -0.18570 | 0.12490 | 1.00040 | 1.000 |
| C2 | -0.14170 | 0.51210 | 0.63960 | 1.000 |
| H2 | -0.23810 | 0.52580 | 0.62760 | 1.000 |
| C3 | 0.39300 | 0.10540 | 0.58910 | 1.000 |
| C6 | -0.03980 | 0.54810 | 0.59580 | 1.000 |
| H6 | -0.06640 | 0.58630 | 0.55320 | 1.000 |
| C7 | 0.52350 | 0.28480 | 0.94710 | 1.000 |
| H7 | 0.61380 | 0.30240 | 0.96880 | 1.000 |
| C17 | 0.40120 | 0.51560 | 0.70290 | 1.000 |
| H17 | 0.39960 | 0.57240 | 0.68340 | 1.000 |
| C9 | 0.49320 | 0.15690 | 0.64030 | 1.000 |
| C19 | 0.41880 | 0.25440 | 0.99130 | 1.000 |
| H19 | 0.42190 | 0.24630 | 1.04800 | 1.000 |
| C10 | 0.03660 | 0.43810 | 0.71920 | 1.000 |
| H10 | 0.06190 | 0.40060 | 0.76270 | 1.000 |
| C11 | -0.08440 | 0.19610 | 0.92190 | 1.000 |

| | | | | |
|-----|----------|----------|---------|-------|
| H11 | -0.16640 | 0.21090 | 0.88890 | 1.000 |
| C12 | 0.14180 | 0.47350 | 0.67560 | 1.000 |
| C13 | 0.04430 | 0.22650 | 0.90280 | 1.000 |
| H13 | 0.05030 | 0.26190 | 0.85690 | 1.000 |
| C14 | 0.16600 | 0.20590 | 0.95040 | 1.000 |
| C18 | 0.15340 | 0.15280 | 1.01650 | 1.000 |
| H18 | 0.23520 | 0.13700 | 1.04920 | 1.000 |
| C15 | 0.28220 | 0.06340 | 0.62110 | 1.000 |
| H15 | 0.26890 | 0.06930 | 0.67680 | 1.000 |
| C1a | 0.19010 | 0.01290 | 0.57360 | 1.000 |
| H1a | 0.11440 | -0.01500 | 0.59670 | 1.000 |
| C1b | 0.63700 | 0.16290 | 0.63760 | 1.000 |
| H1b | 0.69390 | 0.13440 | 0.60170 | 1.000 |
| C1c | 0.20880 | 0.00340 | 0.49310 | 1.000 |
| H1c | 0.14640 | -0.03140 | 0.46040 | 1.000 |
| C1d | 0.41130 | 0.09490 | 0.50760 | 1.000 |
| H1d | 0.48750 | 0.12230 | 0.48450 | 1.000 |
| C1e | -0.10280 | 0.45650 | 0.70030 | 1.000 |
| H1e | -0.17280 | 0.43040 | 0.72970 | 1.000 |
| C20 | 0.51390 | 0.47230 | 0.74010 | 1.000 |
| H20 | 0.60530 | 0.49530 | 0.75200 | 1.000 |
| C1f | 0.31940 | 0.04480 | 0.45970 | 1.000 |
| H1f | 0.33190 | 0.03870 | 0.40390 | 1.000 |

| | | | | |
|-----|---------|---------|---------|-------|
| C1g | 0.10070 | 0.52900 | 0.61340 | 1.000 |
| H1g | 0.16980 | 0.55410 | 0.58260 | 1.000 |
| B2 | 0.55750 | 0.31710 | 0.79770 | 1.000 |
| H2a | 0.65300 | 0.33700 | 0.81600 | 1.000 |

Table C.3. Bond angles in $(Tp^{Ph})FeCl$ ($^{\circ}$).

| | | | |
|-------------|------------|-------------|----------|
| N11—Fe1—N7 | 93.9(2) | C1b—C9—C3 | 128.5(7) |
| N30—Fe1—N7 | 93.2(2) | C7—C19—C4 | 104.8(6) |
| N30—Fe1—N11 | 87.7(2) | H19—C19—C4 | 127.6(4) |
| Cl1—Fe1—N7 | 122.36(18) | H19—C19—C7 | 127.6(4) |
| Cl1—Fe1—N11 | 127.17(18) | C12—C10—H10 | 119.4(4) |
| Cl1—Fe1—N30 | 122.75(18) | C1e—C10—H10 | 119.4(4) |
| C8—N3—N7 | 109.1(5) | C1e—C10—C12 | 121.1(6) |
| B2—N3—N7 | 121.2(6) | H11—C11—C1 | 119.4(5) |
| B2—N3—C8 | 129.3(7) | C13—C11—C1 | 121.1(7) |
| C20—N4—N30 | 109.3(5) | C13—C11—H11 | 119.4(4) |
| B2—N4—N30 | 118.7(6) | C10—C12—C5 | 120.4(7) |
| B2—N4—C20 | 131.9(6) | C1g—C12—C5 | 121.6(7) |
| C7—N6—N11 | 108.9(5) | C1g—C12—C10 | 117.7(6) |
| B2—N6—N11 | 122.2(6) | H13—C13—C11 | 119.8(4) |
| B2—N6—C7 | 128.9(7) | C14—C13—C11 | 120.5(6) |
| N3—N7—Fe1 | 112.2(4) | C14—C13—H13 | 119.8(4) |
| C9—N7—Fe1 | 141.1(5) | C13—C14—C4 | 123.3(7) |

| | | | |
|-------------|----------|-------------|----------|
| C9—N7—N3 | 106.0(5) | C18—C14—C4 | 118.6(7) |
| N6—N11—Fe1 | 112.0(4) | C18—C14—C13 | 118.1(6) |
| C4—N11—Fe1 | 141.0(5) | C14—C18—C16 | 120.7(7) |
| C4—N11—N6 | 107.0(5) | H18—C18—C16 | 119.6(5) |
| N4—N30—Fe1 | 113.8(4) | H18—C18—C14 | 119.6(4) |
| C5—N30—Fe1 | 139.7(5) | H15—C15—C3 | 119.2(4) |
| C5—N30—N4 | 106.0(5) | C1a—C15—C3 | 121.5(7) |
| C19—C4—N11 | 109.3(6) | C1a—C15—H15 | 119.2(5) |
| C14—C4—N11 | 123.4(7) | H1a—C1a—C15 | 120.1(5) |
| C14—C4—C19 | 127.3(7) | C1c—C1a—C15 | 119.7(7) |
| C17—C5—N30 | 110.3(6) | C1c—C1a—H1a | 120.1(4) |
| C12—C5—N30 | 121.4(6) | C9—C1b—C8 | 105.7(6) |
| C12—C5—C17 | 128.0(7) | H1b—C1b—C8 | 127.2(4) |
| C1—C16—H16 | 119.8(5) | H1b—C1b—C9 | 127.2(4) |
| C18—C16—H16 | 119.8(5) | H1c—C1c—C1a | 120.1(4) |
| C18—C16—C1 | 120.4(7) | C1f—C1c—C1a | 119.8(7) |
| H8—C8—N3 | 125.7(4) | C1f—C1c—H1c | 120.1(4) |
| C1b—C8—N3 | 108.7(6) | H1d—C1d—C3 | 119.7(4) |
| C1b—C8—H8 | 125.7(4) | C1f—C1d—C3 | 120.6(6) |
| H1—C1—C16 | 120.4(5) | C1f—C1d—H1d | 119.7(4) |
| C11—C1—C16 | 119.2(7) | C10—C1e—C2 | 120.6(7) |
| C11—C1—H1 | 120.4(5) | H1e—C1e—C2 | 119.7(5) |
| C6—C2—H2 | 120.3(5) | H1e—C1e—C10 | 119.7(4) |

| | | | |
|-------------|----------|-------------|----------|
| C1e—C2—H2 | 120.3(5) | C17—C20—N4 | 109.5(6) |
| C1e—C2—C6 | 119.4(7) | H20—C20—N4 | 125.2(4) |
| C15—C3—C9 | 121.3(7) | H20—C20—C17 | 125.2(4) |
| C1d—C3—C9 | 120.5(6) | C1d—C1f—C1c | 120.1(6) |
| C1d—C3—C15 | 118.2(6) | H1f—C1f—C1c | 119.9(4) |
| H6—C6—C2 | 119.7(5) | H1f—C1f—C1d | 119.9(4) |
| C1g—C6—C2 | 120.5(7) | C12—C1g—C6 | 120.6(7) |
| C1g—C6—H6 | 119.7(5) | H1g—C1g—C6 | 119.7(5) |
| H7—C7—N6 | 125.0(4) | H1g—C1g—C12 | 119.7(4) |
| C19—C7—N6 | 110.0(6) | N4—B2—N3 | 108.2(6) |
| C19—C7—H7 | 125.0(4) | N6—B2—N3 | 111.2(6) |
| H17—C17—C5 | 127.6(4) | N6—B2—N4 | 109.0(6) |
| C20—C17—C5 | 104.8(6) | H2a—B2—N3 | 109(3) |
| C20—C17—H17 | 127.6(4) | H2a—B2—N4 | 108(3) |
| C3—C9—N7 | 120.9(6) | H2a—B2—N6 | 111(3) |
| C1b—C9—N7 | 110.6(6) | | |

Table C.4. Bond lengths in (Tp^{Ph})FeCl (Å).

| | | | |
|---------|------------|---------|----------|
| Fe1—N7 | 2.072(5) | C6—H6 | 0.9500 |
| Fe1—N11 | 2.091(6) | C6—C1g | 1.382(9) |
| Fe1—N30 | 2.091(6) | C7—H7 | 0.9500 |
| Fe1—Cl1 | 2.2141(19) | C7—C19 | 1.370(9) |
| N3—N7 | 1.390(7) | C17—H17 | 0.9500 |

| | | | |
|---------|-----------|---------|-----------|
| N3—C8 | 1.342(8) | C17—C20 | 1.379(9) |
| N3—B2 | 1.543(10) | C9—C1b | 1.377(9) |
| N4—N30 | 1.379(7) | C19—H19 | 0.9500 |
| N4—C20 | 1.330(8) | C10—H10 | 0.9500 |
| N4—B2 | 1.563(10) | C10—C12 | 1.397(9) |
| N6—N11 | 1.366(7) | C10—C1e | 1.373(9) |
| N6—C7 | 1.337(8) | C11—H11 | 0.9500 |
| N6—B2 | 1.523(10) | C11—C13 | 1.375(9) |
| N7—C9 | 1.345(8) | C12—C1g | 1.388(9) |
| N11—C4 | 1.356(8) | C13—H13 | 0.9500 |
| N30—C5 | 1.352(8) | C13—C14 | 1.392(9) |
| C4—C19 | 1.400(9) | C14—C18 | 1.393(9) |
| C4—C14 | 1.468(9) | C18—H18 | 0.9500 |
| C5—C17 | 1.387(9) | C15—H15 | 0.9500 |
| C5—C12 | 1.469(9) | C15—C1a | 1.386(9) |
| C16—H16 | 0.9500 | C1a—H1a | 0.9500 |
| C16—C1 | 1.385(10) | C1a—C1c | 1.373(10) |
| C16—C18 | 1.375(9) | C1b—H1b | 0.9500 |
| C8—H8 | 0.9500 | C1c—H1c | 0.9500 |
| C8—C1b | 1.381(9) | C1c—C1f | 1.390(9) |
| C1—H1 | 0.9500 | C1d—H1d | 0.9500 |
| C1—C11 | 1.366(9) | C1d—C1f | 1.386(9) |
| C2—H2 | 0.9500 | C1e—H1e | 0.9500 |

| | | | |
|--------|-----------|---------|---------|
| C2—C6 | 1.378(10) | C20—H20 | 0.9500 |
| C2—C1e | 1.367(10) | C1f—H1f | 0.9500 |
| C3—C9 | 1.474(9) | C1g—H1g | 0.9500 |
| C3—C15 | 1.386(9) | B2—H2a | 0.99(6) |
| C3—C1d | 1.391(9) | | |

Table C.5. Single crystal X-ray diffraction experimental details for (Tp^{Ph})Fe(thf)Cl.

| | |
|------------------------------------|---|
| Chemical formula | C ₃₁ H ₂₉ BClFeN ₆ O |
| <i>M_r</i> | 603.74 |
| Crystal system, space group | Monoclinic, <i>C2/c</i> |
| Temperature (K) | 100 |
| <i>a</i> , <i>b</i> , <i>c</i> (Å) | 18.2420(5), 14.6476(4), 22.9043(8) |
| β (°) | 110.319(1) |
| <i>V</i> (Å ³) | 5739.2(3) |
| <i>Z</i> | 8 |
| <i>F</i> (000) | 2508.7906 |
| Radiation type | Mo K α λ = 0.71073 Å |
| μ (mm ⁻¹) | 0.66 |
| Crystal size (mm) | 0.44 × 0.30 × 0.28 |
| Diffractometer | Bruker APEX-II CCD |
| Absorption correction | none |

| | |
|--|---|
| No. of measured, independent and observed [$I > 2\sigma(I)$] reflections | 89293, 15182, 12271 |
| R_{int} | 0.044 |
| θ values ($^{\circ}$) | $\theta_{\text{max}} = 41.4$, $\theta_{\text{min}} = 1.8$ |
| $(\sin \theta/\lambda)_{\text{max}}$ (\AA^{-1}) | 0.930 |
| $R[F^2 > 2\sigma(F^2)]$, $wR(F^2)$, S | 0.034, 0.103, 1.02 |
| No. of reflections | 15182 |
| No. of parameters | 370 |
| No. of restraints | 0 |
| No. of constraints | 55 |
| H-atom treatment | H-atom parameters constrained |
| Weighting scheme | $w = 1/[\sigma^2(F_o^2) + (0.0584P)^2 + 2.1213P]$ where $P = (F_o^2 + 2F_c^2)/3$ |
| $(\Delta/\sigma)_{\text{max}}$ | 0.0001 |
| Largest diff. peak/hole ($e \text{\AA}^{-3}$) | 1.06, -0.85 |

Table C.6. Atom coordinates for $(\text{Tp}^{\text{Ph}})\text{Fe}(\text{thf})\text{Cl}$.

| Atom | x | y | z | Occupancy |
|------|---------|---------|---------|-----------|
| Fe1 | 0.36691 | 0.65885 | 0.34517 | 1.000 |
| Cl1 | 0.49241 | 0.61540 | 0.35735 | 1.000 |
| N5 | 0.34884 | 0.54390 | 0.40013 | 1.000 |
| N6 | 0.29934 | 0.56959 | 0.42710 | 1.000 |
| N1 | 0.35299 | 0.75487 | 0.40727 | 1.000 |

| | | | | |
|-----|---------|---------|---------|-------|
| N2 | 0.28509 | 0.74062 | 0.41664 | 1.000 |
| C3 | 0.37592 | 0.84220 | 0.42431 | 1.000 |
| C21 | 0.38749 | 0.46792 | 0.43036 | 1.000 |
| C1 | 0.26548 | 0.81724 | 0.43827 | 1.000 |
| C19 | 0.30871 | 0.51220 | 0.47405 | 1.000 |
| C2 | 0.32167 | 0.88375 | 0.44390 | 1.000 |
| C20 | 0.36492 | 0.44650 | 0.47822 | 1.000 |
| N3 | 0.23975 | 0.64279 | 0.29409 | 1.000 |
| N4 | 0.19642 | 0.63869 | 0.32835 | 1.000 |
| C22 | 0.43937 | 0.41314 | 0.41032 | 1.000 |
| C10 | 0.11685 | 0.62907 | 0.29020 | 1.000 |
| C11 | 0.10744 | 0.62726 | 0.22956 | 1.000 |
| C4 | 0.44797 | 0.88359 | 0.42203 | 1.000 |
| C12 | 0.18634 | 0.63558 | 0.23401 | 1.000 |
| B1 | 0.23922 | 0.64873 | 0.40015 | 1.000 |
| C27 | 0.42365 | 0.40843 | 0.34767 | 1.000 |
| C26 | 0.47103 | 0.35422 | 0.32851 | 1.000 |
| O1 | 0.35418 | 0.77054 | 0.28133 | 1.000 |
| C23 | 0.50267 | 0.36059 | 0.45377 | 1.000 |
| C13 | 0.21241 | 0.63747 | 0.18358 | 1.000 |
| C9 | 0.51179 | 0.83062 | 0.42272 | 1.000 |
| C24 | 0.54964 | 0.30574 | 0.43436 | 1.000 |
| C25 | 0.53439 | 0.30307 | 0.37205 | 1.000 |

| | | | | |
|-----|---------|---------|---------|-------|
| C14 | 0.16702 | 0.68635 | 0.12942 | 1.000 |
| C28 | 0.29345 | 0.84254 | 0.26269 | 1.000 |
| C31 | 0.41189 | 0.78864 | 0.25544 | 1.000 |
| C8 | 0.57858 | 0.87158 | 0.41939 | 1.000 |
| C6 | 0.52118 | 1.01938 | 0.41834 | 1.000 |
| C5 | 0.45344 | 0.97888 | 0.42014 | 1.000 |
| C15 | 0.19173 | 0.69003 | 0.08183 | 1.000 |
| C7 | 0.58327 | 0.96605 | 0.41701 | 1.000 |
| C18 | 0.28245 | 0.59154 | 0.18933 | 1.000 |
| C30 | 0.39611 | 0.88653 | 0.23329 | 1.000 |
| C29 | 0.30444 | 0.89471 | 0.21187 | 1.000 |
| C17 | 0.30736 | 0.59555 | 0.14168 | 1.000 |
| C16 | 0.26188 | 0.64490 | 0.08806 | 1.000 |
| H23 | 0.51137 | 0.36481 | 0.49705 | 1.000 |
| H24 | 0.59079 | 0.27124 | 0.46275 | 1.000 |
| H25 | 0.56642 | 0.26636 | 0.35648 | 1.000 |
| H26 | 0.46240 | 0.34965 | 0.28525 | 1.000 |
| H27 | 0.38168 | 0.44146 | 0.31899 | 1.000 |
| H5 | 0.41059 | 1.01576 | 0.42010 | 1.000 |
| H6 | 0.52509 | 1.08404 | 0.41800 | 1.000 |
| H7 | 0.62903 | 0.99408 | 0.41448 | 1.000 |
| H8 | 0.62130 | 0.83501 | 0.41873 | 1.000 |
| H9 | 0.50940 | 0.76604 | 0.42549 | 1.000 |

| | | | | |
|------|---------|---------|---------|-------|
| H18 | 0.31071 | 0.55891 | 0.22611 | 1.000 |
| H17 | 0.35445 | 0.56617 | 0.14329 | 1.000 |
| H16 | 0.28019 | 0.64758 | 0.05401 | 1.000 |
| H15 | 0.16320 | 0.72195 | 0.04479 | 1.000 |
| H14 | 0.11985 | 0.71573 | 0.12761 | 1.000 |
| H1 | 0.21965 | 0.82543 | 0.44843 | 1.000 |
| H19 | 0.28012 | 0.51581 | 0.50163 | 1.000 |
| H2 | 0.32223 | 0.94471 | 0.45822 | 1.000 |
| H20 | 0.38284 | 0.39846 | 0.50762 | 1.000 |
| H10 | 0.07508 | 0.62445 | 0.30582 | 1.000 |
| H11 | 0.06126 | 0.62195 | 0.19400 | 1.000 |
| H1a | 0.19936 | 0.64723 | 0.42105 | 1.000 |
| H28a | 0.24075 | 0.81463 | 0.24872 | 1.000 |
| H28b | 0.29850 | 0.88318 | 0.29842 | 1.000 |
| H31 | 0.45158 | 0.74887 | 0.25248 | 1.000 |
| H30a | 0.42191 | 0.92985 | 0.26744 | 1.000 |
| H30b | 0.41468 | 0.89839 | 0.19820 | 1.000 |
| H29a | 0.27800 | 0.86596 | 0.17079 | 1.000 |
| H29b | 0.28698 | 0.95884 | 0.21109 | 1.000 |

Table C.7. Bond angles in (Tp^{Ph})Fe(thf)Cl (°).

| | | | |
|------------|-----------|-------------|-----------|
| N5—Fe1—Cl1 | 93.42(2) | C23—C22—C21 | 122.20(8) |
| N1—Fe1—Cl1 | 117.25(2) | C23—C22—C27 | 121.31(8) |

| | | | |
|------------|------------|-------------|------------|
| N1—Fe1—N5 | 92.77(3) | C11—C10—N4 | 112.10(7) |
| N3—Fe1—Cl1 | 148.21(2) | C12—C11—C10 | 99.39(9) |
| N3—Fe1—N5 | 83.30(3) | C9—C4—C3 | 121.68(8) |
| N3—Fe1—N1 | 94.52(3) | C5—C4—C3 | 119.20(9) |
| O1—Fe1—Cl1 | 99.257(19) | C5—C4—C9 | 119.11(9) |
| O1—Fe1—N5 | 166.06(3) | C11—C12—N3 | 115.18(7) |
| O1—Fe1—N1 | 86.59(3) | C13—C12—N3 | 119.76(8) |
| O1—Fe1—N3 | 82.87(3) | C13—C12—C11 | 125.06(9) |
| N6—N5—Fe1 | 108.34(5) | N2—B1—N6 | 107.43(7) |
| C21—N5—Fe1 | 139.45(5) | N4—B1—N6 | 111.73(7) |
| C21—N5—N6 | 108.20(6) | N4—B1—N2 | 111.45(7) |
| C19—N6—N5 | 106.45(7) | C26—C27—C22 | 116.49(9) |
| B1—N6—N5 | 121.86(7) | C25—C26—C27 | 121.84(9) |
| B1—N6—C19 | 131.48(7) | C28—O1—Fe1 | 129.09(5) |
| N2—N1—Fe1 | 110.03(5) | C31—O1—Fe1 | 120.77(6) |
| C3—N1—Fe1 | 137.26(5) | C31—O1—C28 | 109.88(7) |
| C3—N1—N2 | 107.99(7) | C24—C23—C22 | 122.04(9) |
| C1—N2—N1 | 108.13(7) | C14—C13—C12 | 118.02(9) |
| B1—N2—N1 | 122.78(6) | C18—C13—C12 | 118.18(9) |
| B1—N2—C1 | 129.01(7) | C18—C13—C14 | 123.80(8) |
| C2—C3—N1 | 109.15(8) | C8—C9—C4 | 120.38(10) |
| C4—C3—N1 | 124.71(8) | C25—C24—C23 | 116.07(10) |
| C4—C3—C2 | 126.13(8) | C24—C25—C26 | 122.24(8) |

| | | | |
|-------------|-----------|-------------|------------|
| C20—C21—N5 | 110.77(7) | C15—C14—C13 | 118.64(11) |
| C22—C21—N5 | 125.08(7) | C29—C28—O1 | 107.80(8) |
| C22—C21—C20 | 123.90(8) | C30—C31—O1 | 103.74(8) |
| C2—C1—N2 | 110.06(8) | C7—C8—C9 | 120.11(11) |
| C20—C19—N6 | 112.30(7) | C7—C6—C5 | 120.28(10) |
| C1—C2—C3 | 104.67(8) | C6—C5—C4 | 120.12(11) |
| C19—C20—C21 | 102.24(8) | C16—C15—C14 | 117.29(11) |
| N4—N3—Fe1 | 115.60(6) | C6—C7—C8 | 119.95(10) |
| C12—N3—Fe1 | 141.01(5) | C17—C18—C13 | 117.54(11) |
| C12—N3—N4 | 103.39(7) | C29—C30—C31 | 103.53(8) |
| C10—N4—N3 | 109.94(7) | C30—C29—C28 | 97.83(8) |
| B1—N4—N3 | 116.52(7) | C16—C17—C18 | 118.18(11) |
| B1—N4—C10 | 133.49(7) | C17—C16—C15 | 124.54(9) |
| C27—C22—C21 | 116.39(8) | | |

Table C.8. Bond lengths in $(Tp^{Ph})Fe(thf)Cl$ (Å).

| | | | |
|---------|------------|---------|------------|
| Fe1—Cl1 | 2.2979(3) | C10—C11 | 1.3392(13) |
| Fe1—N5 | 2.1947(7) | C11—C12 | 1.4123(13) |
| Fe1—N1 | 2.0778(7) | C4—C9 | 1.3947(14) |
| Fe1—N3 | 2.2182(8) | C4—C5 | 1.4011(13) |
| Fe1—O1 | 2.1524(6) | C12—C13 | 1.3940(11) |
| N5—N6 | 1.3136(9) | C27—C26 | 1.3542(12) |
| N5—C21 | 1.3697(11) | C26—C25 | 1.4461(16) |

| | | | |
|---------|------------|---------|------------|
| N6—C19 | 1.3285(11) | O1—C28 | 1.4810(12) |
| N6—B1 | 1.5677(12) | O1—C31 | 1.4012(10) |
| N1—N2 | 1.3448(10) | C23—C24 | 1.3572(12) |
| N1—C3 | 1.3602(11) | C13—C14 | 1.4225(15) |
| N2—C1 | 1.3251(11) | C13—C18 | 1.4089(14) |
| N2—B1 | 1.5604(12) | C9—C8 | 1.3837(14) |
| C3—C2 | 1.3637(12) | C24—C25 | 1.3566(15) |
| C3—C4 | 1.4646(13) | C14—C15 | 1.3174(13) |
| C21—C20 | 1.3354(11) | C28—C29 | 1.4633(13) |
| C21—C22 | 1.4323(11) | C31—C30 | 1.5148(14) |
| C1—C2 | 1.3873(13) | C8—C7 | 1.3887(17) |
| C19—C20 | 1.3851(13) | C6—C5 | 1.3843(15) |
| N3—N4 | 1.2942(9) | C6—C7 | 1.3848(19) |
| N3—C12 | 1.3867(12) | C15—C16 | 1.403(2) |
| N4—C10 | 1.4177(13) | C18—C17 | 1.3212(13) |
| N4—B1 | 1.5633(13) | C30—C29 | 1.5754(16) |
| C22—C27 | 1.3640(13) | C17—C16 | 1.418(2) |
| C22—C23 | 1.4554(14) | | |

Table C.9. Single crystal X-ray diffraction experimental details for (Tp^{Ph})Fe(phpy)Cl•solvent.

| | |
|-----------------------------|---|
| Chemical formula | C ₃₇ H ₃₀ BCl ₃ FeN ₈ |
| <i>M_r</i> | 759.73 |
| Crystal system, space group | Triclinic, <i>P</i> 1 |

| | |
|---|--|
| Temperature (K) | 100 |
| a, b, c (Å) | 12.004(3), 12.117(3), 13.617(4) |
| α, β, γ (°) | 81.334(14), 82.298(14), 68.116(15) |
| V (Å ³) | 1810.4(9) |
| Z | 2 |
| $F(000)$ | 781.8104 |
| Radiation type | Mo $K\alpha$ $\lambda = 0.71073$ Å |
| μ (mm ⁻¹) | 0.68 |
| Crystal size (mm) | 0.28 × 0.18 × 0.17 |
| Diffractometer | Bruker APEX-II CCD |
| Absorption correction | none |
| No. of measured, independent and observed [$I > 2\sigma(I)$] reflections | 52898, 11011, 6997 |
| R_{int} | 0.208 |
| θ values (°) | $\theta_{\text{max}} = 31.0$, $\theta_{\text{min}} = 1.8$ |
| $(\sin \theta/\lambda)_{\text{max}}$ (Å ⁻¹) | 0.725 |
| $R[F^2 > 2\sigma(F^2)]$, $wR(F^2)$, S | 0.121, 0.425, 1.48 |
| No. of reflections | 11011 |
| No. of parameters | 436 |
| No. of restraints | 0 |
| No. of constraints | 60 |
| H-atom treatment | H-atom parameters constrained |

| | |
|--|--------------------------------------|
| Weighting scheme | $w = 1/[\sigma^2(F_o^2) + (0.2P)^2]$ |
| | where $P = (F_o^2 + 2F_c^2)/3$ |
| $(\Delta/\sigma)_{\max}$ | 15.000 |
| Largest diff. peak/hole ($e \text{ \AA}^{-3}$) | 2.84, -9.54 |

Table C.10. Atom coordinates for in $(Tp^{Ph})Fe(phpy)Cl \cdot \text{solvent}$.

| Atom | x | y | z | Occupancy |
|------|---------|---------|---------|-----------|
| Fe1 | 0.57646 | 0.27188 | 0.27213 | 1.000 |
| Cl2 | 0.71636 | 0.22887 | 0.13566 | 1.000 |
| N6aa | 0.73820 | 0.00200 | 0.29530 | 1.000 |
| H6aa | 0.77350 | 0.01360 | 0.23580 | 1.000 |
| N7aa | 0.36140 | 0.50340 | 0.27830 | 1.000 |
| N8aa | 0.65730 | 0.09050 | 0.34450 | 1.000 |
| N9aa | 0.47690 | 0.46490 | 0.23250 | 1.000 |
| N0ba | 0.41080 | 0.24150 | 0.27970 | 1.000 |
| N1ba | 0.53410 | 0.32730 | 0.41730 | 1.000 |
| N2ba | 0.31300 | 0.31700 | 0.32970 | 1.000 |
| C3ba | 0.72580 | 0.25790 | 0.49310 | 1.000 |
| C1aa | 0.59320 | 0.31180 | 0.49780 | 1.000 |
| C2aa | 0.22240 | 0.27340 | 0.34350 | 1.000 |
| H2aa | 0.14460 | 0.31020 | 0.37570 | 1.000 |
| C3aa | 0.51020 | 0.36020 | 0.57630 | 1.000 |
| H3aa | 0.52740 | 0.36060 | 0.64230 | 1.000 |

| | | | | |
|------|---------|----------|----------|-------|
| C4aa | 0.62540 | 0.03620 | 0.43000 | 1.000 |
| H4aa | 0.56830 | 0.07610 | 0.48050 | 1.000 |
| N5aa | 0.41450 | 0.38730 | 0.44300 | 1.000 |
| C15 | 0.46500 | 0.04970 | 0.21010 | 1.000 |
| C16 | 0.39920 | 0.40680 | 0.54000 | 1.000 |
| H16 | 0.32490 | 0.44580 | 0.57630 | 1.000 |
| C17 | 0.68670 | -0.08600 | 0.43530 | 1.000 |
| H17 | 0.68010 | -0.14400 | 0.48880 | 1.000 |
| C18 | 0.29780 | 0.61360 | 0.23540 | 1.000 |
| H18 | 0.21570 | 0.65880 | 0.25290 | 1.000 |
| C19 | 0.84460 | -0.21860 | 0.31170 | 1.000 |
| C20 | 0.59980 | 0.59050 | 0.00180 | 1.000 |
| H20 | 0.52720 | 0.62070 | -0.03040 | 1.000 |
| C21 | 0.48360 | 0.55410 | 0.16240 | 1.000 |
| C22 | 0.38140 | 0.14880 | 0.26330 | 1.000 |
| C23 | 0.37190 | 0.64930 | 0.16200 | 1.000 |
| H23 | 0.35170 | 0.72280 | 0.11990 | 1.000 |
| B24 | 0.31990 | 0.42750 | 0.36680 | 1.000 |
| H24 | 0.23950 | 0.47620 | 0.39790 | 1.000 |
| C25 | 0.59740 | 0.54970 | 0.10350 | 1.000 |
| C26 | 0.79770 | 0.26850 | 0.40520 | 1.000 |
| H26 | 0.76040 | 0.30920 | 0.34610 | 1.000 |
| C27 | 0.75900 | -0.10680 | 0.34780 | 1.000 |

| | | | | |
|-----|---------|----------|----------|-------|
| C28 | 0.61150 | -0.02540 | 0.07250 | 1.000 |
| H28 | 0.65670 | -0.01100 | 0.01250 | 1.000 |
| C29 | 0.78280 | 0.19740 | 0.57720 | 1.000 |
| H29 | 0.73610 | 0.18810 | 0.63780 | 1.000 |
| C30 | 0.70850 | 0.58750 | -0.05320 | 1.000 |
| H30 | 0.70910 | 0.61450 | -0.12250 | 1.000 |
| C31 | 0.70540 | 0.50920 | 0.14840 | 1.000 |
| H31 | 0.70600 | 0.48310 | 0.21780 | 1.000 |
| C32 | 0.81420 | 0.54550 | -0.00720 | 1.000 |
| H32 | 0.88760 | 0.54350 | -0.04440 | 1.000 |
| C2 | 0.26250 | 0.16720 | 0.30290 | 1.000 |
| H2 | 0.21880 | 0.11630 | 0.30170 | 1.000 |
| C3 | 0.90740 | -0.22150 | 0.21820 | 1.000 |
| H3 | 0.89490 | -0.14980 | 0.17450 | 1.000 |
| C4 | 0.53110 | 0.07110 | 0.12190 | 1.000 |
| H4 | 0.52180 | 0.15080 | 0.09520 | 1.000 |
| C5 | 0.86270 | -0.32460 | 0.37400 | 1.000 |
| H5 | 0.82050 | -0.32410 | 0.43820 | 1.000 |
| C6 | 0.47890 | -0.06760 | 0.24820 | 1.000 |
| H6 | 0.43360 | -0.08300 | 0.30790 | 1.000 |
| C7 | 0.90550 | 0.15070 | 0.57450 | 1.000 |
| H7 | 0.94260 | 0.11050 | 0.63370 | 1.000 |
| C8 | 0.81280 | 0.50650 | 0.09280 | 1.000 |

| | | | | |
|------|---------|----------|----------|-------|
| H8 | 0.88570 | 0.47750 | 0.12450 | 1.000 |
| C9 | 0.55960 | -0.16220 | 0.19850 | 1.000 |
| H9 | 0.56970 | -0.24220 | 0.22500 | 1.000 |
| C11 | 0.98960 | -0.33090 | 0.18860 | 1.000 |
| H11 | 1.03250 | -0.33220 | 0.12460 | 1.000 |
| C12 | 1.00910 | -0.43470 | 0.24940 | 1.000 |
| H12 | 1.06640 | -0.50780 | 0.22910 | 1.000 |
| C1 | 0.62490 | -0.14110 | 0.11120 | 1.000 |
| H1 | 0.67920 | -0.20630 | 0.07770 | 1.000 |
| C0aa | 0.94410 | -0.43230 | 0.34120 | 1.000 |
| H0aa | 0.95480 | -0.50500 | 0.38300 | 1.000 |
| C5aa | 0.92380 | 0.22010 | 0.40250 | 1.000 |
| H5aa | 0.97140 | 0.22860 | 0.34230 | 1.000 |
| C6aa | 0.97780 | 0.16060 | 0.48710 | 1.000 |
| H6ab | 1.06310 | 0.12660 | 0.48640 | 1.000 |
| Cl1 | 0.89910 | -0.20420 | -0.08730 | 1.000 |
| Cl0a | 0.88960 | 0.04230 | -0.13900 | 1.000 |
| C7aa | 0.97510 | -0.10950 | -0.08170 | 1.000 |

Table C.11. Bond angles in (Tp^{Ph})Fe(phpy)Cl·solvent (°).

| | | | |
|---------------|------------|---------------|----------|
| N8aa—Fe1—Cl2 | 91.16(13) | N5aa—C16—C3aa | 107.6(5) |
| N9aa—Fe1—Cl2 | 100.84(12) | C27—C17—C4aa | 106.3(5) |
| N9aa—Fe1—N8aa | 167.29(16) | C23—C18—N7aa | 108.7(5) |

| | | | |
|----------------|------------|---------------|----------|
| N0ba—Fe1—Cl2 | 121.28(13) | C3—C19—C27 | 122.4(5) |
| N0ba—Fe1—N8aa | 88.32(18) | C5—C19—C27 | 118.3(5) |
| N0ba—Fe1—N9aa | 88.96(16) | C5—C19—C3 | 119.3(6) |
| N1ba—Fe1—Cl2 | 147.39(13) | C30—C20—C25 | 120.7(5) |
| N1ba—Fe1—N8aa | 86.62(17) | C23—C21—N9aa | 109.9(5) |
| N1ba—Fe1—N9aa | 81.03(16) | C25—C21—N9aa | 122.2(5) |
| N1ba—Fe1—N0ba | 91.20(17) | C25—C21—C23 | 127.8(5) |
| C27—N6aa—N8aa | 112.3(4) | C15—C22—N0ba | 122.4(5) |
| C18—N7aa—N9aa | 109.5(4) | C2—C22—N0ba | 109.1(5) |
| B24—N7aa—N9aa | 122.1(4) | C2—C22—C15 | 128.5(5) |
| B24—N7aa—C18 | 128.4(5) | C21—C23—C18 | 105.4(5) |
| N6aa—N8aa—Fe1 | 122.1(3) | N2ba—B24—N7aa | 109.4(4) |
| C4aa—N8aa—Fe1 | 131.3(4) | N5aa—B24—N7aa | 107.6(4) |
| C4aa—N8aa—N6aa | 105.2(4) | N5aa—B24—N2ba | 109.3(4) |
| N7aa—N9aa—Fe1 | 112.7(3) | C21—C25—C20 | 121.2(5) |
| C21—N9aa—Fe1 | 139.2(4) | C31—C25—C20 | 117.8(5) |
| C21—N9aa—N7aa | 106.5(4) | C31—C25—C21 | 120.9(5) |
| N2ba—N0ba—Fe1 | 117.2(3) | C5aa—C26—C3ba | 121.2(6) |
| C22—N0ba—Fe1 | 134.3(4) | C17—C27—N6aa | 105.6(5) |
| C22—N0ba—N2ba | 107.0(4) | C19—C27—N6aa | 123.4(5) |
| C1aa—N1ba—Fe1 | 136.7(4) | C19—C27—C17 | 131.0(5) |
| N5aa—N1ba—Fe1 | 115.8(3) | C1—C28—C4 | 120.0(6) |
| N5aa—N1ba—C1aa | 107.3(4) | C7—C29—C3ba | 120.8(7) |

| | | | |
|----------------|----------|---------------|----------|
| C2aa—N2ba—N0ba | 109.8(4) | C32—C30—C20 | 120.2(6) |
| B24—N2ba—N0ba | 120.1(4) | C8—C31—C25 | 120.9(5) |
| B24—N2ba—C2aa | 129.9(5) | C8—C32—C30 | 119.6(6) |
| C26—C3ba—C1aa | 121.8(5) | C22—C2—C2aa | 106.0(5) |
| C29—C3ba—C1aa | 120.2(5) | C11—C3—C19 | 119.7(6) |
| C29—C3ba—C26 | 117.9(6) | C28—C4—C15 | 119.9(6) |
| C3ba—C1aa—N1ba | 121.1(4) | C0aa—C5—C19 | 119.3(6) |
| C3aa—C1aa—N1ba | 108.8(5) | C9—C6—C15 | 119.8(6) |
| C3aa—C1aa—C3ba | 130.0(5) | C6aa—C7—C29 | 121.7(7) |
| C2—C2aa—N2ba | 108.1(5) | C32—C8—C31 | 120.7(6) |
| C16—C3aa—C1aa | 106.8(5) | C1—C9—C6 | 120.7(7) |
| C17—C4aa—N8aa | 110.7(5) | C12—C11—C3 | 121.4(7) |
| C16—N5aa—N1ba | 109.4(4) | C0aa—C12—C11 | 118.8(6) |
| B24—N5aa—N1ba | 121.9(4) | C9—C1—C28 | 120.1(7) |
| B24—N5aa—C16 | 128.6(4) | C12—C0aa—C5 | 121.3(7) |
| C4—C15—C22 | 120.9(5) | C6aa—C5aa—C26 | 119.6(7) |
| C6—C15—C22 | 119.6(5) | C5aa—C6aa—C7 | 118.8(6) |
| C6—C15—C4 | 119.5(6) | Cl0a—C7aa—Cl1 | 109.8(6) |

Table C.12. Bond lengths in $(Tp^{Ph})Fe(phpy)Cl \cdot \text{solvent}$ (Å).

| | | | |
|----------|------------|---------|----------|
| Fe1—Cl2 | 2.3126(16) | C15—C6 | 1.394(9) |
| Fe1—N8aa | 2.182(5) | C17—C27 | 1.374(8) |
| Fe1—N9aa | 2.213(4) | C18—C23 | 1.376(8) |

| | | | |
|-----------|----------|----------|-----------|
| Fe1—N0ba | 2.140(4) | C19—C27 | 1.469(7) |
| Fe1—N1ba | 2.119(4) | C19—C3 | 1.388(9) |
| N6aa—N8aa | 1.344(6) | C19—C5 | 1.389(8) |
| N6aa—C27 | 1.353(7) | C20—C25 | 1.399(7) |
| N7aa—N9aa | 1.380(6) | C20—C30 | 1.406(9) |
| N7aa—C18 | 1.353(7) | C21—C23 | 1.406(8) |
| N7aa—B24 | 1.547(7) | C21—C25 | 1.476(7) |
| N8aa—C4aa | 1.331(8) | C22—C2 | 1.403(8) |
| N9aa—C21 | 1.348(6) | C25—C31 | 1.394(8) |
| N0ba—N2ba | 1.360(6) | C26—C5aa | 1.403(9) |
| N0ba—C22 | 1.352(7) | C28—C4 | 1.404(9) |
| N1ba—C1aa | 1.337(6) | C28—C1 | 1.378(10) |
| N1ba—N5aa | 1.370(6) | C29—C7 | 1.365(10) |
| N2ba—C2aa | 1.356(7) | C30—C32 | 1.378(10) |
| N2ba—B24 | 1.535(7) | C31—C8 | 1.397(8) |
| C3ba—C1aa | 1.475(7) | C32—C8 | 1.372(9) |
| C3ba—C26 | 1.397(9) | C3—C11 | 1.404(9) |
| C3ba—C29 | 1.379(8) | C5—C0aa | 1.402(9) |
| C1aa—C3aa | 1.396(7) | C6—C9 | 1.393(10) |
| C2aa—C2 | 1.369(9) | C7—C6aa | 1.393(12) |
| C3aa—C16 | 1.367(8) | C9—C1 | 1.379(11) |
| C4aa—C17 | 1.382(8) | C11—C12 | 1.357(10) |
| N5aa—C16 | 1.353(6) | C12—C0aa | 1.381(11) |

| | | | |
|----------|----------|-----------|-----------|
| N5aa—B24 | 1.534(7) | C5aa—C6aa | 1.367(11) |
| C15—C22 | 1.464(8) | Cl1—C7aa | 1.726(11) |
| C15—C4 | 1.394(8) | Cl0a—C7aa | 1.850(11) |

Table C. 13. Single crystal X-ray diffraction experimental details for $(Tp^{Ph})Fe(phpy)Br \cdot CH_2Cl_2$.

| | |
|--|---------------------------------------|
| Chemical formula | $C_{37}H_{32}BCl_2BrFeN_8$ |
| M_r | 806.20 |
| Crystal system, space group | Triclinic, $P1$ |
| Temperature (K) | 100 |
| a, b, c (Å) | 11.8688(4), 12.0462(4), 13.6051(4) |
| α, β, γ (°) | 81.5926(17), 81.4590(17), 68.2233(19) |
| V (Å ³) | 1777.51(10) |
| Z | 1 |
| $F(000)$ | 820.9616 |
| Radiation type | Mo $K\alpha$ $\lambda = 0.71073$ Å |
| μ (mm ⁻¹) | 1.74 |
| Crystal size (mm) | 0.34 × 0.26 × 0.19 |
| Diffractometer | Bruker APEX-II CCD |
| Absorption correction | none |
| No. of measured, independent and observed [$I > 2\sigma(I)$] reflections | 54678, 11896, 9349 |
| R_{int} | 0.085 |

| | |
|--|--|
| θ values ($^{\circ}$) | $\theta_{\max} = 31.9, \theta_{\min} = 1.8$ |
| $(\sin \theta / \lambda)_{\max}$ (\AA^{-1}) | 0.744 |
| $R[F^2 > 2\sigma(F^2)], wR(F^2), S$ | 0.062, 0.174, 1.10 |
| No. of reflections | 11896 |
| No. of parameters | 450 |
| No. of restraints | 0 |
| No. of constraints | 63 |
| H-atom treatment | H-atom parameters constrained |
| Weighting scheme | $w = 1/[\sigma^2(F_o^2) + (0.1P)^2]$ where $P = (F_o^2 + 2F_c^2)/3$ |
| $(\Delta/\sigma)_{\max}$ | 0.005 |
| Largest diff. peak/hole ($e \text{\AA}^{-3}$) | 1.52, -1.04 |

Table C.14. Atom coordinates for $(Tp^{Ph})Fe(phpy)Br \cdot CH_2Cl_2$.

| Atom | x | y | z | Occupancy |
|------|---------|----------|---------|-----------|
| Br1 | 0.26998 | 0.77907 | 0.87772 | 1.000 |
| Fe2 | 0.42251 | 0.73048 | 0.72903 | 1.000 |
| Cl3 | 0.10420 | 0.20103 | 0.08424 | 1.000 |
| Cl4 | 0.10080 | -0.03673 | 0.15688 | 1.000 |
| N5 | 0.68807 | 0.68457 | 0.67016 | 1.000 |
| N6 | 0.46446 | 0.67295 | 0.58342 | 1.000 |
| N7 | 0.63900 | 0.49824 | 0.72149 | 1.000 |

| | | | | |
|-----|----------|---------|---------|-------|
| C8 | 0.40460 | 0.68780 | 0.50290 | 1.000 |
| N9 | 0.52222 | 0.53769 | 0.76850 | 1.000 |
| N10 | 0.34130 | 0.90988 | 0.65573 | 1.000 |
| N11 | 0.58521 | 0.61321 | 0.55533 | 1.000 |
| N12 | 0.25789 | 1.00092 | 0.70441 | 1.000 |
| N13 | 0.58789 | 0.76165 | 0.72077 | 1.000 |
| C14 | 0.23850 | 1.10920 | 0.65100 | 1.000 |
| C15 | 0.51580 | 1.07300 | 0.74890 | 1.000 |
| C16 | 0.15330 | 1.22270 | 0.68680 | 1.000 |
| C17 | 0.73990 | 0.83530 | 0.69760 | 1.000 |
| C18 | 0.29120 | 0.49200 | 0.85230 | 1.000 |
| C19 | 0.39840 | 0.41030 | 0.99950 | 1.000 |
| C20 | 0.31470 | 1.08710 | 0.56300 | 1.000 |
| C21 | -0.00970 | 1.44140 | 0.74810 | 1.000 |
| C22 | 0.46820 | 0.93580 | 0.88090 | 1.000 |
| C23 | 0.18210 | 0.45370 | 1.00940 | 1.000 |
| C24 | 0.36880 | 1.14920 | 0.88770 | 1.000 |
| C25 | 0.51510 | 0.44750 | 0.83810 | 1.000 |
| C26 | 0.13690 | 1.32880 | 0.62360 | 1.000 |
| C27 | 0.37560 | 0.96210 | 0.56940 | 1.000 |
| C28 | 0.59950 | 0.59270 | 0.45830 | 1.000 |
| B29 | 0.68040 | 0.57310 | 0.63230 | 1.000 |
| C30 | 0.08810 | 1.22730 | 0.77970 | 1.000 |

| | | | | |
|-----|----------|---------|---------|-------|
| C31 | 0.77970 | 0.72800 | 0.65590 | 1.000 |
| C32 | 0.39980 | 0.45130 | 0.89790 | 1.000 |
| C33 | 0.00610 | 1.33630 | 0.81100 | 1.000 |
| C34 | 0.28970 | 0.41130 | 1.05520 | 1.000 |
| C35 | 0.07150 | 0.78420 | 0.60440 | 1.000 |
| C36 | 0.61940 | 0.85360 | 0.73720 | 1.000 |
| C37 | 0.38610 | 1.03330 | 0.92920 | 1.000 |
| C38 | 0.08520 | 0.85240 | 0.42960 | 1.000 |
| C39 | 0.62750 | 0.35150 | 0.83760 | 1.000 |
| C40 | 0.18340 | 0.49380 | 0.90880 | 1.000 |
| C41 | 0.26950 | 0.74330 | 0.50960 | 1.000 |
| C42 | 0.43400 | 1.16950 | 0.79830 | 1.000 |
| C43 | 0.21220 | 0.80320 | 0.42450 | 1.000 |
| C44 | 0.70270 | 0.38740 | 0.76300 | 1.000 |
| C45 | 0.53270 | 0.95510 | 0.78980 | 1.000 |
| C46 | 0.48700 | 0.63920 | 0.42240 | 1.000 |
| C47 | 0.06530 | 0.08070 | 0.06170 | 1.000 |
| C48 | 0.05540 | 1.43810 | 0.65510 | 1.000 |
| C49 | 0.19850 | 0.73400 | 0.59900 | 1.000 |
| C50 | 0.01580 | 0.84240 | 0.51890 | 1.000 |
| H49 | 0.23680 | 0.69310 | 0.65720 | 1.000 |
| H35 | 0.02350 | 0.77850 | 0.66600 | 1.000 |
| H50 | -0.07070 | 0.87560 | 0.52190 | 1.000 |

| | | | | |
|-----|----------|---------|---------|-------|
| H38 | 0.04650 | 0.89290 | 0.37150 | 1.000 |
| H43 | 0.25980 | 0.81030 | 0.36290 | 1.000 |
| H19 | 0.47190 | 0.38160 | 1.03060 | 1.000 |
| H34 | 0.28900 | 0.38330 | 1.12420 | 1.000 |
| H23 | 0.10770 | 0.45510 | 1.04730 | 1.000 |
| H40 | 0.10960 | 0.52290 | 0.87810 | 1.000 |
| H18 | 0.29150 | 0.51820 | 0.78300 | 1.000 |
| H22 | 0.48020 | 0.85620 | 0.91010 | 1.000 |
| H37 | 0.34180 | 1.01970 | 0.99100 | 1.000 |
| H24 | 0.31210 | 1.21510 | 0.92060 | 1.000 |
| H42 | 0.42290 | 1.24950 | 0.77050 | 1.000 |
| H15 | 0.56020 | 1.08730 | 0.68740 | 1.000 |
| H30 | 0.09920 | 1.15550 | 0.82290 | 1.000 |
| H33 | -0.03880 | 1.33850 | 0.87500 | 1.000 |
| H21 | -0.06540 | 1.51580 | 0.76920 | 1.000 |
| H48 | 0.04470 | 1.51030 | 0.61240 | 1.000 |
| H26 | 0.18120 | 1.32660 | 0.55930 | 1.000 |
| H12 | 0.22051 | 0.99082 | 0.76406 | 1.000 |
| H17 | 0.78460 | 0.88600 | 0.69910 | 1.000 |
| H20 | 0.32390 | 1.14430 | 0.50960 | 1.000 |
| H27 | 0.43350 | 0.92030 | 0.51890 | 1.000 |
| H28 | 0.67480 | 0.55270 | 0.42120 | 1.000 |
| H29 | 0.76210 | 0.52390 | 0.60070 | 1.000 |

| | | | | |
|------|----------|---------|----------|-------|
| H31 | 0.85850 | 0.69070 | 0.62270 | 1.000 |
| H39 | 0.64740 | 0.27790 | 0.87940 | 1.000 |
| H44 | 0.78560 | 0.34180 | 0.74400 | 1.000 |
| H46 | 0.46920 | 0.63840 | 0.35670 | 1.000 |
| H47a | -0.02320 | 0.10960 | 0.05530 | 1.000 |
| H47b | 0.10940 | 0.05050 | -0.00230 | 1.000 |

Table C.15. Bond Angles in $(Tp^{Ph})Fe(phpy)Br \cdot CH_2Cl_2$ ($^\circ$).

| | | | |
|-------------|------------|-------------|----------|
| N6—Fe2—Br1 | 147.13(6) | C34—C19—C32 | 120.3(2) |
| N9—Fe2—Br1 | 100.81(6) | C27—C20—C14 | 105.5(2) |
| N9—Fe2—N6 | 81.26(8) | C48—C21—C33 | 120.2(3) |
| N10—Fe2—Br1 | 91.44(6) | C45—C22—C37 | 120.1(3) |
| N10—Fe2—N6 | 85.89(8) | C40—C23—C34 | 120.1(3) |
| N10—Fe2—N9 | 166.87(9) | C42—C24—C37 | 120.1(3) |
| N13—Fe2—Br1 | 120.44(6) | C32—C25—N9 | 122.2(2) |
| N13—Fe2—N6 | 92.28(8) | C39—C25—N9 | 110.5(2) |
| N13—Fe2—N9 | 89.16(8) | C39—C25—C32 | 127.2(2) |
| N13—Fe2—N10 | 88.67(8) | C48—C26—C16 | 119.9(3) |
| B29—N5—N13 | 119.96(19) | C20—C27—N10 | 111.0(2) |
| C31—N5—N13 | 109.8(2) | C46—C28—N11 | 108.7(2) |
| C31—N5—B29 | 130.1(2) | N7—B29—N5 | 108.6(2) |
| C8—N6—Fe2 | 137.09(16) | N11—B29—N5 | 109.7(2) |
| N11—N6—Fe2 | 115.84(16) | N11—B29—N7 | 108.7(2) |

| | | | |
|-------------|------------|-------------|----------|
| N11—N6—C8 | 106.7(2) | C33—C30—C16 | 120.8(3) |
| B29—N7—N9 | 121.67(19) | C17—C31—N5 | 108.6(2) |
| C44—N7—N9 | 109.8(2) | C19—C32—C18 | 119.4(2) |
| C44—N7—B29 | 128.5(2) | C25—C32—C18 | 120.1(2) |
| C41—C8—N6 | 120.8(2) | C25—C32—C19 | 120.4(2) |
| C46—C8—N6 | 110.0(2) | C30—C33—C21 | 119.7(3) |
| C46—C8—C41 | 129.2(2) | C23—C34—C19 | 119.7(3) |
| N7—N9—Fe2 | 112.79(15) | C50—C35—C49 | 119.5(3) |
| C25—N9—Fe2 | 139.87(17) | C17—C36—N13 | 110.1(2) |
| C25—N9—N7 | 105.95(19) | C45—C36—N13 | 121.5(2) |
| N12—N10—Fe2 | 122.52(17) | C45—C36—C17 | 128.4(2) |
| C27—N10—Fe2 | 130.77(17) | C24—C37—C22 | 120.4(3) |
| C27—N10—N12 | 105.1(2) | C50—C38—C43 | 120.1(3) |
| C28—N11—N6 | 109.3(2) | C44—C39—C25 | 104.9(2) |
| B29—N11—N6 | 120.7(2) | C23—C40—C18 | 120.7(2) |
| B29—N11—C28 | 129.9(2) | C43—C41—C8 | 119.9(2) |
| C14—N12—N10 | 112.4(2) | C49—C41—C8 | 120.9(2) |
| N5—N13—Fe2 | 116.86(16) | C49—C41—C43 | 119.1(2) |
| C36—N13—Fe2 | 135.50(16) | C24—C42—C15 | 120.1(3) |
| C36—N13—N5 | 106.31(19) | C41—C43—C38 | 120.2(3) |
| C16—C14—N12 | 123.5(2) | C39—C44—N7 | 108.8(2) |
| C20—C14—N12 | 106.0(2) | C22—C45—C15 | 119.2(2) |
| C20—C14—C16 | 130.4(2) | C36—C45—C15 | 119.8(2) |

| | | | |
|-------------|----------|-------------|----------|
| C45—C15—C42 | 120.1(3) | C36—C45—C22 | 121.0(2) |
| C26—C16—C14 | 118.6(2) | C28—C46—C8 | 105.3(2) |
| C30—C16—C14 | 122.0(2) | Cl4—C47—Cl3 | 112.2(2) |
| C30—C16—C26 | 119.3(2) | C26—C48—C21 | 120.1(3) |
| C36—C17—C31 | 105.2(2) | C41—C49—C35 | 120.7(3) |
| C40—C18—C32 | 119.8(3) | C38—C50—C35 | 120.4(2) |

Table C.16. Bond lengths in (TpPh)Fe(phpy)Br·CH₂Cl₂ (°).

| | | | |
|---------|-----------|---------|----------|
| Br1—Fe2 | 2.4869(4) | C16—C30 | 1.378(4) |
| Fe2—N6 | 2.123(2) | C17—C31 | 1.377(4) |
| Fe2—N9 | 2.206(2) | C17—C36 | 1.399(3) |
| Fe2—N10 | 2.169(2) | C18—C32 | 1.402(3) |
| Fe2—N13 | 2.116(2) | C18—C40 | 1.385(4) |
| Cl3—C47 | 1.754(4) | C19—C32 | 1.398(4) |
| Cl4—C47 | 1.743(4) | C19—C34 | 1.392(4) |
| N5—N13 | 1.369(3) | C20—C27 | 1.403(4) |
| N5—B29 | 1.544(4) | C21—C33 | 1.388(4) |
| N5—C31 | 1.350(3) | C21—C48 | 1.378(4) |
| N6—C8 | 1.348(3) | C22—C37 | 1.395(4) |
| N6—N11 | 1.368(3) | C22—C45 | 1.393(4) |
| N7—N9 | 1.376(3) | C23—C34 | 1.393(4) |
| N7—B29 | 1.535(4) | C23—C40 | 1.383(4) |
| N7—C44 | 1.353(3) | C24—C37 | 1.379(4) |

| | | | |
|---------|----------|---------|----------|
| C8—C41 | 1.485(3) | C24—C42 | 1.382(4) |
| C8—C46 | 1.394(4) | C25—C32 | 1.473(3) |
| N9—C25 | 1.352(3) | C25—C39 | 1.404(3) |
| N10—N12 | 1.354(3) | C26—C48 | 1.396(4) |
| N10—C27 | 1.331(3) | C28—C46 | 1.377(4) |
| N11—C28 | 1.352(3) | C30—C33 | 1.394(4) |
| N11—B29 | 1.551(4) | C35—C49 | 1.396(4) |
| N12—C14 | 1.354(3) | C35—C50 | 1.389(4) |
| N13—C36 | 1.349(3) | C36—C45 | 1.473(4) |
| C14—C16 | 1.466(3) | C38—C43 | 1.395(4) |
| C14—C20 | 1.384(4) | C38—C50 | 1.379(4) |
| C15—C42 | 1.394(4) | C39—C44 | 1.379(4) |
| C15—C45 | 1.399(4) | C41—C43 | 1.396(4) |
| C16—C26 | 1.398(4) | C41—C49 | 1.390(4) |

Table C.17. Single crystal X-ray diffraction experimental details for $(Tp^{Ph})CoN_3$.

| | |
|-----------------------------|-------------------------------------|
| Chemical formula | $C_{27}H_{22}BCoN_9$ |
| M_r | 542.27 |
| Crystal system, space group | Monoclinic, $P2_1/c$ |
| Temperature (K) | 100 |
| a, b, c (Å) | 16.2428(13), 9.2163(7), 18.4858(14) |
| β (°) | 114.998(4) |
| V (Å ³) | 2508.1(3) |

| | |
|--|---|
| Z | 4 |
| $F(000)$ | 1116 |
| Radiation type | Mo $K\alpha$ $\lambda = 0.71073 \text{ \AA}$ |
| μ (mm^{-1}) | 0.72 |
| Crystal size (mm) | 0.28 × 0.20 × 0.11 |
| Absorption correction | Multi-scan <i>SADABS2014/5</i> (Bruker,2014/5) was used for absorption correction. $wR2(\text{int})$ was 0.0812 before and 0.0632 after correction. |
| $T_{\text{min}}, T_{\text{max}}$ | 0.687, 0.746 |
| No. of measured, independent and observed [$I > 2\sigma(I)$] reflections | 58659, 8043, 6205 |
| R_{int} | 0.069 |
| θ values ($^{\circ}$) | $\theta_{\text{max}} = 31.2, \theta_{\text{min}} = 2.2$ |
| $(\sin \theta / \lambda)_{\text{max}}$ (\AA^{-1}) | 0.729 |
| $R[F^2 > 2\sigma(F^2)], wR(F^2), S$ | 0.038, 0.095, 1.03 |
| No. of reflections | 8043 |
| No. of parameters | 343 |
| No. of restraints | 0 |
| H-atom treatment | H-atom parameters constrained |
| Weighting scheme | $w = 1/[\sigma^2(F_o^2) + (0.0357P)^2 + 1.3195P]$ where $P = (F_o^2 + 2F_c^2)/3$ |

| | |
|--|-------------|
| $(\Delta/\sigma)_{\max}$ | 0.002 |
| Largest diff. peak/hole ($e \text{ \AA}^{-3}$) | 0.52, -0.42 |

Table C.18. Atom coordinates for $(Tp^{Ph})CoN_3$.

| Atom | x | y | z | Occupancy |
|------|---------|----------|---------|-----------|
| Co1 | 0.27151 | 0.43167 | 0.33983 | 1.000 |
| N1 | 0.25672 | 0.60092 | 0.40265 | 1.000 |
| N2 | 0.26323 | 0.55732 | 0.47611 | 1.000 |
| N5 | 0.38264 | 0.34654 | 0.43202 | 1.000 |
| N3 | 0.17896 | 0.30953 | 0.36049 | 1.000 |
| N7 | 0.28175 | 0.44340 | 0.24033 | 1.000 |
| N8 | 0.23144 | 0.48470 | 0.17479 | 1.000 |
| N4 | 0.20089 | 0.30314 | 0.44078 | 1.000 |
| N9 | 0.18673 | 0.52267 | 0.11036 | 1.000 |
| N6 | 0.36935 | 0.34340 | 0.50067 | 1.000 |
| B1 | 0.27941 | 0.39588 | 0.50140 | 1.000 |
| H1 | 0.28190 | 0.38420 | 0.55500 | 1.000 |
| C5 | 0.27908 | 0.96473 | 0.33755 | 1.000 |
| H5 | 0.31180 | 1.00250 | 0.38840 | 1.000 |
| C14 | 0.02120 | 0.06925 | 0.20414 | 1.000 |
| H14 | 0.01930 | -0.00480 | 0.23760 | 1.000 |

| | | | | |
|-----|---------|---------|---------|-------|
| C19 | 0.43989 | 0.27733 | 0.55905 | 1.000 |
| H19 | 0.44630 | 0.26210 | 0.61090 | 1.000 |
| C1 | 0.25554 | 0.67369 | 0.51659 | 1.000 |
| H1A | 0.25790 | 0.67200 | 0.56770 | 1.000 |
| C21 | 0.46294 | 0.28131 | 0.44924 | 1.000 |
| C13 | 0.06484 | 0.19962 | 0.23690 | 1.000 |
| C27 | 0.50417 | 0.37334 | 0.34099 | 1.000 |
| H27 | 0.47650 | 0.46170 | 0.34090 | 1.000 |
| C3 | 0.24466 | 0.74616 | 0.39913 | 1.000 |
| C22 | 0.50202 | 0.26153 | 0.39103 | 1.000 |
| C12 | 0.10849 | 0.21842 | 0.32403 | 1.000 |
| C2 | 0.24360 | 0.79589 | 0.47030 | 1.000 |
| H2 | 0.23640 | 0.89100 | 0.48350 | 1.000 |
| C8 | 0.18003 | 0.85410 | 0.18535 | 1.000 |
| H8 | 0.14690 | 0.81730 | 0.13430 | 1.000 |
| C17 | 0.02560 | 0.28975 | 0.10287 | 1.000 |
| H17 | 0.02680 | 0.36360 | 0.06900 | 1.000 |
| C18 | 0.06609 | 0.31003 | 0.18518 | 1.000 |
| H18 | 0.09430 | 0.39780 | 0.20610 | 1.000 |
| C10 | 0.14609 | 0.20741 | 0.45386 | 1.000 |
| H10 | 0.14840 | 0.18300 | 0.50350 | 1.000 |
| C11 | 0.08604 | 0.15161 | 0.38177 | 1.000 |
| H11 | 0.04030 | 0.08400 | 0.37300 | 1.000 |

| | | | | |
|-----|----------|----------|---------|-------|
| C23 | 0.54278 | 0.12830 | 0.38928 | 1.000 |
| H23 | 0.54150 | 0.05310 | 0.42230 | 1.000 |
| C4 | 0.23629 | 0.82945 | 0.32838 | 1.000 |
| C20 | 0.50122 | 0.23588 | 0.52943 | 1.000 |
| H20 | 0.55620 | 0.18810 | 0.55660 | 1.000 |
| C9 | 0.18623 | 0.77585 | 0.25168 | 1.000 |
| H9 | 0.15670 | 0.68700 | 0.24480 | 1.000 |
| C24 | 0.58503 | 0.10760 | 0.33877 | 1.000 |
| H24 | 0.61130 | 0.01850 | 0.33760 | 1.000 |
| C6 | 0.27281 | 1.04245 | 0.27110 | 1.000 |
| H6 | 0.30190 | 1.13160 | 0.27760 | 1.000 |
| C7 | 0.22346 | 0.98760 | 0.19534 | 1.000 |
| H7 | 0.21930 | 1.04010 | 0.15090 | 1.000 |
| C25 | 0.58797 | 0.21970 | 0.29007 | 1.000 |
| H25 | 0.61690 | 0.20610 | 0.25660 | 1.000 |
| C26 | 0.54785 | 0.35230 | 0.29097 | 1.000 |
| H26 | 0.55010 | 0.42740 | 0.25820 | 1.000 |
| C15 | -0.01947 | 0.04950 | 0.12189 | 1.000 |
| H15 | -0.04870 | -0.03750 | 0.10070 | 1.000 |
| C16 | -0.01672 | 0.15830 | 0.07141 | 1.000 |
| H16 | -0.04310 | 0.14370 | 0.01650 | 1.000 |

Table C.19. Bond angles in $(Tp^{Ph})CoN_3$ ($^\circ$).

| | | | |
|------------|------------|-------------|------------|
| N1—Co1—N5 | 95.44(5) | N5—C21—C20 | 109.55(14) |
| N1—Co1—N3 | 92.43(5) | C20—C21—C22 | 126.69(15) |
| N3—Co1—N5 | 95.34(5) | C14—C13—C12 | 119.87(15) |
| N7—Co1—N1 | 125.98(6) | C14—C13—C18 | 118.66(15) |
| N7—Co1—N5 | 114.65(6) | C18—C13—C12 | 121.48(14) |
| N7—Co1—N3 | 125.46(6) | C22—C27—C26 | 119.92(16) |
| N2—N1—Co1 | 111.33(9) | N1—C3—C2 | 109.78(14) |
| C3—N1—Co1 | 142.03(11) | N1—C3—C4 | 121.10(14) |
| C3—N1—N2 | 106.62(12) | C2—C3—C4 | 129.11(14) |
| N1—N2—B1 | 120.72(12) | C27—C22—C21 | 122.14(14) |
| C1—N2—N1 | 109.27(13) | C27—C22—C23 | 119.16(15) |
| C1—N2—B1 | 130.00(13) | C23—C22—C21 | 118.60(15) |
| N6—N5—Co1 | 110.49(9) | N3—C12—C13 | 122.38(14) |
| C21—N5—Co1 | 142.60(11) | N3—C12—C11 | 109.32(14) |
| C21—N5—N6 | 106.66(13) | C11—C12—C13 | 128.29(15) |
| N4—N3—Co1 | 110.56(9) | C1—C2—C3 | 105.17(14) |
| C12—N3—Co1 | 141.96(11) | C9—C8—C7 | 119.90(17) |
| C12—N3—N4 | 106.93(12) | C18—C17—C16 | 119.67(16) |
| N8—N7—Co1 | 133.38(12) | C17—C18—C13 | 120.77(15) |
| N9—N8—N7 | 176.22(18) | N4—C10—C11 | 108.85(14) |
| N3—N4—B1 | 121.04(12) | C10—C11—C12 | 105.44(14) |
| C10—N4—N3 | 109.46(13) | C24—C23—C22 | 120.62(17) |
| C10—N4—B1 | 129.50(13) | C5—C4—C3 | 120.07(15) |

| | | | |
|-------------|------------|-------------|------------|
| N5—N6—B1 | 121.31(12) | C9—C4—C5 | 118.99(15) |
| C19—N6—N5 | 109.76(13) | C9—C4—C3 | 120.94(14) |
| C19—N6—B1 | 128.61(14) | C19—C20—C21 | 105.32(14) |
| N2—B1—N4 | 109.19(13) | C8—C9—C4 | 120.51(16) |
| N6—B1—N2 | 109.81(13) | C25—C24—C23 | 119.88(17) |
| N6—B1—N4 | 108.25(13) | C7—C6—C5 | 120.14(17) |
| C6—C5—C4 | 120.30(17) | C6—C7—C8 | 120.15(16) |
| C15—C14—C13 | 120.44(16) | C24—C25—C26 | 120.25(16) |
| N6—C19—C20 | 108.72(14) | C25—C26—C27 | 120.14(17) |
| N2—C1—C2 | 109.17(14) | C16—C15—C14 | 120.46(16) |
| N5—C21—C22 | 123.76(14) | C15—C16—C17 | 119.98(16) |

Table C.20. Bond lengths in (Tp^{Ph})CoN₃ (Å).

| | | | |
|--------|------------|---------|----------|
| Co1—N1 | 2.0188(13) | C1—C2 | 1.378(2) |
| Co1—N5 | 2.0442(13) | C21—C22 | 1.474(2) |
| Co1—N3 | 2.0391(13) | C21—C20 | 1.407(2) |
| Co1—N7 | 1.9187(14) | C13—C12 | 1.470(2) |
| N1—N2 | 1.3767(17) | C13—C18 | 1.402(2) |
| N1—C3 | 1.350(2) | C27—C22 | 1.395(2) |
| N2—B1 | 1.548(2) | C27—C26 | 1.397(2) |
| N2—C1 | 1.343(2) | C3—C2 | 1.400(2) |
| N5—N6 | 1.3745(18) | C3—C4 | 1.473(2) |
| N5—C21 | 1.346(2) | C22—C23 | 1.402(2) |

| | | | |
|---------|------------|---------|----------|
| N3—N4 | 1.3735(17) | C12—C11 | 1.407(2) |
| N3—C12 | 1.348(2) | C8—C9 | 1.389(2) |
| N7—N8 | 1.201(2) | C8—C7 | 1.391(3) |
| N8—N9 | 1.156(2) | C17—C18 | 1.392(2) |
| N4—B1 | 1.551(2) | C17—C16 | 1.393(2) |
| N4—C10 | 1.346(2) | C10—C11 | 1.376(2) |
| N6—B1 | 1.544(2) | C23—C24 | 1.386(2) |
| N6—C19 | 1.343(2) | C4—C9 | 1.393(2) |
| C5—C4 | 1.402(2) | C24—C25 | 1.385(3) |
| C5—C6 | 1.388(2) | C6—C7 | 1.382(3) |
| C14—C13 | 1.396(2) | C25—C26 | 1.389(3) |
| C14—C15 | 1.390(2) | C15—C16 | 1.383(3) |
| C19—C20 | 1.378(2) | | |

Table C.21. Single crystal X-ray diffraction experimental details for $(Tp^{Ph})Co(thf)Cl$.

| | |
|-----------------------------|-------------------------------------|
| Chemical formula | $C_{31}H_{30}BClCoN_6O$ |
| M_r | 607.80 |
| Crystal system, space group | Monoclinic, $C2/c$ |
| Temperature (K) | 100 |
| a, b, c (Å) | 18.2368(9), 14.5530(7), 22.8613(15) |
| β (°) | 110.296(2) |
| V (Å ³) | 5690.7(5) |
| Z | 8 |

| | |
|---|-------------------------------------|
| Radiation type | Mo K α λ = 0.71073 Å |
| μ (mm ⁻¹) | 0.73 |
| Crystal size (mm) | 0.55 × 0.51 × 0.50 |
| Absorption correction | Multi-scan SADABS v2014/5 |
| T_{\min} , T_{\max} | 0.743, 0.802 |
| No. of measured, independent and observed [$I > 2\sigma(I)$] reflections | 70872, 13882, 11698 |
| R_{int} | 0.030 |
| $(\sin \theta/\lambda)_{\text{max}}$ (Å ⁻¹) | 0.835 |
| $R[F^2 > 2\sigma(F^2)]$, $wR(F^2)$, S | 0.034, 0.101, 1.04 |
| No. of reflections | 13882 |
| No. of parameters | 370 |
| H-atom treatment | H-atom parameters constrained |
| Largest diff. peak/hole (e Å ⁻³) | 0.62, -0.68 |

Table C.22. Atom coordinates for $(Tp^{Ph})Co(thf)Cl$.

| Atom | x | y | z | Occupancy |
|------|---------|---------|---------|-----------|
| Co1 | 0.73096 | 0.59214 | 0.34501 | 1.000 |
| Cl1 | 0.61770 | 0.63792 | 0.35501 | 1.000 |
| O1 | 0.67686 | 0.48177 | 0.28355 | 1.000 |
| N1 | 0.80144 | 0.70630 | 0.40041 | 1.000 |

| | | | | |
|-----|---------|---------|---------|-------|
| N2 | 0.87802 | 0.68147 | 0.42736 | 1.000 |
| N3 | 0.80515 | 0.49697 | 0.40639 | 1.000 |
| N4 | 0.88243 | 0.51029 | 0.41597 | 1.000 |
| N5 | 0.80506 | 0.60964 | 0.29483 | 1.000 |
| N6 | 0.88273 | 0.61398 | 0.32842 | 1.000 |
| C1 | 0.91508 | 0.73939 | 0.47449 | 1.000 |
| H1 | 0.96850 | 0.73570 | 0.50050 | 1.000 |
| C2 | 0.86251 | 0.80467 | 0.47850 | 1.000 |
| H2 | 0.87170 | 0.85400 | 0.50740 | 1.000 |
| C3 | 0.79224 | 0.78250 | 0.43047 | 1.000 |
| C4 | 0.72056 | 0.83784 | 0.41020 | 1.000 |
| C5 | 0.69982 | 0.88972 | 0.45355 | 1.000 |
| H5 | 0.73110 | 0.88710 | 0.49650 | 1.000 |
| C6 | 0.63371 | 0.94505 | 0.43402 | 1.000 |
| H6 | 0.61990 | 0.98020 | 0.46370 | 1.000 |
| C7 | 0.58770 | 0.94932 | 0.37146 | 1.000 |
| H7 | 0.54200 | 0.98640 | 0.35840 | 1.000 |
| C8 | 0.60868 | 0.89907 | 0.32785 | 1.000 |
| H8 | 0.57760 | 0.90230 | 0.28490 | 1.000 |
| C9 | 0.67490 | 0.84431 | 0.34720 | 1.000 |
| H9 | 0.68940 | 0.81080 | 0.31720 | 1.000 |
| C10 | 0.92302 | 0.43295 | 0.43802 | 1.000 |
| H10 | 0.97770 | 0.42520 | 0.44790 | 1.000 |

| | | | | |
|-----|---------|---------|---------|-------|
| C11 | 0.87183 | 0.36694 | 0.44386 | 1.000 |
| H11 | 0.88380 | 0.30560 | 0.45830 | 1.000 |
| C12 | 0.79833 | 0.40964 | 0.42386 | 1.000 |
| C13 | 0.72373 | 0.36923 | 0.42174 | 1.000 |
| C14 | 0.71537 | 0.27366 | 0.42027 | 1.000 |
| H14 | 0.75780 | 0.23570 | 0.42040 | 1.000 |
| C15 | 0.64553 | 0.23400 | 0.41865 | 1.000 |
| H15 | 0.64070 | 0.16900 | 0.41850 | 1.000 |
| C16 | 0.58281 | 0.28853 | 0.41732 | 1.000 |
| H16 | 0.53460 | 0.26120 | 0.41510 | 1.000 |
| C17 | 0.59072 | 0.38357 | 0.41931 | 1.000 |
| H17 | 0.54790 | 0.42130 | 0.41860 | 1.000 |
| C18 | 0.66112 | 0.42362 | 0.42230 | 1.000 |
| H18 | 0.66660 | 0.48860 | 0.42470 | 1.000 |
| C19 | 0.92343 | 0.62387 | 0.28973 | 1.000 |
| H19 | 0.97870 | 0.62870 | 0.30200 | 1.000 |
| C20 | 0.87149 | 0.62590 | 0.22921 | 1.000 |
| H20 | 0.88340 | 0.63190 | 0.19210 | 1.000 |
| C21 | 0.79735 | 0.61718 | 0.23435 | 1.000 |
| C22 | 0.72056 | 0.61501 | 0.18434 | 1.000 |
| C23 | 0.65609 | 0.66011 | 0.19045 | 1.000 |
| H23 | 0.66170 | 0.69410 | 0.22720 | 1.000 |
| C24 | 0.58352 | 0.65562 | 0.14291 | 1.000 |

| | | | | |
|------|---------|---------|---------|-------|
| H24 | 0.53970 | 0.68610 | 0.14740 | 1.000 |
| C25 | 0.57534 | 0.60633 | 0.08889 | 1.000 |
| H25 | 0.52580 | 0.60290 | 0.05650 | 1.000 |
| C26 | 0.63951 | 0.56208 | 0.08237 | 1.000 |
| H26 | 0.63380 | 0.52880 | 0.04530 | 1.000 |
| C27 | 0.71188 | 0.56628 | 0.12969 | 1.000 |
| H27 | 0.75560 | 0.53600 | 0.12490 | 1.000 |
| C28 | 0.71876 | 0.41027 | 0.26359 | 1.000 |
| H28A | 0.74550 | 0.36830 | 0.29860 | 1.000 |
| H28B | 0.75820 | 0.43750 | 0.24790 | 1.000 |
| C29 | 0.65668 | 0.35940 | 0.21197 | 1.000 |
| H29A | 0.67180 | 0.29470 | 0.20910 | 1.000 |
| H29B | 0.64600 | 0.38970 | 0.17110 | 1.000 |
| C30 | 0.58674 | 0.36626 | 0.23382 | 1.000 |
| H30A | 0.53690 | 0.35620 | 0.19890 | 1.000 |
| H30B | 0.59090 | 0.32150 | 0.26740 | 1.000 |
| C31 | 0.59323 | 0.46404 | 0.25762 | 1.000 |
| H31A | 0.56730 | 0.50730 | 0.22320 | 1.000 |
| H31B | 0.56900 | 0.47020 | 0.29010 | 1.000 |
| B1 | 0.91200 | 0.60292 | 0.40011 | 1.000 |
| H1A | 0.97040 | 0.60490 | 0.41740 | 1.000 |

Table C.23. Bond angles for $(Tp^{Ph})Co(thf)Cl$ ($^{\circ}$).

| | | | |
|------------|-----------|-------------|------------|
| N5—Co1—N3 | 93.34(3) | C15—C14—H14 | 119.8 |
| N5—Co1—O1 | 88.24(3) | C13—C14—H14 | 119.8 |
| N3—Co1—O1 | 89.26(3) | C16—C15—C14 | 120.41(10) |
| N5—Co1—N1 | 82.15(3) | C16—C15—H15 | 119.8 |
| N3—Co1—N1 | 90.06(3) | C14—C15—H15 | 119.8 |
| O1—Co1—N1 | 170.32(3) | C15—C16—C17 | 119.64(10) |
| N5—Co1—Cl1 | 144.76(2) | C15—C16—H16 | 120.2 |
| N3—Co1—Cl1 | 121.86(2) | C17—C16—H16 | 120.2 |
| O1—Co1—Cl1 | 93.35(2) | C16—C17—C18 | 120.17(12) |
| N1—Co1—Cl1 | 95.21(2) | C16—C17—H17 | 119.9 |
| C28—O1—C31 | 109.62(7) | C18—C17—H17 | 119.9 |
| C28—O1—Co1 | 124.82(6) | C17—C18—C13 | 120.48(10) |
| C31—O1—Co1 | 125.51(6) | C17—C18—H18 | 119.8 |
| C3—N1—N2 | 106.08(7) | C13—C18—H18 | 119.8 |
| C3—N1—Co1 | 139.58(6) | N6—C19—C20 | 108.56(8) |
| N2—N1—Co1 | 111.11(5) | N6—C19—H19 | 125.7 |
| C1—N2—N1 | 110.21(7) | C20—C19—H19 | 125.7 |
| C1—N2—B1 | 129.00(8) | C19—C20—C21 | 105.09(8) |
| N1—N2—B1 | 120.58(7) | C19—C20—H20 | 127.5 |
| C12—N3—N4 | 106.41(7) | C21—C20—H20 | 127.5 |
| C12—N3—Co1 | 135.62(6) | N5—C21—C20 | 109.47(8) |
| N4—N3—Co1 | 113.87(5) | N5—C21—C22 | 122.00(8) |
| C10—N4—N3 | 110.19(7) | C20—C21—C22 | 128.53(8) |

| | | | |
|------------|-----------|--------------|------------|
| C10—N4—B1 | 128.90(8) | C23—C22—C27 | 119.36(9) |
| N3—N4—B1 | 120.88(7) | C23—C22—C21 | 121.39(8) |
| C21—N5—N6 | 107.11(7) | C27—C22—C21 | 119.25(9) |
| C21—N5—Co1 | 136.42(6) | C24—C23—C22 | 120.38(10) |
| N6—N5—Co1 | 116.46(5) | C24—C23—H23 | 119.8 |
| C19—N6—N5 | 109.76(7) | C22—C23—H23 | 119.8 |
| C19—N6—B1 | 129.93(8) | C25—C24—C23 | 119.83(12) |
| N5—N6—B1 | 120.23(7) | C25—C24—H24 | 120.1 |
| N2—C1—C2 | 108.48(8) | C23—C24—H24 | 120.1 |
| N2—C1—H1 | 125.8 | C26—C25—C24 | 119.98(11) |
| C2—C1—H1 | 125.8 | C26—C25—H25 | 120.0 |
| C1—C2—C3 | 104.90(8) | C24—C25—H25 | 120.0 |
| C1—C2—H2 | 127.6 | C27—C26—C25 | 120.34(11) |
| C3—C2—H2 | 127.6 | C27—C26—H26 | 119.8 |
| N1—C3—C2 | 110.29(8) | C25—C26—H26 | 119.8 |
| N1—C3—C4 | 123.13(8) | C26—C27—C22 | 120.11(11) |
| C2—C3—C4 | 126.29(8) | C26—C27—H27 | 119.9 |
| C9—C4—C5 | 118.96(8) | C22—C27—H27 | 119.9 |
| C9—C4—C3 | 120.71(8) | O1—C28—C29 | 105.19(8) |
| C5—C4—C3 | 120.19(8) | O1—C28—H28A | 110.7 |
| C6—C5—C4 | 120.22(9) | C29—C28—H28A | 110.7 |
| C6—C5—H5 | 119.9 | O1—C28—H28B | 110.7 |
| C4—C5—H5 | 119.9 | C29—C28—H28B | 110.7 |

| | | | |
|-------------|-----------|---------------|-----------|
| C7—C6—C5 | 120.35(9) | H28A—C28—H28B | 108.8 |
| C7—C6—H6 | 119.8 | C28—C29—C30 | 101.33(8) |
| C5—C6—H6 | 119.8 | C28—C29—H29A | 111.5 |
| C6—C7—C8 | 119.78(9) | C30—C29—H29A | 111.5 |
| C6—C7—H7 | 120.1 | C28—C29—H29B | 111.5 |
| C8—C7—H7 | 120.1 | C30—C29—H29B | 111.5 |
| C9—C8—C7 | 119.94(9) | H29A—C29—H29B | 109.3 |
| C9—C8—H8 | 120.0 | C31—C30—C29 | 102.08(8) |
| C7—C8—H8 | 120.0 | C31—C30—H30A | 111.4 |
| C8—C9—C4 | 120.71(9) | C29—C30—H30A | 111.4 |
| C8—C9—H9 | 119.6 | C31—C30—H30B | 111.4 |
| C4—C9—H9 | 119.6 | C29—C30—H30B | 111.4 |
| N4—C10—C11 | 108.44(8) | H30A—C30—H30B | 109.2 |
| N4—C10—H10 | 125.8 | O1—C31—C30 | 104.68(8) |
| C11—C10—H10 | 125.8 | O1—C31—H31A | 110.8 |
| C10—C11—C12 | 105.22(8) | C30—C31—H31A | 110.8 |
| C10—C11—H11 | 127.4 | O1—C31—H31B | 110.8 |
| C12—C11—H11 | 127.4 | C30—C31—H31B | 110.8 |
| N3—C12—C11 | 109.73(8) | H31A—C31—H31B | 108.9 |
| N3—C12—C13 | 123.15(8) | N2—B1—N4 | 109.46(7) |
| C11—C12—C13 | 127.12(8) | N2—B1—N6 | 108.29(7) |
| C18—C13—C14 | 118.86(9) | N4—B1—N6 | 108.67(7) |
| C18—C13—C12 | 121.69(8) | N2—B1—H1A | 110.1 |

| | | | |
|-------------|------------|-----------|-------|
| C14—C13—C12 | 119.44(9) | N4—B1—H1A | 110.1 |
| C15—C14—C13 | 120.40(11) | N6—B1—H1A | 110.1 |

Table C.24. Bond Lengths in $(Tp^{Ph})Co(thf)Cl$ (Å).

| | | | |
|---------|------------|---------|------------|
| Co1—N5 | 2.0693(8) | C13—C18 | 1.3929(14) |
| Co1—N3 | 2.0978(7) | C13—C14 | 1.3982(13) |
| Co1—O1 | 2.1367(7) | C14—C15 | 1.3872(16) |
| Co1—N1 | 2.2106(8) | C14—H14 | 0.9500 |
| Co1—Cl1 | 2.2562(3) | C15—C16 | 1.384(2) |
| O1—C28 | 1.4548(12) | C15—H15 | 0.9500 |
| O1—C31 | 1.4551(12) | C16—C17 | 1.3896(18) |
| N1—C3 | 1.3454(11) | C16—H16 | 0.9500 |
| N1—N2 | 1.3652(10) | C17—C18 | 1.3901(14) |
| N2—C1 | 1.3500(11) | C17—H17 | 0.9500 |
| N2—B1 | 1.5319(12) | C18—H18 | 0.9500 |
| N3—C12 | 1.3509(11) | C19—C20 | 1.3794(14) |
| N3—N4 | 1.3629(10) | C19—H19 | 0.9500 |
| N4—C10 | 1.3454(11) | C20—C21 | 1.4031(13) |
| N4—B1 | 1.5412(12) | C20—H20 | 0.9500 |
| N5—C21 | 1.3449(11) | C21—C22 | 1.4691(13) |
| N5—N6 | 1.3584(11) | C22—C23 | 1.3951(14) |
| N6—C19 | 1.3453(11) | C22—C27 | 1.3971(14) |
| N6—B1 | 1.5458(12) | C23—C24 | 1.3926(16) |

| | | | |
|---------|------------|----------|------------|
| C1—C2 | 1.3752(13) | C23—H23 | 0.9500 |
| C1—H1 | 0.9500 | C24—C25 | 1.391(2) |
| C2—C3 | 1.4055(13) | C24—H24 | 0.9500 |
| C2—H2 | 0.9500 | C25—C26 | 1.388(2) |
| C3—C4 | 1.4670(12) | C25—H25 | 0.9500 |
| C4—C9 | 1.3945(13) | C26—C27 | 1.3875(16) |
| C4—C5 | 1.3983(12) | C26—H26 | 0.9500 |
| C5—C6 | 1.3885(13) | C27—H27 | 0.9500 |
| C5—H5 | 0.9500 | C28—C29 | 1.5152(14) |
| C6—C7 | 1.3859(15) | C28—H28A | 0.9900 |
| C6—H6 | 0.9500 | C28—H28B | 0.9900 |
| C7—C8 | 1.3928(15) | C29—C30 | 1.5260(16) |
| C7—H7 | 0.9500 | C29—H29A | 0.9900 |
| C8—C9 | 1.3852(14) | C29—H29B | 0.9900 |
| C8—H8 | 0.9500 | C30—C31 | 1.5134(14) |
| C9—H9 | 0.9500 | C30—H30A | 0.9900 |
| C10—C11 | 1.3779(13) | C30—H30B | 0.9900 |
| C10—H10 | 0.9500 | C31—H31A | 0.9900 |
| C11—C12 | 1.4025(13) | C31—H31B | 0.9900 |
| C11—H11 | 0.9500 | B1—H1A | 1.0000 |
| C12—C13 | 1.4674(13) | | |

Table C.25. Single crystal X-ray diffraction experimental details for $(Tp^{Ph})_2Ni_2 \cdot 2thf$.

| | |
|-----------------------------|--|
| Chemical formula | $C_{54}H_{44}B_2N_{12}Ni_2 \cdot 2(C_4H_8O)$ |
| M_r | 1144.26 |
| Crystal system, space group | Triclinic, $P1$ |
| Temperature (K) | 100 |
| a, b, c (Å) | 9.5953 (8), 12.2934 (11), 12.8107 (12) |
| α, β, γ (°) | 65.681 (3), 84.333 (2), 82.250 (2) |
| V (Å ³) | 1362.9 (2) |
| Z | 1 |
| $F(000)$ | 598 |
| D_x (Mg m ⁻³) | 1.394 |
| Radiation type | Mo $K\alpha$ $\lambda = 0.71073$ Å |
| μ (mm ⁻¹) | 0.75 |
| Crystal shape | Rectangular |
| Colour | Red |
| Crystal size (mm) | 0.30 × 0.16 × 0.14 |
| Diffractometer | Bruker APEX-II CCD |
| Scan method | φ and ω scans |

| | |
|---|---|
| Absorption correction | Multi-scan |
| | SADABS v2014/2 |
| T_{\min} , T_{\max} | 0.770, 0.862 |
| No. of measured, independent and observed [$I > 2\sigma(I)$] reflections | 14515, 6226, 5254 |
| R_{int} | 0.028 |
| θ values ($^{\circ}$) | $\theta_{\max} = 27.5$, $\theta_{\min} = 1.8$ |
| $(\sin \theta/\lambda)_{\max}$ (\AA^{-1}) | 0.651 |
| $R[F^2 > 2\sigma(F^2)]$, $wR(F^2)$, S | 0.035, 0.080, 1.02 |
| No. of reflections | 6226 |
| No. of parameters | 377 |
| No. of restraints | 70 |
| H-atom treatment | H-atom parameters constrained |
| Weighting scheme | $w = 1/[\sigma^2(F_o^2) + (0.0289P)^2 + 0.9187P]$ where $P = (F_o^2 + 2F_c^2)/3$ |
| $(\Delta/\sigma)_{\max}$ | 0.001 |
| $\Delta\rho_{\max}$, $\Delta\rho_{\min}$ ($e \text{\AA}^{-3}$) | 0.65, -0.39 |

Table C.26. Atom coordinates for $(Tp^{Ph})_2Ni_2 \cdot 2thf$.

| Atom | x | y | z | Occupancy |
|------|---------|---------|---------|-----------|
| Ni1 | 0.56316 | 0.59955 | 0.47963 | 1.000 |
| N1 | 0.81250 | 0.42675 | 0.50878 | 1.000 |

| | | | | |
|-----|---------|---------|---------|-------|
| N2 | 0.72466 | 0.48988 | 0.55999 | 1.000 |
| N3 | 0.63005 | 0.61624 | 0.32547 | 1.000 |
| N4 | 0.73186 | 0.53723 | 0.30502 | 1.000 |
| N5 | 0.69785 | 0.31387 | 0.41297 | 1.000 |
| N6 | 0.56049 | 0.30370 | 0.45389 | 1.000 |
| C1 | 0.92785 | 0.37498 | 0.57074 | 1.000 |
| H1 | 1.00430 | 0.32730 | 0.55220 | 1.000 |
| C2 | 0.91623 | 0.40263 | 0.66433 | 1.000 |
| H2 | 0.98140 | 0.37820 | 0.72300 | 1.000 |
| C3 | 0.78799 | 0.47456 | 0.65564 | 1.000 |
| C4 | 0.72627 | 0.52680 | 0.73676 | 1.000 |
| C5 | 0.81293 | 0.57250 | 0.78700 | 1.000 |
| H5 | 0.91080 | 0.57200 | 0.76650 | 1.000 |
| C6 | 0.75790 | 0.61853 | 0.86635 | 1.000 |
| H6 | 0.81790 | 0.64930 | 0.90000 | 1.000 |
| C7 | 0.61470 | 0.61966 | 0.89672 | 1.000 |
| H7 | 0.57660 | 0.65120 | 0.95110 | 1.000 |
| C8 | 0.52781 | 0.57454 | 0.84729 | 1.000 |
| H8 | 0.42980 | 0.57590 | 0.86750 | 1.000 |
| C9 | 0.58283 | 0.52749 | 0.76870 | 1.000 |
| H9 | 0.52260 | 0.49550 | 0.73630 | 1.000 |
| C10 | 0.77491 | 0.58300 | 0.19335 | 1.000 |
| H10 | 0.84470 | 0.54490 | 0.15810 | 1.000 |

| | | | | |
|-----|---------|---------|---------|-------|
| C11 | 0.70183 | 0.69339 | 0.13885 | 1.000 |
| H11 | 0.71100 | 0.74630 | 0.06030 | 1.000 |
| C12 | 0.61090 | 0.71112 | 0.22392 | 1.000 |
| C13 | 0.50765 | 0.81526 | 0.21214 | 1.000 |
| C14 | 0.37434 | 0.80162 | 0.26684 | 1.000 |
| H14 | 0.34800 | 0.72350 | 0.31260 | 1.000 |
| C15 | 0.27950 | 0.90177 | 0.25494 | 1.000 |
| H15 | 0.18890 | 0.89170 | 0.29280 | 1.000 |
| C16 | 0.31670 | 1.01623 | 0.18814 | 1.000 |
| H16 | 0.25160 | 1.08450 | 0.17940 | 1.000 |
| C17 | 0.44940 | 1.03023 | 0.13426 | 1.000 |
| H17 | 0.47580 | 1.10850 | 0.08940 | 1.000 |
| C18 | 0.54390 | 0.93100 | 0.14520 | 1.000 |
| H18 | 0.63420 | 0.94170 | 0.10680 | 1.000 |
| C19 | 0.74153 | 0.22657 | 0.37587 | 1.000 |
| H19 | 0.83300 | 0.21420 | 0.34420 | 1.000 |
| C20 | 0.63367 | 0.15831 | 0.39082 | 1.000 |
| H20 | 0.63470 | 0.09130 | 0.37170 | 1.000 |
| C21 | 0.52190 | 0.20871 | 0.44029 | 1.000 |
| C22 | 0.37796 | 0.17165 | 0.47135 | 1.000 |
| C23 | 0.30990 | 0.14512 | 0.39482 | 1.000 |
| H23 | 0.35720 | 0.14890 | 0.32490 | 1.000 |
| C24 | 0.17330 | 0.11324 | 0.42029 | 1.000 |

| | | | | |
|------|---------|---------|----------|-------|
| H24 | 0.12700 | 0.09700 | 0.36680 | 1.000 |
| C25 | 0.10414 | 0.10496 | 0.52263 | 1.000 |
| H25 | 0.01030 | 0.08380 | 0.53940 | 1.000 |
| C26 | 0.17288 | 0.12780 | 0.60078 | 1.000 |
| H26 | 0.12690 | 0.12010 | 0.67230 | 1.000 |
| C27 | 0.30874 | 0.16195 | 0.57475 | 1.000 |
| H27 | 0.35450 | 0.17880 | 0.62810 | 1.000 |
| B1 | 0.78850 | 0.41557 | 0.39700 | 1.000 |
| H1A | 0.88350 | 0.39390 | 0.36690 | 1.000 |
| O1 | 0.99390 | 0.19970 | 0.10970 | 0.687 |
| C28 | 0.96720 | 0.11750 | 0.06310 | 0.687 |
| H28A | 0.94690 | 0.03980 | 0.12550 | 0.687 |
| H28B | 1.05010 | 0.10320 | 0.01620 | 0.687 |
| C29 | 0.83750 | 0.17560 | -0.01260 | 0.687 |
| H29A | 0.86690 | 0.21590 | -0.09460 | 0.687 |
| H29B | 0.77330 | 0.11530 | -0.00320 | 0.687 |
| C30 | 0.77000 | 0.26470 | 0.03420 | 0.687 |
| H30A | 0.70920 | 0.22620 | 0.10360 | 0.687 |
| H30B | 0.71360 | 0.33190 | -0.02380 | 0.687 |
| C31 | 0.89640 | 0.30640 | 0.06230 | 0.687 |
| H31A | 0.93870 | 0.36680 | -0.00770 | 0.687 |
| H31B | 0.86990 | 0.34230 | 0.11880 | 0.687 |
| O1' | 1.01710 | 0.22250 | 0.06250 | 0.313 |

| | | | | |
|------|---------|---------|----------|-------|
| C28' | 0.98760 | 0.14970 | 0.00480 | 0.313 |
| H28C | 1.04370 | 0.07040 | 0.03550 | 0.313 |
| H28D | 1.01010 | 0.18960 | -0.07860 | 0.313 |
| C29' | 0.83550 | 0.13650 | 0.02740 | 0.313 |
| H29C | 0.81920 | 0.06390 | 0.09780 | 0.313 |
| H29D | 0.79550 | 0.12950 | -0.03760 | 0.313 |
| C30' | 0.76840 | 0.24760 | 0.04200 | 0.313 |
| H30C | 0.69580 | 0.22760 | 0.10600 | 0.313 |
| H30D | 0.72470 | 0.30620 | -0.02890 | 0.313 |
| C31' | 0.89010 | 0.29640 | 0.06940 | 0.313 |
| H31C | 0.89730 | 0.38040 | 0.01390 | 0.313 |
| H31D | 0.87510 | 0.29530 | 0.14740 | 0.313 |

Table C.27. Bond angles for $(Tp^{Ph})_2Ni_2 \cdot 2thf$ (°).

| | | | |
|---------------------------------------|------------|-------------|------------|
| N6 ⁱ —Ni1—N3 | 136.07(6) | C19—C20—C21 | 104.90(15) |
| N6 ⁱ —Ni1—N2 | 122.40(6) | C19—C20—H20 | 127.6 |
| N3—Ni1—N2 | 96.60(6) | C21—C20—H20 | 127.6 |
| N6 ⁱ —Ni1—Ni1 ⁱ | 107.58(4) | N6—C21—C20 | 110.25(15) |
| N3—Ni1—Ni1 ⁱ | 92.73(4) | N6—C21—C22 | 122.19(15) |
| N2—Ni1—Ni1 ⁱ | 86.81(4) | C20—C21—C22 | 127.51(16) |
| C1—N1—N2 | 109.90(14) | C27—C22—C23 | 118.96(16) |
| C1—N1—B1 | 123.62(15) | C27—C22—C21 | 121.98(16) |
| N2—N1—B1 | 126.48(14) | C23—C22—C21 | 119.05(16) |

| | | | |
|-------------------------|------------|-------------|------------|
| C3—N2—N1 | 105.92(14) | C24—C23—C22 | 120.33(18) |
| C3—N2—Ni1 | 132.30(12) | C24—C23—H23 | 119.8 |
| N1—N2—Ni1 | 120.78(11) | C22—C23—H23 | 119.8 |
| C12—N3—N4 | 106.35(14) | C25—C24—C23 | 120.56(18) |
| C12—N3—Ni1 | 129.61(12) | C25—C24—H24 | 119.7 |
| N4—N3—Ni1 | 122.90(11) | C23—C24—H24 | 119.7 |
| C10—N4—N3 | 109.48(14) | C24—C25—C26 | 119.41(17) |
| C10—N4—B1 | 125.94(15) | C24—C25—H25 | 120.3 |
| N3—N4—B1 | 124.57(14) | C26—C25—H25 | 120.3 |
| C19—N5—N6 | 109.20(14) | C25—C26—C27 | 120.23(18) |
| C19—N5—B1 | 123.03(15) | C25—C26—H26 | 119.9 |
| N6—N5—B1 | 127.44(14) | C27—C26—H26 | 119.9 |
| C21—N6—N5 | 106.18(14) | C22—C27—C26 | 120.46(17) |
| C21—N6—Ni1 ⁱ | 124.05(12) | C22—C27—H27 | 119.8 |
| N5—N6—Ni1 ⁱ | 129.77(11) | C26—C27—H27 | 119.8 |
| N1—C1—C2 | 108.69(16) | N1—B1—N4 | 111.28(14) |
| N1—C1—H1 | 125.7 | N1—B1—N5 | 114.24(15) |
| C2—C1—H1 | 125.7 | N4—B1—N5 | 112.09(14) |
| C1—C2—C3 | 105.51(16) | N1—B1—H1A | 106.2 |
| C1—C2—H2 | 127.2 | N4—B1—H1A | 106.2 |
| C3—C2—H2 | 127.2 | N5—B1—H1A | 106.2 |
| N2—C3—C2 | 109.98(16) | C28—O1—C31 | 108.1(4) |
| N2—C3—C4 | 123.30(16) | O1—C28—C29 | 106.9(4) |

| | | | |
|-------------|------------|---------------|----------|
| C2—C3—C4 | 126.72(16) | O1—C28—H28A | 110.3 |
| C5—C4—C9 | 118.70(16) | C29—C28—H28A | 110.3 |
| C5—C4—C3 | 119.81(16) | O1—C28—H28B | 110.3 |
| C9—C4—C3 | 121.43(15) | C29—C28—H28B | 110.3 |
| C6—C5—C4 | 120.81(17) | H28A—C28—H28B | 108.6 |
| C6—C5—H5 | 119.6 | C30—C29—C28 | 102.1(5) |
| C4—C5—H5 | 119.6 | C30—C29—H29A | 111.4 |
| C5—C6—C7 | 119.96(17) | C28—C29—H29A | 111.4 |
| C5—C6—H6 | 120.0 | C30—C29—H29B | 111.4 |
| C7—C6—H6 | 120.0 | C28—C29—H29B | 111.4 |
| C8—C7—C6 | 119.67(17) | H29A—C29—H29B | 109.2 |
| C8—C7—H7 | 120.2 | C29—C30—C31 | 101.8(6) |
| C6—C7—H7 | 120.2 | C29—C30—H30A | 111.4 |
| C9—C8—C7 | 120.48(17) | C31—C30—H30A | 111.4 |
| C9—C8—H8 | 119.8 | C29—C30—H30B | 111.4 |
| C7—C8—H8 | 119.8 | C31—C30—H30B | 111.4 |
| C8—C9—C4 | 120.38(16) | H30A—C30—H30B | 109.3 |
| C8—C9—H9 | 119.8 | O1—C31—C30 | 105.1(6) |
| C4—C9—H9 | 119.8 | O1—C31—H31A | 110.7 |
| N4—C10—C11 | 109.09(16) | C30—C31—H31A | 110.7 |
| N4—C10—H10 | 125.5 | O1—C31—H31B | 110.7 |
| C11—C10—H10 | 125.5 | C30—C31—H31B | 110.7 |
| C10—C11—C12 | 105.05(16) | H31A—C31—H31B | 108.8 |

| | | | |
|-------------|------------|----------------|-----------|
| C10—C11—H11 | 127.5 | C31'—O1'—C28' | 108.1(8) |
| C12—C11—H11 | 127.5 | O1'—C28'—C29' | 105.5(8) |
| N3—C12—C11 | 110.02(16) | O1'—C28'—H28C | 110.6 |
| N3—C12—C13 | 122.02(16) | C29'—C28'—H28C | 110.6 |
| C11—C12—C13 | 127.96(17) | O1'—C28'—H28D | 110.6 |
| C14—C13—C18 | 118.75(18) | C29'—C28'—H28D | 110.6 |
| C14—C13—C12 | 121.71(17) | H28C—C28'—H28D | 108.8 |
| C18—C13—C12 | 119.53(17) | C28'—C29'—C30' | 106.2(9) |
| C15—C14—C13 | 120.39(18) | C28'—C29'—H29C | 110.5 |
| C15—C14—H14 | 119.8 | C30'—C29'—H29C | 110.5 |
| C13—C14—H14 | 119.8 | C28'—C29'—H29D | 110.5 |
| C16—C15—C14 | 120.31(19) | C30'—C29'—H29D | 110.5 |
| C16—C15—H15 | 119.8 | H29C—C29'—H29D | 108.7 |
| C14—C15—H15 | 119.8 | C29'—C30'—C31' | 103.7(9) |
| C17—C16—C15 | 119.49(19) | C29'—C30'—H30C | 111.0 |
| C17—C16—H16 | 120.3 | C31'—C30'—H30C | 111.0 |
| C15—C16—H16 | 120.3 | C29'—C30'—H30D | 111.0 |
| C16—C17—C18 | 120.50(19) | C31'—C30'—H30D | 111.0 |
| C16—C17—H17 | 119.8 | H30C—C30'—H30D | 109.0 |
| C18—C17—H17 | 119.8 | O1'—C31'—C30' | 108.3(10) |
| C17—C18—C13 | 120.55(19) | O1'—C31'—H31C | 110.0 |
| C17—C18—H18 | 119.7 | C30'—C31'—H31C | 110.0 |
| C13—C18—H18 | 119.7 | O1'—C31'—H31D | 110.0 |

| | | | |
|-------------|------------|----------------|-------|
| N5—C19—C20 | 109.46(16) | C30'—C31'—H31D | 110.0 |
| N5—C19—H19 | 125.3 | H31C—C31'—H31D | 108.4 |
| C20—C19—H19 | 125.3 | | |

Symmetry code: (i) $-x+1, -y+1, -z+1$.

Table C.28. Bond lengths in (Tp^{Ph})₂Ni₂•2thf (Å).

| | | | |
|----------------------|------------|---------|----------|
| Ni1—N6 ⁱ | 1.9498(14) | C17—C18 | 1.384(3) |
| Ni1—N3 | 1.9509(15) | C17—H17 | 0.9500 |
| Ni1—N2 | 1.9716(15) | C18—H18 | 0.9500 |
| Ni1—Ni1 ⁱ | 2.7121(5) | C19—C20 | 1.369(3) |
| N1—C1 | 1.352(2) | C19—H19 | 0.9500 |
| N1—N2 | 1.370(2) | C20—C21 | 1.395(2) |
| N1—B1 | 1.536(2) | C20—H20 | 0.9500 |
| N2—C3 | 1.354(2) | C21—C22 | 1.478(2) |
| N3—C12 | 1.351(2) | C22—C27 | 1.388(3) |
| N3—N4 | 1.3673(19) | C22—C23 | 1.394(2) |
| N4—C10 | 1.348(2) | C23—C24 | 1.387(3) |
| N4—B1 | 1.542(2) | C23—H23 | 0.9500 |
| N5—C19 | 1.346(2) | C24—C25 | 1.381(3) |
| N5—N6 | 1.3717(19) | C24—H24 | 0.9500 |
| N5—B1 | 1.552(2) | C25—C26 | 1.389(3) |
| N6—C21 | 1.352(2) | C25—H25 | 0.9500 |
| N6—Ni1 ⁱ | 1.9497(14) | C26—C27 | 1.390(3) |

| | | | |
|---------|----------|-----------|-----------|
| C1—C2 | 1.365(3) | C26—H26 | 0.9500 |
| C1—H1 | 0.9500 | C27—H27 | 0.9500 |
| C2—C3 | 1.400(2) | B1—H1A | 1.0000 |
| C2—H2 | 0.9500 | O1—C28 | 1.428(5) |
| C3—C4 | 1.473(2) | O1—C31 | 1.446(7) |
| C4—C5 | 1.397(2) | C28—C29 | 1.558(6) |
| C4—C9 | 1.397(2) | C28—H28A | 0.9900 |
| C5—C6 | 1.386(3) | C28—H28B | 0.9900 |
| C5—H5 | 0.9500 | C29—C30 | 1.500(7) |
| C6—C7 | 1.390(3) | C29—H29A | 0.9900 |
| C6—H6 | 0.9500 | C29—H29B | 0.9900 |
| C7—C8 | 1.387(3) | C30—C31 | 1.507(7) |
| C7—H7 | 0.9500 | C30—H30A | 0.9900 |
| C8—C9 | 1.385(3) | C30—H30B | 0.9900 |
| C8—H8 | 0.9500 | C31—H31A | 0.9900 |
| C9—H9 | 0.9500 | C31—H31B | 0.9900 |
| C10—C11 | 1.371(3) | O1'—C31' | 1.438(12) |
| C10—H10 | 0.9500 | O1'—C28' | 1.442(9) |
| C11—C12 | 1.398(3) | C28'—C29' | 1.478(12) |
| C11—H11 | 0.9500 | C28'—H28C | 0.9900 |
| C12—C13 | 1.474(2) | C28'—H28D | 0.9900 |
| C13—C14 | 1.393(3) | C29'—C30' | 1.506(12) |
| C13—C18 | 1.397(3) | C29'—H29C | 0.9900 |

| | | | |
|---------|----------|-----------|-----------|
| C14—C15 | 1.392(3) | C29'—H29D | 0.9900 |
| C14—H14 | 0.9500 | C30'—C31' | 1.512(12) |
| C15—C16 | 1.387(3) | C30'—H30C | 0.9900 |
| C15—H15 | 0.9500 | C30'—H30D | 0.9900 |
| C16—C17 | 1.384(3) | C31'—H31C | 0.9900 |
| C16—H16 | 0.9500 | C31'—H31D | 0.9900 |

Symmetry code: (i) $-x+1, -y+1, -z+1$.

Table C.29. Single crystal X-ray diffraction experimental details for [(Tp)Fe(CN)₂-μCN-Ni(NCMe)(Tp^{Ph})].*

| | |
|--|---|
| Chemical formula | C ₄₇ H ₄₇ B ₂ FeN ₁₆ Ni·C ₂ H ₃ N·CH ₂ Cl ₂ |
| <i>M_r</i> | 1098.16 |
| Crystal system, space group | Monoclinic, <i>P</i> 2 ₁ / <i>c</i> |
| Temperature (K) | 100 |
| <i>a</i> , <i>b</i> , <i>c</i> (Å) | 10.8728 (4), 21.5195 (8), 22.2856 (8) |
| β (°) | 95.0484 (14) |
| <i>V</i> (Å ³) | 5194.1 (3) |
| <i>Z</i> | 4 |
| <i>F</i> (000) | 2276 |
| <i>D_x</i> (Mg m ⁻³) | 1.404 |
| Radiation type | Mo Kα λ = 0.71073 Å |
| μ (mm ⁻¹) | 0.80 |
| Crystal shape | Rectangle |

| | |
|---|---|
| Colour | Orange |
| Crystal size (mm) | 0.26 × 0.14 × 0.08 |
| Diffractometer | Bruker <i>APEX-II</i> CCD |
| Scan method | φ and ω scans |
| Absorption correction | Multi-scan twinabs v2012/1 |
| T_{\min} , T_{\max} | 0.602, 0.746 |
| No. of measured, independent and observed [$I > 2\sigma(I)$] reflections | 56124, 14321, 11901 |
| R_{int} | 0.059 |
| θ values ($^{\circ}$) | $\theta_{\max} = 28.3$, $\theta_{\min} = 1.8$ |
| $(\sin \theta / \lambda)_{\max}$ (\AA^{-1}) | 0.668 |
| $R[F^2 > 2\sigma(F^2)]$, $wR(F^2)$, S | 0.052, 0.122, 1.08 |
| No. of reflections | 14321 |
| No. of parameters | 674 |
| No. of restraints | 41 |
| H-atom treatment | H-atom parameters constrained |
| Weighting scheme | $w = 1/[\sigma^2(F_o^2) + (0.0335P)^2 + 8.8776P]$ where $P = (F_o^2 + 2F_c^2)/3$ |
| $(\Delta/\sigma)_{\max}$ | 0.005 |
| $\Delta\rho_{\max}$, $\Delta\rho_{\min}$ ($e \text{\AA}^{-3}$) | 0.76, -0.63 |

Table C.30. Atom coordinates for $[(Tp^*)Fe(CN)_2-\mu CN-Ni(NCMe)(Tp^{Ph})]$.

| Atom | x | y | z | Occupancy |
|------|----------|---------|---------|-----------|
| Ni1 | 0.20132 | 0.17915 | 0.33288 | 1.000 |
| Fe1 | 0.21181 | 0.40980 | 0.37076 | 1.000 |
| N1 | 0.27660 | 0.44143 | 0.29505 | 1.000 |
| N2 | 0.36170 | 0.48867 | 0.30120 | 1.000 |
| N3 | 0.18540 | 0.49912 | 0.39536 | 1.000 |
| N4 | 0.27710 | 0.54105 | 0.38648 | 1.000 |
| N5 | 0.38280 | 0.41114 | 0.41000 | 1.000 |
| N6 | 0.44930 | 0.46555 | 0.40549 | 1.000 |
| N7 | 0.21040 | 0.27196 | 0.33735 | 1.000 |
| N8 | 0.27130 | 0.17829 | 0.24915 | 1.000 |
| N9 | 0.21100 | 0.13837 | 0.20911 | 1.000 |
| N10 | 0.02470 | 0.15591 | 0.30213 | 1.000 |
| N11 | 0.01530 | 0.11286 | 0.25685 | 1.000 |
| N12 | 0.24870 | 0.08692 | 0.33587 | 1.000 |
| N13 | 0.20590 | 0.05355 | 0.28619 | 1.000 |
| N14 | 0.16590 | 0.18149 | 0.42255 | 1.000 |
| N15 | -0.05000 | 0.40481 | 0.30527 | 1.000 |
| N16 | 0.13190 | 0.36483 | 0.49294 | 1.000 |
| C1 | 0.25700 | 0.42894 | 0.23577 | 1.000 |
| C2 | 0.32960 | 0.46870 | 0.20466 | 1.000 |
| H2 | 0.33380 | 0.47000 | 0.16230 | 1.000 |

| | | | | |
|------|----------|---------|---------|-------|
| C3 | 0.39400 | 0.50590 | 0.24657 | 1.000 |
| C4 | 0.17050 | 0.37980 | 0.20985 | 1.000 |
| H4A | 0.18750 | 0.34060 | 0.23140 | 1.000 |
| H4B | 0.18230 | 0.37410 | 0.16710 | 1.000 |
| H4C | 0.08520 | 0.39260 | 0.21400 | 1.000 |
| C5 | 0.48630 | 0.55640 | 0.23860 | 1.000 |
| H5A | 0.45640 | 0.59550 | 0.25460 | 1.000 |
| H5B | 0.49730 | 0.56130 | 0.19570 | 1.000 |
| H5C | 0.56550 | 0.54540 | 0.26050 | 1.000 |
| C6 | 0.08950 | 0.53101 | 0.41337 | 1.000 |
| C7 | 0.12010 | 0.59462 | 0.41623 | 1.000 |
| H7 | 0.06960 | 0.62770 | 0.42800 | 1.000 |
| C8 | 0.23860 | 0.59912 | 0.39833 | 1.000 |
| C9 | -0.03060 | 0.50271 | 0.42598 | 1.000 |
| H9A | -0.07720 | 0.49140 | 0.38790 | 1.000 |
| H9B | -0.07820 | 0.53270 | 0.44760 | 1.000 |
| H9C | -0.01530 | 0.46540 | 0.45070 | 1.000 |
| C10 | 0.31570 | 0.65534 | 0.38814 | 1.000 |
| H10A | 0.39780 | 0.65020 | 0.40950 | 1.000 |
| H10B | 0.27600 | 0.69230 | 0.40340 | 1.000 |
| H10C | 0.32370 | 0.66020 | 0.34490 | 1.000 |
| C11 | 0.45500 | 0.37258 | 0.44560 | 1.000 |
| C12 | 0.56650 | 0.40205 | 0.46277 | 1.000 |

| | | | | |
|------|---------|---------|---------|-------|
| H12 | 0.63410 | 0.38520 | 0.48740 | 1.000 |
| C13 | 0.55980 | 0.46005 | 0.43728 | 1.000 |
| C14 | 0.65320 | 0.51128 | 0.44220 | 1.000 |
| H14A | 0.68390 | 0.51850 | 0.40270 | 1.000 |
| H14B | 0.72220 | 0.49950 | 0.47130 | 1.000 |
| H14C | 0.61480 | 0.54940 | 0.45580 | 1.000 |
| C15 | 0.41760 | 0.30859 | 0.46295 | 1.000 |
| H15A | 0.35270 | 0.31140 | 0.49070 | 1.000 |
| H15B | 0.48920 | 0.28680 | 0.48270 | 1.000 |
| H15C | 0.38630 | 0.28570 | 0.42680 | 1.000 |
| C16 | 0.21600 | 0.32415 | 0.34907 | 1.000 |
| C17 | 0.04640 | 0.40713 | 0.33093 | 1.000 |
| C18 | 0.15750 | 0.38112 | 0.44646 | 1.000 |
| C19 | 0.34480 | 0.21370 | 0.21766 | 1.000 |
| C20 | 0.32870 | 0.19709 | 0.15658 | 1.000 |
| H20 | 0.36800 | 0.21500 | 0.12430 | 1.000 |
| C21 | 0.24430 | 0.14946 | 0.15323 | 1.000 |
| H21 | 0.21440 | 0.12800 | 0.11760 | 1.000 |
| C22 | 0.43450 | 0.25754 | 0.24745 | 1.000 |
| C23 | 0.49730 | 0.24244 | 0.30294 | 1.000 |
| H23 | 0.48000 | 0.20440 | 0.32220 | 1.000 |
| C24 | 0.58520 | 0.28305 | 0.33020 | 1.000 |
| H24 | 0.62760 | 0.27230 | 0.36780 | 1.000 |

| | | | | |
|-----|----------|---------|---------|-------|
| C25 | 0.61150 | 0.33880 | 0.30310 | 1.000 |
| H25 | 0.67020 | 0.36660 | 0.32230 | 1.000 |
| C26 | 0.55150 | 0.35330 | 0.24800 | 1.000 |
| H26 | 0.57030 | 0.39120 | 0.22890 | 1.000 |
| C27 | 0.46290 | 0.31310 | 0.21930 | 1.000 |
| H27 | 0.42270 | 0.32360 | 0.18110 | 1.000 |
| C28 | -0.08930 | 0.16207 | 0.32041 | 1.000 |
| C29 | -0.17240 | 0.12409 | 0.28546 | 1.000 |
| H29 | -0.25870 | 0.12020 | 0.28820 | 1.000 |
| C30 | -0.10250 | 0.09392 | 0.24656 | 1.000 |
| H30 | -0.13230 | 0.06440 | 0.21710 | 1.000 |
| C31 | -0.11970 | 0.20227 | 0.37096 | 1.000 |
| C32 | -0.18370 | 0.17600 | 0.41635 | 1.000 |
| H32 | -0.20690 | 0.13350 | 0.41410 | 1.000 |
| C33 | -0.21380 | 0.21200 | 0.46500 | 1.000 |
| H33 | -0.25500 | 0.19380 | 0.49650 | 1.000 |
| C34 | -0.18310 | 0.27450 | 0.46709 | 1.000 |
| H34 | -0.20380 | 0.29920 | 0.50010 | 1.000 |
| C35 | -0.12290 | 0.30115 | 0.42170 | 1.000 |
| H35 | -0.10360 | 0.34420 | 0.42310 | 1.000 |
| C36 | -0.09030 | 0.26506 | 0.37369 | 1.000 |
| H36 | -0.04790 | 0.28350 | 0.34270 | 1.000 |
| C37 | 0.29870 | 0.04569 | 0.37635 | 1.000 |

| | | | | |
|------|---------|----------|---------|-------|
| C38 | 0.28640 | -0.01442 | 0.35216 | 1.000 |
| H38 | 0.31330 | -0.05220 | 0.37110 | 1.000 |
| C39 | 0.22730 | -0.00744 | 0.29542 | 1.000 |
| H39 | 0.20540 | -0.03990 | 0.26760 | 1.000 |
| C40 | 0.35300 | 0.06320 | 0.43600 | 0.864 |
| C41 | 0.42170 | 0.11740 | 0.44640 | 0.864 |
| H41 | 0.43620 | 0.14380 | 0.41370 | 0.864 |
| C42 | 0.46960 | 0.13320 | 0.50480 | 0.864 |
| H42 | 0.51400 | 0.17090 | 0.51220 | 0.864 |
| C43 | 0.45050 | 0.09210 | 0.55210 | 0.864 |
| H43 | 0.47980 | 0.10260 | 0.59220 | 0.864 |
| C44 | 0.39000 | 0.03700 | 0.54090 | 0.864 |
| H44 | 0.38210 | 0.00860 | 0.57300 | 0.864 |
| C45 | 0.34060 | 0.02220 | 0.48390 | 0.864 |
| H45 | 0.29780 | -0.01590 | 0.47690 | 0.864 |
| C40' | 0.36000 | 0.07000 | 0.43480 | 0.136 |
| C41' | 0.43600 | 0.12300 | 0.43570 | 0.136 |
| H41' | 0.44800 | 0.14340 | 0.39910 | 0.136 |
| C42' | 0.49400 | 0.14500 | 0.49040 | 0.136 |
| H42' | 0.55560 | 0.17620 | 0.49070 | 0.136 |
| C43' | 0.46000 | 0.11950 | 0.54460 | 0.136 |
| H43' | 0.50250 | 0.13030 | 0.58220 | 0.136 |
| C44' | 0.36200 | 0.07900 | 0.54170 | 0.136 |

| | | | | |
|------|----------|----------|---------|-------|
| H44' | 0.32860 | 0.06780 | 0.57810 | 0.136 |
| C45' | 0.31100 | 0.05360 | 0.48900 | 0.136 |
| H45' | 0.24400 | 0.02550 | 0.48900 | 0.136 |
| C46 | 0.14440 | 0.19397 | 0.47001 | 1.000 |
| C47 | 0.11750 | 0.21110 | 0.53110 | 1.000 |
| H47A | 0.09900 | 0.25560 | 0.53250 | 1.000 |
| H47B | 0.18920 | 0.20180 | 0.55940 | 1.000 |
| H47C | 0.04600 | 0.18740 | 0.54230 | 1.000 |
| B1 | 0.39690 | 0.51730 | 0.36370 | 1.000 |
| H1 | 0.45800 | 0.55180 | 0.36120 | 1.000 |
| B2 | 0.13170 | 0.08570 | 0.23248 | 1.000 |
| H2A | 0.10880 | 0.05500 | 0.19970 | 1.000 |
| CI1 | -0.22660 | 0.32488 | 0.13245 | 1.000 |
| CI2 | -0.02279 | 0.24642 | 0.17762 | 1.000 |
| C3S | -0.14830 | 0.29040 | 0.19820 | 1.000 |
| H3SA | -0.11860 | 0.32320 | 0.22700 | 1.000 |
| H3SB | -0.20600 | 0.26330 | 0.21820 | 1.000 |
| N1S | 0.04290 | -0.06990 | 0.46870 | 0.746 |
| C2S | -0.03070 | 0.01330 | 0.38810 | 0.746 |
| H2S1 | 0.01830 | 0.05040 | 0.39920 | 0.746 |
| H2S2 | -0.11880 | 0.02330 | 0.38770 | 0.746 |
| H2S3 | -0.01260 | -0.00070 | 0.34800 | 0.746 |
| N1S' | 0.08200 | -0.07690 | 0.42980 | 0.254 |

| | | | | |
|------|----------|----------|---------|-------|
| C2S' | -0.13000 | -0.00700 | 0.44170 | 0.254 |
| H2S4 | -0.18170 | -0.04070 | 0.45530 | 0.254 |
| H2S5 | -0.17010 | 0.01110 | 0.40460 | 0.254 |
| H2S6 | -0.12020 | 0.02510 | 0.47300 | 0.254 |
| C1S | -0.00140 | -0.03320 | 0.42950 | 1.000 |

angles

Table C.31. Bond angles for $[(Tp^*)Fe(CN)_2-\mu CN-Ni(NCMe)(Tp^{Ph})]$ ($^\circ$).

| | | | |
|-------------|------------|-------------|----------|
| N7—Ni1—N10 | 107.56(13) | N9—C21—C20 | 108.3(3) |
| N7—Ni1—N12 | 162.40(13) | N9—C21—H21 | 125.8 |
| N10—Ni1—N12 | 89.99(13) | C20—C21—H21 | 125.8 |
| N7—Ni1—N14 | 86.57(12) | C23—C22—C27 | 119.1(4) |
| N10—Ni1—N14 | 94.60(13) | C23—C22—C19 | 120.2(3) |
| N12—Ni1—N14 | 93.43(12) | C27—C22—C19 | 120.6(3) |
| N7—Ni1—N8 | 91.91(12) | C24—C23—C22 | 120.2(4) |
| N10—Ni1—N8 | 95.99(12) | C24—C23—H23 | 119.9 |
| N12—Ni1—N8 | 84.82(12) | C22—C23—H23 | 119.9 |
| N14—Ni1—N8 | 169.26(13) | C25—C24—C23 | 120.9(4) |
| C16—Fe1—C17 | 84.08(14) | C25—C24—H24 | 119.6 |
| C16—Fe1—C18 | 85.91(14) | C23—C24—H24 | 119.6 |
| C17—Fe1—C18 | 92.73(15) | C26—C25—C24 | 119.1(4) |
| C16—Fe1—N5 | 94.78(14) | C26—C25—H25 | 120.4 |

| | | | |
|------------|------------|-------------|----------|
| C17—Fe1—N5 | 178.55(14) | C24—C25—H25 | 120.4 |
| C18—Fe1—N5 | 88.07(14) | C25—C26—C27 | 121.2(4) |
| C16—Fe1—N1 | 95.57(13) | C25—C26—H26 | 119.4 |
| C17—Fe1—N1 | 90.29(14) | C27—C26—H26 | 119.4 |
| C18—Fe1—N1 | 176.76(14) | C22—C27—C26 | 119.5(4) |
| N5—Fe1—N1 | 88.92(13) | C22—C27—H27 | 120.3 |
| C16—Fe1—N3 | 173.00(14) | C26—C27—H27 | 120.3 |
| C17—Fe1—N3 | 90.23(13) | N10—C28—C29 | 109.9(3) |
| C18—Fe1—N3 | 90.29(13) | N10—C28—C31 | 124.1(3) |
| N5—Fe1—N3 | 90.96(12) | C29—C28—C31 | 126.0(4) |
| N1—Fe1—N3 | 88.53(12) | C30—C29—C28 | 105.2(4) |
| C1—N1—N2 | 107.0(3) | C30—C29—H29 | 127.4 |
| C1—N1—Fe1 | 136.2(3) | C28—C29—H29 | 127.4 |
| N2—N1—Fe1 | 116.8(2) | N11—C30—C29 | 108.8(3) |
| C3—N2—N1 | 109.9(3) | N11—C30—H30 | 125.6 |
| C3—N2—B1 | 130.0(3) | C29—C30—H30 | 125.6 |
| N1—N2—B1 | 119.9(3) | C36—C31—C32 | 119.3(4) |
| C6—N3—N4 | 107.5(3) | C36—C31—C28 | 122.4(4) |
| C6—N3—Fe1 | 134.4(2) | C32—C31—C28 | 118.2(4) |
| N4—N3—Fe1 | 117.5(2) | C33—C32—C31 | 120.3(4) |
| C8—N4—N3 | 109.8(3) | C33—C32—H32 | 119.9 |
| C8—N4—B1 | 131.5(3) | C31—C32—H32 | 119.9 |
| N3—N4—B1 | 118.7(3) | C34—C33—C32 | 119.5(4) |

| | | | |
|-------------|----------|--------------|----------|
| C11—N5—N6 | 106.4(3) | C34—C33—H33 | 120.2 |
| C11—N5—Fe1 | 136.4(3) | C32—C33—H33 | 120.2 |
| N6—N5—Fe1 | 117.1(2) | C35—C34—C33 | 120.6(4) |
| C13—N6—N5 | 109.6(3) | C35—C34—H34 | 119.7 |
| C13—N6—B1 | 130.7(3) | C33—C34—H34 | 119.7 |
| N5—N6—B1 | 119.4(3) | C34—C35—C36 | 120.1(4) |
| C16—N7—Ni1 | 169.8(3) | C34—C35—H35 | 120.0 |
| C19—N8—N9 | 106.8(3) | C36—C35—H35 | 120.0 |
| C19—N8—Ni1 | 138.2(2) | C31—C36—C35 | 120.2(4) |
| N9—N8—Ni1 | 113.6(2) | C31—C36—H36 | 119.9 |
| C21—N9—N8 | 109.9(3) | C35—C36—H36 | 119.9 |
| C21—N9—B2 | 130.2(3) | N12—C37—C38 | 109.3(3) |
| N8—N9—B2 | 119.5(3) | N12—C37—C40 | 123.3(9) |
| C28—N10—N11 | 106.2(3) | C38—C37—C40 | 127.4(9) |
| C28—N10—Ni1 | 137.6(3) | N12—C37—C40' | 118(6) |
| N11—N10—Ni1 | 114.8(2) | C38—C37—C40' | 132(6) |
| C30—N11—N10 | 109.8(3) | C39—C38—C37 | 105.9(3) |
| C30—N11—B2 | 128.8(3) | C39—C38—H38 | 127.1 |
| N10—N11—B2 | 120.6(3) | C37—C38—H38 | 127.1 |
| C37—N12—N13 | 106.6(3) | N13—C39—C38 | 107.9(3) |
| C37—N12—Ni1 | 138.2(3) | N13—C39—H39 | 126.0 |
| N13—N12—Ni1 | 114.6(2) | C38—C39—H39 | 126.0 |
| C39—N13—N12 | 110.3(3) | C41—C40—C45 | 119.1(7) |

| | | | |
|-------------|----------|----------------|----------|
| C39—N13—B2 | 128.8(3) | C41—C40—C37 | 122.6(7) |
| N12—N13—B2 | 120.6(3) | C45—C40—C37 | 118.3(7) |
| C46—N14—Ni1 | 167.6(3) | C40—C41—C42 | 120.7(6) |
| N1—C1—C2 | 108.6(4) | C40—C41—H41 | 119.7 |
| N1—C1—C4 | 124.0(3) | C42—C41—H41 | 119.7 |
| C2—C1—C4 | 127.4(4) | C41—C42—C43 | 118.4(6) |
| C3—C2—C1 | 107.3(4) | C41—C42—H42 | 120.8 |
| C3—C2—H2 | 126.4 | C43—C42—H42 | 120.8 |
| C1—C2—H2 | 126.4 | C44—C43—C42 | 120.7(5) |
| N2—C3—C2 | 107.2(4) | C44—C43—H43 | 119.7 |
| N2—C3—C5 | 122.4(4) | C42—C43—H43 | 119.7 |
| C2—C3—C5 | 130.4(4) | C43—C44—C45 | 120.8(6) |
| C1—C4—H4A | 109.5 | C43—C44—H44 | 119.6 |
| C1—C4—H4B | 109.5 | C45—C44—H44 | 119.6 |
| H4A—C4—H4B | 109.5 | C44—C45—C40 | 120.2(6) |
| C1—C4—H4C | 109.5 | C44—C45—H45 | 119.9 |
| H4A—C4—H4C | 109.5 | C40—C45—H45 | 119.9 |
| H4B—C4—H4C | 109.5 | C41'—C40'—C45' | 117(3) |
| C3—C5—H5A | 109.5 | C41'—C40'—C37 | 121(4) |
| C3—C5—H5B | 109.5 | C45'—C40'—C37 | 119(4) |
| H5A—C5—H5B | 109.5 | C40'—C41'—C42' | 120(3) |
| C3—C5—H5C | 109.5 | C40'—C41'—H41' | 119.8 |
| H5A—C5—H5C | 109.5 | C42'—C41'—H41' | 119.8 |

| | | | |
|---------------|----------|----------------|----------|
| H5B—C5—H5C | 109.5 | C43'—C42'—C41' | 119(2) |
| N3—C6—C7 | 109.0(3) | C43'—C42'—H42' | 120.7 |
| N3—C6—C9 | 124.4(3) | C41'—C42'—H42' | 120.7 |
| C7—C6—C9 | 126.6(3) | C44'—C43'—C42' | 118(2) |
| C8—C7—C6 | 106.1(3) | C44'—C43'—H43' | 121.0 |
| C8—C7—H7 | 127.0 | C42'—C43'—H43' | 121.0 |
| C6—C7—H7 | 127.0 | C45'—C44'—C43' | 123(2) |
| N4—C8—C7 | 107.7(3) | C45'—C44'—H44' | 118.4 |
| N4—C8—C10 | 122.0(3) | C43'—C44'—H44' | 118.4 |
| C7—C8—C10 | 130.2(3) | C44'—C45'—C40' | 119(2) |
| C6—C9—H9A | 109.5 | C44'—C45'—H45' | 120.6 |
| C6—C9—H9B | 109.5 | C40'—C45'—H45' | 120.6 |
| H9A—C9—H9B | 109.5 | N14—C46—C47 | 179.1(4) |
| C6—C9—H9C | 109.5 | C46—C47—H47A | 109.5 |
| H9A—C9—H9C | 109.5 | C46—C47—H47B | 109.5 |
| H9B—C9—H9C | 109.5 | H47A—C47—H47B | 109.5 |
| C8—C10—H10A | 109.5 | C46—C47—H47C | 109.5 |
| C8—C10—H10B | 109.5 | H47A—C47—H47C | 109.5 |
| H10A—C10—H10B | 109.5 | H47B—C47—H47C | 109.5 |
| C8—C10—H10C | 109.5 | N4—B1—N6 | 108.9(3) |
| H10A—C10—H10C | 109.5 | N4—B1—N2 | 106.5(3) |
| H10B—C10—H10C | 109.5 | N6—B1—N2 | 108.0(3) |
| N5—C11—C12 | 109.2(3) | N4—B1—H1 | 111.1 |

| | | | |
|---------------|----------|----------------|----------|
| N5—C11—C15 | 124.0(3) | N6—B1—H1 | 111.1 |
| C12—C11—C15 | 126.8(3) | N2—B1—H1 | 111.1 |
| C13—C12—C11 | 106.7(3) | N11—B2—N9 | 110.0(3) |
| C13—C12—H12 | 126.6 | N11—B2—N13 | 106.6(3) |
| C11—C12—H12 | 126.6 | N9—B2—N13 | 108.7(3) |
| N6—C13—C12 | 108.1(3) | N11—B2—H2A | 110.5 |
| N6—C13—C14 | 122.9(3) | N9—B2—H2A | 110.5 |
| C12—C13—C14 | 129.0(4) | N13—B2—H2A | 110.5 |
| C13—C14—H14A | 109.5 | CI2—C3S—CI1 | 109.5(3) |
| C13—C14—H14B | 109.5 | CI2—C3S—H3SA | 109.8 |
| H14A—C14—H14B | 109.5 | CI1—C3S—H3SA | 109.8 |
| C13—C14—H14C | 109.5 | CI2—C3S—H3SB | 109.8 |
| H14A—C14—H14C | 109.5 | CI1—C3S—H3SB | 109.8 |
| H14B—C14—H14C | 109.5 | H3SA—C3S—H3SB | 108.2 |
| C11—C15—H15A | 109.5 | C1S—C2S—H2S1 | 109.5 |
| C11—C15—H15B | 109.5 | C1S—C2S—H2S2 | 109.5 |
| H15A—C15—H15B | 109.5 | H2S1—C2S—H2S2 | 109.5 |
| C11—C15—H15C | 109.5 | C1S—C2S—H2S3 | 109.5 |
| H15A—C15—H15C | 109.5 | H2S1—C2S—H2S3 | 109.5 |
| H15B—C15—H15C | 109.5 | H2S2—C2S—H2S3 | 109.5 |
| N7—C16—Fe1 | 175.2(3) | C1S—C2S'—H2S4 | 109.5 |
| N15—C17—Fe1 | 177.4(3) | C1S—C2S'—H2S5 | 109.5 |
| N16—C18—Fe1 | 176.1(3) | H2S4—C2S'—H2S5 | 109.5 |

| | | | |
|-------------|----------|----------------|-----------|
| N8—C19—C20 | 109.4(3) | C1S—C2S'—H2S6 | 109.5 |
| N8—C19—C22 | 121.9(3) | H2S4—C2S'—H2S6 | 109.5 |
| C20—C19—C22 | 128.4(3) | H2S5—C2S'—H2S6 | 109.5 |
| C21—C20—C19 | 105.6(3) | N1S—C1S—C2S | 169.6(10) |
| C21—C20—H20 | 127.2 | N1S'—C1S—C2S' | 153.4(16) |
| C19—C20—H20 | 127.2 | | |

Table C.32. Bond lengths for $[(Tp^*)Fe(CN)_2-\mu CN-Ni(NCMe)(Tp^{Ph})]$ (Å).

| | | | |
|---------|----------|---------|----------|
| Ni1—N7 | 2.002(3) | C21—H21 | 0.9500 |
| Ni1—N10 | 2.044(3) | C22—C23 | 1.397(6) |
| Ni1—N12 | 2.050(3) | C22—C27 | 1.398(5) |
| Ni1—N14 | 2.069(3) | C23—C24 | 1.394(6) |
| Ni1—N8 | 2.076(3) | C23—H23 | 0.9500 |
| Fe1—C16 | 1.907(3) | C24—C25 | 1.384(6) |
| Fe1—C17 | 1.935(4) | C24—H24 | 0.9500 |
| Fe1—C18 | 1.937(4) | C25—C26 | 1.375(7) |
| Fe1—N5 | 1.984(3) | C25—H25 | 0.9500 |
| Fe1—N1 | 2.004(3) | C26—C27 | 1.406(6) |
| Fe1—N3 | 2.026(3) | C26—H26 | 0.9500 |
| N1—C1 | 1.347(5) | C27—H27 | 0.9500 |
| N1—N2 | 1.373(4) | C28—C29 | 1.402(5) |
| N2—C3 | 1.348(5) | C28—C31 | 1.480(5) |
| N2—B1 | 1.540(5) | C29—C30 | 1.366(6) |

| | | | |
|---------|----------|----------|-----------|
| N3—C6 | 1.339(4) | C29—H29 | 0.9500 |
| N3—N4 | 1.372(4) | C30—H30 | 0.9500 |
| N4—C8 | 1.351(4) | C31—C36 | 1.388(5) |
| N4—B1 | 1.527(5) | C31—C32 | 1.397(6) |
| N5—C11 | 1.351(5) | C32—C33 | 1.395(6) |
| N5—N6 | 1.384(4) | C32—H32 | 0.9500 |
| N6—C13 | 1.346(5) | C33—C34 | 1.385(7) |
| N6—B1 | 1.529(5) | C33—H33 | 0.9500 |
| N7—C16 | 1.154(4) | C34—C35 | 1.378(7) |
| N8—C19 | 1.346(5) | C34—H34 | 0.9500 |
| N8—N9 | 1.364(4) | C35—C36 | 1.393(5) |
| N9—C21 | 1.348(5) | C35—H35 | 0.9500 |
| N9—B2 | 1.542(5) | C36—H36 | 0.9500 |
| N10—C28 | 1.345(5) | C37—C38 | 1.403(5) |
| N10—N11 | 1.367(4) | C37—C40 | 1.456(8) |
| N11—C30 | 1.345(5) | C37—C40' | 1.51(4) |
| N11—B2 | 1.536(5) | C38—C39 | 1.375(6) |
| N12—C37 | 1.346(5) | C38—H38 | 0.9500 |
| N12—N13 | 1.367(4) | C39—H39 | 0.9500 |
| N13—C39 | 1.346(5) | C40—C41 | 1.393(7) |
| N13—B2 | 1.547(5) | C40—C45 | 1.401(12) |
| N14—C46 | 1.135(5) | C41—C42 | 1.399(7) |
| N15—C17 | 1.150(5) | C41—H41 | 0.9500 |

| | | | |
|----------|----------|-----------|-----------|
| N16—C18 | 1.151(5) | C42—C43 | 1.406(8) |
| C1—C2 | 1.390(6) | C42—H42 | 0.9500 |
| C1—C4 | 1.496(6) | C43—C44 | 1.367(10) |
| C2—C3 | 1.374(6) | C43—H43 | 0.9500 |
| C2—H2 | 0.9500 | C44—C45 | 1.372(8) |
| C3—C5 | 1.501(6) | C44—H44 | 0.9500 |
| C4—H4A | 0.9800 | C45—H45 | 0.9500 |
| C4—H4B | 0.9800 | C40'—C41' | 1.40(2) |
| C4—H4C | 0.9800 | C40'—C45' | 1.41(2) |
| C5—H5A | 0.9800 | C41'—C42' | 1.407(19) |
| C5—H5B | 0.9800 | C41'—H41' | 0.9500 |
| C5—H5C | 0.9800 | C42'—C43' | 1.41(2) |
| C6—C7 | 1.409(5) | C42'—H42' | 0.9500 |
| C6—C9 | 1.489(5) | C43'—C44' | 1.37(2) |
| C7—C8 | 1.386(5) | C43'—H43' | 0.9500 |
| C7—H7 | 0.9500 | C44'—C45' | 1.37(2) |
| C8—C10 | 1.500(5) | C44'—H44' | 0.9500 |
| C9—H9A | 0.9800 | C45'—H45' | 0.9500 |
| C9—H9B | 0.9800 | C46—C47 | 1.465(5) |
| C9—H9C | 0.9800 | C47—H47A | 0.9800 |
| C10—H10A | 0.9800 | C47—H47B | 0.9800 |
| C10—H10B | 0.9800 | C47—H47C | 0.9800 |
| C10—H10C | 0.9800 | B1—H1 | 1.0000 |

| | | | |
|----------|----------|-----------|-----------|
| C11—C12 | 1.391(5) | B2—H2A | 1.0000 |
| C11—C15 | 1.496(5) | C11—C3S | 1.790(5) |
| C12—C13 | 1.371(5) | C12—C3S | 1.754(6) |
| C12—H12 | 0.9500 | C3S—H3SA | 0.9900 |
| C13—C14 | 1.497(5) | C3S—H3SB | 0.9900 |
| C14—H14A | 0.9800 | N1S—C1S | 1.243(12) |
| C14—H14B | 0.9800 | C2S—C1S | 1.380(12) |
| C14—H14C | 0.9800 | C2S—H2S1 | 0.9800 |
| C15—H15A | 0.9800 | C2S—H2S2 | 0.9800 |
| C15—H15B | 0.9800 | C2S—H2S3 | 0.9800 |
| C15—H15C | 0.9800 | N1S'—C1S | 1.30(3) |
| C19—C20 | 1.403(5) | C2S'—C1S | 1.56(3) |
| C19—C22 | 1.472(5) | C2S'—H2S4 | 0.9800 |
| C20—C21 | 1.374(6) | C2S'—H2S5 | 0.9800 |
| C20—H20 | 0.9500 | C2S'—H2S6 | 0.9800 |

Table C.33. Single crystal X-ray diffraction experimental details for $[(Tp^*)Fe(CN)_2-\mu CN-Co(dmf)(Tp^{Ph})] \cdot 2dmf$.

| | |
|-----------------------------|---|
| Chemical formula | $4(C_{48}H_{51}B_2CoFeN_{16}O) \cdot 8(C_3H_7NO)$ |
| M_r | 4602.66 |
| Crystal system, space group | Monoclinic, $P2_1/n$ |
| Temperature (K) | 101 |
| a, b, c (Å) | 13.370 (5), 13.064 (5), 32.181 (14) |
| β (°) | 95.961 (14) |

| | |
|---|-------------------------------------|
| V (Å ³) | 5590 (4) |
| Z | 1 |
| $F(000)$ | 2411.5669 |
| D_x (Mg m ⁻³) | 1.367 |
| Radiation type | Mo K α $\lambda = 0.71073$ Å |
| μ (mm ⁻¹) | 0.62 |
| Crystal shape | Hexagonal |
| Colour | Red |
| Crystal size (mm) | 0.43 × 0.21 × 0.09 |
| Data collection | |
| Diffractometer | Bruker APEX-II CCD |
| Scan method | φ and ω scans |
| Absorption correction | – |
| No. of measured, independent and observed [$I > 2\sigma(I)$] reflections | 26677, 7350, 2997 |
| R_{int} | 0.156 |
| θ_{max} (°) | 23.4 |
| $(\sin \theta/\lambda)_{\text{max}}$ (Å ⁻¹) | 0.560 |
| $R[F^2 > 2\sigma(F^2)]$, $wR(F^2)$, S | 0.275, 0.677, 2.25 |
| No. of reflections | 7350 |
| No. of parameters | 329 |
| No. of restraints | 0 |
| No. of constraints | 106 |

| | |
|---|--|
| H-atom treatment | H-atom parameters constrained |
| Weighting scheme | $w = 1/[\sigma^2(F_o^2) + (0.2P)^2]$ where $P = (F_o^2 + 2F_c^2)/3$ |
| $(\Delta/\sigma)_{\max}$ | 2.943 |
| $\Delta\rho_{\max}, \Delta\rho_{\min}$ (e Å ⁻³) | 10.86, -5.78 |

Table C.34. Atom coordinates for $[(Tp^*)Fe(CN)_2-\mu CN-Co(dmf)(Tp^{Ph})] \cdot 2dmf$.

| Atom | x | y | z | Occupancy |
|------|---------|---------|---------|-----------|
| Ni1 | 0.20132 | 0.17915 | 0.33288 | 1.000 |
| Fe1 | 0.21181 | 0.40980 | 0.37076 | 1.000 |
| N1 | 0.27660 | 0.44143 | 0.29505 | 1.000 |
| N2 | 0.36170 | 0.48867 | 0.30120 | 1.000 |
| N3 | 0.18540 | 0.49912 | 0.39536 | 1.000 |
| N4 | 0.27710 | 0.54105 | 0.38648 | 1.000 |
| N5 | 0.38280 | 0.41114 | 0.41000 | 1.000 |
| N6 | 0.44930 | 0.46555 | 0.40549 | 1.000 |
| N7 | 0.21040 | 0.27196 | 0.33735 | 1.000 |
| N8 | 0.27130 | 0.17829 | 0.24915 | 1.000 |
| N9 | 0.21100 | 0.13837 | 0.20911 | 1.000 |
| N10 | 0.02470 | 0.15591 | 0.30213 | 1.000 |
| N11 | 0.01530 | 0.11286 | 0.25685 | 1.000 |
| N12 | 0.24870 | 0.08692 | 0.33587 | 1.000 |

| | | | | |
|-----|----------|---------|---------|-------|
| N13 | 0.20590 | 0.05355 | 0.28619 | 1.000 |
| N14 | 0.16590 | 0.18149 | 0.42255 | 1.000 |
| N15 | -0.05000 | 0.40481 | 0.30527 | 1.000 |
| N16 | 0.13190 | 0.36483 | 0.49294 | 1.000 |
| C1 | 0.25700 | 0.42894 | 0.23577 | 1.000 |
| C2 | 0.32960 | 0.46870 | 0.20466 | 1.000 |
| H2 | 0.33380 | 0.47000 | 0.16230 | 1.000 |
| C3 | 0.39400 | 0.50590 | 0.24657 | 1.000 |
| C4 | 0.17050 | 0.37980 | 0.20985 | 1.000 |
| H4A | 0.18750 | 0.34060 | 0.23140 | 1.000 |
| H4B | 0.18230 | 0.37410 | 0.16710 | 1.000 |
| H4C | 0.08520 | 0.39260 | 0.21400 | 1.000 |
| C5 | 0.48630 | 0.55640 | 0.23860 | 1.000 |
| H5A | 0.45640 | 0.59550 | 0.25460 | 1.000 |
| H5B | 0.49730 | 0.56130 | 0.19570 | 1.000 |
| H5C | 0.56550 | 0.54540 | 0.26050 | 1.000 |
| C6 | 0.08950 | 0.53101 | 0.41337 | 1.000 |
| C7 | 0.12010 | 0.59462 | 0.41623 | 1.000 |
| H7 | 0.06960 | 0.62770 | 0.42800 | 1.000 |
| C8 | 0.23860 | 0.59912 | 0.39833 | 1.000 |
| C9 | -0.03060 | 0.50271 | 0.42598 | 1.000 |
| H9A | -0.07720 | 0.49140 | 0.38790 | 1.000 |
| H9B | -0.07820 | 0.53270 | 0.44760 | 1.000 |

| | | | | |
|------|----------|---------|---------|-------|
| H9C | -0.01530 | 0.46540 | 0.45070 | 1.000 |
| C10 | 0.31570 | 0.65534 | 0.38814 | 1.000 |
| H10A | 0.39780 | 0.65020 | 0.40950 | 1.000 |
| H10B | 0.27600 | 0.69230 | 0.40340 | 1.000 |
| H10C | 0.32370 | 0.66020 | 0.34490 | 1.000 |
| C11 | 0.45500 | 0.37258 | 0.44560 | 1.000 |
| C12 | 0.56650 | 0.40205 | 0.46277 | 1.000 |
| H12 | 0.63410 | 0.38520 | 0.48740 | 1.000 |
| C13 | 0.55980 | 0.46005 | 0.43728 | 1.000 |
| C14 | 0.65320 | 0.51128 | 0.44220 | 1.000 |
| H14A | 0.68390 | 0.51850 | 0.40270 | 1.000 |
| H14B | 0.72220 | 0.49950 | 0.47130 | 1.000 |
| H14C | 0.61480 | 0.54940 | 0.45580 | 1.000 |
| C15 | 0.41760 | 0.30859 | 0.46295 | 1.000 |
| H15A | 0.35270 | 0.31140 | 0.49070 | 1.000 |
| H15B | 0.48920 | 0.28680 | 0.48270 | 1.000 |
| H15C | 0.38630 | 0.28570 | 0.42680 | 1.000 |
| C16 | 0.21600 | 0.32415 | 0.34907 | 1.000 |
| C17 | 0.04640 | 0.40713 | 0.33093 | 1.000 |
| C18 | 0.15750 | 0.38112 | 0.44646 | 1.000 |
| C19 | 0.34480 | 0.21370 | 0.21766 | 1.000 |
| C20 | 0.32870 | 0.19709 | 0.15658 | 1.000 |
| H20 | 0.36800 | 0.21500 | 0.12430 | 1.000 |

| | | | | |
|-----|----------|---------|---------|-------|
| C21 | 0.24430 | 0.14946 | 0.15323 | 1.000 |
| H21 | 0.21440 | 0.12800 | 0.11760 | 1.000 |
| C22 | 0.43450 | 0.25754 | 0.24745 | 1.000 |
| C23 | 0.49730 | 0.24244 | 0.30294 | 1.000 |
| H23 | 0.48000 | 0.20440 | 0.32220 | 1.000 |
| C24 | 0.58520 | 0.28305 | 0.33020 | 1.000 |
| H24 | 0.62760 | 0.27230 | 0.36780 | 1.000 |
| C25 | 0.61150 | 0.33880 | 0.30310 | 1.000 |
| H25 | 0.67020 | 0.36660 | 0.32230 | 1.000 |
| C26 | 0.55150 | 0.35330 | 0.24800 | 1.000 |
| H26 | 0.57030 | 0.39120 | 0.22890 | 1.000 |
| C27 | 0.46290 | 0.31310 | 0.21930 | 1.000 |
| H27 | 0.42270 | 0.32360 | 0.18110 | 1.000 |
| C28 | -0.08930 | 0.16207 | 0.32041 | 1.000 |
| C29 | -0.17240 | 0.12409 | 0.28546 | 1.000 |
| H29 | -0.25870 | 0.12020 | 0.28820 | 1.000 |
| C30 | -0.10250 | 0.09392 | 0.24656 | 1.000 |
| H30 | -0.13230 | 0.06440 | 0.21710 | 1.000 |
| C31 | -0.11970 | 0.20227 | 0.37096 | 1.000 |
| C32 | -0.18370 | 0.17600 | 0.41635 | 1.000 |
| H32 | -0.20690 | 0.13350 | 0.41410 | 1.000 |
| C33 | -0.21380 | 0.21200 | 0.46500 | 1.000 |
| H33 | -0.25500 | 0.19380 | 0.49650 | 1.000 |

| | | | | |
|------|----------|----------|---------|-------|
| C34 | -0.18310 | 0.27450 | 0.46709 | 1.000 |
| H34 | -0.20380 | 0.29920 | 0.50010 | 1.000 |
| C35 | -0.12290 | 0.30115 | 0.42170 | 1.000 |
| H35 | -0.10360 | 0.34420 | 0.42310 | 1.000 |
| C36 | -0.09030 | 0.26506 | 0.37369 | 1.000 |
| H36 | -0.04790 | 0.28350 | 0.34270 | 1.000 |
| C37 | 0.29870 | 0.04569 | 0.37635 | 1.000 |
| C38 | 0.28640 | -0.01442 | 0.35216 | 1.000 |
| H38 | 0.31330 | -0.05220 | 0.37110 | 1.000 |
| C39 | 0.22730 | -0.00744 | 0.29542 | 1.000 |
| H39 | 0.20540 | -0.03990 | 0.26760 | 1.000 |
| C40 | 0.35300 | 0.06320 | 0.43600 | 0.864 |
| C41 | 0.42170 | 0.11740 | 0.44640 | 0.864 |
| H41 | 0.43620 | 0.14380 | 0.41370 | 0.864 |
| C42 | 0.46960 | 0.13320 | 0.50480 | 0.864 |
| H42 | 0.51400 | 0.17090 | 0.51220 | 0.864 |
| C43 | 0.45050 | 0.09210 | 0.55210 | 0.864 |
| H43 | 0.47980 | 0.10260 | 0.59220 | 0.864 |
| C44 | 0.39000 | 0.03700 | 0.54090 | 0.864 |
| H44 | 0.38210 | 0.00860 | 0.57300 | 0.864 |
| C45 | 0.34060 | 0.02220 | 0.48390 | 0.864 |
| H45 | 0.29780 | -0.01590 | 0.47690 | 0.864 |
| C40' | 0.36000 | 0.07000 | 0.43480 | 0.136 |

| | | | | |
|------|----------|---------|---------|-------|
| C41' | 0.43600 | 0.12300 | 0.43570 | 0.136 |
| H41' | 0.44800 | 0.14340 | 0.39910 | 0.136 |
| C42' | 0.49400 | 0.14500 | 0.49040 | 0.136 |
| H42' | 0.55560 | 0.17620 | 0.49070 | 0.136 |
| C43' | 0.46000 | 0.11950 | 0.54460 | 0.136 |
| H43' | 0.50250 | 0.13030 | 0.58220 | 0.136 |
| C44' | 0.36200 | 0.07900 | 0.54170 | 0.136 |
| H44' | 0.32860 | 0.06780 | 0.57810 | 0.136 |
| C45' | 0.31100 | 0.05360 | 0.48900 | 0.136 |
| H45' | 0.24400 | 0.02550 | 0.48900 | 0.136 |
| C46 | 0.14440 | 0.19397 | 0.47001 | 1.000 |
| C47 | 0.11750 | 0.21110 | 0.53110 | 1.000 |
| H47A | 0.09900 | 0.25560 | 0.53250 | 1.000 |
| H47B | 0.18920 | 0.20180 | 0.55940 | 1.000 |
| H47C | 0.04600 | 0.18740 | 0.54230 | 1.000 |
| B1 | 0.39690 | 0.51730 | 0.36370 | 1.000 |
| H1 | 0.45800 | 0.55180 | 0.36120 | 1.000 |
| B2 | 0.13170 | 0.08570 | 0.23248 | 1.000 |
| H2A | 0.10880 | 0.05500 | 0.19970 | 1.000 |
| CI1 | -0.22660 | 0.32488 | 0.13245 | 1.000 |
| CI2 | -0.02279 | 0.24642 | 0.17762 | 1.000 |
| C3S | -0.14830 | 0.29040 | 0.19820 | 1.000 |
| H3SA | -0.11860 | 0.32320 | 0.22700 | 1.000 |

| | | | | |
|------|----------|----------|---------|-------|
| H3SB | -0.20600 | 0.26330 | 0.21820 | 1.000 |
| N1S | 0.04290 | -0.06990 | 0.46870 | 0.746 |
| C2S | -0.03070 | 0.01330 | 0.38810 | 0.746 |
| H2S1 | 0.01830 | 0.05040 | 0.39920 | 0.746 |
| H2S2 | -0.11880 | 0.02330 | 0.38770 | 0.746 |
| H2S3 | -0.01260 | -0.00070 | 0.34800 | 0.746 |
| N1S' | 0.08200 | -0.07690 | 0.42980 | 0.254 |
| C2S' | -0.13000 | -0.00700 | 0.44170 | 0.254 |
| H2S4 | -0.18170 | -0.04070 | 0.45530 | 0.254 |
| H2S5 | -0.17010 | 0.01110 | 0.40460 | 0.254 |
| H2S6 | -0.12020 | 0.02510 | 0.47300 | 0.254 |
| C1S | -0.00140 | -0.03320 | 0.42950 | 1.000 |

Table C.35. Bond angles for $[(Tp^*)Fe(CN)_2-\mu CN-Co(dmf)(Tp^{Ph})]\cdot 2dmf$ ($^\circ$).

| | | | |
|-------------|----------|-------------|-----------|
| N14—Co1—N10 | 93.4(7) | B2—N13—N12 | 123.7(18) |
| N1—Co1—N10 | 88.1(8) | C15—C16—C17 | 107(2) |
| N1—Co1—N14 | 106.3(8) | N7—C5—C6 | 105(2) |
| N12—Co1—N10 | 83.9(8) | C4—C5—C6 | 133(2) |
| N12—Co1—N14 | 91.2(8) | C4—C5—N7 | 121(2) |
| N12—Co1—N1 | 161.2(8) | C27—C26—C25 | 113(2) |
| O1—Co1—N10 | 161.8(7) | N13—C28—C29 | 105(2) |
| O1—Co1—N14 | 102.4(7) | N9—C10—C9 | 118(2) |
| O1—Co1—N1 | 95.8(7) | C11—C10—C9 | 134(2) |

| | | | |
|-------------|-----------|-------------|-----------|
| O1—Co1—N12 | 86.9(7) | C11—C10—N9 | 106(2) |
| N6—Fe1—N4 | 87.1(9) | N13—N12—Co1 | 112.5(14) |
| C3—Fe1—N4 | 97.6(11) | C30—N12—Co1 | 143.8(18) |
| C3—Fe1—N6 | 172.6(12) | C30—N12—N13 | 103(2) |
| C2—Fe1—N4 | 179.1(10) | B2—N15—N14 | 125.5(18) |
| C2—Fe1—N6 | 92.1(10) | C37—N15—N14 | 113.1(19) |
| C2—Fe1—C3 | 83.1(12) | C37—N15—B2 | 121.2(19) |
| N8—Fe1—N4 | 91.9(8) | C16—C15—N5 | 110(2) |
| N8—Fe1—N6 | 94.2(9) | C14—C15—N5 | 117(2) |
| N8—Fe1—C3 | 91.3(11) | C14—C15—C16 | 132(2) |
| N8—Fe1—C2 | 88.6(9) | C12—N8—Fe1 | 139.1(17) |
| C1—Fe1—N4 | 89.9(8) | N9—N8—Fe1 | 118.4(14) |
| C1—Fe1—N6 | 88.2(9) | N9—N8—C12 | 102.5(17) |
| C1—Fe1—C3 | 86.2(11) | N2—C1—Fe1 | 176.3(19) |
| C1—Fe1—C2 | 89.6(9) | N8—N9—C10 | 110.4(19) |
| C1—Fe1—N8 | 177.1(9) | B1—N9—C10 | 132(2) |
| C17—N4—Fe1 | 139.3(19) | B1—N9—N8 | 116.9(19) |
| N5—N4—Fe1 | 114.3(12) | N13—B2—N11 | 105.2(17) |
| N5—N4—C17 | 106(2) | N15—B2—N11 | 109(2) |
| C40—C45—C44 | 124(2) | N15—B2—N13 | 103.3(17) |
| C21—N10—Co1 | 137.7(16) | C19—C20—C21 | 109(2) |
| N11—N10—Co1 | 116.2(14) | C10—C11—C12 | 107(2) |
| N11—N10—C21 | 105.1(18) | C25—C24—C23 | 124(3) |

| | | | |
|-------------|-----------|-------------|-----------|
| C22—C21—N10 | 120(2) | N5—B1—N7 | 107(2) |
| C20—C21—N10 | 108(2) | N9—B1—N7 | 112(2) |
| C20—C21—C22 | 131(2) | N9—B1—N5 | 109(2) |
| C7—N6—Fe1 | 137.2(18) | C24—C25—C26 | 122(3) |
| N7—N6—Fe1 | 115.0(17) | C32—C31—C30 | 123(2) |
| N7—N6—C7 | 105.1(19) | C36—C31—C30 | 119(2) |
| N1—C3—Fe1 | 166(2) | C36—C31—C32 | 117(2) |
| N15—N14—Co1 | 114.9(15) | N12—C30—C29 | 114(2) |
| C39—N14—Co1 | 136.7(17) | C31—C30—C29 | 124(2) |
| C39—N14—N15 | 107.9(19) | C31—C30—N12 | 122(2) |
| C3—N1—Co1 | 160(2) | C39—C40—C45 | 121(2) |
| C43—C44—C45 | 121(3) | C41—C40—C45 | 114(2) |
| N3—C2—Fe1 | 178(2) | C41—C40—C39 | 124(2) |
| C5—C6—C7 | 111(2) | C40—C39—N14 | 126(2) |
| C6—C7—N6 | 108(2) | C38—C39—N14 | 108(2) |
| C8—C7—N6 | 120(2) | C38—C39—C40 | 126(2) |
| C8—C7—C6 | 131(2) | C37—C38—C39 | 110(2) |
| C24—C23—C22 | 114(2) | C42—C43—C44 | 118(3) |
| C16—C17—N4 | 112(2) | C41—C42—C43 | 118(3) |
| C18—C17—N4 | 123(2) | C38—C37—N15 | 100.7(19) |
| C18—C17—C16 | 125(2) | C42—C41—C40 | 124(2) |
| C5—N7—N6 | 109.4(19) | C33—C32—C31 | 124(3) |
| B1—N7—N6 | 120(2) | C35—C36—C31 | 119(3) |

| | | | |
|-------------|-----------|-------------|-----------|
| B1—N7—C5 | 131(2) | C34—C33—C32 | 120(3) |
| C20—C19—N11 | 105(2) | C35—C34—C33 | 120(3) |
| C23—C22—C21 | 114(2) | C26—C27—C22 | 125(3) |
| C27—C22—C21 | 124(3) | C34—C35—C36 | 120(3) |
| C27—C22—C23 | 122(3) | C46—O1—Co1 | 130.4(15) |
| C19—N11—N10 | 112(2) | N16—C46—O1 | 127(2) |
| B2—N11—N10 | 120.0(18) | C48—N16—C46 | 123(2) |
| B2—N11—C19 | 128(2) | C47—N16—C46 | 121(2) |
| C30—C29—C28 | 105(2) | C47—N16—C48 | 116.3(18) |
| C15—N5—N4 | 104.7(17) | C49—N17—C50 | 131(3) |
| B1—N5—N4 | 117.8(19) | C51—N17—C50 | 112(3) |
| B1—N5—C15 | 137(2) | C51—N17—C49 | 117(3) |
| C11—C12—N8 | 114(2) | O2—C49—N17 | 121(4) |
| C13—C12—N8 | 124(2) | C54—N18—C52 | 116(3) |
| C13—C12—C11 | 123(2) | C53—N18—C52 | 123(3) |
| N12—N13—C28 | 113.2(18) | C53—N18—C54 | 121(3) |
| B2—N13—C28 | 122.9(18) | O3—C52—N18 | 128(4) |

Table C.36 Bond lengths for $[(Tp^*)Fe(CN)_2-\mu CN-Co(dmf)(Tp^{Ph})] \cdot 2dmf$ (Å).

| | | | |
|---------|-----------|---------|---------|
| Co1—N10 | 2.10(2) | C12—C13 | 1.55(3) |
| Co1—N14 | 2.093(19) | N13—C28 | 1.35(3) |
| Co1—N1 | 2.03(2) | N13—N12 | 1.37(3) |

| | | | |
|---------|-----------|---------|---------|
| Co1—N12 | 2.12(2) | N13—B2 | 1.68(3) |
| Co1—O1 | 2.012(15) | C16—C15 | 1.29(3) |
| Fe1—N4 | 2.022(19) | C5—C4 | 1.41(3) |
| Fe1—N6 | 2.03(2) | C26—C25 | 1.45(4) |
| Fe1—C3 | 1.86(3) | C26—C27 | 1.45(4) |
| Fe1—C2 | 1.92(3) | N2—C1 | 1.13(3) |
| Fe1—N8 | 1.916(18) | C10—C9 | 1.49(3) |
| Fe1—C1 | 1.880(19) | C10—N9 | 1.39(3) |
| N4—C17 | 1.23(3) | C10—C11 | 1.36(4) |
| N4—N5 | 1.48(3) | N12—C30 | 1.30(3) |
| C45—C44 | 1.36(4) | C14—C15 | 1.51(4) |
| C45—C40 | 1.39(3) | N15—B2 | 1.54(3) |
| N10—C21 | 1.39(3) | N15—C37 | 1.39(3) |
| N10—N11 | 1.39(3) | N8—N9 | 1.46(3) |
| C21—C22 | 1.49(3) | N9—B1 | 1.50(3) |
| C21—C20 | 1.35(3) | C24—C25 | 1.22(4) |
| N6—C7 | 1.37(3) | C31—C30 | 1.49(3) |
| N6—N7 | 1.41(3) | C31—C32 | 1.40(3) |
| C3—N1 | 1.26(4) | C31—C36 | 1.36(4) |
| N14—N15 | 1.32(3) | C40—C39 | 1.42(3) |
| N14—C39 | 1.37(3) | C40—C41 | 1.36(3) |
| C44—C43 | 1.41(4) | C39—C38 | 1.34(3) |
| N3—C2 | 1.16(3) | C38—C37 | 1.44(3) |

| | | | |
|---------|---------|---------|---------|
| C6—C7 | 1.39(4) | C43—C42 | 1.37(4) |
| C6—C5 | 1.35(3) | C42—C41 | 1.45(4) |
| C7—C8 | 1.49(3) | C32—C33 | 1.31(4) |
| C23—C22 | 1.42(4) | C36—C35 | 1.44(4) |
| C23—C24 | 1.46(3) | C33—C34 | 1.39(4) |
| C17—C16 | 1.41(3) | C34—C35 | 1.36(4) |
| C17—C18 | 1.55(3) | O1—C46 | 1.23(3) |
| N7—C5 | 1.40(3) | C46—N16 | 1.31(3) |
| N7—B1 | 1.51(4) | N16—C48 | 1.43(3) |
| C19—N11 | 1.32(3) | N16—C47 | 1.49(3) |
| C19—C20 | 1.41(4) | N17—C50 | 1.54(4) |
| C22—C27 | 1.23(3) | N17—C49 | 1.33(4) |
| N11—B2 | 1.56(3) | N17—C51 | 1.49(4) |
| C29—C28 | 1.37(3) | O2—C49 | 1.29(4) |
| C29—C30 | 1.38(4) | N18—C52 | 1.35(5) |
| N5—C15 | 1.36(3) | N18—C54 | 1.41(4) |
| N5—B1 | 1.55(3) | N18—C53 | 1.44(4) |
| C12—N8 | 1.32(3) | O3—C52 | 1.18(4) |
| C12—C11 | 1.41(3) | | |
